UNIVERSITY OF SOUTHAMPTON

DEPARTMENT OF AERONAUTICS AND ASTRONAUTICS

WAVE RECEPTANCE ANALYSIS OF VIBRATING BEAMS AND STIFFENED PLATES

by

Yavuz YAMAN, M.Sc.

Under the Supervision of Professor D.J. Mead

Thesis submitted for the Degree of
Doctor of Philosophy

1989

This work is dedicated to my mother, Nebiye, and my father ,Mehmet Tevfik, who have sacrificed everything in their lives for me.

Bu çalışma yaşamlarındaki herşeyi benim için feda eden annem Nebiye ve babam Mehmet Tevfik YAMAN'a ithaf edilmiştir.

UNIVERSITY OF SOUTHAMPTON

ABSTRACT

FACULTY OF ENGINEERING AND APPLIED SCIENCE
AERONAUTICS AND ASTRONAUTICS

Doctor of Philosophy

WAVE RECEPTANCE ANALYSIS OF VIBRATING BEAMS AND STIFFENED PLATES

by Yavuz YAMAN

This study develops analytical methods for the analysis of harmonically forced vibrations of multi-supported beams and stiffened plates. The methods are based on the response of infinite, uninterrupted structures to a single external excitation from which families of waves propagate outwards in all directions. The structures considered are uniform in thickness. The beams have a single-point force. The plates are finite in width with the two opposite parallel edges being simply-supported along the length. A line forcing varies sinusoidally between those edges.

The first part of the thesis analyses the dynamics of infinite, uninterrupted structures. Special attention is subsequently paid to three-layered sandwich structures and their dispersion characteristics are also investigated.

The second part considers finite structures. An analytical approach is presented for single-bay and multi-bay structures with arbitrary support spacing. Influences of support elastic/inertial characteristics are investigated in detail. Effects of end reflections are fully dealt with.

The third part deals with the free and forced vibrations of infinite, periodic structures. Particular attention is focused on the effects of stiffness characteristics and cross-sectional distortion of the stiffeners.

Part four outlines experimental work undertaken to validate the above theories. The experimental and theoretical results are compared.

ACKNOWLEDGEMENTS

The author wishes to express his warmest gratitude to his supervisor, Professor D.J. Mead, for the guidance, supervision and encouragement given during the course of the work.

Acknowledgement is also given to the stimulating discussions and help provided by Dr. R. Joannides for the computer plots.

The author is particularly indebted to Mrs. G. Snelgrove for endless and patient time she had spent for the computer outputs and plots.

The expert and flawless typing of Mrs. M. Strickland and her understanding are deeply appreciated.

Thanks are also extended to Mr. J. Hawkes, Mr. I. Smart and the Workshop staff.

Finally, the author wishes to thank wholeheartedly the Turkish Government and the British Council for the financial help and opportunity provided to conduct this work.

TABLE OF CONTENTS

Section 3: Dynamic Behaviour of Infinite, Periodic Structures

LIST OF FIGURES

LIST OF TABLES

Table

NOMENCLATURE

a	Acceleration
a_n, b_n, c_n, d_n	n^{th} coefficients of infinite-system point/line response and receptance functions
A	Current
A_n, B_n, C_n	Coefficients of n^{th} wave amplitudes
b	Width of beams
b_{eff}	Effective width of stiffened plate skin
d	Sandwich structure parameter ($d = h + h_c$) Appendix C: Width of flange
D	Flexural rigidity of Euler-Bernoulli plates
D_t	Total flexural rigidity of face-plates of sandwich structures
e	Exponential symbol
E	Young's modulus
f	Frequency
F_o	Magnitude of externally applied transverse point/line force Appendix C: Magnitude of the transverse line force
G_c	Magnitude of core shear stiffness of sandwich structures
G_c^*	Complex core shear stiffness of sandwich structures ($G_c^* = G_c(1 + \imath\beta)$)
h	Thickness of Euler-Bernoulli beams and plates Face-plate thickness of sandwich structures Appendix C: Height of web
h_c	Core thickness of sandwich structures
$\imath$	$\sqrt{-1}$
I	Second moment of area of unit-width Euler-Bernoulli beams
I_f	Second moment of area of the upper flange of stiffener
I_{xx}	Second moment of area of stiffener cross-section
I_{xz}	Product moment of area of stiffener cross-section

k_n	n^{th} wave number
K_c	Stiffness coupling
KC	Non-dimensional stiffness coupling
K_r	Rotational stiffness
KR	Non-dimensional rotational stiffness
K_t	Transverse stiffness
KT	Non-dimensional transverse stiffness
L	Total length of the finite structure
L_y	Width of plate Appendix C: Length of stiffener
m	Number of half-wavelengths across the width of plates
m_b	Mass/length of unit-width Euler-Bernoulli beam
m_s	Mass/area of sandwich structures
M	Point mass
M	Bending moment on Euler-Bernoulli beam cross-section
M_{af}	Bending moment due to face-plate axial forces on sandwich structure cross-section
M_{fp}	Total bending moment of face-plates on sandwich structure cross-section
M_j	Reaction moment applied on the structure by the j^{th} support at x_j
M_x	Total bending moment on sandwich structure cross-section
M_{x_j}	Moment applied on the j^{th} support by the structure at x_j
M_{xx}	Bending moment on uniform plate cross-section
M_{xy}	Twisting moment on sandwich plate cross-section
M_o	Magnitude of externally applied point/line bending moment Appendix C: Magnitude of line bending moment
M_1, M_3	Bending moments of individual face-plates on sandwich structure cross-section
N	Number of degrees of freedom of the structure cross-section Force unit(Newton)
N_b	Number of bays in finite multi-bay structures

N_1, N_3	Axial forces of face-plates on sandwich beam cross-section
R_j	Transverse reaction force applied on the structure by the j^{th} support at x_j
R_{x_j}	Transverse force applied on the j^{th} support by the structure at x_j
S	Shear force on Euler-Bernoulli beam cross-section
S_{eff}	Effective shear force on plate cross-section
S_n	Shear force of the n^{th} layer on sandwich beam cross-section
S_x	Total shear force on the sandwich structure cross-section
t	Time Appendix C: Uniform thickness of stiffener cross-section
T	Temperature Appendix C: Kinetic energy
u	Axial displacement in x direction
u_3	Mid-plane axial displacement of the bottom plate of sandwich structure in x direction
v	Axial displacement in y direction Chapter 11: Velocity
v_3	Mid-plane axial displacement of the bottom plate of sandwich plates in y direction
V	Potential energy Chapter 11: Voltage
w	Transverse displacement in z direction
w'	$\partial w/\partial x$
w"	$\partial^2 w/\partial x^2$
w'"	$\partial^3 w/\partial x^3$
XL	Bay length of infinite, periodic structures
α_{FF}, α_{FM} α_{MF}, α_{MM}	Generalized phased array receptance functions
β	Core loss factor of sandwich structures
Γ_c	Torsion-bending constant of the stiffener cross-section
η	Material loss factor

θ	Rotation ($\theta = \partial w/\partial x$)
μ	Complex propagation constant ($\mu = \mu_r + i\mu_i$)
ν	Poisson's ratio
π	3.14159
ρ	Material density
σ_1, σ_3	Direct stresses of face-plates on sandwich plate cross-section
τ_{xy}	Shear stress of face-plates on sandwich plate cross-section
ω	Circular frequency
∇^2	$\partial^2/\partial x^2 + \partial^2/\partial y^2$
∇^4	$\partial^4/\partial x^4 + 2\ \partial^4/\partial x^2 \partial y^2 + \partial^4/\partial y^4$
$\dot{}$	$\partial/\partial t$
$\ddot{}$	$\partial^2/\partial t^2$
$\lvert\ \rvert$	Absolute value
$\{\ \}$	Column matrix
$\lfloor\ \rfloor$	Row matrix
$[\ ]$	Square matrix

The dummy variables confined to certain chapters are clearly defined wherever applicable.

CHAPTER 1

INTRODUCTION

1.1 Background to the Study

Even though technological advances in composite materials are gathering pace, many aeroplane structures are still made of stiffened metal plates or shells. These parts have to endure a wide range of external pressure fluctuations during the different phases of take-off and flight and they may readily vibrate in consequence. Fatigue failure and unacceptable sound transmission can be the result of these severe working conditions. For a long time now, engineers have been trying to develop analytical models which can give an accurate insight into the complicated dynamic response of these stiffened structures.

The stiffening provides stability under the heavy compressive stresses carried in the course of flight and landing. In the case of plate-like structures stiffening is achieved by using orthogonal sets of frames and stringers (stiffeners). The frames run along the length of the plate and generally have very high transverse stiffness. The stringers are attached to the plate across the width and provide both transverse and rotational constraints. The whole plate is then divided into smaller plate components (bays). If the stiffener spacing is equal and the stiffeners are the same, the plate can be considered as a periodic structure but practical limitations often render it non-periodic.

The external pressure fluctuations which act on aeroplane structures are generally random in time and their peak spectral densities usually occur in the range of 300-1000 Hz. These may be jet noise acoustic pressure at take-off, shock noise in high-altitude flight or boundary layer hydrodynamic pressure fluctuations at high speed.

In the frequency range of interest there are many modes which contribute to the response. Around the resonant regions their

individual resonant peaks often overlap because of high modal density. The prediction of the many natural modes, their corresponding natural frequencies and the total forced response has been a difficult task to achieve.

Finding effective ways of damping the excessive response created by these resonant modes is another problem which has been challenging engineers. Material hysteretic damping, structural joints and the adjacent air into which acoustic energy can be radiated are the sources of damping of a structure. In addition, unconstrained or constrained layers of materials which have high damping capacity have been incorporated for the purpose of controlling the vibration. Sandwich structures with constrained layers of viscoelastic damping material are of particular interest. As well as providing high damping, some other features such as the high stiffness for a given weight and in some cases the absence of stress-raising rivets lead to much higher fatigue life than that of pure metal skin-stringer construction when exposed to the same working conditions.

However, from the analytical point of view, high damping brings its own problems. Due to the high modal density and heavy modal coupling there are no predominant modes in the resonant regions.

On the other hand, certain analytical advantages of high damping also exist. In a heavily damped structure the waves created by the excitation quickly die out as they travel away from the source. Therefore, if the structural boundaries are sufficiently far from the point of disturbance, the effect at that point of wave reflection from the boundaries can be ignored. This in turn suggests that the structure can be regarded as being infinite in extent and this simplifies the analytical procedures.

1.2 Review of Existing Methods of Theoretical Modal Analysis

1.2.1 Theory of Single and Multi-Bay Structures

The dynamic behaviour of single-bay structures has long been analyzed by classical methods such as the receptance theory, the direct solution of differential equation and various energy methods. If the plate structure has many stiffeners with complicated support characteristics, the required algebra becomes so unwieldy that these methods no longer offer an easy method of analysis.

Gorman developed a method applicable to the vibrations of multi-bay beams [1]. When the number of bays got large (in his case ≥ 3) he assumed all the intermediate supports as simple. Clearly this situation is difficult, if not impossible, to satisfy in practice. The supports generally provide elastic and inertial constraints on the structure and further complicates the problem.

Effects of stiffening on the plate response were analyzed and presented by Kirk in two articles [2,3]. He first obtained the natural frequencies of transverse vibration of rectangular plates which had stiffeners parallel to one edge. Later he determined the ratio of the fundamental natural frequency of a rectangular plate with a single stiffener to the fundamental natural frequency of the unstiffened plate of equal mass.

One of the first studies on the dynamic response of stiffened multi-bay plates was made by Lin [4]. By considering the dynamics of open-section beams, he developed a model for the representation of stiffener characteristics [5]. He showed that the natural frequencies of an N_b bay structure, in which the bays are comparable or equal in length, falls into groups of N_b. By assuming each bay to be identical he was able to predict the bounding frequencies of each group as N_b became infinite. Later, by using the finite difference method, Lin *et al* [6] predicted the natural frequencies, but not the normal modes, of vibrations of a plate with identically constructed bays and stiffeners. However, the support characteristics were simplified and either transverse stiffness or rotational stiffness effects were

considered. Mercer *et al* [7] presented a transfer matrix method and analysed the natural frequencies and normal modes of multi-bay flat plates. But the method required time-consuming computations particularly when the number of bays was large. The stiffeners were modelled as in [5].

All the work so far outlined dealt with the free vibration of structures.

1.2.2 Theory of Periodic Structures

Wave propagation and periodic structure theories were first studied by physicists and electrical engineers [8]. The applications to engineering structures are relatively new. Heckl [9] considered a system of grillages and found that waves can propagate in some frequency bands but not in others. Mead *et al* [10] included the effects of damping and demonstrated the influence of support stiffnesses on the random response.

Advances in periodic structures theory allowed researchers to provide some approximate solutions for the vibrations of finite structures. By using the vibration characteristics of infinite, periodic undamped structures, Sen Gupta studied the free vibrations of finite multi-bay beams and plates in two articles. He considered equi-spaced beams on intermediate simple supports having either simply-supported or clamped extreme ends [11]. Later he extended the theory to skin-stringer structures [12]. However, he only analysed the simplified boundary conditions of [6].

In another study [13] Mead solved the differential equation of motion directly and studied the responses of periodic beams on flexible supports. In two articles [14,15] Mead determined the relations between the limiting frequencies of the bands at which the waves can freely propagate and the natural frequencies of the individual periodic element. Abdel-Rahman *et al* [16] used finite element methods in the analysis of two-dimensional periodic structures.

Mead in [17] approached the problem from a different angle. He viewed the infinite, periodic structure as an infinite uniform structure on which the supports at regular intervals impose reactions depending on their stiffnesses. He then combined those reactions and proceeded to obtain closed form formulae for the propagation constants of Euler-Bernoulli beams, Timoshenko beams and stiffened uniform plates for various support conditions.

By using transfer matrix methods, Munjal *et al* [18] presented an approach for the analysis of an infinite, periodic beam when it is forced only in one of its bays. A useful review covering some other recent works was published by Sen Gupta [19].

1.3 Analysis of Damping of Multi-Layered Structures

A study conducted by Mead [20] discussed the controlling of acoustic fatigue stresses in stiffened plate structures and compared the unconstrained and constrained damping treatments.

Multi-layered plate configurations with a constrained layer of damping materials have been exploited as an effective method of vibration control. Most work has concentrated on three-layered plates with elastic face-plates and a soft viscoelastic damping layer sandwiched between them. They have been used to obtain a high damping capacity when the plate is undergoing transverse motion at relatively moderate frequencies. This is the range in which the wavelength of the transverse vibration is much greater than the plate thickness. Hence the assumptions made in the analyses that the elastic face-plates deform in accordance with elementary theory of bending have been justified. To predict the vibration levels of such plates the analyses concentrated on determining the effective flexural stiffnesses and loss factors of the plates.

Kerwin presented the first study [21]. This was followed by Mead [22], DiTaranto [23] and Mead *et al* [24]. These theories allowed the cross-section to move as a whole in the transverse direction.

Furthermore they all assumed that the longitudinal and rotatory inertias of the face-plates and core were negligible.

This thesis follows the basic principles put forward by these investigators in the analysis of three-layered sandwich beams and plates.

The effects of different sandwich beam boundary conditions were analysed by Mead *et al* [25]. The damping properties of single-bay and periodic three-layered sandwich plates were investigated in [26] and [27] respectively. Two opposite edges along the length were assumed as being simply-supported and across the width stiffeners having elastic characteristics provided the constraints. A purely experimental study on multi-bay stiffened sandwich plates was published [28]. Nakra in [29] included a useful bibliography on the dynamics of damped sandwich plates.

1.4 The Response Functions of Infinite, Uninterrupted Beams and Plates

If an infinite, uninterrupted structure is forced at a point (or line), the response of the structure to that excitation is that of waves emanating from the point (or line) of excitation. The response can be expressed in terms of 'Infinite-System Point/Line Response Functions' of the structure defined by Cremer *et al* [30].

If the structure has any intermediate supports, each support exerts reaction(s) on the structure which depend on its characteristics. The structure then can be viewed as a uniform structure which is under the action of externally applied force(s) and reaction(s). These reactions create their own wave fields identical in form to that of the external excitation but proportional to the support stiffnesses.

If the structure is spatially infinite there are no reflected waves from the ends. The total response of the structure is then

composed of the contributions from the 'Infinite-System Point/Line Response Functions' of all the reactions and the externally applied force. On the other hand if the structure is finite, the reflected waves from the boundaries also contribute to the total response and must be considered in the analysis.

In order to find the response of the structure, the amplitudes of all the intermediate support reactions are to be determined. This can be achieved by satisfying the appropriate compatibility and equilibrium conditions at selected support locations. If reflected waves also exist then the extreme end boundary conditions should also be considered.

1.5 The Contents and Scope of This Study

This thesis studies the harmonic responses of uniform structures. Euler-Bernoulli beams, three-layered sandwich beams, Euler-Bernoulli plates and three-layered sandwich plates are investigated. The beam structures have a single-point external harmonic force. The plate structures have two opposite edges simply-supported along the length and a harmonic line forcing varies sinusoidally between those edges.

The first part of the thesis deals with the dynamics of infinite, uninterrupted structures. Chapter 2 lays down the underlying theory for beam structures and Chapter 3 gives the extension for plate structures. Both damped and undamped analyses are undertaken. Special attention is paid to sandwich structures and the analyses are concentrated on structures having equal face-plates. Effects of core characteristics are investigated in detail. Also analysed in this part are the dispersion characteristics of three-layered sandwich beams and plates.

The second part of the thesis considers the harmonically forced vibrations of finite structures. An analytical approach is presented for multi-bay structures which is based upon the 'Infinite-System

Point/Line Response Functions' of external forcing and intermediate support reactions. The effects of reflections are fully dealt with.

Chapter 4 gives the full theory for Euler-Bernoulli beams. Incorporation of different support characteristics is shown. The condition of multi-forcing is given. Multi-bay beams with intermediate simple supports and different end boundary conditions are studied. The effects of elastic supports are investigated. It is explained how both the frequency response and the corresponding mode shapes may be obtained.

Chapter 5 studies the harmonically forced vibrations of a single-bay sandwich beam and shows that the method can successfully incorporate the relevant complicated boundary conditions.

Chapter 6 analyses the forced vibrations of multi-bay, stiffened plates. Both Euler-Bernoulli plate and three-layered sandwich plate theories are considered. Sandwich plates are assumed to have equal face-plates. Effects of damping, sandwich plate core shear stiffness, line of application of forcing, cross-sectional distortion and dynamic stiffness coupling of the stiffeners are studied. Frequency responses and mode shapes are presented.

The third part of the thesis deals with the dynamics of infinite, periodic structures. Chapter 7 gives the theory of free vibrations. The 'Infinite-System Point/Line Response Functions' of the support reactions are combined to form the 'Phased-Array Receptance Functions' of the structures. These functions have nothing to do with the support characteristics. However, the propagation constants of wave motion in infinite, periodic structures are easily obtained by combining these functions with the support characteristics. In this way closed-form equations are obtained for the determination of propagation constants for various support conditions. Simple supports, sliding supports, elastic supports which only provide transverse constraints and general supports which provide both transverse and rotational constraints are studied for Euler-Bernoulli and three-layered sandwich structures.

The application of the theories is carried out in Chapter 8. The relation between the individual periodic element response and 'Phased-Array Receptance Functions' response is studied. The free vibration characteristics of infinite, periodic three-layered sandwich structures are investigated in detail. Effects of core properties are analysed and shown. Influences of support characteristics are presented. Particular attention is focussed on the effects of dynamic characteristics and cross-sectional distortion of the stiffeners.

Chapter 9 analyses the forced vibrations of infinite, periodic structures excited harmonically in a single bay. It utilizes the 'Infinite-System Point/Line Response Functions' of the structure in effect. It is shown how the problem may be reduced from the determination of an infinite number of unknown support reactions to the determination of a finite number of different wave amplitudes. Specific equations are set for structures on simple supports, transversely elastic supports and general supports.

Computations based on Chapter 9 are presented in Chapter 10. Resonances in the harmonic response curves are studied in detail. Effects of support stiffness characteristics are analysed.

In Part 4, Chapter 11 outlines the experimental work undertaken to validate the above theories. The transverse responses of single-layered and three-layered stiffened plates have been measured. Some experiments on simple sandwich beams have also been conducted. The experimental and theoretical results are compared.

1.6 Limitations of the Study

Developed analytical methods can only apply to structures which are uniform in thickness. The beams must be straight and the plates flat. The plate structures should have two opposite edges along the length as simply-supported and the forcing (and hence the response) should be taken as sinusoidally varying between those edges.

Although three-layered sandwich structures having equal face-plates have been considered in this thesis, the approaches presented are equally applicable to sandwich structures with a higher number of equal or unequal layers.

This study only considers the transverse and rotational stiffnesses of the stiffener and the stiffness coupling which may exist between them. The effects of lateral stiffness of the stiffener (*i.e.*, in the plane of the plate) have been ignored.

SECTION 1: DYNAMIC BEHAVIOUR OF INFINITE, UNINTERRUPTED STRUCTURES

CHAPTER 2

POINT RECEPTANCE FUNCTIONS OF INFINITE UNIFORM BEAMS

2.1 Introduction

The response of a uniform infinite beam to a harmonic point force or moment can be found in closed form by solving the corresponding wave equation. The motion of the infinite structure can then be easily studied in terms of the wave motion generated by the source. The feature of being infinite in extent prevents the occurrence of waves being reflected back to the source and hence simplifies the analysis and the motion.

The contents of this chapter present this theory for the uniform Euler-Bernoulli and the three-layered sandwich beams. This is to provide the background for the reader who is not closely familiar with the wave approach to beam vibration analysis.

This chapter develops the full theory for Euler-Bernoulli beams then outlines the relevant points for three-layered sandwich beams with equal face-plates. The beams are assumed to have unit width. Subsequent numerical analysis has been carried out through extensive computer programs. The responses are found at the points of application of external excitations. In the case of force excitation, attention is focussed on the transverse displacement, whereas rotation is considered for moment excitation. The dispersion characteristics of sandwich beams have also been investigated with particular attention being given to the effects of core properties upon them.

2.2 Euler-Bernoulli Beams

2.2.1 Theoretical Approach

The wave equation for the transverse motion of the beam is

$$EI \frac{\partial^4 w}{\partial x^4} + m_b \frac{\partial^2 w}{\partial t^2} = 0 \qquad (2.1)$$

where m_b is the mass/length of a unit-width beam.

When the motion is harmonic with frequency ω, this becomes

$$\frac{d^4 w}{dx^4} - k^4 w = 0 \qquad (2.2)$$

where $k^4 = m_b \omega^2 / EI$.

There are evidently four distinctly different values of k on the complex plane, and they can be shown to be $k_1 = k$, $k_2 = ik$, $k_3 = -k$, $k_4 = -ik$ where $k = (m_b \omega^2 / EI)^{1/4}$.

Consider the infinite beam of Figure 1(a) subjected to the harmonic force $F_o e^{i\omega t}$ acting at $x = 0$. In all the subsequent work of this thesis, it will be assumed that the excitations and responses are harmonic, so the $e^{i\omega t}$ term will usually be omitted.

The transverse responses due to the force can be expressed as [30]

$$w_{right}(x) = F_o \sum_{n=1}^{N} a_n e^{-k_n(+|x|)} \qquad (x \geq 0)$$

$$w_{left}(x) = F_o \sum_{n=1}^{N} a_n e^{k_n(-|x|)} \qquad (x \leq 0) \qquad (2.3)$$

Therefore, the transverse displacement at the distance $|x|$ to the right and left of the force can be found to be,

$$w(x) = F_o \sum_{n=1}^{N} a_n e^{-k_n x} \qquad (-\infty < x < \infty) \qquad (2.4)$$

The k_n's are the wave numbers (real or imaginary for undamped beams and complex for damped beams) of the N waves which the applied force sends out in both directions. A purely real wave number implies a decaying motion, whereas a purely imaginary one defines a propagating motion with constant amplitude and wavelength $\lambda = 2\pi/k$. N depends on the number of degrees of freedom of the cross-section of the structure. For an Euler-Bernoulli beam, N = 2, the freedoms being transverse motion and rotation, though they are not independent. In this case $k_1 = k$, $k_2 = ik$.

Figure 1(b) shows the infinite beam subjected to a moment M_o. Now, since the transverse displacements due to a moment are antisymmetric with respect to the point of application, they can be expressed at a distance |x| as,

$$w_{right}(x) = M_o \sum_{n=1}^{2} b_n e^{-k_n x} \qquad (x \geq 0)$$

$$w_{left}(x) = -M_o \sum_{n=1}^{2} b_n e^{-k_n x} \qquad (x \leq 0) \qquad (2.5)$$

By invoking the symmetry and antisymmetry arguments, similar expressions involving rotations, $\theta = \partial w/\partial x$, can be written as

$$\theta_{right}(x) = F_o \sum_{n=1}^{2} c_n e^{-k_n x} \qquad (x \geq 0)$$

$$\theta_{left}(x) = -F_o \sum_{n=1}^{2} c_n e^{-k_n x} \qquad (x \leq 0)$$

$$\theta(x) = M_o \sum_{n=1}^{2} d_n e^{-k_n x} \qquad (-\infty < x < \infty) \qquad (2.6)$$

The quantities described in equations (2.4) to (2.6) define the 'Infinite-System Point Response Functions' of Euler-Bernoulli beams.

The expressions for the coefficients a_n, b_n, c_n and d_n's can be obtained by considering the relevant equilibrium and compatibility conditions at the point of application of the force or moment.

To start with, consider Figure 2. External excitations F_o or M_o act at $x = 0$. Consider first the case when F_o alone is applied. The boundary conditions to be satisfied in the positive x region are:

$$\left.\frac{\partial w}{\partial x}\right|_{x=0} = 0 \qquad \text{and} \qquad EI \left.\frac{\partial^3 w}{\partial x^3}\right|_{x=0} = \frac{F_o}{2} \tag{2.7}$$

By applying equation (2.4) they lead to two simultaneous equations, given as

$$F_o(-k_1 a_1 - k_2 a_2) = 0$$

$$EI\, F_o(-k_1^3 a_1 - k_2^3 a_2) = \frac{F_o}{2} \tag{2.8}$$

The coefficients a_1 and a_2 required in the analysis are therefore

$$a_1 = -1/4EIk^3, \qquad a_2 = ia_1 \tag{2.9}$$

Since the rotation, θ, is $\partial w/\partial x$, the coefficients c_1 and c_2 corresponding to the force loading are $c_n = -k_n a_n$ $(n = 1,2)$, hence

$$c_1 = 1/4EIk^2, \qquad c_2 = -c_1. \tag{2.10}$$

When the infinite beam is excited by the moment M_o, the first of equations (2.5) must satisfy the boundary conditions,

$$w|_{x=0} = 0 \qquad \text{and} \qquad EI \left.\frac{\partial^2 w}{\partial x^2}\right|_{x=0} = -\frac{M_o}{2} \tag{2.11}$$

Following similar arguments to those above, the required coefficients for the moment loading are found to be

$$b_1 = -1/4EIk^2, \qquad b_2 = -b_1$$

$$d_1 = 1/4EIk, \qquad d_2 = id_1 \tag{2.12}$$

Now suppose that one finds the response at the points of application of excitations. By using equations (2.4) to (2.6), together with (2.9), (2.10) and (2.12), they can be written as

$$w(0)/F_o = \sum_{n=1}^{2} a_n = -(1 + i)/4EIk^3 \qquad (2.13)$$

$$\theta(0)/F_o = \sum_{n=1}^{2} c_n = 0 \qquad (2.14)$$

$$w(0)/M_o = \sum_{n=1}^{2} b_n = 0 \qquad (2.15)$$

$$\theta(0)/M_o = \sum_{n=1}^{2} d_n = (1 + i)/4EIk \qquad (2.16)$$

These equations define 'Infinite-System Point Receptance Functions' of uniform Euler-Bernoulli beams and they are complex quantities.

2.2.2 Calculations and Discussion

Consider a rectangular beam with depth 'h' and excited at frequency 'f' Hz. The frequency and the responses are non-dimensionalized as follows:

ND Frequency: $2\pi f(m_b h^4/EI)^{1/2}$

ND Transverse Point Receptance: $(w(0)/F_o)(EI/h^3)$

ND Rotational Point Receptance: $(\theta(0)/M_o)(EI/h)$

Damping may be included through the complex flexural rigidity of the beam as $EI(1 + i\eta)$. $I = h^3/12$ and η is the loss factor of the beam material.

Figure 3 shows the variation with frequency of the magnitude of the receptances for two different damping values ($\eta = 0$ and $\eta = 0.3$). It can be seen that they vary linearly on log-log scale. The transverse receptance follows a trend of -30 dB per decade. On the

other hand the rotational receptance goes down by 10 dB per decade. These can theoretically be verified by considering equations (2.13) and (2.16) with $k = (m_b\omega^2/EI)^{1/4}$.

The phase angles of the receptances (*i.e.*, phase between response and excitation) are considered in Figure 4. It can be seen that a constant phase angle exists between response and excitation for all frequencies. In the case of no damping this is $\pi/4$ for both receptances. The introduction of damping increases this phase for the rotational receptance but lowers it for the transverse receptance.

2.3 Three-Layered Sandwich Beams

The beams which will be considered in this section have two equal, linearly elastic outer layers (face-plates) and a linearly viscoelastic central layer (core). Numerous authors have studied the response of sandwich structures in recent years. This section follows the theory developed by Mead and Markus [24]. It assumes no significant direct strain normal to the thickness of the layers and no shear strain in the face-plates. It therefore allows the cross-section to move as a whole in the transverse direction. The longitudinal direct stresses in the core are assumed to be negligible and the rotatory and longitudinal inertia effects of the face-plates are excluded from the analysis. Damping is introduced through the core shear modulus in the form of $G_c^* = G_c(1 + i\beta)$.

2.3.1 Theoretical Approach

To begin with, consider Figure 5. The intermediate steps which are omitted here can easily be deduced by studying this figure. It has been shown [24] that the total shear force on the cross-section S_x, the total bending moment of the face-plates M_{fp}, and the bending moment M_{af} due to axial forces N_1 $(= -N_3)$, can be written as:

$$S_x = S_1 + S_3 - S_2 = D_t \frac{\partial^3 w}{\partial x^3} - G_c^* d\left(\frac{d}{h_c}\frac{\partial w}{\partial x} - \frac{2u_3}{h_c}\right)$$

$$M_{fp} = M_1 + M_3 = D_t \frac{\partial^2 w}{\partial x^2}$$

$$M_{af} = N_3.d = (Eh \frac{\partial u_3}{\partial x})d \qquad (2.17)$$

where $d = h + h_c$, D_t is the total flexural rigidity of the individual face-plates and in this case is given by $2(Eh^3/12)$. u_3 is the mid-plane axial displacement of the bottom face-plate. Subscripts 1 and 3 refer to top and bottom face-plates respectively and 2 denotes the core.

Furthermore it has also been proved that the equation of motion of the sandwich can be expressed in two simultaneous equations as,

$$\frac{\partial^4 w}{\partial x^4} - g^* Y \frac{\partial^2 w}{\partial x^2} + g^* \frac{Ehd}{D_t}\frac{\partial u_3}{\partial x} = -\frac{m_s}{D_t}\frac{\partial^2 w}{\partial t^2}$$

$$\frac{\partial^2 u_3}{\partial x^2} - g^* u_3 = -g^* Y \frac{D_t}{Ehd}\frac{\partial w}{\partial x} \qquad (2.18)$$

where m_s is the total mass/area of the whole sandwich.

In the above equations two important parameters have been introduced as follows:

$$g^* = 2G_c^*/Ehh_c \qquad \text{(shear parameter)}$$
$$Y = Ehd^2/2D_t \qquad \text{(geometric parameter)} \qquad (2.19)$$

Mead and Markus [24] have eliminated u_3 from the pairs of (2.18) and have expressed the total motion in terms of the transverse displacement w as:

$$\frac{\partial^6 w}{\partial x^6} - g^*(1 + Y)\frac{\partial^4 w}{\partial x^4} + \frac{m_s}{D_t}\left(\frac{\partial^4 w}{\partial x^2 \partial t^2} - g^* \frac{\partial^2 w}{\partial t^2}\right) = 0 \qquad (2.20)$$

This is satisfied by

$$w(x) = A_n e^{k_n x} \qquad (2.21)$$

Substitution of it into (2.20) yields

$$k_n^6 - g^*(1 + Y)k_n^4 - \frac{m_s\omega^2}{D_t} k_n^2 + \frac{m_s g^*\omega^2}{D_t} = 0 \qquad (2.22)$$

This is a sixth-order equation for the wave number k_n of a three-layered sandwich beam and is bi-cubic in k_n^2. There are six distinctly different solutions for k_n in three positive/negative pairs.

Sandwich beams of the type being considered have three inter-related degrees of freedom on any cross-section. These are transverse displacement w, rotation $\partial w/\partial x$ and the mid-plane axial displacements u_1 $(= -u_3)$ of the face-plates. Therefore in this case the expressions for the 'Infinite-System Point Response Functions' and the 'Infinite-System Point Receptance Functions' have the same general form as those developed for Euler-Bernoulli beams but with $N = 3$.

Now introduce

$$w(x) = \sum_{n=1}^{6} A_n e^{k_n x}$$

$$u_3(x) = \sum_{n=1}^{6} B_n e^{k_n x} \qquad (2.23)$$

By substituting them into (2.18) and ensuring satisfaction of the equations for all x, it can be shown that

$$B_n = \left(-\frac{g^* d}{2(k_n^2 - g^*)} k_n\right) A_n \qquad (2.24)$$

The positive sign convention of the forces and moments on a whole sandwich beam section is shown in Figure 6. We can express the transverse displacement in the positive x region, due to a single point harmonic force F_o, as

$$w(x) = F_o \sum_{n=1}^{3} a_n \, e^{-k_n x} \qquad (2.25)$$

The boundary conditions to be satisfied by this for the determination of a_n's are

$$\frac{\partial w}{\partial x}\Big|_{x=0} = 0 \quad : \quad F_o \sum_{n=1}^{3} -k_n \, a_n = 0$$

$$u_3\Big|_{x=0} = 0 \quad : \quad F_o\left(\frac{g^*d}{2}\right) \sum_{n=1}^{3} \frac{k_n}{(k_n^2 - g^*)} \, a_n = 0$$

$$S_x\Big|_{x=0} = \frac{F_o}{2} \quad : \quad F_o \, D_t \sum_{n=1}^{3} - k_n^3 \, a_n = \frac{F_o}{2} \qquad (2.26)$$

Note that, the first two equations of (2.26) simplify the form of S_x given in equation (2.17) to that above.

Hence, the a_n's can be obtained from the following matrix equation:

$$\begin{bmatrix} -k_1 & -k_2 & -k_3 \\ \Gamma \dfrac{k_1}{k_1^2 - g^*} & \Gamma \dfrac{k_2}{k_2^2 - g^*} & \Gamma \dfrac{k_3}{k_3^2 - g^*} \\ -D_t k_1^3 & -D_t k_2^3 & -D_t k_3^3 \end{bmatrix} \begin{Bmatrix} a_1 \\ a_2 \\ a_3 \end{Bmatrix} = \begin{Bmatrix} 0 \\ 0 \\ \frac{1}{2} \end{Bmatrix} \qquad (2.27)$$

where $\Gamma = (g^*d)/2$.

Now consider the application of the single point moment, M_o, and express the w in the positive x region by

$$w(x) = M_o \sum_{n=1}^{3} b_n \, e^{-k_n x} \qquad (2.28)$$

The required coefficients, b_n's, can be achieved by satisfying the following boundary conditions:

$$M_{fp}\,|_{x=0} = -\frac{M_o}{2} \;:\; M_o\, D_t \sum_{n=1}^{3} k_n^2\, b_n = -\frac{M_o}{2}$$

$$w\,|_{x=0} = 0 \;:\; M_o \sum_{n=1}^{3} b_n = 0$$

$$M_{af}\,|_{x=0} = 0 \;:\; M_o\,(-\frac{Eg^*hd^2}{2}) \sum_{n=1}^{3} \frac{k_n^2}{(k_n^2 - g^*)}\, b_n = 0 \qquad (2.29)$$

Since there is no axial force created, the moment due to them is zero. Hence, it has been assumed that the whole of the applied moment is balanced by the total bending moment of the face-plates. The b_n's can be found from the following matrix equation:

$$\begin{bmatrix} D_t k_1^2 & D_t k_2^2 & D_t k_3^2 \\ 1 & 1 & 1 \\ Y\frac{k_1^2}{k_1^2 - g^*} & Y\frac{k_2^2}{k_2^2 - g^*} & Y\frac{k_3^2}{k_3^2 - g^*} \end{bmatrix} \begin{Bmatrix} b_1 \\ b_2 \\ b_3 \end{Bmatrix} = \begin{Bmatrix} -\frac{1}{2} \\ 0 \\ 0 \end{Bmatrix} \qquad (2.30)$$

where $Y = -(Eg^*hd^2)/2$.

Now $\theta = \partial w/\partial x$, and the rotational coefficients can be obtained as:

$$c_n = -k_n\, a_n \quad \text{and} \quad d_n = -k_n\, b_n \quad (n = 1,2,3) \qquad (2.31)$$

Due to the great complexity involved in algebra, analytical expressions for these coefficients will not be attempted, and the solutions will be achieved numerically.

2.3.2 Calculations and Discussion

This section first presents computed values of one pair of the wave numbers of three-layered sandwich beams with equal face-plates. It then studies the 'Infinite-System Point Receptance Functions' of the beams. The non-dimensional parameters used are as follows:

ND Wave Number : $k_n h_t$

ND Frequency* : $2\pi f((m_s h_t^4)/D_t)^{1/2}$

ND Transverse Point Receptance : $(w(0)/F_o)(D_t/h_t^3)$

ND Rotational Point Receptance : $(\theta(0)/M_o)(D_t/h_t)$

where $h_t = 2h + h_c$.

The sandwich structures analysed in this work have frequency and temperature dependent core shear moduli and core damping values. The actual characteristics of the viscoelastic material to be used [28] are shown in Figure 7. Calculations carried out were conducted for constant temperature. For simplicity, the shear modulus has been assumed to vary linearly with frequency on a logarithmic basis. G_c values corresponding to $T = 15^oC$ and $T = 18^oC$ have been determined from Figure 7 by appropriate interpolation. Unless otherwise stated, the temperature is assumed at 18^oC in this study. The variation of core loss factor with frequency has been ignored and it has been taken as constant. On the other hand, in order to offer comparative results, on certain figures constant G_c values have been assumed. These correspond to the values at the extreme ends of the relevant frequency ranges. The sandwich is then assumed to have constant G_c throughout the range.

Figure 8 shows the non-dimensional magnitudes for three non-dimensional wave numbers of the sandwich beam plotted against non-dimensional frequency. Core damping is zero. The beam has two purely real and one purely imaginary wave number. The magnitude of the imaginary part is asymptotic to the real values at the extreme frequencies. It has been found that at low frequencies, the beam behaves as a uniform beam having the properties of the whole sandwich section with a shear-rigid core. At high frequencies it acts as two separate beams each having the flexural stiffness of one face plate and the mass of half the sandwich [25].

---

*For a sandwich beam with aluminium face plates if $h = 0.87$ [mm], $h_c = 1.1$ [mm], $\rho_c = 1000$ [kg/m^3], the ND Frequency is $\simeq$ 4.4E-05 f.

Figures 9 and 10 show the non-dimensional magnitudes of the wave numbers when the core loss factor is taken as $\beta = 1$. Each wave number now has both real and imaginary parts and all of these are plotted on the same graph. In Figure 10 the core shear modulus is allowed to vary with frequency, starting from the fixed G_c value of Figure 9. With decreasing frequency, the imaginary part of the second wave number and the real part of the third wave number approach the same asymptote. This tendency can also be observed between the imaginary part of the third and the real part of the second. The first wave number exhibits distinct real and imaginary parts. At high frequencies the roles of the first and third wave numbers reverse. The third one now has distinct real and imaginary parts and the first one converges with the second in the above mentioned way. It can also be noticed that the high frequency asymptotic behaviour moves to higher frequencies with increasing G_c.

'Infinite-System Point Receptances' of the three-layered sandwich beams are shown in Figures 11 and 12 for zero core damping. Investigation of the non-dimensional magnitudes in Figure 11 shows that they behave in a similar manner to the uniform Euler-Bernoulli beams but with variable slopes. Increasing G_c results in lowering the magnitudes of both receptances. On the other hand the phase curves of Figure 12 show that when G_c is low and the frequency is high, the relative phases become asymptotic to the uniform beam value of $\pi/4$.

2.4 Conclusions

The dynamic behaviour of uniform, infinite, uninterrupted beams has been studied by considering the wave motion generated by the single-point external excitation. The parameters called 'Infinite-System Point Response Functions' have been defined and will be used in studying more complicated systems in later chapters. These are functions of wave numbers and of structural properties. They have been developed for Euler-Bernoulli beams and for three-layered sandwich beams having equal face-plates. It has been found that the

properties of the viscoelastic core greatly influence the wave numbers in the latter case and this change has reflected itself in dynamic response.

The investigation of 'Infinite-System Point Receptances' has revealed that even in the absence of damping they are complex quantities. The introduction of damping reduces their magnitudes. The phase between excitation and response is found to be constant with frequency for Euler-Bernoulli beams. In the case of sandwich beams, though this relation varies with frequency, it approaches a constant value at high frequencies. It has also been obtained that the inclusion of damping increases the phase difference of rotational receptances but reduces it for the transverse receptances for all the beams considered in this chapter.

For the beam structures analysed, it has been shown that the coefficients required in the functions are easy to calculate. This feature will be utilised in the study of more complicated structures, provided they are uniform. This task will be undertaken in the next chapter for plate structures.

CHAPTER 3

LINE RECEPTANCE FUNCTIONS OF INFINITE UNIFORM PLATES

3.1 Introduction

This chapter extends the concept of infinite system analysis to the harmonic vibrations of two-dimensional structures. The plates considered are of infinite length and finite width and are simply supported along the two opposite parallel edges which are distance L_y apart. The excitation acts along a line perpendicular to those edges and is assumed to be sinusoidally-varying across the finite width (*i.e.*, $F(y) = F_o \sin m\pi y/L_y$ per unit length and $M(y) = M_o \sin m\pi y/L_y$ per unit length). The response varies across the width in the same way and one can readily analyse the wave motion along the infinite direction. With this excitation and response the problem is effectively reduced from two dimensions to one.

Euler-Bernoulli plates and three-layered sandwich plates with equal face-plates will be considered here. All the plates are taken to be uniform, flat and rectangular. The assumptions previously made for three-layered sandwich beams in Chapter 2 are equally valid for the three-layered sandwich plates concerned. Sandwich plate wave numbers will be studied in detail.

This chapter serves to complement Chapter 2. Therefore many of the detailed points made in it are omitted and only the features, which are thought to be important for the better understanding of the plate theory will be outlined.

3.2 Euler-Bernoulli Plates

3.2.1 Theoretical Approach

Let the width of the plate be L_y. Under the given excitation free harmonic waves can propagate of the form

$$w(x,y) = w(x) \sin k_y y \tag{3.1}$$

where $k_y = m\pi/L_y$ and m defines the number of half-wavelengths across the width.

Equation (3.1) must satisfy the plate equation

$$D\nabla^4 w + \rho h \frac{\partial^2 w}{\partial t^2} = 0 \tag{3.2}$$

where $\nabla^4 = \partial^4/\partial x^4 + 2\partial^4/\partial x^2 \partial y^2 + \partial^4/\partial y^4$. The plate flexural rigidity $D = Eh^3/12(1 - \nu^2)$.

If one assumes

$$w(x) = A_n e^{k_n x} \tag{3.3}$$

then the wave numbers can easily be found as having the forms

$$\begin{aligned} k_1 &= \{k_y^2 + \omega(\rho h/D)^{1/2}\}^{1/2} \\ k_2 &= \{k_y^2 - \omega(\rho h/D)^{1/2}\}^{1/2} \\ k_3 &= -k_1 \\ k_4 &= -k_2 \end{aligned} \tag{3.4}$$

Suppose the infinite plate is excited by a line force distributed across the plate at $x = 0$, in the form

$$F(y) = F_o \sin k_y y \quad \text{per unit length} \tag{3.5}$$

The transverse displacement in the positive x region may be expressed in the form

$$w(x,y) = F_o \sum_{n=1}^{N} a_n e^{-k_n x} \sin k_y y \tag{3.6}$$

For Euler-Bernoulli plates $N = 2$, as the degrees of freedom of a cross-section are the transverse displacement and rotation but these are not independent of each other.

The rotational response due to distributed force $F(y)$ can be expressed for the positive x region as

$$\theta(x,y) = F_o \sum_{n=1}^{2} c_n e^{-k_n x} \sin k_y y \qquad (3.7)$$

When the infinite plate is excited by the moment distributed across the plate at $x = 0$, in the form of

$$M(y) = M_o \sin k_y y \quad \text{per unit length} \qquad (3.8)$$

the corresponding responses in the positive x region can be written as

$$w(x,y) = M_o \sum_{n=1}^{2} b_n e^{-k_n x} \sin k_y y$$

$$\theta(x,y) = M_o \sum_{n=1}^{2} d_n e^{-k_n x} \sin k_y y \qquad (3.9)$$

Equations (3.6), (3.7) and (3.9) define the 'Infinite-System Line Response Functions' of Euler-Bernoulli plates and in general they are complex quantities.

The determination of coefficients can be achieved by satisfying the relevant equilibrium and geometric boundary conditions at the line of application of the excitation. This has been done in [17] in detail so only their final forms will be given here.

$$\begin{aligned}
a_1 &= -1/2Dk_1(k_1^2 - k_2^2) & a_2 &= 1/2Dk_2(k_1^2 - k_2^2) \\
b_1 &= -1/2D(k_1^2 - k_2^2) & b_2 &= -b_1 \\
c_1 &= 1/2D(k_1^2 - k_2^2) & c_2 &= -c_1 \\
d_1 &= k_1/2D(k_1^2 - k_2^2) & d_2 &= -k_2/2D(k_1^2 - k_2^2)
\end{aligned} \qquad (3.10)$$

The 'Infinite-System Line Receptance Functions' of the Euler-Bernoulli plates are those functions determined by letting $F_o = 1$, $M_o = 1$ and by substituting $x = 0$ in 'Infinite-System Line Response Functions'.

3.2.2 Calculations and Discussion

The number of half-wavelengths across the width, m, greatly alters the dynamic characteristics of plate structures. Unless defined otherwise, m = 1 will be taken throughout this thesis. Now assume a rectangular plate with thickness 'h', density 'ρ' and excited at 'f' Hz. In the analysis of these plates the following non-dimensional quantities are used:

ND Frequency : $2\pi f((\rho h)h^4/D)^{1/2}$

ND Transverse Line Receptance : $(w(0,y)/F_0(y))(D/h^3)$

ND Rotational Line Receptance : $(\theta(0,y)/M_0(y))(D/h)$

Damping has been introduced through the complex flexural rigidity, in the form of $D(1 + i\eta)$. Poisson's ratio, ν, is taken to be 0.3.

The receptances have been computed for two different damping values (η = 0.0001 and η = 0.3) and their non-dimensional magnitudes are plotted against non-dimensional frequency in Figure 13. The 'resonance peak' in the transverse receptance curve occurs at the 'cut-on frequency' of the plate. At this frequency, the plate resonates in its fundamental simply-supported mode across the width. It therefore results in the high transverse displacement. It is also the frequency at which one of the purely real wave numbers of the undamped plate becomes zero before becoming purely imaginary. Below this frequency, wave motion with m = 1 cannot propagate without attenuation. Note that the rotational receptance curve shows a discontinuity at this frequency. This is a kink rather than a peak.

Inspection of the receptance phases in Figure 14 reveals that, in the case of very low damping and below the cut-on frequency, the excitations and the responses are in phase. This means that the 'Infinite-System Line Receptance Functions' of undamped Euler-Bernoulli plates are purely real below the cut-on frequency. At that frequency the transverse receptance undergoes a sudden phase change of $\pi/2$ and then approaches the value of $\pi/4$ at high frequencies. On the other hand the phase of the rotational receptance starts from 0 at the cut-on frequency and gradually increases to $\pi/4$.

Higher damping results in an increase of rotational phase, but lowers the transverse phase at high frequencies. At low frequencies the two damped plate receptances have the same phase.

3.3 Three-Layered Sandwich Plates

3.3.1 Theoretical Approach

The coordinate, displacement and stress system to be used in this section is given in Figure 15. When the two face-plates are equal, their mid-plane axial displacements, u and v, are also equal but opposite (*i.e.*, $u_3 = -u_1$, $v_3 = -v_1$). The differential equations of this plate has been derived by Mead [22] as,

$$\frac{E}{1-\nu^2}\frac{\partial^2 u_3}{\partial x^2} + \frac{E}{2(1+\nu)}\frac{\partial^2 u_3}{\partial y^2} - \frac{2G_c^*}{hh_c}u_3 + \frac{E}{2(1-\nu)}\frac{\partial^2 v_3}{\partial x \partial y} = -\frac{G_c^* d}{hh_c}\frac{\partial w}{\partial x} \tag{3.11}$$

$$\frac{E}{1-\nu^2}\frac{\partial^2 v_3}{\partial y^2} + \frac{E}{2(1+\nu)}\frac{\partial^2 v_3}{\partial x^2} - \frac{2G_c^*}{hh_c}v_3 + \frac{E}{2(1-\nu)}\frac{\partial^2 u_3}{\partial x \partial y} = -\frac{G_c^* d}{hh_c}\frac{\partial w}{\partial y} \tag{3.12}$$

$$D_t \nabla^4 w - \frac{G_c^* d}{h_c}\left[d\nabla^2 w - 2\left(\frac{\partial u_3}{\partial x} + \frac{\partial v_3}{\partial y}\right)\right] - \omega^2 m_s w = 0 \tag{3.13}$$

where w is the transverse displacement and u_3 and v_3 are the mid-plane axial displacements of the bottom face-plate in the x and y directions respectively. $\nabla^2 = \partial^2/\partial x^2 + \partial^2/\partial y^2$ and the parameters d, G_c^*, m_s are the same as those defined for sandwich beams. D_t is the total flexural rigidity of the two face-plates and $2(Eh^3/12(1-\nu^2))$.

Under the action of the distributed line force F(y) at x = 0, the displacements have the general form

$$w(x,y) = \sum_{n=1}^{6} A_n e^{k_n x} \sin k_y y$$

$$u_3(x,y) = \sum_{n=1}^{6} B_n e^{k_n x} \sin k_y y$$

$$v_3(x,y) = \sum_{n=1}^{6} C_n e^{k_n x} \cos k_y y \qquad (3.14)$$

where the k_n's are the wave numbers which are to be determined.

If the above equations are inserted into (3.11) and (3.12), long algebraic manipulation leads to

$$B_n = \left(- \frac{g^* d}{2(k_n^2 - k_y^2 - g^*)} k_n\right) A_n$$

$$C_n = \left(- \frac{g^* d}{2(k_n^2 - k_y^2 - g^*)} k_y\right) A_n \qquad (3.15)$$

where g^* is defined as the 'shear parameter' and is given by

$$g^* = \frac{2G_c^*(1 - \nu^2)}{Ehh_c} \qquad (3.16)$$

Substituting equations (3.15) to (3.14) one can express u_3 and v_3 in terms of w. Further substitution of these back into (3.13) and further long manipulation leads to the equation for the wave number k_n in the form:

$$(k_n^2 - k_y^2)^3 - g^*(1 + Y)(k_n^2 - k_y^2)^2 - (m_s\omega^2/D_t)(k_n^2 - k_y^2 - g^*) = 0 \qquad (3.17)$$

In this, Y is the 'geometric parameter' and is defined by

$$Y = 3\left(1 + \frac{h_c}{h}\right)^2 \qquad (3.18)$$

The bi-cubic form of equation (3.17) shows the existence of six wave numbers in the form of positive and negative-going pairs.

Since the three-layered sandwich plate cross-section has the same three degrees of freedom as the sandwich beams of Chapter 2, its 'Infinite-System Line Response Functions' and 'Infinite-System Line Receptance Functions' retain the same form of the uniform plate functions with N = 3. Due to the great complexity involved, the determination of the relevant coefficients is presented in Appendix A.

3.3.2 Calculations and Discussion

A three-layered sandwich plate is considered with equal face-plate thicknesses 'h' and core thickness 'h_c'. The face-plates are of Young's modulus E. For computational purposes, it was assumed that the temperature is constant at T = 18°C and the core damping β is included through the core shear modulus as $G_c^* = G_c(1 + i\beta)$. The non- dimensional parametes are defined as:

ND Wave Number : $k_n h_t$

ND Frequency : $2\pi f((m_s h_t^4)/D_t)^{1/2}$

ND Transverse Line Receptance : $(w(0,y)/F_o(y))(D_t/h_t^3)$

ND Rotational Line Receptance : $(\theta(0,y)/M_o(y))(D_t/h_t)$

where $h_t = 2h + h_c$.

The wave number/frequency relationship of the sandwich plate has been investigated, taking into account the frequency dependent values of the core shear modulus. Figure 16 shows the results when there is no damping in the viscoelastic core. Below the cut-on frquency the sandwich plate has three purely real wave numbers. With decreasing frequency two of them are asymptotic to one another, whereas the third one is significantly higher in magnitude. At the cut-on frequency one of the two lower magnitude wave numbers becomes zero while the others remain real. At higher frequencies the zero wave number becomes imaginary and shows a steep increase with frequency, crossing the lower real and approaching the value of the higher real at high frequencies.

The effect of core damping on wave numbers is shown in Figure 17 by taking β =1. With decreasing frequency the real parts and the imaginary parts of the second and third wave numbers converge, but the first one has different real and imaginary parts. At high frequencies the real part of the first wave number and the imaginary part of the third converge. The second wave number is now different. The same holds for the imaginary part of the first and the real part of the third wave numbers. The frequency characterised by the crossing of the real and the imaginary parts of the third wave number is the cut-on frequency of the sandwich plate.

Figure 18 shows the effect of the number of excitation half-wavelengths, m, across the plate width, by taking m = 2. Comparing this with Figure 17 clearly shows that the cut-on frequency is now different. At low frequencies the real parts of the second and third wave numbers have increased while their imaginary parts have decreased. In the frequency region considered, at high frequencies changing 'm' does not affect the wave number magnitudes.

Infinite-System Line Receptances of the sandwich plates are shown in four figures. Figures 19 and 20 represent the magnitude and phase characteristics for the plate with very low core damping (β = 0.0001) and different core shear moduli. Again as for Euler-Bernoulli plates, the transverse receptances have a peak at the cut-on frequency and the rotational receptances have a discontinuity in Figure 19. Increasing G_c reduces the off-peak magnitudes of both receptances. The phase relation in Figure 20 indicates that with zero damping and below the cut-on frequencies all the receptances are purely real. At the cut-on frequencies a sudden phase change of $\pi/2$ occurs as observed in the Euler-Bernoulli plates. At higher frequencies the sandwich plate with low constant G_c value gives phase characteristics similar to those of an Euler-Bernoulli plate.

Figures 21 and 22 show the effect of increasing core damping when the same, frequency dependent, G_c is used. Non-dimensional magnitudes of Figure 21 indicate that high damping reduces the magnitudes of both receptances. Figure 22 represents the phases and reveals that increasing the damping increases the phase of the rotational

receptance but reduces the phase of the transverse receptance at high frequencies. Another point worthy of mention is that, when the core is damped the excitation and response are never in phase. Also in contrast to the Euler-Bernoulli plates, the phase of receptances of damped sandwich plates are not equal at low frequencies.

3.4 Conclusions

This chapter has focussed on the dynamic response of uniform, flat and rectangular plates of finite width, infinite length, uninterrupted and simply-supported along the two opposite parallel edges. They are subjected to harmonic line excitations which are sinusoidally varying across the width. The generated responses have the same width-wise variation. The relations between response and excitation have been obtained and lead to the concept of the 'Infinite-System Line Receptance Functions'. These receptance functions have been computed for Euler-Bernoulli and three-layered sandwich plates having equal face plates.

Propagating wave motion in the undamped plate cannot occur below particular cut-on frequencies. It has been observed that at these frequencies the line receptance functions have large peak values or display discontinuities. Their magnitudes always fall off above those particular frequencies. In the absence of damping, the phase angle between transverse response and excitation undergoes a sudden change of $\pi/2$ at those frequencies. Increasing the number of half-wavelengths of excitation across the width results in higher cut-on frequencies.

The behaviour of the wave numbers of the three-layered sandwich plates has also been investigated. It has emerged that in addition to the frequency the core properties G_c and β are the principal factors which influence the variation of wave numbers. These changes are reflected in the behaviour of receptance functions. Increasing G_c and β have lowered the magnitude of the response.

SECTION 2: DYNAMIC BEHAVIOUR OF FINITE STRUCTURES

CHAPTER 4

FORCED VIBRATIONS OF UNIFORM FINITE EULER-BERNOULLI BEAMS

4.1 Introduction

The dynamic analysis of finite structures is always more complex than the study of infinite structures, owing to the wave reflections which occur at the structural boundaries and discontinuities.

The dynamic characteristics of single bay structures have long been studied by a variety of methods. They include the classical receptance theory, direct solution of the differential equation of motion, and energy methods. Gorman developed a theory for the dynamic analysis of multi-bay beams [1] (albeit by considering the free vibrations) but when the number of bays get large (≥ 3 in his case) he assumed all the intermediate supports as being simple. Clearly this condition is unrealistic in practice. Most supports, if not all of them, provide constraints which further complicate the task that an engineer faces.

One of the aims of this thesis is to develop an easy-to-apply yet accurate, analytical method for the forced dynamic analysis of multi-bay finite structures. An approach is sought which relaxes the previously accepted constraints and reduces the otherwise unwieldy algebraic manipulations.

When a structure is harmonically excited at any point, the source sends out N waves in each direction. The waves are reflected at boundaries and discontinuities. If a uniform Euler-Bernoulli beam is harmonically excited at a single point, two waves are sent out in each direction (*i.e.*, one propagating and one near-field wave). These are reflected from each end and travel back to the other end of the beam. The total motion in the beam is therefore the sum of the motion generated by the known applied force as if it were acting on an infinite beam, together with the motion due to the four unknown reflected waves. The characteristic motion of the force on the infinite beam is related to the 'Infinite-System Point Response

Functions' of Chapter 2. If the beam has many supports each intermediate support applies a reaction force and/or moment to the structure depending on the nature of the support. The motions generated by these unknown reactions have the same form as those considered when studying the corresponding infinite-system functions. There are still four waves reflected from the extreme ends of the beam. Hence the total unknowns in this case are the magnitudes of the reactions at the intermediate supports and the magnitudes of the four reflected waves.

Within the context of this thesis, the reflected waves are called 'free waves', whereas the motion generated by the excitations is referred to as 'forced waves'. The relationship between them is found by satisfying the boundary conditions at the extreme ends and, if any, at the intermediate support locations. In this way a matrix equation is obtained for the unknowns and is solved numerically. Once the unknowns are determined the response at any point is easily determined.

This chapter develops the proposed theory for uniform Euler-Bernoulli beams. In order to offer clarity and simplicity, a single bay beam is first studied with a variety of possible boundary conditions. After this the effects of intermediate supports are investigated. The general equations of motion are then derived for an N_b bay beam on simple supports at irregular support spacing. The necessary modifications for other types of support are illustrated. The capability of the method for dealing with multi and combined forcing conditions is highlighted. The determination of resonant mode shapes is explained and some are presented, together with the relevant frequency response curves. The usually-overlooked problem of the effects of coupling between deflection and rotation at the supports is also considered. Both damped and undamped analyses are undertaken by introducing damping through the complex flexural rigidity as $EI(1 + i\eta)$. The beams are assumed to have unit width.

4.2 Response of a Single Bay Beam Under a Single Point Harmonic Load

Consider the finite beam of Figure 23(a) which is excited by the harmonic force F_o at $x = x_o$. The forced waves generated by the force together with the free waves reflected from the ends constitute the total motion. The transverse displacement at any point x_r ($0 \leq x_r \leq L$) is then given by

$$w(x_r,t) = \left\{ \sum_{n=1}^{4} A_n e^{k_n x_r} + F_o \sum_{n=1}^{2} a_n e^{-k_n|x_o-x_r|} \right\} e^{i\omega t} \qquad (4.1a)$$

Now consider the finite beam of Figure 23(b) which is excited by the harmonic moment M_o at x_o. The transverse displacement in this case is given by

$$w(x_r,t) = \left\{ \sum_{n=1}^{4} A_n e^{k_n x_r} + (jm)\, M_o \sum_{n=1}^{2} b_n e^{-k_n|x_o-x_r|} \right\} e^{i\omega t} \qquad (4.1b)$$

where $jm = -1$ if $x_o > x_r$, $jm = 1$ if $x_o < x_r$.

There are four unknown A_n's in these equations and hence four equations are required in order to find them. These equations are derived from the boundary conditions at $x = 0$ and $x = L$. Before these are considered it is helpful to list the expressions for the shear force and bending moment in the beam due to F_o and M_o to the right and left of F_o and M_o. They are:

$$M(x) = EIw''(x) = EI\left(F_o \sum_{n=1}^{2} k_n^2\, a_n\, e^{-k_n x}\right)$$

$$M_{right}(x) = EIw''_{right}(x) = EI\left(M_o \sum_{n=1}^{2} k_n^2\, b_n\, e^{-k_n x}\right)$$

$$M_{left}(x) = EIw''_{left}(x) = -EI\left(M_o \sum_{n=1}^{2} k_n^2\, b_n\, e^{-k_n x}\right)$$

$$S_{right}(x) = EIw'''_{right}(x) = EI\left(F_o \sum_{n=1}^{2} -k_n^3\, a_n\, e^{-k_n x}\right)$$

$$S_{left}(x) = EIw'''_{left}(x) = -EI(F_o \sum_{n=1}^{2} -k_n^3 a_n e^{-k_n x})$$

$$S(x) = EIw'''(x) = EI(M_o \sum_{n=1}^{2} -k_n^3 b_n e^{-k_n x}) \qquad (4.2)$$

where 'x' is the distance measured from the point of application of the excitation.

A variety of possible end boundary conditions will now be considered. They will be outlined by assuming a single harmonic force excitation. Any modifications necessary for moment excitation can be carried out by considering equation (4.2) and the infinite-system point response functions of Section 2.2.

4.2.1 Simply-Supported Ends

At a simple support $w = 0$ and Moment $= 0$. Hence

$$w(0) = 0 : \sum_{n=1}^{4} A_n e^{k_n(0)} + F_o \sum_{n=1}^{2} a_n e^{-k_n|x_o-0|} = 0$$

or

$$\sum_{n=1}^{4} A_n = -F_o \sum_{n=1}^{2} a_n e^{-k_n x_o} \qquad (4.3)$$

$$M(0) = 0 : w''(0) = 0 : \sum_{n=1}^{4} k_n^2 A_n e^{k_n(0)} + F_o \sum_{n=1}^{2} k_n^2 a_n e^{-k_n|x_o-0|} = 0$$

so

$$\sum_{n=1}^{4} k_n^2 A_n = -F_o \sum_{n=1}^{2} k_n^2 a_n e^{-k_n x_o} \qquad (4.4)$$

Likewise $w(L) = 0$ leads to

$$\sum_{n=1}^{4} A_n e^{k_n L} = -F_o \sum_{n=1}^{2} a_n e^{-k_n|L-x_o|} \qquad (4.5)$$

and $M(L) = 0$ results in

$$\sum_{n=1}^{4} k_n^2 A_n e^{k_n L} = -F_o \sum_{n=1}^{2} k_n^2 a_n e^{-k_n |L-x_o|} \qquad (4.6)$$

Equations (4.3) to (4.6) constitute the four simultaneous equations required to find the A_n's. In matrix form they become

$$\begin{bmatrix} 1 & 1 & 1 & 1 \\ k^2 & -k^2 & k^2 & -k^2 \\ e^{kL} & e^{ikL} & e^{-kL} & e^{-ikL} \\ k^2 e^{kL} & -k^2 e^{ikL} & k^2 e^{-kL} & -k^2 e^{-ikL} \end{bmatrix} \begin{Bmatrix} A_1 \\ A_2 \\ A_3 \\ A_4 \end{Bmatrix} = -F_o \begin{Bmatrix} \sum_{n=1}^{2} a_n e^{-k_n x_o} \\ \sum_{n=1}^{2} k_n^2 a_n e^{-k_n x_o} \\ \sum_{n=1}^{2} a_n e^{-k_n (L-x_o)} \\ \sum_{n=1}^{2} k_n^2 a_n e^{-k_n (L-x_o)} \end{Bmatrix} \qquad (4.7)$$

In this and all the relevant cases of this chapter, use has been made of the relations $k_1 = k$, $k_2 = ik$, $k_3 = -k$, $k_4 = -ik$. Equation (4.7) will be used in Appendix B to formally prove that the response of undamped structures is purely real.

4.2.2 Clamped Ends

These beams have zero displacement and zero slope at each end. Hence

$$w(0) = 0, \quad w'(0) = 0, \quad w(L) = 0, \quad w'(L) = 0 \qquad (4.8)$$

These conditions imposed upon equation (4.1a) lead to the equation

$$\begin{bmatrix} 1 & 1 & 1 & 1 \\ k & ik & -k & -ik \\ e^{kL} & e^{ikL} & e^{-kL} & e^{-ikL} \\ ke^{kL} & ike^{ikL} & -ke^{-kL} & -ike^{-ikL} \end{bmatrix} \begin{Bmatrix} A_1 \\ A_2 \\ A_3 \\ A_4 \end{Bmatrix} = -F_o \begin{Bmatrix} \sum_{n=1}^{2} a_n e^{-k_n x_o} \\ -\sum_{n=1}^{2} -k_n a_n e^{-k_n x_o} \\ \sum_{n=1}^{2} a_n e^{-k_n (L-x_o)} \\ \sum_{n=1}^{2} -k_n a_n e^{-k_n (L-x_o)} \end{Bmatrix} \tag{4.9}$$

4.2.3 Free Ends

In this case, the bending moment and shear force at each end must vanish. Therefore,

$$w''(0) = 0, \quad w'''(0) = 0, \quad w''(L) = 0, \quad w'''(0) = 0 \tag{4.10}$$

If equation (4.1a) is set to satisfy these conditions, one can obtain

$$\begin{bmatrix} k^2 & -k^2 & k^2 & -k^2 \\ k^3 & -ik^3 & -k^3 & ik^3 \\ k^2e^{kL} & -k^2e^{ikL} & k^2e^{-kL} & -k^2e^{-ikL} \\ k^3e^{kL} & -ik^3e^{ikL} & -k^3e^{-kL} & ik^3e^{-ikL} \end{bmatrix} \begin{Bmatrix} A_1 \\ A_2 \\ A_3 \\ A_4 \end{Bmatrix} = -F_o \begin{Bmatrix} \sum_{n=1}^{2} k_n^2 a_n e^{-k_n x_o} \\ -\sum_{n=1}^{2} -k_n^3 a_n e^{-k_n x_o} \\ \sum_{n=1}^{2} k_n^2 a_n e^{-k_n (L-x_o)} \\ \sum_{n=1}^{2} -k_n^3 a_n e^{-k_n (L-x_o)} \end{Bmatrix} \tag{4.11}$$

4.2.4 Linear Transverse Spring at Each End

Let the spring resist the transverse displacement w by the force $-K_t w$ as shown in Figure 24(a). The spring force exerts a shear force on the end of the beam but rotation is unconstrained. Therefore

$$w''(0) = 0, \quad w''(L) = 0 \tag{4.12}$$

and also

$$\begin{aligned} EI\, w'''(0) &= -K_t\, w(0) \\ EI\, w'''(L) &= K_t\, w(L) \end{aligned} \tag{4.13}$$

These four conditions imposed upon equation (4.1a) lead to

$$\begin{bmatrix} k^2 & -k^2 & k^2 & -k^2 \\ EIk^3+K_t & -iEIk^3+K_t & -EIk^3+K_t & iEIk^3+K_t \\ k^2e^{kL} & -k^2e^{ikL} & k^2e^{-kL} & -k^2e^{-ikL} \\ (EIk^3-K_t)e^{kL} & (-iEIk^3-K_t)e^{ikL} & (-EIk^3-K_t)e^{-kL} & (iEIk^3-K_t)e^{-ikL} \end{bmatrix} \begin{Bmatrix} A_1 \\ A_2 \\ A_3 \\ A_4 \end{Bmatrix}$$

$$= -F_o \begin{Bmatrix} \sum_{n=1}^{2} k_n^2\, a_n\, e^{-k_n x_o} \\ \left(-EI \sum_{n=1}^{2} -k_n^3\, a_n\, e^{-k_n x_o} + K_t \sum_{n=1}^{2} a_n\, e^{-k_n x_o}\right) \\ \sum_{n=1}^{2} k_n^2\, a_n\, e^{-k_n (L-x_o)} \\ \left(EI \sum_{n=1}^{2} -k_n^3\, a_n\, e^{-k_n (L-x_o)} - K_t \sum_{n=1}^{2} a_n\, e^{-k_n (L-x_o)}\right) \end{Bmatrix} \tag{4.14}$$

4.2.5 Rotational Spring and Simple Support at Each End

Consider Figure 24(b). The simple supports prevent end transverse displacements. So $w(0) = w(L) = 0$. The rotational spring resists

rotation w' by the moment K_r per unit rotation and exert bending moments on the beam given by

$$EI\, w''(0) = K_r\, w'(0)$$
$$EI\, w''(L) = -K_r\, w'(L) \qquad (4.15)$$

Application of these four boundary conditions to equation (4.1a) leads to

$$\begin{bmatrix} 1 & 1 & 1 & 1 \\ EIk^2-K_rk & -EIk^2-iK_rk & EIk^2+K_rk & -EIk^2+iK_rk \\ e^{kL} & e^{ikL} & e^{-kL} & e^{-ikL} \\ (EIk^2+K_rk)e^{kL} & (-EIk^2+iK_rk)e^{ikL} & (EIk^2-K_rk)e^{-kL} & (-EIk^2-iK_rk)e^{-ikL} \end{bmatrix} \begin{Bmatrix} A_1 \\ A_2 \\ A_3 \\ A_4 \end{Bmatrix}$$

$$= -F_o \begin{Bmatrix} \sum_{n=1}^{2} a_n e^{-k_n x_o} \\ (EI \sum_{n=1}^{2} k_n^2 a_n e^{-k_n x_o} - K_r \sum_{n=1}^{2} -(-k_n) a_n e^{-k_n x_o}) \\ \sum_{n=1}^{2} a_n e^{-k_n (L-x_o)} \\ (EI \sum_{n=1}^{2} k_n^2 a_n e^{-k_n (L-x_o)} + K_r \sum_{n=1}^{2} -k_n a_n e^{-k_n (L-x_o)}) \end{Bmatrix} \qquad (4.16)$$

4.2.6 Point Mass at Each End

Now consider Figure 24(c). The mass M which has no rotational inertia is added at an otherwise free end. Therefore $M(0) = M(L) = 0$. The inertia force on the mass is $-\omega^2 Mw$ and this creates a shear force on the ends of the beam. We see

$$EI\, w'''(0) = M\omega^2\, w(0)$$
$$EI\, w'''(L) = -M\omega^2\, w(L) \qquad (4.17)$$

These four boundary conditions lead to

$$\begin{bmatrix} k^2 & -k^2 & k^2 & -k^2 \\ EIk^3-M\omega^2 & -iEIk^3-M\omega^2 & -EIk^3-M\omega^2 & iEIk^3-M\omega^2 \\ k^2e^{kL} & -k^2e^{ikL} & k^2e^{-kL} & -k^2e^{-ikL} \\ (EIk^3+M\omega^2)e^{kL} & (-iEIk^3+M\omega^2)e^{ikL} & (-EIk^3+M\omega^2)e^{-kL} & (iEIk^3+M\omega^2)e^{-ikL} \end{bmatrix} \begin{Bmatrix} A_1 \\ A_2 \\ A_3 \\ A_4 \end{Bmatrix}$$

$$= -F_o \begin{Bmatrix} \sum_{n=1}^{2} k_n^2 a_n e^{-k_n x_o} \\ (-EI \sum_{n=1}^{2} -k_n^3 a_n e^{-k_n x_o} - M\omega^2 \sum_{n=1}^{2} a_n e^{-k_n x_o}) \\ \sum_{n=1}^{2} k_n^2 a_n e^{-k_n(L-x_o)} \\ (EI \sum_{n=1}^{2} -k_n^3 a_n e^{-k_n(L-x_o)} + M\omega^2 \sum_{n=1}^{2} a_n e^{-k_n(L-x_o)}) \end{Bmatrix} \qquad (4.18)$$

4.2.7 Determination of Magnitudes of Free Waves and Resonant Modes

Any one of the complex matrix equations (4.7), (4.9), (4.11), (4.14), (4.16) and (4.18) can be solved for the A_n's in terms of F_o. Once the A_n's are known for a given frequency, the mode of vibration $w(x_r)$ can be calculated for any x_r using equation (4.1a). The same equation can also be used to determine the frequency response.

4.3 Response of Multi-Bay Beams

4.3.1 Simply-Supported Multi-Bay Beam

Consider an N_b bay finite uniform Euler-Bernoulli beam represented by Figure 25. Since the intermediate simple supports

supply unknown transverse forces, their magnitudes need to be determined. This is achieved by satisfying the boundary conditions at each of the $N_b - 1$ intermediate supports. As an illustrative example, consider the support at $x = x_3$. The displacement at this point, due to all the intermediate support reactions R_j ($j = 1, N_b - 1$), the external force F_o and the waves reflected from the ends, is

$$w(x_3) = \sum_{n=1}^{4} A_n e^{k_n x_3} + F_o \sum_{n=1}^{2} a_n e^{-k_n |x_o - x_3|} + \sum_{j=1}^{N_b-1} R_j \sum_{n=1}^{2} a_n e^{-k_n |x_j - x_3|} \qquad (4.19)$$

Similar expressions can be written for the other $N_b - 2$ intermediate supports. Since these supports do not deflect, the corresponding equations should be set to zero. This yields $N_b - 1$ equations. Another four equations can be written down to express the boundary conditions at the extreme ends of the simply-supported beam. They are the modified versions of equations (4.3) to (4.6) which now also include the effects of the intermediate supports. In this way equation (4.3) can be rewritten as:

$$w(0) = 0 : \sum_{n=1}^{4} A_n + \sum_{j=1}^{N_b-1} R_j \sum_{n=1}^{2} a_n e^{-k_n x_j} = -F_o \sum_{n=1}^{2} a_n e^{-k_n x_o} \qquad (4.20)$$

Altogether we now have $N_b + 3$ equations for $N_b + 3$ unknowns ($N_b - 1$ R_j's and 4 A_n's). The R_j's and A_n's are found by numerical solution of the final matrix equation.

The transverse displacement at x_r on the beam is now found from

$$w(x_r) = \sum_{n=1}^{4} A_n e^{k_n x_r} + F_o \sum_{n=1}^{2} a_n e^{-k_n |x_o - x_r|} + \sum_{j=1}^{N_b-1} R_j \sum_{n=1}^{2} a_n e^{-k_n |x_j - x_r|} \qquad (4.21)$$

4.3.2 Beams with Different Intermediate Conditions

A number of different types of intermediate supports are now considered. Also analysed is the case where point masses are attached to a simply-supported beam.

4.3.2.1 The Linear Transverse Spring

Suppose that the support at x_j is elastic, requiring a transverse force of K_t to produce unit $w(x_j)$. When the beam moves vertically by $w(x_j)$ the reaction force from the spring is $R_j = -K_t w(x_j)$. The displacement of the beam at x_j is given by equation (4.19) with x_3 set to x_j. Substituting equation (4.19) into this reaction force equation and rearranging, one obtains the modified boundary condition, for the j'th intermediate support

$$\sum_{n=1}^{4} A_n e^{k_n x_j} + \sum_{\substack{\ell=1 \\ \ell \neq j}}^{N_b-1} R_\ell \sum_{n=1}^{2} a_n e^{-k_n|x_\ell - x_j|}$$

$$+ R_j\left(\sum_{n=1}^{2} a_n e^{-k_n|x_j - x_j|} + \frac{1}{K_t}\right) = -F_o \sum_{n=1}^{2} a_n e^{-k_n|x_o - x_j|} \qquad (4.22)$$

Each of the remaining $N_b - 2$ intermediate supports yields an equation of similar form. Allowance is easily made for each support having a different stiffness. Four more boundary conditions relating to the ends at $x = 0$ and $x = L$ can be written down (*e.g.*, equations (4.4), (4.6), (4.13) but during setting-up of their modified versions, the contributions of $N_b - 1$ intermediate supports should also be considered) so that a matrix equation of order $N_b + 3$ can be set up for the $N_b + 3$ unknowns. This can be solved numerically to yield the unknown R_j's and A_n's. Once the unknowns are found, the required response can be found again from equation (4.21).

4.3.2.2 The Point Mass

Suppose that a simply-supported uniform Euler-Bernoulli beam of length L has $N_b - 1$ masses attached to it at irregular intervals. Further assume that these masses, M's, have no rotational inertias. When the beam vibrates under the influence of F_o these masses apply vertical forces on the beam given by $R_j = M\omega^2 w(x_j)$ at points of attachment x_j's. Substituting the beam transverse displacement $w(x_j)$ from equation (4.19) by setting x_s to x_j in it, to the above equation and rearranging, the modified boundary condition for the j'th mass location can be found to be

$$\sum_{n=1}^{4} A_n e^{k_n x_j} + \sum_{\substack{\ell=1 \\ \ell \neq j}}^{N_b-1} R_\ell \sum_{n=1}^{2} a_n e^{-k_n|x_\ell - x_j|}$$

$$+ R_j\left(\sum_{n=1}^{2} a_n e^{-k_n|x_j - x_j|} - \frac{1}{M\omega^2} \right) = -F_o \sum_{n=1}^{2} a_n e^{-k_n|x_o - x_j|} \qquad (4.23)$$

Similar equations can be written down for the other $N_b - 2$ mass locations. If the masses are different their appropriate values should be used in corresponding equations. Since the ends are simply-supported the required boundary conditions for the determination of free waves are the modified versions of equations (4.3) to (4.6). Their new forms must include the effects of the reaction forces due to masses (*e.g.*, equation (4.20)). Altogether we again have $N_b + 3$ equations and $N_b + 3$ unknowns. The unknowns A_n's and R_j's can be found by the numerical solution of the final matrix equation and equation (4.21) gives the transverse displacement at any x_r on the beam.

4.3.2.3 Combined Effects of the Rotational and Transverse Springs

Now let there be also a rotational spring K_r at the support in addition to the linear spring K_t. K_r is its rotational stiffness

and is the moment required to produce a unit $w'(x_j)$. This now introduces an additional unknown reaction applied on the beam given by $M_j = -K_r\, w'(x_j)$. M_j must satisfy the rotational boundary condition at x_j. Suppose each support has a rotational spring. Each reaction moment M_j and each reaction force R_j generates a displacement and rotation at the support x_j, and these are given by the infinite-system point response functions. Summing these and adding the contributions from F_o and the four free waves from the ends enables an expression for $w'(x_j)$ to be obtained. Putting $-M_j/K_r = w'(x_j)$ (from above) and rearranging, one obtains

$$\sum_{n=1}^{4} k_n A_n e^{k_n x_j} + (jk) \sum_{\substack{\ell=1 \\ \ell\neq j}}^{N_b-1} R_\ell \sum_{n=1}^{2} c_n e^{-k_n|x_\ell - x_j|}$$

$$+ \sum_{\substack{mn=1 \\ mn\neq j}}^{N_b-1} M_{mn} \sum_{n=1}^{2} d_n e^{-k_n|x_{mn}-x_j|} + R_j \sum_{n=1}^{2} c_n e^{-k_n|x_j-x_j|}$$

$$+ M_j\left(\sum_{n=1}^{2} d_n e^{-k_n|x_j-x_j|} + \frac{1}{K_r} \right) = -(jj)F_o \sum_{n=1}^{2} c_n e^{-k_n|x_o-x_j|} \qquad (4.24)$$

where $jj = -1$ if $x_o > x_j$, $jj = 1$ if $x_o < x_j$

$jk = -1$ if $x_\ell > x_j$, $jk = 1$ if $x_\ell < x_j$

It must be remembered that, if the supports have different K_r's, their appropriate values should be utilized in setting-up of equation (4.24).

The sign of R_j is actually irrelevant in this rotational equation as, in the absence of coupling, a transverse force produces no rotation at its point of application. This can also be seen from equation (2.14). However R_j is included in equation (4.24) to preserve the form which involves all the unknowns. By pursuing a similar argument, it can be concluded that in the corresponding displacement equation M_j makes no contribution to the displacement boundary conditions at support x_j. The condition at that support can be shown to be

$$\sum_{n=1}^{4} A_n e^{k_n x_j} + \sum_{\substack{\ell=1 \\ \ell \neq j}}^{N_b-1} R_\ell \sum_{n=1}^{2} a_n e^{-k_n|x_\ell - x_j|}$$

$$+ (jn) \sum_{\substack{mn=1 \\ mn \neq j}}^{N_b-1} M_{mn} \sum_{n=1}^{2} b_n e^{-k_n|x_{mn} - x_j|} + M_j \sum_{n=1}^{2} b_n e^{-k_n|x_j - x_j|}$$

$$+ R_j\left(\sum_{n=1}^{2} a_n e^{-k_n|x_j - x_j|} + \frac{1}{K_t} \right) = -F_o \sum_{n=1}^{2} a_n e^{-k_n|x_o - x_j|} \qquad (4.25)$$

where $jn = -1$ if $x_{mn} > x_j$, $jn = 1$ if $x_{mn} < x_j$.

By considering equation (2.15) it can be seen that the coefficient of M_j in this must be zero.

This general case leads to a matrix equation having the order $2(N_b + 1)$. Satisfaction of the transverse and rotational equilibrium and compatibility conditions at the $(N_b - 1)$ intermediate supports leads to $2(N_b - 1)$ equations involving $2(N_b - 1)$ unknowns. The determination of four free-waves requires the appropriate applications of the relevant boundary conditions of Section 4.2. The $2(N_b + 1)$ equations can numerically be solved for the A_n's, R_j's and M_j's. The transverse displacement at any x_r can then be found as:

$$w(x_r) = \sum_{n=1}^{4} A_n e^{k_n x_r} + F_o \sum_{n=1}^{2} a_n e^{-k_n|x_o - x_r|}$$

$$+ \sum_{j=1}^{N_b-1} R_j \sum_{n=1}^{2} a_n e^{-k_n|x_j - x_r|}$$

$$+ (jk) \sum_{j=1}^{N_b-1} M_j \sum_{n=1}^{2} b_n e^{-k_n|x_j - x_r|} \qquad (4.26)$$

where $jk = -1$ if $x_j > x_r$ and $jk = 1$ if $x_j < x_r$.

The rotational response $w'(x_r)$ can easily be found from equation (4.26), by replacing A_n's with $k_n A_n$'s, a_n's with c_n's, b_n's with

d_n's and by considering the appropriate signs of the relevant functions.

4.3.2.4 Effects of the Coupled Motions of the General Support

Now, assume that the support at x_j is asymmetric. In this case the force R_{x_j} acting on it creates rotation $w'(x_j)$ and the moment M_{x_j} induces the transverse displacement $w(x_j)$. This support may be characterized by a symmetric linear stiffness matrix (static or dynamic), through the equation.

$$\begin{Bmatrix} R_{x_j} \\ M_{x_j} \end{Bmatrix} = \begin{bmatrix} K_t & K_c \\ K_c & K_r \end{bmatrix} \begin{Bmatrix} w(x_j) \\ w'(x_j) \end{Bmatrix} \tag{4.27}$$

Rearranging this, one can find that

$$w(x_j) = \frac{K_r}{K_{tot}^2} R_{x_j} - \frac{K_c}{K_{tot}^2} M_{x_j}$$

$$w'(x_j) = -\frac{K_c}{K_{tot}^2} R_{x_j} + \frac{K_t}{K_{tot}^2} M_{x_j} \tag{4.28}$$

where $K_{tot}^2 = K_t K_r - K_c^2$.

Now, because of the equilibrium of the forces and moments at x_j, $R_{x_j} = -R_j$ and $M_{x_j} = -M_j$. Put the expressions for $w(x_j)$ and $w'(x_j)$ in terms of F_o, the A_n's, R_j's and M_j's into the modified (4.28). They yield the two boundary condition equations corresponding to support x_j. These have the same forms as equations (4.24) and (4.25) but the coefficients corresponding to R_j and M_j should be changed in equation (4.24) to

$$R_j\left(\sum_{n=1}^{2} c_n e^{-k_n|x_j-x_j|} - \frac{K_c}{K_{tot}^2}\right)$$

$$M_j\left(\sum_{n=1}^{2} d_n e^{-k_n|x_j-x_j|} + \frac{K_t}{K_{tot}^2}\right) \tag{4.29}$$

and in equation (4.25)

$$R_j\left(\sum_{n=1}^{2} a_n e^{-k_n|x_j-x_j|} + \frac{K_r}{K_{tot}^2}\right)$$

$$M_j\left(\sum_{n=1}^{2} b_n e^{-k_n|x_j-x_j|} - \frac{K_c}{K_{tot}^2}\right) \qquad (4.30)$$

As can be seen, the motion coupling does not introduce any extra unknowns.

4.4 Response of Beams under Multi-Point Excitation

Consider once more the single bay beam of Figure 23(a). Suppose a moment of magnitude M_o also acts at x_1. If the ends are simply-supported the resultant matrix equation for the A_n's can be shown to be:

$$\begin{bmatrix} 1 & 1 & 1 & 1 \\ k^2 & -k^2 & k^2 & -k^2 \\ e^{kL} & e^{ikL} & e^{-kL} & e^{-ikL} \\ k^2e^{kL} & -k^2e^{ikL} & k^2e^{-kL} & -k^2e^{-ikL} \end{bmatrix} \begin{Bmatrix} A_1 \\ A_2 \\ A_3 \\ A_4 \end{Bmatrix}$$

$$= -\begin{Bmatrix} F_o \sum_{n=1}^{2} a_n e^{-k_n x_o} - M_o \sum_{n=1}^{2} b_n e^{-k_n x_1} \\ F_o \sum_{n=1}^{2} k_n^2 a_n e^{-k_n x_o} - M_o \sum_{n=1}^{2} k_n^2 b_n e^{-k_n x_1} \\ F_o \sum_{n=1}^{2} a_n e^{-k_n(L-x_o)} + M_o \sum_{n=1}^{2} b_n e^{-k_n(L-x_1)} \\ F_o \sum_{n=1}^{2} k_n^2 a_n e^{-k_n(L-x_o)} + M_o \sum_{n=1}^{2} k_n^2 b_n e^{-k_n(L-x_1)} \end{Bmatrix} \qquad (4.31)$$

Again the terms relating to the known external forces appear on the right hand side and those relating to the four unknown free waves are contained on the left hand side. Notice that the left hand side of equation (4.31) is identical to that of equation (4.7). Any other external forces or moments can likewise be included in the problem simply by adding extra terms to the right hand side. The left hand side remains unchanged. This is true for the beam on a pair of simple supports or on multiple supports which provide elastic and inertial constraints.

4.5 Calculations and Discussion

Various multi-bay beams, having different support conditions, have been studied through computer calculations. The following non-dimensional quantities are also used.

ND Frequency: $2\pi f(m_b X_b^4/EI)^{1/2}$

ND Inertance : $(\ddot{w}/F_o)\rho h(X_b)$ (Inertance = Acceleration/Force)

ND Transverse Stiffness KT : $(K_t(X_b)^3)/EI$

ND Rotational Stiffness KR : $(K_r(X_b))/EI$

ND Stiffness Coupling KC : $(K_c(X_b)^2)/EI$

where X_b is the equi-distant bay length and $\ddot{w} = -\omega^2 w$.

The supports are assumed to have stiffnesses but no inertia. Any inertia characteristics can conveniently be included by using the dynamic stiffness concept.

In order to verify the method, it has first been applied to some simple cases where results from previous investigations are available. Two uniform Euler-Bernoulli beams, having three and six equi-length bays, are considered. In both cases the intermediate supports are taken as simple supports, whereas the extreme end conditions are in turn made (i) Simply-Supported, (ii) Clamped, (iii) Free. Excitation is provided by a single harmonic force. Frequency response curves have been computed by using equation (4.21). These apply to beams with $\eta = 0.001$. The transverse harmonic force is assumed to act at

one-fourth of the total beam lengths. Figures 26 and 27 give the transverse responses in terms of non-dimensional direct inertances against non-dimensional frequency for three and six-bay beams, respectively. The natural frequencies were identified by very precisely locating the frequencies for peak response with $\eta = 10^{-6}$. The values obtained are compared in Tables 1 and 2 with the natural frequencies quoted in [31] for three and six bay beams respectively. It can be seen that, on the whole, the agreement reached is impeccable with a maximum difference of 0.2%.

The undamped modes of forced vibration at the resonance frequencies of the three-bay beam have also been computed and are presented in Figures 28 to 30 in normalized form. Even though the beam is forced at the middle of the first bay (x_o = L/6) the mode shapes are independent of the point of application of the excitation. It can be seen that the odd-numbered modes are symmetric with respect to the centre of the beam and the even-numbered ones are antisymmetric. This well known fact [1] is due to the structure having an odd number of equi-length bays. If it had an even number of bays, the reverse of the statement applies.

The damped mode shapes of the three-bay beam with all supports being simple are plotted for the lowest resonance frequency and presented in Figure 31. Forcing in turn is applied at the middle of the first bay (x_o = L/6) and the second bay (x_o = L/2). The cases correspond to $\eta = 0.3$. These illustrate the effect of the point of application on damped structure response. As can be seen, the response levels fall off with distance from the source and are no longer symmetric about the centre if the excitation is off-centre. These can be explained on the grounds that the inclusion of damping results in waves which have complex wave numbers and attenuate as they travel away from the source or back from the supports.

The three-bay beam is next allowed to have identical general supports, which provide both transverse and rotational flexibilities at each end and at the two intermediate support locations. Motion coupling at the supports is excluded from the analysis. The direct transverse responses are computed by using equation (4.26) and

presented in the form of non-dimensional inertances. Force is applied at one-fourth of the beam length. Material loss factor is $\eta = 0.001$. First investigated is the effect of changing the transverse support stiffness on the response. Two cases corresponding to KT = 1000 and KT = 10000 are studied. The value of rotational stiffness is KR = 1 in each case. Figure 32 represents the responses against the square-root of the non-dimensional frequency. Then the transverse stiffness is kept constant as KT = 10000 and the cases corresponding to rotational stiffnesses KR = 1 and KR = 10 are considered. Their responses are given in Figure 33 against the non-dimensional frequency. These figures show that the resonance frequencies increase as the elastic constraints increase. The undamped mode shapes corresponding to the resonance frequencies of the case KT = 10000, KR = 10 are obtained again by using equation (4.26) and are given in Figure 34 in normalized forms. The inclusion of the stiffness coupling (K_C) has been found to reduce the resonance frequencies, though not appreciably. Its effect on the mode shapes has been hardly visible.

4.6 Conclusions

This chapter has analysed the forced vibrations of the single and multi-bay finite uniform Euler-Bernoulli beams by introducing a new approach.

The total motion in the beam has been defined in terms of free and forced components. In multi-bay beams, each intermediate support has been assumed to supply excitation(s) with unknown magnitude(s). In this way, the beam has been viewed as being under the influence of multiple excitations each of which generates a 'forced' wave field. Their wave fields have been taken to be those of the infinite-system point response functions of the infinite uninterrupted beam. The so-called 'free' waves are those which are reflected from the extreme ends of the beam and their magnitudes are found by considering the boundary conditions at the extreme ends in conjunction with the relevant boundary conditions at the intermediate support locations. Altogether these boundary conditions permit the determination of the unknown reaction forces and/or moments and the free wave magnitudes.

The resultant simultaneous equations have been put into a matrix form and solved numerically.

The developed method has been verified by comparing the resonance frequencies obtained for very lightly damped beams with natural frequencies in existing literature. Due to the scarcity of existing results, only a few and relatively simple cases have been considered but remarkable agreement has been obtained. The responses of various multi-bay beams have then been investigated with particular attention being given to the effects of damping and the support characteristics.

It has been demonstrated that the proposed method possesses some novel features. It conveniently incorporates any number and combination of excitations. It relaxes the possible restrictions imposed on the type and spacing of the intermediate supports and can easily include their individual dynamic characteristics. Furthermore it also allows each support condition to be different.

CHAPTER 5

FORCED VIBRATIONS OF UNIFORM FINITE SANDWICH BEAMS

5.1 Introduction

This short chapter details the forced vibration analysis of a single-bay three-layered sandwich beam under the influence of a transverse harmonic force. Such beams have been investigated in Section 2.3. The assumptions made in that section and the derivations which have been undertaken still apply in this chapter and will not be repeated here.

The analytical method is the one which has been developed in Chapter 4. This chapter concentrates purely on the theoretical considerations and sets up the corresponding six simultaneous equations for simply-supported, clamped-clamped and free-free beams.

5.2 Response of a Single Bay Three-Layered Sandwich Beam

Expressions for the displacements, rotation, shear force and bending moments in the sandwich beam have been explicitly detailed in Section 2.3. The 'Infinite-System Point Response Functions' due to a force have also been given in that section for the transverse displacement and rotation. Other relevant quantities are found to take the following forms:

$$S_{x,right}(x) = F_o \sum_{n=1}^{3} -k_n \Gamma_n a_n e^{-k_n x} \qquad (5.1)$$

$$S_{x,left}(x) = -S_{x,right}(x) \qquad (5.2)$$

$$M_{fp}(x) = F_o D_t \sum_{n=1}^{3} k_n^2 a_n e^{-k_n x} \qquad (5.3)$$

$$M_{af}(x) = F_o (-Ehd) \sum_{n=1}^{3} \gamma_n k_n a_n e^{-k_n x} \qquad (5.4)$$

$$u_{3,right}(x) = F_o \sum_{n=1}^{3} \Upsilon_n a_n e^{-k_n x} \tag{5.5}$$

$$u_{3,left}(x) = -u_{3,right}(x) \tag{5.6}$$

where x is the distance measured from F_o and

$$\Gamma_n = D_t k_n^2 - (G_c^* d^2/h_c)\,(1 + g^*/(k_n^2 - g^*))$$

$$\Upsilon_n = (k_n/(k_n^2 - g^*))\,(g^* d/2)$$

5.2.1 Boundary Conditions for Simply-Supported Ends

Suppose that the sandwich beam has a length L and the force F_o acts at x_o. The required boundary conditions and their parametric forms can be written as:

$$w(0) = 0 : \quad \sum_{n=1}^{6} A_n + F_o \sum_{n=1}^{3} a_n e^{-k_n x_o} = 0 \tag{5.7}$$

$$M_{fp}(0) = 0 : \quad D_t\left\{ \sum_{n=1}^{6} k_n^2 A_n + F_o \sum_{n=1}^{3} k_n^2 a_n e^{-k_n x_o} \right\} = 0 \tag{5.8}$$

$$M_{af}(0) = 0 : \quad (-Ehd)\left\{ \sum_{n=1}^{6} \Upsilon_n k_n A_n + F_o \sum_{n=1}^{3} \Upsilon_n k_n a_n e^{-k_n x_o} \right\} = 0 \tag{5.9}$$

$$M_{af}(L) = 0 : \quad (-Ehd)\left\{ \sum_{n=1}^{6} \Upsilon_n k_n A_n e^{k_n L} + F_o \sum_{n=1}^{3} \Upsilon_n k_n a_n e^{-k_n (L-x_o)} \right\} = 0 \tag{5.10}$$

$$M_{fp}(L) = 0 : \quad D_t\left\{ \sum_{n=1}^{6} k_n^2 A_n e^{k_n L} + F_o \sum_{n=1}^{3} a_n e^{-k_n (L-x_o)} \right\} = 0 \tag{5.11}$$

$$w(L) = 0 : \quad \sum_{n=1}^{6} A_n e^{k_n L} + F_o \sum_{n=1}^{3} a_n e^{-k_n (L-x_o)} = 0 \tag{5.12}$$

These equations can be expressed in the matrix form of $[C]\{A_n\} = F_o\{D\}$. The six unknown free wave magnitudes can be computed numerically. Once they are found, the transverse response at any point x_r ($0 \leq x_r \leq L$) can be determined as:

$$w(x_r) = \sum_{n=1}^{6} A_n e^{k_n x_r} + F_o \sum_{n=1}^{3} a_n e^{-k_n |x_o - x_r|} \qquad (5.13)$$

5.2.2 Boundary Conditions for Clamped Ends

In addition to equations (5.7) and (5.12), this condition requires that the rotation, $\theta = \partial w/\partial x$, and the axial displacement, u_3, at each end must be zero. These conditions are expressed by:

$$\theta(0) = 0 \; : \quad \sum_{n=1}^{6} k_n A_n - F_o \sum_{n=1}^{3} c_n e^{-k_n x_o} = 0 \qquad (5.14)$$

$$u_3(0) = 0 \; : \quad \left\{ - \sum_{n=1}^{6} \gamma_n A_n - F_o \sum_{n=1}^{3} \gamma_n a_n e^{-k_n x_o} \right\} = 0 \qquad (5.15)$$

$$u_3(L) = 0 \; : \quad \left\{ - \sum_{n=1}^{6} \gamma_n A_n e^{k_n L} + F_o \sum_{n=1}^{3} \gamma_n a_n e^{-k_n (L - x_o)} \right\} = 0 \qquad (5.16)$$

$$\theta(L) = 0 \; : \quad \left\{ \sum_{n=1}^{6} k_n A_n e^{k_n L} + F_o \sum_{n=1}^{3} c_n e^{-k_n (L - x_o)} \right\} = 0 \qquad (5.17)$$

Equations (5.7) and (5.12) together with equations (5.14) to (5.17) can be cast into a matrix form and solved for the A_n's. Equation (5.13) can then be used to obtain transverse response $w(x_r)$.

5.2.3 Boundary Conditions for Free Ends

The free condition requires all the forces and moments acting on the end section to be zero. Moment boundary conditions are given by

equations (5.8) to (5.11). The total shear force at either ends can be expressed as:

$$S_x(0) = 0 : \quad \sum_{n=1}^{6} k_n \Gamma_n A_n + F_o \sum_{n=1}^{3} k_n \Gamma_n a_n e^{-k_n x_o} = 0 \qquad (5.18)$$

$$S_x(L) = 0 : \quad \sum_{n=1}^{6} k_n \Gamma_n A_n e^{k_n L} - F_o \sum_{n=1}^{3} k_n \Gamma_n a_n e^{-k_n (L-x_o)} = 0 \qquad (5.19)$$

Again a 6 × 6 matrix equation can be set up for the A_n's and they can be computed. Equation (5.13) can then be used to determine the response at any point x_r on the beam.

5.3 Conclusions

This chapter has outlined the necessary theoretical background for the analysis of the forced vibrations of single-bay, three-layered sandwich beams with classical boundary conditions. The developed and proven analytical method of Chapter 4 has been utilized to solve a considerably more complicated problem. Full attention has been given to the difficult boundary conditions of the sandwich beam. The theory presented can easily be extended to multi-bay sandwich beams, simply by following the relevant sections of Chapter 4.

No computed results are given for sandwich beams. The theory which has been presented is intended as a pre-cursor to the theory and calculations of Chapter 6 which relate to a two-dimensional sandwich plate.

CHAPTER 6

FORCED VIBRATIONS OF UNIFORM FINITE STIFFENED PLATES

6.1 Introduction

Stiffened plate structures are widely used in aircraft and are often subjected to intense acoustic loading. A knowledge of natural frequencies and normal modes of vibration of such structures is essential in the study of acoustic fatigue failure.

Various authors have studied the dynamics of stiffened structures. Kirk [2] obtained the natural frequencies of transverse vibration of rectangular plates which had stiffeners parallel to one edge. He later [3] determined the ratio of the fundamental natural frequency of a rectangular plate having a single stiffener to the fundamental natural frequency of the unstiffened plate of equal mass.

The earliest attempts at analysing the response of a multi-bay stiffened structure were based on the normal mode approach, but this became extremely tedious when the number of bays was large. Lin proposed a model consisting of a row of flat plates supported by open section stringers between two frames to represent an aircraft fuselage [4]. He initially considered each stringer (stiffener) and each panel (bay) to be different. For an 'N_b' bay plate he set up a matrix equation of order $4N_b$ and showed that the natural frequencies of these structures fall into groups. By assuming each bay to be identical Lin was able to predict the limiting frequencies and modes of each group as N_b became infinite. In this study Lin modelled the stiffeners by considering the dynamics of open sections [5]. Later Lin *et al* [6] employed a finite difference method to predict the natural frequencies, but not the modes of a multi-bay plate with identically constructed and evenly spaced stiffeners. Each bay element was taken to be equal to the others. They only considered some special classes of stiffeners which provided finite constraints either in transverse motion or rotation. Mercer *et al* [7] developed a transfer matrix approach to study both natural frequencies and mode shapes of stiffened plates.

Their technique allowed for individual bay and stiffener characteristics to be different but suffered from mathematical instability. Sen Gupta developed a graphical method to determine the natural frequencies of finite multi-bay beams [11]. He made use of propagation constants of the infinite periodic structure (a concept which will be analysed in Chapter 7) and obtained the frequencies for the cases where the extreme ends of the structure either had simple or clamped supports. Intermediate supports were assumed as simple and the bays were taken as equal in length. He later extended his theory to skin-stringer structures [12] where the extreme ends were either clamped or having half the stiffener. Cases considered were confined to those of [6]. In all these attempts the frames have been modelled as simple supports. This has been justified on the grounds that if the aspect ratio of the bay (frame spacing/stiffener spacing) is greater than two, the frames have little effect on the frequencies.

All the above-mentioned theoretical models apply to the study of free vibrations of the structures. A new approach will be presented in this chapter which analyses the harmonically forced vibrations of Euler-Bernoulli plates and three-layered sandwich plates having equal face-plates with multiple stiffening. All the plates are assumed to be uniform, flat and rectangular. The free vibration characteristics are readily deduced from the forced vibrations of the undamped structures.

In this approach, the plate of finite length L is mounted along one pair of edges on frames which are at a distance L_y apart and are assumed to provide simple supports. A set of stiffeners is attached to the plate normal to these edges. A spatially sinusoidal line force, $F(y) = F_o \sin m\pi y/L_y$ per unit length, acts across the uniform plate and sends out N waves to either side. These are the waves studied in Chapter 3 where it was shown that N = 2 for uniform, flat, rectangular plates and N = 3 for uniform, flat, three-layered sandwich plates. When one of these waves encounters the plate boundary at its extreme end, it is reflected in the form of two free waves back to the other end. As in the beam problems of Chapter 4, the magnitudes of these 2N free waves constitute some of the unknowns of the problem. Any stiffeners acting across the plate impose line forces and moments on the plate which also send out N waves in both directions. The total

plate motion due to all of these wave systems must satisfy the boundary conditions at the extreme ends of the plate, as well as the equilibrium and compatibility conditions at each stiffener location. Satisfaction of all of these conditions leads to a set of equations in the various unknowns which are sufficient to determine the complex amplitudes of the unknowns. When these have been found, the response at any point on the finite stiffened plate can be computed.

The method developed in this chapter also determines the natural frequencies and mode shapes of the plates. Each bay may be of different length and each stiffener may have different characteristics. The theoretical analysis is carried out for a single transverse distributed line force but any number and/or type of such forces can easily be included. Even though the method will be outlined for multi-bay plates, it is equally applicable to the forced analysis of single bay plates.

6.2 Euler-Bernoulli Plates

6.2.1 Theoretical Approach

To begin with, consider Figure 35. It represents an N_b bay finite Euler-Bernoulli plate of length L, width L_y. It has $N_b - 1$ stiffeners and a single externally applied harmonic line force $F(y,t) = F_o \sin m\pi y/L_y \, e^{i\omega t}$ per unit length acts on the plate at (x_o,y); $m = 1$ is illustrated. The plate harmonic transverse displacement at any distance 'x' from the force due to that force alone is given by

$$w(x,y,t) = F_o \sum_{n=1}^{2} a_n \, e^{-k_n x} \sin k_y y \, e^{i\omega t} \qquad (6.1)$$

where the terms have their usual meanings as described in Section 3.2.1. The method of determining the wave numbers, k_n, was also given in the same section.

The stiffener at location (x_j,y) reacts against the plate motion and exerts on the plate a distributed line force, $R_j \sin k_y y$ per unit length, together with a distributed line moment, $M_j \sin k_y y$ per unit

length. These reaction forces create their own forced wave fields, identical in form to the infinite-system line response functions given by Equations (3.6), (3.7) and (3.9) but proportional to the unknown reactions R_j's and M_j's. When the total motion due to the externally applied force and the stiffener reaction forces and moments impinges on the extreme x-wise ends, a pair of waves is reflected from each end. The transverse displacement due to these four reflected waves is given by

$$w(x,y) = \sum_{n=1}^{4} A_n e^{k_n x} \sin k_y y \qquad (6.2)$$

The total transverse displacement at any (x_r,y) can then be found to be

$$w(x_r,y) = \Big(\sum_{n=1}^{4} A_n e^{k_n x_r} + \sum_{j=1}^{N_b-1} R_j \sum_{n=1}^{2} a_n e^{-k_n|x_j-x_r|}$$

$$+ (jj) \sum_{j=1}^{N_b-1} M_j \sum_{n=1}^{2} b_n e^{-k_n|x_j-x_r|}$$

$$+ F_o \sum_{n=1}^{2} a_n e^{-k_n|x_o-x_r|} \Big) \sin k_y y \qquad (6.3)$$

where $jj = -1$ if $x_j > x_r$, $jj = 1$ if $x_j < x_r$.

There are $2(N_b+1)$ unknowns in this equation ((N_b-1) R_j's, (N_b-1) M_j's and 4 A_n's). These are found from the group of equations set up by considering the boundary conditions at the extreme ends and at each stiffener location. In this study the finite Euler-Bernoulli plate is assumed to have (i) Free Ends and (ii) Ends supported by the stiffeners. The first case is selected, because the plate which was analysed during the experimental stages of the study had that type of edge conditions. The second case is included because it provides the ultimate condition.

Now consider Figure 36 which shows the positive sign convention followed in the analysis of Euler-Bernoulli plates. The bending

moment and the effective shear force on a uniform plate section are well known to be (*i.e.*, Kirchhoff's boundary conditions)

$$S_{eff} = D\{\frac{\partial^3 w}{\partial x^3} + (2 - \nu)\frac{\partial^3 w}{\partial x \partial y^2}\} \qquad \text{per unit length} \tag{6.4}$$

$$M_{xx} = D\{\frac{\partial^2 w}{\partial x^2} + \nu\frac{\partial^2 w}{\partial y^2}\} \qquad \text{per unit length} \tag{6.5}$$

Due to a line force $R_j \sin m\pi y/L_y$ and a line moment $M_j \sin m\pi y/L_y$, the bending moment and the effective shear force at a distance x from R_j and M_j are found to take the following forms

$$S_{eff,right}(x,y) = -R_j \sum_{n=1}^{2} \Lambda_n a_n e^{-k_n x} \sin k_y y \tag{6.6}$$

$$S_{eff,left}(x,y) = R_j \sum_{n=1}^{2} \Lambda_n a_n e^{-k_n x} \sin k_y y \tag{6.7}$$

$$S_{eff}(x,y) = -M_j \sum_{n=1}^{2} \Lambda_n b_n e^{-k_n x} \sin k_y y \tag{6.8}$$

$$M_{xx}(x,y) = R_j \sum_{n=1}^{2} \Psi_n a_n e^{-k_n x} \sin k_y y \tag{6.9}$$

$$M_{xx,right}(x,y) = M_j \sum_{n=1}^{2} \Psi_n b_n e^{-k_n x} \sin k_y y \tag{6.10}$$

$$M_{xx,left}(x,y) = -M_j \sum_{n=1}^{2} \Psi_n b_n e^{-k_n x} \sin k_y y \tag{6.11}$$

In these

$$\Lambda_n = D\, k_n \{k_n^2 - (2 - \nu)k_y^2\}$$

$$\Psi_n = D(k_n^2 - \nu k_y^2).$$

When the plate has free x-wise edges, S_{eff} and M_{xx} due to the whole set of free and forced waves should be zero at both ends. The end boundary conditions are then given by

$$S_{eff}(0,y) = 0 \quad : \quad \{ \sum_{n=1}^{4} \Lambda_n A_n + \sum_{j=1}^{N_b-1} R_j \sum_{n=1}^{2} \Lambda_n a_n e^{-k_n x_j}$$

$$- \sum_{j=1}^{N_b-1} M_j \sum_{n=1}^{2} \Lambda_n b_n e^{-k_n x_j} \} \sin k_y y$$

$$= -(F_o \sum_{n=1}^{2} \Lambda_n a_n e^{-k_n x_o}) \sin k_y y \qquad (6.12)$$

$$M_{xx}(0,y) = 0 \quad : \quad \{ \sum_{n=1}^{4} \Psi_n A_n + \sum_{j=1}^{N_b-1} R_j \sum_{n=1}^{2} \Psi_n a_n e^{-k_n x_j}$$

$$- \sum_{j=1}^{N_b-1} M_j \sum_{n=1}^{2} \Psi_n b_n e^{-k_n x_j} \} \sin k_y y$$

$$= -(F_o \sum_{n=1}^{2} \Psi_n a_n e^{-k_n x_o}) \sin k_y y \qquad (6.13)$$

$$M_{xx}(L,y) = 0 \quad : \quad \{ \sum_{n=1}^{4} \Psi_n A_n e^{k_n L} + \sum_{j=1}^{N_b-1} R_j \sum_{n=1}^{2} \Psi_n a_n e^{-k_n(L-x_j)}$$

$$+ \sum_{j=1}^{N_b-1} M_j \sum_{n=1}^{2} \Psi_n b_n e^{-k_n(L-x_j)} \} \sin k_y y$$

$$= -(F_o \sum_{n=1}^{2} \Psi_n a_n e^{-k_n(L-x_o)}) \sin k_y y \qquad (6.14)$$

$$S_{eff}(L,y) = 0 \quad : \quad \{ \sum_{n=1}^{4} \Lambda_n A_n e^{k_n L} - \sum_{j=1}^{N_b-1} R_j \sum_{n=1}^{2} \Lambda_n a_n e^{-k_n(L-x_j)}$$

$$- \sum_{j=1}^{N_b-1} M_j \sum_{n=1}^{2} \Lambda_n b_n e^{-k_n(L-x_j)} \} \sin k_y y$$

$$= -(-F_o \sum_{n=1}^{2} \Lambda_n a_n e^{-k_n(L-x_o)}) \sin k_y y \qquad (6.15)$$

If the plate extreme x-wise edges are elastically supported, it can be deduced from Figure 37 that the boundary conditions become

$$\begin{aligned} S_{eff}(0,y) &= -K_t\, w(0,y) \\ M_{xx}(0,y) &= K_r\, w'(0,y) \\ S_{eff}(L,y) &= K_t\, w(L,y) \\ M_{xx}(L,y) &= -K_r\, w'(L,y) \end{aligned} \qquad (6.16)$$

The first of Equations (6.16) can be shown to be

$$\Big\{ \{ \sum_{n=1}^{4} \Lambda_n A_n + \sum_{j=1}^{N_b-1} R_j \sum_{n=1}^{2} \Lambda_n a_n e^{-k_n x_j} - \sum_{j=1}^{N_b-1} M_j \sum_{n=1}^{2} \Lambda_n b_n e^{-k_n x_j} \}$$

$$+ K_t \{ \sum_{n=1}^{4} A_n + \sum_{j=1}^{N_b-1} R_j \sum_{n=1}^{2} a_n e^{-k_n x_j} - \sum_{j=1}^{N_b-1} M_j \sum_{n=1}^{2} b_n e^{-k_n x_j} \} \Big\} \sin k_y y$$

$$= -F_o \{ \sum_{n=1}^{2} \Lambda_n a_n e^{-k_n x_o} + K_t \sum_{n=1}^{2} a_n e^{-k_n x_o} \} \sin k_y y \qquad (6.17)$$

In addition to the end boundary conditions, one needs $2(N_b - 1)$ more equations for the remaining $2(N_b - 1)$ unknowns. These are satisfied by considering the equilibrium and compatibility conditions at the $(N_b - 1)$ stiffener locations.

The stiffener transverse displacement and rotation and the sinusoidal distributions of force and moment per unit length acting on it are related by

$$\begin{bmatrix} K_t & K_c \\ K_c & K_r \end{bmatrix} \begin{Bmatrix} w(x_j,y) \\ w'(x_j,y) \end{Bmatrix} = \begin{Bmatrix} R_{x_j} \\ M_{x_j} \end{Bmatrix} \sin k_y y \qquad (6.18)$$

where the transverse stiffness K_t, rotational stiffnes K_r and the stiffness coupling K_c are derived in Appendix C.

Now because of the equilibrium of the forces and moments at line (x_j,y), $R_{x_j} = -R_j$ and $M_{x_j} = -M_j$. Hence it can be obtained through equation (6.18) that

$$w(x_j,y) = \left(-\frac{K_r}{K_{tot}^2} R_j + \frac{K_c}{K_{tot}^2} M_j\right) \sin k_y y$$

$$w'(x_j,y) = \left(+\frac{K_c}{K_{tot}^2} R_j - \frac{K_t}{K_{tot}^2} M_j\right) \sin k_y y \qquad (6.19)$$

where $K_{tot}^2 = K_t K_r - K_c^2$.

The transverse displacement and rotation of the stiffener at (x_j,y) are equal to the transverse displacement and rotation of the finite plate due to externally applied force F_o, the free waves A_n's and the intermediate support reactions R_j's and M_j's. The total transverse displacement of the plate can be obtained from equation (6.3) by setting x_r to x_j. In this way, it can be found that compatibility of transverse displacements at the stiffener location (x_j,y) gives

$$\left\{ \sum_{n=1}^{4} A_n e^{k_n x_j} + \sum_{\substack{\ell=1 \\ \ell \neq j}}^{N_b-1} R_\ell \sum_{n=1}^{2} a_n e^{-k_n|x_\ell - x_j|} + R_j \left(\sum_{n=1}^{2} a_n e^{-k_n|x_j - x_j|} \right.\right.$$

$$\left. + \frac{K_r}{K_{tot}^2} \right) + (jp) \sum_{\substack{mj=1 \\ mj \neq j}}^{N_b-1} M_{mj} \sum_{n=1}^{2} b_n e^{-k_n|x_{mj} - x_j|}$$

$$\left. + M_j \left(\sum_{n=1}^{2} b_n e^{-k_n|x_j - x_j|} - \frac{K_c}{K_{tot}^2} \right) \right\} \sin k_y y$$

$$= -\left\{ F_o \sum_{n=1}^{2} a_n e^{-k_n|x_o - x_j|} \right\} \sin k_y y \qquad (6.20)$$

where $jp = -1$ if $x_{mj} > x_j$, $jp = 1$ if $x_{mj} < x_j$
and rotational compatibility at (x_j, y) yields

$$\left\{ \sum_{n=1}^{4} k_n A_n e^{k_n x_j} + (jt) \sum_{\substack{\ell\ell=1 \\ \ell\ell \neq j}}^{N_b-1} R_{\ell\ell} \sum_{n=1}^{2} c_n e^{-k_n|x_{\ell\ell} - x_j|} \right.$$

$$+ R_j \left(\sum_{n=1}^{2} c_n e^{-k_n|x_j - x_j|} - \frac{K_c}{K_{tot}^2} \right) + \sum_{\substack{mt=1 \\ mt \neq j}}^{N_b-1} M_{mt} \sum_{n=1}^{2} d_n e^{-k_n|x_{mt} - x_j|}$$

$$\left. + M_j \left(\sum_{n=1}^{2} d_n e^{-k_n|x_j - x_j|} + \frac{K_t}{K_{tot}^2} \right) \right\} \sin k_y y$$

$$= -\left\{ (\ell t) F_o \sum_{n=1}^{2} c_n e^{-k_n|x_o - x_j|} \right\} \sin k_y y \qquad (6.21)$$

where $jt = -1$ if $x_{\ell\ell} > x_j$, $jt = 1$ if $x_{\ell\ell} < x_j$
$\ell t = -1$ if $x_o > x_j$, $\ell t = 1$ if $x_o < x_j$.

$2(N_b-1)$ similar equations can be obtained from the (N_b-1) stiffeners. If the stiffeners are all different, allowance can easily be made for their individual characteristics by using the required stiffness values in the appropriate equations. These $2(N_b-1)$

equations are independent of the end boundary conditions and together with the four extreme end boundary conditions (which are different for different ends) constitute the set of equations which must be solved to find the A_n's, R_j's and M_j's. The whole set of equations has the general form

$$\underset{2(N_b+1)\times 2(N_b+1)}{\begin{bmatrix} & X_{i,j} & \end{bmatrix}} \underset{2(N_b+1)\times 1}{\begin{Bmatrix} A_1 \\ A_2 \\ A_3 \\ A_4 \\ R_1 \\ M_1 \\ \vdots \\ R_{N_b-1} \\ M_{N_b-1} \end{Bmatrix}} = -F_o \underset{2(N_b+1)\times 1}{\begin{Bmatrix} & & \end{Bmatrix}} \qquad (6.22)$$

Numerical solution of the above equation gives the complex amplitudes of the unknowns. Once they are determined, the transverse displacement at any (x_r,y) can be found from Equation (6.3).

6.2.2 The Stiffener Characteristics to be Used

The dynamic stiffnesses of the Z-section stiffeners used throughout this thesis, are computed from a method which is significantly different from that of [5]. The difference lies in the fact that distortion (deformation) of the stiffener cross-section is allowed for in the current work. The stiffener cross-section is deflected transversely and rotated about the root of the web and in addition the web of the cross-section is allowed to deform. The distortion of the flange is ignored. Figure 38 gives the stiffener cross-section and its exaggerated final shape when all the allowed freedoms take place. The effective width of the plate which works with the stiffener is also accounted for. An energy approach is employed to determine the stiffnesses. Appendix C gives the detailed analysis. From this, the

dynamic stiffness matrix of the stiffener is found and evaluated numerically. Appendix C presents stiffness calculations carried out both by excluding and including cross-sectional deformation and shows the importance of inclusion.

6.2.3 Calculations and Discussion

6.2.3.1 Natural Frequency Prediction

Firstly the validity of the developed analytical method of Section 6.2.1 has been verified by comparing the natural frequencies obtained through it with those given in [7] which were found by the transfer matrix method. A six equal-bay uniform plate is considered where the stiffeners provide dynamic constraints at the ends as well as at the intermediate support locations. Since the purpose is to compare the two methods, the stiffeners are taken as being those used in [7] which were found by the methods of [5]. The dimensions and material properties of the plate are given in Table 3. The line forcing is applied at x_o = 0.11 [m] and equation (6.3) is used to determine the direct transverse response. The first group of six frequencies at which the response of a very lightly damped plate ($\eta = 10^{-6}$) reaches peak values (*i.e.*, the resonance frequencies which are almost exactly equal to the natural undamped frequencies) are computed by an iterative method. These are then compared in Table 4 with the natural frequencies quoted in [7]. The agreement achieved is excellent.

6.2.3.2 The Response to a Line Loading

A response curve has been computed for a stiffened Euler-Bernoulli plate with eight bays and free ends (*i.e.*, seven intermediate supports). The dimensions and material properties are given in Figure 39, which are those of the plate used in the experimental studies. The transverse direct line inertances of the plate are computed using equation (6.3) for two different damping values (η = 0.001 and η = 0.1). The external line force is applied at x_o = 0.37 [m]. The intermediate supports are general, in that they are stiffeners which

undergo transverse displacement, rotation and cross-sectional distortion. Their dynamic stiffnesses include coupling between flexure and torsion. The dimensions and material properties of the stiffeners are given in Appendix C. Each stiffener is the same.

In this case the order of the final matrix equation is 18 (4 unknown free waves and 2 × 7 unknown intermediate support reactions). Figure 40 gives the resultant magnitudes against the frequency. Notice that the lightly damped plate has resonance frequencies in a bunch of six. Other bunches of six occur at high frequencies. When the damping is high, the response peak levels drop and the distinct peaks combine to form a much broader and flatter response.

6.2.3.3 The Effects of Different Theories for the Stiffener Stiffnesses

The effects of stiffener characteristics on the plate response have been investigated by computing the plate resonance frequencies. Four different cases have been studied:

(i) Stiffeners with stiffness but no inertia and no cross-sectional distortion. Coupling between flexure and torsion is ignored.

(ii) Stiffeners with stiffness and inertia but without any distortion. Coupling is again ignored.

(iii) Stiffeners having stiffness, inertia and with coupling but no cross-sectional distortion.

(iv) The general stiffener.

The plate of Section 6.2.3.2 is used in each case. The stiffeners are those analysed in Appendix C. External line forcing is applied at x_o = 0.36 [m] and the direct transverse response is obtained from Equation (6.3). Very low damping ($\eta = 10^{-6}$) is assigned to the plate and the frequencies at which the response reaches peak values are

precisely located by iteration. They are virtually the natural frequencies of undamped plate. The results are presented in Table 5.

It can be seen from Table 5 that cases (i) and (iv) provide the limits of the variation of each resonance frequency. Frequencies are highest in case (i) but progressive relaxation of constraints lowers them accordingly, though the differences are not too appreciable between cases (i) to (iii). Case (iv) reflects the importance of cross-sectional deformation. Its inclusion significantly reduces the values of the lower frequencies of the group considered. It is well-known that these frequencies are highly influenced by the rotational stiffnesses of the stiffeners. Since the cross-sectional distortion significantly lowers the rotational stiffness magnitude at low frequencies (see Figure C.4) its consideration consequently results in drastic reduction of the resonance frequencies.

6.3 Three-Layered Sandwich Plate

6.3.1 Theoretical Approach

In this section a three-layered sandwich plate having equal face-plates will be considered. The two opposite edges along the length, distance L_y apart, are assumed to be simply supported. The total plate length is L and $N_b - 1$ general stiffeners are attached to the plate across the width to provide the intermediate constraints. A sinusoidal harmonic line force $F(y,t) = F_o \sin k_y y \, e^{i\omega t}$ acts on the plate at (x_o, y).

It was explained in Chapter 3 that any line excitation acting on such a sandwich plate sends out three waves in both directions. It can hence be deduced that Equation (6.2) will represent the free wave transverse displacement of the sandwich plate provided a total of six waves is allowed. The total transverse displacement of the sandwich plate at any (x_r, y) can thus be found to be

$$w(x_r,y) = \Big(\sum_{n=1}^{6} A_n e^{k_n x_r} + \sum_{j=1}^{N_b-1} R_j \sum_{n=1}^{3} a_n e^{-k_n|x_j-x_r|}$$

$$+ (jp) \sum_{j=1}^{N_b-1} M_j \sum_{n=1}^{3} b_n e^{-k_n|x_j-x_r|}$$

$$+ F_o \sum_{n=1}^{3} a_n e^{-k_n|x_o-x_r|} \Big) \sin k_y y \qquad (6.23)$$

where $jp = -1$ if $x_j > x_r$, $jp = 1$ if $x_j < x_r$.

In this $R_j \sin k_y y$ and $M_j \sin k_y y$ define the force and moment per unit length applied on the sandwich plate by the stiffener at (x_j,y). The required coefficients, a_n's and b_n's, are given by equations (A.12) and (A.16) respectively. The wave numbers, k_n's, were derived in Section 3.3.1. The total number of unknowns is now seen to be $2(N_b + 2)$ (*i.e.*, 6 A_n's, $(N_b - 1)$ R_j's and $(N_b - 1)$ M_j's).

We now require the equations expressing compatibility between the displacement of the plate and of each stiffener. The equations of Section 6.2.1 for the stiffened Euler-Bernoulli plate may be used for the sandwich simply by changing the number of terms in each summation from 2 to 3. By doing this the compatibility of transverse displacements of the plate and the stiffener at (x_j,y) yields

$$\Big\{ \sum_{n=1}^{6} A_n e^{k_n x_j} + \sum_{\substack{\ell=1 \\ \ell\neq j}}^{N_b-1} R_\ell \sum_{n=1}^{3} a_n e^{-k_n|x_\ell-x_j|}$$

$$+ R_j \Big(\sum_{n=1}^{3} a_n e^{-k_n|x_j-x_j|} + \frac{K_r}{K_{tot}^2} \Big)$$

$$+ (js) \sum_{\substack{\ell n=1 \\ \ell n\neq j}}^{N_b-1} M_{\ell n} \sum_{n=1}^{3} b_n e^{-k_n|x_{\ell n}-x_j|}$$

$$+ M_j \Big(\sum_{n=1}^{3} b_n e^{-k_n|x_j-x_j|} - \frac{K_c}{K_{tot}^2} \Big) \Big\} \sin k_y y$$

$$= -\Big\{ F_o \sum_{n=1}^{3} a_n e^{-k_n|x_o-x_j|} \Big\} \sin k_y y \qquad (6.24)$$

where $js = -1$ if $x_{\ell n} > x_j$, $js = 1$ if $x_{\ell n} < x_j$

and the compatibility of rotations leads to

$$\Bigg\{ \sum_{n=1}^{6} k_n A_n e^{k_n x_j} + (jk) \sum_{\substack{\ell s=1 \\ \ell s \neq j}}^{N_b-1} R_{\ell s} \sum_{n=1}^{3} c_n e^{-k_n |x_{\ell s} - x_j|}$$

$$+ R_j \Big(\sum_{n=1}^{3} c_n e^{-k_n |x_j - x_j|} - \frac{K_c}{K_{tot}^2} \Big)$$

$$+ \sum_{\substack{mp=1 \\ mp \neq j}}^{N_b-1} M_{mp} \sum_{n=1}^{3} d_n e^{-k_n |x_{mp} - x_j|}$$

$$+ M_j \Big(\sum_{n=1}^{3} d_n e^{-k_n |x_j - x_j|} + \frac{K_t}{K_{tot}^2} \Big) \Bigg\} \sin k_y y$$

$$= -\Big\{ (\ell k) F_o \sum_{n=1}^{3} c_n e^{-k_n |x_o - x_j|} \Big\} \sin k_y y \qquad (6.25)$$

where $jk = -1$ if $x_{\ell s} > x_j$, $jk = 1$ if $x_{\ell s} < x_j$

$\ell k = -1$ if $x_o > x_j$, $\ell k = 1$ if $x_o < x_j$.

The coefficients, c_n's and d_n's are given by equations (A.13) and (A.17) respectively.

These $2(N_b - 1)$ equations which are obtained at the $N_b - 1$ intermediate stiffener locations are independent of the extreme end boundary conditions.

For the same reasons which were stated in Section 6.2.1, the sandwich plates with (i) free ends, (ii) stiffener supported ends will be considered in this section.

Expressions for the effective shear force and bending moments per unit length on a section through a three-layered sandwich plate are derived in Appendix A. It can be found that due to $R_j \sin k_y y$ and $M_j \sin k_y y$ they can be expressed in the following forms:

$$S_{eff,right}(x,y) = R_j \sum_{n=1}^{3} \Gamma_n a_n e^{-k_n x} \sin k_y y \qquad (6.26)$$

$$S_{eff,left}(x,y) = -R_j \sum_{n=1}^{3} \Gamma_n a_n e^{-k_n x} \sin k_y y \qquad (6.27)$$

$$S_{eff}(x,y) = M_j \sum_{n=1}^{3} \Gamma_n b_n e^{-k_n x} \sin k_y y \qquad (6.28)$$

$$M_{fp}(x,y) = R_j \sum_{n=1}^{3} \Delta_n a_n e^{-k_n x} \sin k_y y \qquad (6.29)$$

$$M_{fp,right}(x,y) = M_j \sum_{n=1}^{3} \Delta_n b_n e^{-k_n x} \sin k_y y \qquad (6.30)$$

$$M_{fp,left}(x,y) = -M_j \sum_{n=1}^{3} \Delta_n b_n e^{-k_n x} \sin k_y y \qquad (6.31)$$

$$M_{af}(x,y) = R_j \sum_{n=1}^{3} \Omega_n a_n e^{-k_n x} \sin k_y y \qquad (6.32)$$

$$M_{af,right}(x,y) = M_j \sum_{n=1}^{3} \Omega_n b_n e^{-k_n x} \sin k_y y \qquad (6.33)$$

$$M_{af,left}(x,y) = -M_j \sum_{n=1}^{3} \Omega_n b_n e^{-k_n x} \sin k_y y \qquad (6.34)$$

where 'x' is measured from the line of application of the excitation and

$$\Gamma_n = k_n \{D_t[k_n^2 - (2 - \nu)k_y^2][1 + (g^*Y) / (k_n^2 - k_y^2 - g^*)]\}$$

$$\Delta_n = D_t(k_n^2 - \nu k_y^2)$$

$$\Omega_n = (-G^*d^2/h_c)[(k_n^2 - \nu k_y^2) / (k_n^2 - k_y^2 - g^*)]$$

The parameters used above were defined in Section 3.3.1.

If the ends of an N_b bay finite sandwich plate are free, the required boundary conditions are:

$$S_{eff}(0,y) = 0 \qquad S_{eff}(L,y) = 0$$
$$M_{fp}(0,y) = 0 \qquad M_{fp}(L,y) = 0$$
$$M_{af}(0,y) = 0 \qquad M_{af}(L,y) = 0 \tag{6.35}$$

Their final forms, as explained before, include the effects of the free waves, the unknown intermediate support reactions at (x_j,y) $(j = 1, N_{b-1})$ and the known externally applied excitation. Assuming a single force excitation $F_o \sin k_y y$ acting at (x_o,y), they can be shown to be:

$$S_{eff}(0,y) = 0: \quad \Big\{ \sum_{n=1}^{6} -\Gamma_n A_n - \sum_{j=1}^{N_b-1} R_j \sum_{n=1}^{3} \Gamma_n a_n e^{-k_n x_j}$$
$$+ \sum_{j=1}^{N_b-1} M_j \sum_{n=1}^{3} \Gamma_n b_n e^{-k_n x_j} \Big\} \sin k_y y = -(-F_o \sum_{n=1}^{3} \Gamma_n a_n e^{-k_n x_o}) \sin k_y y \tag{6.36}$$

$$M_{fp}(0,y) = 0: \quad \Big\{ \sum_{n=1}^{6} \Delta_n A_n + \sum_{j=1}^{N_b-1} R_j \sum_{n=1}^{3} \Delta_n a_n e^{-k_n x_j}$$
$$- \sum_{j=1}^{N_b-1} M_j \sum_{n=1}^{3} \Delta_n b_n e^{-k_n x_j} \Big\} \sin k_y y = -(F_o \sum_{n=1}^{3} \Delta_n a_n e^{-k_n x_o}) \sin k_y y \tag{6.37}$$

$$M_{af}(0,y) = 0: \quad \Big\{ \sum_{n=1}^{6} \Omega_n A_n + \sum_{j=1}^{N_b-1} R_j \sum_{n=1}^{3} \Omega_n a_n e^{-k_n x_j}$$
$$- \sum_{j=1}^{N_b-1} M_j \sum_{n=1}^{3} \Omega_n b_n e^{-k_n x_j} \Big\} \sin k_y y = -(F_o \sum_{n=1}^{3} \Omega_n a_n e^{-k_n x_o}) \sin k_y y \tag{6.38}$$

$$S_{eff}(L,y) = 0: \quad \Big\{ \sum_{n=1}^{6} -\Gamma_n A_n e^{k_n L} + \sum_{j=1}^{N_b-1} R_j \sum_{n=1}^{3} \Gamma_n a_n e^{-k_n(L-x_j)}$$

$$+ \sum_{j=1}^{N_b-1} M_j \sum_{n=1}^{3} \Gamma_n b_n e^{-k_n(L-x_j)} \Big\} \sin k_y y = -\Big(F_o \sum_{n=1}^{3} \Gamma_n a_n e^{-k_n(L-x_o)}\Big) \sin k_y y \tag{6.39}$$

$$M_{fp}(L,y) = 0: \quad \Big\{ \sum_{n=1}^{6} \Delta_n A_n e^{k_n L} + \sum_{j=1}^{N_b-1} R_j \sum_{n=1}^{3} \Delta_n a_n e^{-k_n(L-x_j)}$$

$$+ \sum_{j=1}^{N_b-1} M_j \sum_{n=1}^{3} \Delta_n b_n e^{-k_n(L-x_j)} \Big\} \sin k_y y = -\Big(F_o \sum_{n=1}^{3} \Delta_n a_n e^{-k_n(L-x_o)}\Big) \sin k_y y \tag{6.40}$$

$$M_{af}(L,y) = 0: \quad \Big\{ \sum_{n=1}^{6} \Omega_n A_n e^{k_n L} + \sum_{j=1}^{N_b-1} R_j \sum_{n=1}^{3} \Omega_n a_n e^{-k_n(L-x_j)}$$

$$+ \sum_{j=1}^{N_b-1} M_j \sum_{n=1}^{3} \Omega_n b_n e^{-k_n(L-x_j)} \Big\} \sin k_y y = -\Big(F_o \sum_{n=1}^{3} \Omega_n a_n e^{-k_n(L-x_o)}\Big) \sin k_y y \tag{6.41}$$

Figure 41 represents the positive sign convention for the effective shear force and face-plate bending moment of a three-layered sandwich plate. It can easily be shown that if the stiffeners provide the constraints at the extreme edges of the sandwich plate, the boundary conditions to be satisfied become:

$$\begin{aligned} S_{eff}(0,y) &= K_t\, w(0,y) & S_{eff}(L,y) &= -K_t\, w(L,y) \\ M_{fp}(0,y) &= K_r\, w'(0,y) & M_{fp}(L,y) &= -K_r\, w'(L,y) \\ M_{af}(0,y) &= 0 & M_{af}(L,y) &= 0 \end{aligned} \tag{6.42}$$

It is to be noted that all the applied moment is assumed to be carried by the face-plates. Since there is no axial force, the moment due to them is zero.

The first of equations (6.42) can be shown to be

$$\Big\{\Big(\sum_{n=1}^{6} -\Gamma_n A_n - \sum_{j=1}^{N_b-1} R_j \sum_{n=1}^{3} \Gamma_n a_n e^{-k_n x_j} + \sum_{j=1}^{N_b-1} M_j \sum_{n=1}^{3} \Gamma_n b_n e^{-k_n x_j}\Big)$$

$$- K_t\Big(\sum_{n=1}^{6} A_n + \sum_{j=1}^{N_b-1} R_j \sum_{n=1}^{3} a_n e^{-k_n x_j} - \sum_{j=1}^{N_b-1} M_j \sum_{n=1}^{3} b_n e^{-k_n x_j}\Big)\Big\}\sin k_y y$$

$$= -F_o\Big\{-\sum_{n=1}^{3} \Gamma_n a_n e^{-k_n x_o} - K_t \sum_{n=1}^{3} a_n e^{-k_n x_o}\Big\}\sin k_y y \qquad (6.43)$$

Depending on the end boundary conditions, $2(N_b + 2)$ obtained equations can be cast into a matrix form similar to equation (6.22). The numerical solution gives the unknowns (6 A_n's, $(N_b - 1)$ R_j's and $(N_b - 1)$ M_j's). Once they have been determined, the total transverse displacement at any (x_r, y) can be found from equation (6.23).

6.3.2 Calculations and Discussion

6.3.2.1 The Models Studied

This section analyses two different multi-bay, three-layered sandwich plates. Dimensions of the first plate (an eight-bay plate) are given in Figure 42. It actually represents the plate on which the experiments to be detailed in Chapter 11 were carried out. The second plate is a fictitious one and is assumed to have six bays. It retains the same material properties and thicknesses of the eight-bay plate but has an equal bay length of 0.172 [m] and an aspect ratio of two for each bay. Poisson's ratio, ν, is now taken as 0.34. The plate has no overhangs at x-wise edges. At the extreme ends as well as at the intermediate support locations the stiffeners provide the constraints. In the study of both plates the stiffeners are assumed as being general and their specifications are given in Appendix C.

It can easily be shown that the order of the final matrix equation for the response is 16 (6 unknown free waves and 2 × 5 unknown intermediate reactions) for the six-bay plate. It increases to 20 (6 unknown free waves and 2 × 7 unknown intermediate reactions) for the eight-bay plate.

6.3.2.2 Natural Frequency Prediction

First, the developed analytical method of Section 6.3.1 has been verified by comparing the natural frequencies obtained from it with those found by using Sen Gupta's graphical approach [11]. It is assumed that the stiffeners of the six-bay plate considered in Section 6.3.2.1 provide infinite transverse constraint but no rotational constraint. Hence they act like simple line supports. Since there are no reaction moments an 11^{th} order matrix equation is set up (6 A_n's and 5 R_j's) and the direct transverse response is determined from the modified version of Equation (6.23) (*i.e.*, the terms corresponding to M_j's are ignored). The external line forcing is assumed to act at $x_o = 0.086$ [m]. By using an iterative procedure the first six resonance frequencies are precisely located for a core loss factor of $\beta = 10^{-6}$. These frequencies are then compared in Table 6 to those estimated from the propagation constants curve of infinite, periodic undamped sandwich plate on simple line supports. The bay dimensions and material properties of the infinite, periodic sandwich plate are equal to those of the finite plate. Despite the probable inaccuracies of reading from a curve, the obtained agreement is another point to validate the developed method.

6.3.2.3 The Response to a Line Loading; The Effect of Damping

The effect of core damping on the response has been demonstrated by computing the direct transverse line inertances of the eight-bay plate for a range of frequencies. The external line forcing is applied at $x_o = 0.12$ [m] and equation (6.23) is used to determine the response. Figure 43 gives the results for two different core loss factors (β = 0.001 and β = 1). Since the two overhangs are relatively small as

compared to the six intermediate bays which are comparable, one would expect the response peaks to occur in bunches of six. This can be seen to be the case for $\beta = 0.001$. With the introduction of heavy core damping, the peaks and troughs merge to form a much flatter resonant response. Figure 44 shows further results for four other core loss factors ($\beta = 0.3$, $\beta = 0.5$, $\beta = 0.7$, $\beta = 0.9$). It is apparent that lower damping reduces the location of the resonance plateau at which the resonance peaks merge together but increases the response level, mainly around the resonance region, up to approximately 310 Hz. The slight increase in response in the low frequency region is due to the lower magnitude of the effective shear stiffness (*i.e.*, $G_C^* = G_C(1 + i\beta)$). Around frequency 310 Hz as far as the magnitude is concerned the amount of the damping is irrelevant.

6.3.2.4 The Response to a Line Loading; The Influence of Plate Effective Width

This section analyses the influence of the stiffener effective width on the response of the eight-bay sandwich plate. As can be seen from Appendix C, the bending and torsional stiffnesses of the stiffeners are dependent on the effective width. In order to highlight the impact of this change, the transfer line inertances are obtained for three different effective width values ($b_{eff} = 0.017$ [m], $b_{eff} = 0.034$ [m], $b_{eff} = 0.085$ [m]). For each case the line force is assumed to act at $x_o = 0.12$ [m] and the response is determined at $x_r = 0.13$ [m] by using equation (6.23). Core loss factor is taken to be $\beta = 1$. Figure 45 gives the determined responses against the frequency.

It can be seen from Figure 45 that the varying of the effective width is not very significant in the frequency region considered. Even though the higher bending stiffness leads to lower transverse response at low frequencies, the results still imply that the plate properties rather than the stiffeners dominate the response. At ≈290 Hz all the response values have the same magnitude.

6.3.2.5 The Response to a Line Loading; The Influence of Excitation Position

The importance of measurement and excitation points has been investigated for both the six and eight-bay sandwich plates. In each case direct line inertances are computed at six different locations. The excitation points are taken to be at the bay centres in the case of the six-bay plate. For the eight-bay plate they are assigned close to the centre values of bays two to seven. They are actually the points where the excitations were applied during the experiments conducted on the sandwich plate. The responses are computed by using equation (6.23) and the results are presented in Figures 46 and 47 for six and eight-bay plates respectively. The core loss factor is taken as $\beta = 1$. The excitation points are indicated in the corresponding figures.

In both figures it can be seen that the response levels are greater in the bays at either end of the whole plate. This is due to the higher contribution of reflected waves from the ends. Because of high damping the reflected waves inevitably die out as they travel away from the ends and hence contribute less to the response.

In the six-bay plate, since the bays are equal one would expect the same direct response obtained at the points which are evenly located at the two sides of the plate centre. The discrepancies encountered in Figure 46 are attributed to the coupling between flexure and torsion of the stiffener motion. The inclusion of it not only lowers the resonance frequencies of the sandwich plate but also makes the plate structure unsymmetrical about the centre. Therefore if coupling exists, the symmetry of the resonant mode shapes with respect to the centre of the finite plate greatly deteriorates. This can be seen from Figures 48 through 53 which show the undamped forced mode shapes of the six-bay plate corresponding to the first six natural frequencies. Line force excitation is applied at the middle of the first bay ($x_o = 0.086$ [m]) and the mode shapes are found from equation (6.23) by varying x_r along the length.

6.3.2.6 The Response to a Line Loading; The Effect of Temperature

Increasing the temperature reduces the magnitude of the core shear stiffness G_c. To demonstrate the effect on the response of the eight-bay plate the core shear modulus is assigned three different frequency-dependent values which correspond to T = 15°C, T = 18°C and T = 20°C. The core loss factor is kept at the constant value of $\beta = 1$. The direct line inertances are computed at $x_o = 0.305$ [m] and equation (6.23) is used in each case. They are shown in Figure 54 against frequency.

It can be observed that the higher temperature results in higher response at low frequencies. This is due to the core shear modulus and sandwich plate stiffness being lower. For the same reason the resonance range also moves to lower frequencies.

6.4 Conclusions

The forced dynamic response of finite, uniform, multi-bay, stiffened, flat and rectangular plate structures has been investigated through the developed analytical method. Euler-Bernoulli plates and three-layered sandwich plates with equal face-plates have been studied. Two opposite edges along the length have been assumed as simply-supported. Stiffeners across the width have provided elastic and inertial constraints. External excitation has been applied as sinusoidally-varying across the width and the responses have been assumed to behave accordingly.

The characteristics of the stiffeners have been investigated. It has been demonstrated that when their cross-sectional distortion is taken into account the consequent resonance frequencies show drastic changes. The differences are prominently apparent at the frequencies which are actually governed by the rotational stiffness value of the stiffener. Another feature, whose impact on the stiffened plate response has been shown, is the coupling between the transverse and rotational motions of the stiffener. When included in the response calculations it has been found to slightly reduce the resonance

frequencies but its effect on the natural mode shapes is far more significant.

It has been demonstrated once again that the resonance frequencies of N_b bay stiffened plates occur in bunches of N_b if the bays are equal or comparable. When the damping is allowed to take high values, the resonance peaks and troughs merge to form a plateau in the frequency response curve.

The consequence of assuming different core damping and temperature in sandwich plate studies have also been indicated.

It can be concluded that the developed analytical method provides an easy tool for the dynamic analysis of multi-bay stiffened plates provided that they are uniform in thickness and two opposite edges are simply-supported. Bay numbers can easily be increased and their spacing need not be equal. Each stiffener may be different. Multi and combined loading conditions can easily be studied by simply modifying the forcing vector of the final matrix equation (*e.g.*, equation (6.22)). Furthermore, any quantity such as curvature or shear force can easily be obtained at the required position.

SECTION 3: DYNAMIC BEHAVIOUR OF INFINITE, PERIODIC STRUCTURES

CHAPTER 7

THEORY OF FREE WAVE MOTION IN UNIFORM INFINITE PERIODIC STRUCTURES

7.1 Introduction

A periodic structure consists of a number of identical elements, coupled together in identical ways to form the whole structure. An aircraft wing component consisting of a uniform plate reinforced at regular intervals by a set of identical stiffeners is an example of such a structure. The identical elements constituting the system are known as *periodic elements*. In the case of the wing component this can be one plate element between adjacent pairs of stiffeners together with the half stiffeners along each side.

A periodic structure can, in principle, be spatially finite or infinite. Free harmonic wave motion can propagate in a periodic structure such that wave vectors at any two corresponding points A and B in adjacent periodic elements are related by $\text{Vector}_B = e^{\mu}\ \text{Vector}_A$. This is known as Floquet's Principle. Points A and B can be anywhere in the infinite structure as long as no external force lies between them. μ is a frequency dependent quantity and is generally known as the *propagation constant*. In general it has the complex form $\mu = \mu_r + i\mu_i$. The real part μ_r is called the *attenuation constant* and defines the growth or decay of the wave as it propagates. The imaginary part μ_i is denoted as the *phase constant* and represents the phase difference between the motions in adjacent bays. The number of propagation constants which can exist at any given frequency is given by two times the number of degrees of freedom, j_c, at the junction of adjacent periodic elements (*e.g.*, a uniform Euler-Bernoulli beam on simple supports only has one rotational freedom, so $j_c = 1$). At any frequency the propagation constants occur in the pairs of equal and opposite values. For an undamped structure free wave propagation can only take place in the frequency ranges where $\mu_r = 0$. These bands are called the *propagation zones*, and through each range the phase constant μ_i varies between 0 and $\mp\pi$. Outside those bands μ_r is non-zero and μ_i is usually 0 or $-\pi$. These frequency ranges are called the *attenuation zones* and in these ranges the magnitude of the

free wave motion decays as it travels. Over a wide frequency range the propagation and attenuation zones alternate. If the structure is damped, each propagation constant becomes complex and the wave motion inevitably dies out as it moves away from the source.

As Brillouin pointed out [8], wave propagation in periodic structures has long been used by physicists and electrical engineers to study crystals, optics and transmission lines. Studies in engineering structures are relatively recent. Heckl [9] considered a system of beams coupled together to form a regular grillage and showed that waves can propagate in some frequency bands but not in others. By considering the receptances of a periodic element, Mead *et al* [10] included the effects of damping and demonstrated the influence of support stiffnesses on the response. Later Mead [32] discussed the nature of the propagating waves and showed that for positive going waves (*i.e.*, waves travelling from left to right) μ_i can be of any sign though μ_r is strictly negative. These were followed by a study [13] which solved the differential equation of motion directly. In that, Mead studied the harmonic and random responses of periodic beams on flexible supports. In two articles [14] and [15] Mead investigated infinite and periodic structures which were coupled through one or more coordinates. He determined the relations between the limiting frequencies of the bands at which the waves can freely propagate and the natural frequencies of the individual periodic element. Hence he indicated the likelihood of occurrence of the natural frequencies of an N_b bay structure in these bands. Three-layered damped periodic sandwich plates were analysed [27] by considering plates of infinite length but finite width with the pair of infinite edges along the length being simply supported. Periodic stiffeners across the width provided elastic constraints. Abdel-Rahman *et al* [16] used the finite element method in the analysis of two-dimensional periodic structures. Roy *et al* [33] studied the wave attenuation. They used a transfer matrix approach and investigated a periodic beam with a number of tuned cantilevers at regular intervals. Mead [17] approached the problem from a different angle. He viewed the infinite, periodic structure as an infinite uniform structure on which the supports, depending on their characteristics, impose forces and/or moments at regular intervals. He then related those reactions through the propagation constant and

proceeded to obtain the closed form formulae for the propagation constants of Euler-Bernoulli beams, Timoshenko beams and stiffened Euler-Bernoulli plates for various support conditions.

Research into wave propagation in periodic structures has gained momentum as time has progressed. A review of all the work is beyond the scope and intention of this thesis. However, some other useful source can be found in [19].

This chapter follows the approach of [17]. It first outlines the method for analysing wave motion in uniform, infinite, periodic Euler-Bernoulli beams and plates. It then extends the theory to the free wave motion analysis of infinite, periodic three-layered sandwich beams and plates. The structures to be considered in this chapter are those studied in Chapters 2 and 3 so a number of detailed derivations and assumptions still apply. The plate structures are taken as being flat and rectangular and are assumed to be simply-supported along the two infinite opposite edges.

Purely theoretical aspects are considered in this chapter. The application of the method will be carried out in Chapter 8.

7.2 Euler-Bernoulli Beams

7.2.1 Phased Array Receptance Functions

To begin with, consider Figure 55(a). When free wave motion takes place in a periodic structure, the reaction forces exerted by the equi-distant supports can be related through the propagation constant μ. Hence the reaction force at the r^{th} support ('r' is the number of the supports to the right of x = 0) can be expressed as $R_o\, e^{r\mu}$. If μ is purely imaginary these forces constitute a set which can be described as a 'phased array' [17]. In this thesis this term will be used in a more general sense where μ can be a complex quantity. First assume that only one of the forces R_o acts on the beam at x = 0. The complex displacement at the point of application of the force is

given by the infinite-system point response function developed in chapter 2, which is

$$w(0) = R_o \sum_{n=1}^{2} a_n \tag{7.1}$$

When the whole array of forces exists, the total response at point x = 0 is the sum of the response due to R_o, together with the responses due to all the forces to the right and left of R_o. This can conveniently be expressed as

$$w(0) = R_o \sum_{n=1}^{2} a_n + \sum_{r=1}^{\infty} R_r \sum_{n=1}^{2} a_n e^{-k_n(XL)r} + \sum_{\ell=1}^{\infty} R_\ell' \sum_{n=1}^{2} a_n e^{-k_n(XL)\ell} \tag{7.2}$$

where 'ℓ' denotes the number of the support to the left of x = 0 and XL is the length of the periodic element.

It can be seen that the total transverse displacement is the sum of the 'infinite-system point response functions' due to each reaction force. Now,

$$R_r = R_o e^{\mu r}, \quad R_\ell' = R_o e^{-\mu \ell} \tag{7.3}$$

Therefore

$$w(0) = R_o \sum_{n=1}^{2} a_n \left\{ 1 + \sum_{r=1}^{\infty} [e^{(-k_n XL+\mu)r} + e^{(-k_n XL-\mu)r}] \right\} \tag{7.4}$$

The infinite series can be summed to yield

$$w_{OF} = R_o \left\{ \sum_{n=1}^{2} - \frac{\sinh k_n XL}{\cosh \mu - \cosh k_n XL} a_n \right\} = R_o \alpha_{FF} \tag{7.5}$$

The rotational response at point x = 0 can be found in a similar way and can be shown to be

$$\theta(0) = \sum_{\ell=1}^{\infty} R_\ell' \sum_{n=1}^{2} c_n e^{-k_n(XL)\ell} - \sum_{r=1}^{\infty} R_r \sum_{n=1}^{2} c_n e^{-k_n(XL)r} \tag{7.6}$$

The symmetry and antisymmetry arguments of Section 2.2.1 have been taken into consideration in these derivations. The term corresponding

to R_o at x = 0 does not occur in equation (7.6) since the transverse force does not create any rotation at its point of application. The summation of the infinite series of the above equation gives

$$\theta_{OF} = R_o \left\{ \sum_{n=1}^{2} \frac{\sinh \mu}{\cosh \mu - \cosh k_n XL} c_n \right\} = R_o \alpha_{MF} \qquad (7.7)$$

Now consider Figure 55(b) which represents a phased array of moments, rather than of forces, applied to the beam in a manner similar to that above. The total transverse displacement and rotation at x = 0 can be shown to be

$$w_{OM} = M_o \left\{ \sum_{n=1}^{2} \frac{\sinh \mu}{\cosh \mu - \cosh k_n XL} b_n \right\} = M_o \alpha_{FM} \qquad (7.8)$$

$$\theta_{OM} = M_o \left\{ \sum_{n=1}^{2} - \frac{\sinh k_n XL}{\cosh \mu - \cosh k_n XL} d_n \right\} = M_o \alpha_{MM} \qquad (7.9)$$

α_{FF}, α_{MF}, α_{FM}, α_{MM} defined by equations (7.5), (7.7), (7.8) and (7.9) are the generalized, 'phased array receptance functions' of the infinite, periodic Euler-Bernoulli beam. It has been found that $\alpha_{FM} = -\alpha_{MF}$ [17]. The required coefficients a_n's, b_n's, c_n's, d_n's were given in Section 2.2.1.

Now consider the transverse beam displacement at any point 'x' due to the phased arrays of forces (see Figure 55(a) once again). The forces R_1 to R_r cause the displacement at 'x', given by

$$\sum_{r=1}^{\infty} R_r \sum_{n=1}^{2} a_n e^{-k_n(rXL-x)} \qquad (7.10)$$

and the forces R_1' to R_ℓ' cause the transverse displacement

$$\sum_{\ell=1}^{\infty} R_\ell' \sum_{n=1}^{2} a_n e^{-k_n(\ell XL+x)} \qquad (7.11)$$

By using equation (7.3) and also by including the transverse displacement caused by R_o itself, one finds the total transverse displacement at 'x' due to the whole phased array of forces to be

$$w_R(x) = R_o \sum_{n=1}^{2} a_n e^{-k_n x} + R_o \sum_{n=1}^{2} a_n \sum_{r=1}^{\infty} [e^{-(k_n XL-\mu)r+k_n x} + e^{-(k_n XL+\mu)r-k_n x}] \quad (7.12)$$

The infinite series can easily be summed and the whole expression reduces to

$$w_R(x) = -R_o \sum_{n=1}^{2} a_n \frac{\sinh k_n(XL-x) + e^{\mu} \sinh k_n x}{\cosh \mu - \cosh k_n XL} \quad (7.13)$$

For each value of μ and the corresponding frequency and wave number k_n equation (7.13) represents a unique displacement pattern between R_o and R_1. Since free motion takes place, the transverse displacement at any corresponding point in the n^{th} right-hand adjacent bay can be obtained simply by multiplying this expression by $e^{-n\mu}$.

In a similar way, the transverse displacement at 'x' due to a phased array of moments (see Figure 55(b)) can be found. This can be shown to be

$$w_M(x) = -M_o \sum_{n=1}^{2} b_n \frac{\cosh k_n(XL-x) - e^{\mu} \cosh k_n x}{\cosh \mu - \cosh k_n XL} \quad (7.14)$$

7.2.2 Propagation Constants

This section sets up equations for the propagation constants of a periodic, infinite Euler-Bernoulli beam for a variety of support conditions.

7.2.2.1 Simple Supports

If a periodic, infinite beam rests on simple supports, the support reactions are pure transverse forces with no moments and the transverse displacement at each support is zero. The total transverse

displacement at x = 0 due to all the reaction forces is given by equation (7.5). Equating this to zero yields an equation for the propagation constant μ as

$$\cosh \mu = (a_1 * T1 * T4 + a_2 * T2 * T3) / (a_1 * T1 + a_2 * T2) \quad (7.15)$$

where $T1 = \sinh k_1XL$, $T2 = \sinh k_2XL$, $T3 = \cosh k_1XL$, $T4 = \cosh k_2XL$

7.2.2.2 Sliding Supports

In this case the rotation at each support is zero whereas the transverse motion is unrestrained. There are no transverse reaction forces but each support exerts reaction moments on the beam. Equation (7.9) gives the rotation due to the phased array of moments. The propagation constants of this case can be obtained by equating this rotation to zero. The resulting equation takes the form

$$\cosh \mu = (d_1 * T1 * T4 + d_2 * T2 * T3) / (d_1 * T1 + d_2 * T2) \quad (7.16)$$

Notice that the general forms of equations (7.15) and (7.16) are the same.

7.2.2.3 Transversely Elastic Supports

Now suppose that the periodic beam rests on supports which only react with linear transverse elastic forces but with no moments. The deflection of the beam at the r^{th} support location is no longer zero but is equal to the deflection of the support which is given by

$$w(x_r) = -\frac{R_r}{K_t} \quad (7.17)$$

The minus sign stems from the fact that the force exerted on the beam by the support and the force applied on the support by the beam are equal and opposite.

Hence $R_o = -K_t w_{OF}$ and this leads to

$$K_t \alpha_{FF} = -1 \quad (7.18)$$

By substituting α_{FF} from equation (7.5) and then expanding equation (7.18) one obtains a quadratic equation for $\cosh \mu$ as

$$\cosh^2\mu - [(a_1 * T1 + a_2 * T2)K_t + (T3 + T4)]\cosh \mu + [(a_1 * T1 * T4 + a_2 * T2 * T3)K_t + T3 * T4] = 0 \qquad (7.19)$$

7.2.2.4 General Elastic Supports

These supports are characterised by a symmetric stiffness matrix (static or dynamic) which relates the applied forces and moments to the displacements and rotations. The relationship was given by equation (4.27) for an arbitrary support location at $x = x_j$.

Now the displacements and rotations of the beam at $x = 0$ are related to the phased array of forces and moments (R_o and M_o) by

$$\begin{Bmatrix} w(0) \\ w'(0) \end{Bmatrix} = \begin{bmatrix} \alpha_{FF} & \alpha_{FM} \\ \alpha_{MF} & \alpha_{MM} \end{bmatrix} \begin{Bmatrix} R_o \\ M_o \end{Bmatrix} \qquad (7.20)$$

Since the beam and supports are joined, one can modify equation (4.27) for the support $x = 0$ by considering that $R_{x_j} = -R_o$, $M_{x_j} = -M_o$, $w(x_j) = w(0)$, $w'(x_j) = w'(0)$. This modified equation (4.27) can be combined with equation (7.20) to give

$$\begin{Bmatrix} R_o \\ M_o \end{Bmatrix} = -\begin{bmatrix} K_t & K_c \\ K_c & K_r \end{bmatrix} \begin{bmatrix} \alpha_{FF} & \alpha_{FM} \\ \alpha_{MF} & \alpha_{MM} \end{bmatrix} \begin{Bmatrix} R_o \\ M_o \end{Bmatrix} \qquad (7.21)$$

which can be expanded and rearranged to yield

$$\begin{bmatrix} K_t\alpha_{FF} + K_c\alpha_{MF} + 1 & K_t\alpha_{FM} + K_c\alpha_{MM} \\ K_c\alpha_{FF} + K_r\alpha_{MF} & K_c\alpha_{FM} + K_r\alpha_{MM} + 1 \end{bmatrix} \begin{Bmatrix} R_o \\ M_o \end{Bmatrix} = 0 \qquad (7.22)$$

Free wave motion occurs at frequencies and μ values which make the determinant of the matrix vanish. Expansion of the determinant gives

$$(K_t K_r - K_c^2)(\alpha_{FF}\alpha_{MM} - \alpha_{FM}\alpha_{MF}) + K_t\alpha_{FF} + K_r\alpha_{MM} + 1 = 0 \qquad (7.23)$$

By making use of $\alpha_{FM} = -\alpha_{MF}$ and inserting the expressions for the α's, a quadratic equation for $\cosh \mu$ can be obtained:

$$\begin{aligned}\cosh^2\mu - [X1 * T1 + X2 * T2 + T3 + T4] \cosh \mu \\ + [-X4 + (1 + X4)*(T3 * T4) + X3 * T1 * T2 \\ + X1 * T1 * T4 + X2 * T2 * T3] = 0 \qquad (7.24)\end{aligned}$$

where $X1 = K_t a_1 + K_r d_1$

$X2 = K_t a_2 + K_r d_2$

$X3 = (a_1 d_2 + a_2 d_1) K_{tot}^2$

$X4 = 2a_1 d_1 K_{tot}^2$

$K_{tot}^2 = K_t K_r - K_c^2$.

In the evaluation of equation (7.24) use has been made of the relation $a_n d_n = b_n c_n$ where $n = 1,2$ [17].

7.3 Euler-Bernoulli Plates

This section extends the theory of free wave propagation for one-dimensional Euler-Bernoulli beams to two-dimensional Euler-Bernoulli plates. They are the uniform, flat, rectangular plates analysed in Chapter 3. The derivations undertaken there and the assumptions made still apply here. Two opposite, infinite edges, which are L_y apart, are simply-supported and all the forcing and response quantities are assumed to vary sinusoidally between those edges.

7.3.1 Phased Array Receptance Functions

Consider Figure 55(c) which represents the periodic, infinite plate under the action of distributed line forcing having the general form $R(y) = R\sin k_y y$ where $k_y = m\pi/L_y$. By considering the corresponding infinite-system line response functions of all the phased array of line forces, the transverse displacement at $x = 0$ can be found to be

$$w(0)\sin k_y y = \Big\{R_o \sum_{n=1}^{2} a_n + \sum_{r=1}^{\infty} R_r \sum_{n=1}^{2} a_n\, e^{-k_n(XL)r} + \sum_{\ell=1}^{\infty} R_\ell' \sum_{n=1}^{2} a_n\, e^{-k_n(XL)\ell}\Big\} \sin k_y y \qquad (7.25)$$

Now the line forces are related by

$$R_r \sin k_y y = R_o\, e^{\mu r} \sin k_y y, \quad R_\ell' \sin k_y y = R_o\, e^{-\mu \ell} \sin k_y y \qquad (7.26)$$

Hence the summation of the infinite series and further manipulations give

$$w_{OF} \sin k_y y = R_o \Big\{ \sum_{n=1}^{2} \frac{-\sinh k_n XL}{\cosh \mu - \cosh k_n XL}\, a_n \Big\} \sin k_y y = R_o \alpha_{FF} \sin k_y y \qquad (7.27)$$

Comparison of equations (7.5) and (7.27) shows that the final forms of the corresponding phased array receptance functions, α_{FF}'s, are the same. Furthermore, the other phased array receptance functions α_{MF}, α_{FM}, α_{MM} of Euler-Bernoulli plates are found to have the same forms as those of Euler-Bernoulli beams given by equations (7.7), (7.8) and (7.9) respectively. The plate coefficients a_n's, b_n's, c_n's and d_n's required in these expressions are those given by equation (3.10).

7.3.2 Propagation Constants

Since the phased array receptance functions of infinite periodic Euler-Bernoulli beams and plates have the same forms, it follows that the propagation constants formulae derived for Euler-Bernoulli beams in Section 7.2.2 apply also to the corresponding cases of Euler-Bernoulli plates. However, the support stiffnesses defined by K_t, K_r and K_c must now contain information about the dynamic characteristics and cross-sectional distortion of the stiffeners, and these are the functions of the y-wise wave number of the motion, k_y. This has been considered in Appendix C in detail.

7.4 Three-Layered Sandwich Beams

This section extends the wave propagation theory for periodic Euler- Bernoulli beams to periodic three-layered sandwich beams.

7.4.1 Phased Array Receptance Functions

It was explained in Chapter 2 that the cross-section of a three-layered sandwich beam has three coupled degrees of freedom. The generalized phase array receptance functions will therefore contain sums of three terms but otherwise will have the same general forms as those of the Euler-Bernoulli beams. These functions for the sandwich beams are given by the following equations:

$$w_{OF} = R_o\left\{\sum_{n=1}^{3} \frac{-\sinh k_n XL}{\cosh \mu - \cosh k_n XL} a_n\right\} = R_o \alpha_{FF}$$

$$\theta_{OF} = R_o\left\{\sum_{n=1}^{3} \frac{\sinh \mu}{\cosh \mu - \cosh k_n XL} c_n\right\} = R_o \alpha_{MF}$$

$$w_{OM} = M_o\left\{\sum_{n=1}^{3} \frac{\sinh \mu}{\cosh \mu - \cosh k_n XL} b_n\right\} = M_o \alpha_{FM}$$

$$\theta_{OM} = M_o\left\{\sum_{n=1}^{3} \frac{-\sinh k_n XL}{\cosh \mu - \cosh k_n XL} d_n\right\} = M_o \alpha_{MM} \qquad (7.28)$$

where a_n's, b_n's, c_n's and d_n's were given by equations (2.27), (2.30) and (2.31). It is again found that $\alpha_{MF} = -\alpha_{FM}$.

7.4.2 Propagation Constants

These are found in the same way as the propagation constants for the uniform Euler-Bernoulli beam but the three-term phased array receptance functions of equation (7.28) are used instead of the two term functions for the Euler-Bernoulli beam. It follows that the

three-layered sandwich beam equations for the propagation constants are one order higher than the corresponding equations for the Euler-Bernoulli beam. The detailed steps of the analysis will not be presented but the final equations are given.

7.4.2.1 Simple Supports

$$(-a_1 * TT1 - a_2 * TT2 - a_3 * TT3)\cosh^2\mu + [a_1 * TT1 * (TT5 + TT6) + a_2 * TT2 * (TT4 + TT6) + a_3 * TT3 * (TT4 + TT5)]\cosh\mu - [a_1 * TT1 * TT5 * TT6 + a_2 * TT2 * TT4 * TT6 + a_3 * TT3 * TT4 * TT5] = 0 \qquad (7.29)$$

where $TT1 = \sinh k_1XL$ $TT2 = \sinh k_2XL$ $TT3 = \sinh k_3XL$
$TT4 = \cosh k_1XL$ $TT5 = \cosh k_2XL$ $TT6 = \cosh k_3XL$.

Note that equation (7.29) is quadratic in cosh μ, whereas equation (7.15) for the Euler-Bernoulli beam was linear in cosh μ.

7.4.2.2 Sliding Supports

$$(-d_1 * TT1 - d_2 * TT2 - d_3 * TT3)\cosh^2\mu + [d_1 * TT1 * (TT5 + TT6) + d_2 * TT2 * (TT4 + TT6) + d_3 * TT3 * (TT4 + TT5)]\cosh\mu - [d_1 * TT1 * TT5 * TT6 + d_2 * TT2 * TT4 * TT6 + d_3 * TT3 * TT4 * TT5] = 0 \qquad (7.30)$$

7.4.2.3 Transversely Elastic Supports

$$\cosh^3\mu + C_2\cosh^2\mu + C_1\cosh\mu + C_0 = 0 \qquad (7.31a)$$

where

$$C_0 = \{-K_t[a_1 * TT1 * TT5 * TT6 + a_2 * TT2 * TT4 * TT6 + a_3 * TT3 * TT4 * TT5] - TT4 * TT5 * TT6\} \qquad (7.31b)$$

$$C_1 = \{K_t[a_1 * TT1 * (TT5 + TT6) + a_2 * TT2 * (TT4 + TT6) + a_3 * TT3 * (TT4 + TT5)] + TT4 * TT5 + TT4 * TT6 + TT5 * TT6\} \quad (7.31c)$$

$$C_2 = \{-K_t(a_1 * TT1 + a_2 * TT2 + a_3 * TT3) - (TT4 + TT5 + TT6)\} \quad (7.31d)$$

7.4.2.4 General Elastic Supports

At its point of attachment to the beam, we assume that the plate does not move in the x-direction. Therefore in this thesis the stiffnesses relating to the x-wise motion of the stiffener are ignored. Appendix D details the derivation of propagation constants equation for this complicated case. The resultant form is cubic in cosh μ and is given by

$$C_3 \cosh^3\mu + C_2 \cosh^2\mu + C_1 \cosh \mu + C_0 = 0 \quad (7.32a)$$

where

$$\begin{aligned} C_0 = \{K_{tot}^2 [&-(a_1 * d_1 + a_2 * d_2 + a_3 * d_3) * TT4 * TT5 * TT6 \\ &- (a_1 * d_2 + a_2 * d_1) * TT1 * TT2 * TT6 \\ &- (b_1 * c_2 + b_2 * c_1) * TT6 \\ &- (a_1 * d_3 + a_3 * d_1) * TT1 * TT3 * TT5 \\ &- (b_1 * d_3 + b_3 * d_1) * TT5 \\ &- (a_2 * d_3 + a_3 * d_2) * TT2 * TT3 * TT4 \\ &- (b_2 * c_3 + b_3 * c_2) * TT4] \\ &- XX1 * TT1 * TT5 * TT6 - XX2 * TT2 * TT4 * TT6 \\ &- XX3 * TT3 * TT4 * TT5 - TT4 * TT5 * TT6\} = 0 \end{aligned} \quad (7.32b)$$

$$C_1 = \{K_{tot}^2\ [a_1 * d_1 * (-TT5 * TT6 + TT4 * (TT5 * TT6))$$
$$+\ a_2 * d_2 * (-TT4 * TT6 + TT5 * (TT4 + TT6))$$
$$+ a_3 * d_3 * (-TT4 * TT5 + TT6 * (TT4 + TT5))$$
$$+ (a_1 * d_2 + a_2 * d_1)*(TT1 * TT2)$$
$$+ (a_1 * d_3 + a_3 * d_1)*(TT1 * TT3)$$
$$+ (a_2 * d_3 + a_3 * d_2)*(TT2 * TT3)$$
$$+ b_1 * c_2 + b_2 * c_1$$
$$+ b_1 * c_3 + b_3 * c_1 + b_2 * c_3 + b_3 * c_2]$$
$$+ XX1 * TT1 * (TT5 + TT6) + XX2 * TT2 * (TT4 + TT6)$$
$$+ XX3 * TT3 * (TT4 + TT5) + TT4 * TT5 + TT4 * TT6$$
$$+ TT5 * TT6\} \qquad (7.32c)$$

$$C_2 = \{K_{tot}^2\ [a_1 * d_1 * (TT5 + TT6 - TT4)$$
$$+\ a_2 * d_2 * (TT4 + TT6 - TT5)$$
$$+ a_3 * d_3 * (TT4 + TT5 - TT6) + (b_1 * c_2 + b_2 * c_1) * TT6$$
$$+ (b_1 * c_3 + b_3 * c_1) * TT5 + (b_2 * c_3 + b_3 * c_2) * TT4]$$
$$- XX1 * TT1 - XX2 * TT2 - XX3 * TT3 - (TT4 + TT5 + TT6)\} \qquad (7.32d)$$

$$C_3 = \{K_{tot}^2(-a_1 * d_1 - a_2 * d_2 - a_3 * d_3 - b_1 * c_2 - b_2 * c_1$$
$$- b_1 * c_3 - b_3 * c_1 - b_2 * c_3 - b_3 * c_2) + 1\} \qquad (7.32e)$$

where $XX1 = K_t a_1 + K_r d_1$ $\qquad XX2 = K_t a_2 + K_r d_2$

$XX3 = K_t a_3 + K_r d_3$.

TT1 to TT6 were given by equation (7.29) and K_{tot}^2 was given by equation (7.24).

Notice that equation (7.32) is cubic whereas equation (7.24) for the Euler-Bernoulli beam was quadratic.

7.5 Three-Layered Sandwich Plates

This section combines the information obtained about infinite, periodic Euler-Bernoulli beams and plates and three-layered sandwich beams to deduce the theory of free wave propagation in three-layered sandwich plates. Like the Euler-Bernoulli plates the three-layered

sandwich plates have two opposite infinite edges which are simply-supported. The externally applied line forces and corresponding response quantities vary sinusoidally across the plate. The sandwich plates to be analysed in this section are those which were studied in Chapter 3. Therefore the detailed derivations and assumptions will not be repeated.

7.5.1 Phased Array Receptance Functions

Sections 7.2 and 7.3 have shown that if the degrees of freedom of the cross-section at periodic junctions of beams and plates are the same in number, their phased array receptance functions have the same general forms. It follows that since the three-layered sandwich plates have the same three degrees of freedom at a periodic junction as the three-layered sandwich beam; phased array receptance functions of the plate will have the same forms as those of the beam given by equation (7.28).

The sandwich plate coefficients a_n's, b_n's, c_n's and d_n's are given by equations (A.12), (A.16), (A.13) and (A.17) respectively.

7.5.2 Propagation Constants

Following the arguments already outlined, it can be concluded that the propagation constant equations for various support conditions of three-layered sandwich beams are also valid for the corresponding cases of periodic three-layered sandwich plates. However, as in the case of periodic Euler-Bernoulli plates, the support stiffnesses must now include dynamic and distortional characteristics, and the effect of the wave number k_y.

7.6 Conclusions

This chapter has developed the method of phased array receptance functions to set-up equations for the propagation constants of uniform, infinite, periodic structures on a variety of supports. Euler-Bernoulli beams and plates, as well as three-layered sandwich beams and plates, have been analysed. The approach has been based on the 'Infinite-System Point and Line Response Functions' of Chapters 2 and 3.

An infinite, periodic structure has been viewed as a uniform infinite structure on which the supports exert forces and/or moments at regular intervals in proportion to the support stiffnesses. Adjacent reactions have been related through the propagation constant of the structure and the total response has been expressed in terms of these reactions.

It has been shown that equations for the required propagation constants can be obtained merely by satisfying the boundary conditions at a single support location. Simple supports, sliding supports, supports which provide only transverse linear constraints and supports which provide general linear constraints have been considered. The method developed can also conveniently include the coupling effects of an asymmetric support.

CHAPTER 8

CALCULATIONS RELATING TO FREE WAVE MOTION IN UNIFORM INFINITE PERIODIC STRUCTURES

8.1 Introduction

This chapter presents computed results relating to the free wave motion in uniform, infinite, periodic structures. It is confined to the applications of the theoretical concepts developed in Chapter 7 and considers the same structures. The examples given are for Euler-Bernoulli beams and plates and for three-layered sandwich beams and plates having equal face-plates.

Section 8.2 considers the phased array receptance functions of the different structures and Section 8.3 considers the propagation constants of those structures with various support conditions. Both undamped and damped structures are investigated. The effects of the structural properties on the phased array receptance functions are illustrated. The influence of the support conditions and structural properties on the propagation constants are demonstrated.

8.2 Phased Array Receptance Functions

8.2.1 Euler-Bernoulli Beams

The following non-dimensional parameters are introduced for Euler-Bernoulli beams.

ND Frequency : $2\pi f(\rho h(XL)^4/EI)^{1/2}$

ND α_{PP} : $\alpha_{PP}\ (EI/XL^3)$

ND α_{MM} : $\alpha_{MM}\ (EI/XL)$

ND α_{PM} : $\alpha_{PM}\ (EI/XL^2)$

where the symbols have the meanings as previously defined.

Figure 56 shows how the magnitude of the non-dimensional phased array receptance function, α_{PF}, of the beam varies with the square-root of non-dimensional frequency. α_{PF} is determined from equation (7.5) and is plotted for four different assigned values of the purely imaginary propagation constant μ (*i.e.*, phase constant). A material loss factor of $\eta = 0.001$ has been assigned.

The curve corresponding to $\mu = 0$ has a peak at frequency $\sqrt{(2\pi)^2}$ and a trough at $\sqrt{(4.73)^2}$. The curve for $\mu = -i\pi$ has its peaks at frequencies $\sqrt{\pi^2}$ and $\sqrt{(3\pi)^2}$ and its trough at $\sqrt{(7.85)^2}$.

These values can be identified with the natural frequencies of isolated periodic beam elements. When $\mu = 0$, the j^{th} peaks of α_{PF} occur at the j^{th} even natural frequencies of an isolated periodic beam element on simple supports. The frequencies at which α_{PF} descends to a trough are the j^{th} odd natural frequencies of an isolated periodic element which is clamped at each end. When $\mu = -i\pi$ the j^{th} peak frequencies of α_{PF} are the j^{th} odd natural frequencies of the isolated simply-supported periodic beam element, whereas the trough frequencies are the j^{th} even natural frequencies of the same element with clamped ends.

The peak frequencies of the α_{PF} curves which correspond to $\mu = -i\pi/2$ and $\mu = -i\pi/4$ can also be related to the isolated periodic element natural frequencies. It is found that when $\mu = -i\pi/2$ the j^{th} peak frequencies are $1/4^{th}$ of the j^{th} odd natural frequencies of isolated simply supported periodic element and the j^{th} trough frequencies are $1/4^{th}$ of the j^{th} even natural frequencies of the same element with clamped ends. The j^{th} peak frequencies of $\mu = -i\pi/4$ are $((4j - 3)\pi)^2/16$ if j is odd and $((4j - 1)\pi)^2/16$ if j is even. Therefore the first two peak frequencies of the case $\mu = -i\pi/4$ are $1/16^{th}$ of the first and the seventh natural frequencies of isolated periodic element with simply-supported ends.

The existence of peaks and troughs in the α_{PF} curve at certain frequencies can best be explained with the help of Figures 57 and 58. These give the normalized vibration displacement of four adjacent bays of the beam due to the phased array of forces at those non-dimensional

frequencies. These displacement modes have been calculated by using equation (7.13). The numbered points 0,1,2,3,4 on the abscissa identify the points at which the forces of the phased array are acting.

First consider Figure 57 which is for $\mu = 0$. At frequency $(2\pi)^2$ the motion is a standing wave and is anti-symmetric about each force. The opposite inertial loading on either side of a force leads to zero nett reaction force at those locations. Now there is no displacement at the forced points in this case. Hence the ratio of w/F (*i.e.*, α_{FF}) at each force location remains finite but high. On the other hand at frequency $(4.73)^2$ the wave motion is symmetric about the forces. There is a non-zero reaction force from the inertial loading but still no displacement. Therefore the ratio of w/F (and consequently α_{FF}) goes to zero.

Figure 58 shows the displacement modes of the same beam at two different frequencies when $\mu = -i\pi$. Again for both frequencies the displacements are zero at the force locations. It can be seen that for the frequency $(7.85)^2$ the wave motion is symmetric about these points but for π^2 it is anti-symmetric. Thus, following the same arguments as given in the above paragraph, it can be concluded that α_{FF} will have a peak at π^2 but a trough at $(7.85)^2$ for $\mu = -i\pi$.

The variation of the non-dimensional phased array receptance function α_{MM} with frequency is shown in Figure 59 for the same frequency range and the same μ values as α_{FF}. The α_{MM} values have been obtained from equation (7.9) with $\eta = 0.001$. A comparison of Figures 56 and 59 reveals that for a given phase constant both α_{FF} and α_{MM} reach peaks at the same frequencies but their troughs occur at different frequencies. It is found that the trough frequencies of α_{MM} for $\mu = 0$ are the j^{th} even natural frequencies of an isolated periodic element with clamped ends. Those for $\mu = -i\pi$ are the j^{th} odd natural frequencies of the same element.

The existence of peaks and troughs in the α_{MM} curves can be explained with the help of Figures 60 and 61. They represent the normalized displacement modes of four adjacent bays of the beam due to

the phased arrays of reaction moments and have been found using equation (7.14).

Figure 60 shows the modes for $\mu = 0$. At frequency $(2\pi)^2$ the inertial moments from either side of the excitation points are equal and opposite so they cancel each other. There is no rotation at these points, so the ratio of θ/M (*i.e.*, α_{MM}) remains finite but high. At frequency $(7.85)^2$ the inertial moments from either side of the excitation points are equal and in the same direction so do not cancel. However there is still no rotation and therefore the ratio of θ/M (and consequently α_{MM}) becomes zero.

By referring to Figure 61 which is for $\mu = -i\pi$ and using similar arguments one can explain the existence of the α_{MM} peak at the frequency π^2 and the trough at the frequency $(4.73)^2$.

It is interesting to note that at frequencies of $(j\pi)^2$ the infinite, periodic beams of Figures 60 and 61 have standing wave modes which are the j^{th} modes of isolated periodic element with sliding ends. This is expected because $(j\pi)^2$ is the non-dimensional j^{th} natural frequency of isolated periodic element with sliding ends.

The variation with frequency of the non-dimensional magnitude of the phased array receptance function α_{FM} is shown in Figure 62 for the same frequency range of α_{FF} and α_{MM} curves but for only three different purely imaginary μ values ($\mu = -i\pi/4$, $\mu = -i\pi/2$, $\mu = -i\pi$). Inspection of equation (7.8) reveals that α_{FM} is zero when $\mu = 0$, so the curve corresponding to $\mu = 0$ is excluded. Since $\alpha_{MF} = -\alpha_{FM}$, Figure 62 also represents α_{MF}. η is again 0.001. By comparing it with Figures 56 and 59, it can be seen that the peak frequencies for a given μ are the same for all four phased array receptance functions.

8.2.2 Euler-Bernoulli Plates

The following non-dimensional parameters are used in this section:

ND Frequency : $2\pi f(\rho h(XL)^4/D)^{1/2}$

ND α_{FF} : $\alpha_{FF}\ (D/XL^3)$

where the symbols have been defined in Chapters 3 and 7.

The plate is simply-supported along the infinite edges. A phased array of spatially-sinusoidal distributions of force is assumed to act across the finite width L_y. The distribution has the form $F(y) = F_o \sin(m\pi/L_y)$ with a single half-wave ($m = 1$). The aspect ratio of each bay (L_y/XL) is two and Poisson's ratio is $\nu = 0.3$.

Figure 63 shows how the non-dimensional magnitude of α_{FF} varies with frequency for $\mu = 0$. The peak at $\sqrt{(2.47)}$ corresponds to the cut-on frequency of the plate (see Chapter 3). At this frequency the whole plate resonates to a large amplitude when the array of forces, all in phase ($\mu = 0$), acts on the plate. The peak at $\sqrt{(6.48)^2}$ corresponds to the second natural frequency of an isolated periodic plate element with all edges simply-supported. The trough at $\sqrt{(4.88)^2}$ corresponds to the first natural frequency of an isolated periodic plate element with two edges along the width clamped and other two edges along the length simply-supported.

No other curves of receptance functions are shown for the plate. However, it has been found that most of the features observed on the Euler-Bernoulli beam curves are also found on the plate curves and can be explained in a similar manner.

8.2.3 Three-Layered Sandwich Beams

The following non-dimensional parameters are used in this section:

*ND Frequency : $2\pi f(m_s(XL)^4/D_t)^{1/2}$

ND α_{FF} : $\alpha_{FF}(D_t/XL^3)$

The terms within these parameters have the meanings defined in Chapters 2 and 7. Equations (7.28) have been used to find the phased array receptance functions.

Computed curves of the phased array receptance functions for sandwich beams show a similar variation with frequency and μ to the curves for the Euler-Bernoulli beams and plates.

For a given μ value the receptances pass through a series of peaks and troughs and for a given μ value α_{FF}, α_{MM}, α_{FM} (= $-\alpha_{MF}$) go to peaks at the same frequency.

Figure 7 which gives the core properties shows that the core shear modulus G_c and core loss factor β are strongly dependent on temperature and frequency hence can significantly vary under different operating conditions.

Figure 64 shows the influence of changing the core shear modulus, G_c, on $|\alpha_{FF}|$. μ is 0 and the core loss factor is $\beta = 0.001$. Three different cases are considered. In the first two cases core shear moduli (G_c's) corresponding to the extreme frequencies of the range studied are computed from Figure 7 for a temperature of T = 18 ^oC. The beam is allowed to take these constant values ($G_c = 2.8*10^6$ [N/m^2] and $G_c = 3.1*10^7$ [N/m^2]) throughout the frequency range. Then the G_c is allowed to vary according to the frequency dependence of Figure 7 at the same temperature.

---

*For a beam with h = 0.87 [mm], h_c = 1.1 [mm], $E = 7*10^{10}$ [N/m^2] XL = 0.172 [m], m_s = 5.798 [kg/m^2], ND Frequency is $\cong$ 0.16 f.

It can be seen from Figure 64 that the increasing G_c increases all the peak and trough frequencies. The array of forces which are in phase ($\mu = 0$) create finite transverse acceleration on the beam. At very low frequencies this finite harmonic acceleration leads to very high transverse displacement. Hence when the frequency is very low, α_{FF} goes to infinity.

Figure 65 shows the effects of different core damping values on $|\alpha_{FF}|$ for a three-layered sandwich beam when $\mu = -i\pi$. Two different core loss factors $\beta = 0.001$ and $\beta = 1$ have been considered. In both curves the core shear modulus is taken as frequency dependent from Figure 7 corresponding to a temperature of $T = 18^{o}C$.

The peak frequencies correspond to the fundamental resonance frequencies of an isolated periodic element which is simply-supported. Increasing the core damping is seen to increase the element resonance frequency. This has formerly been observed by Mead *et al* [25]. Higher β also flattens the otherwise sharp peak.

8.2.4 Three-Layered Sandwich Plates

Curves of phased array receptance functions for the sandwich plate are very similar in form to those of the Euler-Bernoulli plate and are not presented here. As before, all four phased array receptance functions peak at the same frequencies when the assigned phase constant is the same.

8.3 Propagation Constants

8.3.1 Euler-Bernoulli Beams

In this section the support stiffness values are non-dimensionalized as follows:

ND Transverse Stiffness KT : $(K_t(XL)^3)/EI$

ND Rotational Stiffness KR : $(K_r(XL))/EI$

where the symbols have meanings as previously defined.

8.3.1.1 Simple and Sliding Supports

The propagation constants of free wave motion in periodic, undamped Euler-Bernoulli beams with simple supports and sliding supports are shown in Figures 66(a) and 66(b) against the non-dimensional frequency. The propagation constants of these cases have been found by using equations (7.15) and (7.16) respectively.

With these support conditions there is only one degree of freedom at each support (rotation at a simple support and transverse displacement at a sliding support). There is therefore only one pair of propagation constants for each case.

When the attenuation constant is non-zero wave motion attenuates as it progresses and no energy is propagated. Frequency zones in which this occurs are called the *attenuation zones*. When the attenuation constant is zero, wave motion can freely propagate. Frequency zones in which this can occur are called the *propagation zones*. The limiting frequencies of the propagation zones are called the *bounding frequencies*. As the frequency changes in the propagation zones, the phase constant varies between 0 and $-\pi$.

Figures 66(a) and 66(b) show that the propagation zones of the beam with simple supports and those of the beam with sliding supports complement each other. In the beam with sliding supports, free waves can propagate from zero frequency.

The lower bounding frequencies of the j^{th} propagation zones of the undamped beam with simple supports are the j^{th} natural frequencies of an isolated simply-supported periodic beam element. The upper bounding frequencies of the same zones are the j^{th} natural frequencies of an isolated periodic element with clamped ends. The mode shapes of the infinite, periodic simply-supported Euler-Bernoulli beam at the bounding frequencies of the first two propagation zones are those given in Figures 57 and 58.

Similar features apply to the bounding frequencies of a periodic beam with sliding supports. The upper bounding frequency of the j^{th} propagation zone is the corresponding natural frequency of an isolated periodic element with sliding ends. The lower bounding frequency of the j^{th} propagation zone ($j \geq 2$) is the $(j-1)^{st}$ natural frequency of an isolated periodic element with clamped ends. The mode shapes of the infinite, periodic beam at the upper bounding frequency of the first zone and at the lower bounding frequency of the second zone of propagation constants with sliding supports are those presented in Figure 61. Figure 60 depicts the mode shapes at the upper bounding frequency of the second zone and at the lower bounding frequency of the third zone.

8.3.1.2 Transversely Elastic Supports

Now allow each support of the periodic Euler-Bernoulli beam to have a finite transverse stiffness but no rotational stiffness. A non-dimensional transverse stiffness of KT = 10000 is considered in this section. The corresponding propagation constants of the undamped beam are found from equation (7.19). The propagation constants obtained are plotted against the non-dimensional frequency and are compared with those of a simply-supported beam in Figure 67.

When both deflection and rotation are permitted at each support there are two degrees of freedom at each periodic junction and the beam has two propagation constants at each frequency. Up to the frequency of $\cong 185$ the value of the transverse stiffness, KT, governs the *upper* bounding frequencies of the propagation zones. It can be seen from Figure 67 that when KT = 10000 the upper bounding frequencies are then less than those of the beam with simple supports. The reduction of upper bounding frequencies is progressively more pronounced in successively higher propagation zones. Since both cases have no rotational constraint the lower bounding frequencies of the first four propagation zones are the same.

In a very narrow frequency range around frequency $\cong 185$ both pairs of propagation constants of KT = 10000 have the same real part but

their phase constants are the complex-conjugates of each other. (In Figure 67 they are both plotted as negative.) This range is called a Complex Conjugate Zone (CCZ) [17] and is not a free propagation zone. At frequencies above the CCZ the *lower* bounding frequencies of the periodic beam are governed by KT.

8.3.1.3 General Elastic Supports

The propagation constants of a periodic Euler-Bernoulli beam with elastic supports which provide both transverse and rotational constraints are found from equation (7.24) and are compared with the propagation constants of the simply-supported beam in Figure 68. The non-dimensional elastic support stiffnesses are taken as KT = 10000 and KR = 10. There is no stiffness coupling at the supports.

The effect of increasing the rotational stiffness, KR, is to increase the *lower* bounding frequencies below the CCZ. After the CCZ (which is at about the frequency ≅ 160) the roles of KT and KR are reversed. As before, KT governs the lower bounding frequencies and KR in this case governs the upper bounding frequencies.

8.3.2 Euler-Bernoulli Plates

8.3.2.1 Simple and Sliding Supports

The plates to be considered here have the same bay dimensions and properties as those analysed in Section 8.2.2.

The propagation constants of periodic Euler-Bernoulli plates with simple supports and sliding supports are also found from equations (7.15) and (7.16) respectively and are presented in Figures 69(a) and 69(b). Like Euler-Bernoulli beams each case has a single propagation constant and again they complement each other, the propagation zones of one case being the attenuation zones of the other. This is with the exception of the frequency range below frequency ≅ 10. Wave

propagation in the plate with sliding supports does not start from zero frequency as it does in beams on sliding supports. Rather it starts from the cut-on frequency of the plate ($\cong 2.47$).

8.3.3 Three-Layered Sandwich Beams

8.3.3.1 Simple and Sliding Supports

The propagation constants of undamped periodic sandwich beams with simple supports and sliding supports are obtained from equations (7.29) and (7.30) and are shown in Figures 70(a) and 70(b). The dimensions and the material properties are the same as in Section 8.2.3.

Each beam now has two pairs of propagation constants but the propagation zones of sandwich beams with simple supports and sliding supports no longer complement each other.

However the lower bounding frequencies of propagation zones of beams with simple supports and the upper bounding frequencies of corresponding propagation zones of beams with sliding supports are still the same. This is due to the fact that the natural frequencies of simply-supported and sliding-sliding isolated periodic sandwich beam elements are the same.

It is also evident from Figure 70(b) that the starting frequency of the first propagation zone with sliding support is zero.

8.3.3.2 The Effects of Including Core Damping: Simple Supports

Figure 71 shows the effects of core damping on the propagation constants of the simply-supported three-layered sandwich beams by considering two different core loss factors $\beta = 0$ and $\beta = 1$. When damping is present neither the attenuation nor the phase constants ever become zero. Furthermore the phase constants never cover any range with a value of $\mu = -i\pi$. Nevertheless, particular changes in

the propagation constants of the damped beam can be associated with the beginning or end of a propagation zone. Through that zone one of the attenuation constants dips to minimum and one of the phase constants shows a steep change.

The upper attenuation constant of Figure 71 (which represents a very rapidly attenuating wave) is increased by the inclusion of damping in the core of the beam.

8.3.3.3 The Effects of Temperature: Simple Supports

Figure 72 shows the influence of temperature on the propagation constants of the simply-supported three-layered undamped sandwich beams. Frequency dependent G_c values corresponding to the temperatures T = 15°C and T = 18°C are obtained from Figure 7 and are used in the generation of the curves. Figure 72 shows that the propagation zones of a sandwich beam with softer core (corresponding to T = 18°C) take place at lower frequencies than the zones of a beam with stiffer core (corresponding to T = 15°C). Also the upper attenuation constant is less when T = 18°C.

8.3.4 Three-Layered Sandwich Plates

8.3.4.1 Simple and Sliding Supports

The following non-dimensional parameter is used in this section:

ND Frequency : $2\pi f(m_s(XL)^4/D_t)^{1/2}$.

The terms within this parameter have the meanings defined in Chapters 3 and 7.

The sinusoidal distribution of displacement across the width is the same as that considered for the Euler-Bernoulli plates. The cases studied consider a periodic plate element with an aspect ratio of two. Poisson's ratio is $\nu = 0.3$.

Propagation constants curves for sandwich plates with simple supports and sliding supports are determined by using equations (7.29) and (7.30) respectively and are presented in Figures 73(a) and 73(b) against the non-dimensional frequency.

The curves for the two different support conditions do not complement each other as in the case of three-layered sandwich beams. The upper bounding frequencies of the plate with sliding supports and the corresponding lower bounding frequencies of the plate with simple supports are, however, the same for the reasons given for sandwich beams. With sliding supports propagation starts from the plate cut-on frequency.

8.3.5 The Effects of the Stiffener Properties on the Propagation Constants of Three-Layered Sandwich Plates

Next investigated are the effects of the stiffener properties on the propagation constants by considering a particular sandwich-plate/stiffener configuration. The dimensions of the periodic sandwich plate element are the same as those of an element of the six-bay sandwich plate considered in Section 6.3.2.1. The same material properties are also used. The dimensions and material properties of the stiffeners are given in Appendix C. The required stiffness values of the stiffener (*i.e.*, K_t, K_r and K_c) for each case to be considered have been computed by using the procedures outlined in Appendix C. The propagation constants are determined from equation (7.32).

8.3.5.1. The Stiffener with Pure Stiffnesses and No Inertia

Figure 74 shows the propagation constants when the inertia, stiffness coupling and the cross-sectional distortion of the stiffeners are all excluded from the analysis. The stiffeners are assumed to possess transverse and rotational stiffness only.

There are three propagation constants at any frequency. One of the attenuation constants is considerably higher than the other two. There is a Complex Conjugate Zone at very low frequencies ($\cong$ 20 to 90 Hz) and despite its existence it is found that the lower bounding frequency of the first propagation zone is still controlled by the value of K_r. This appears to contradict the findings on Euler-Bernoulli beams and certainly deserves greater attention. It is also found that above $\cong$ 530 Hz the value of the upper bounding frequency is affected by K_r but not by K_t.

8.3.5.2 The Effects of Including the Rotational Inertia of the Stiffener

Next, the rotational inertia is added in the analysis. The resulting propagation constants are presented in Figure 75. As compared to Figure 74 the differences are not significant at low frequencies but the upper bounding frequency of the second propagation zone is reduced. This is because of the fact that the inclusion of the rotational inertia reduces the dynamic rotational stiffness. Since the upper bounding frequency of second propagation zone is controlled by the value of K_r (see previous section), addition of the stiffener rotational inertia lowers the bounding frequency.

8.3.5.3 The Effects of Including the Transverse Inertia of the Stiffener

Figure 76 shows the propagation constants when the effect of transverse inertia (but not the rotational inertia) is added to the stiffener properties used in Section 8.3.5.1. Comparison of Figures 74 and 76 shows that the lower bounding frequency of the second propagation zone is now reduced for the same reasons as given in the previous section.

Figure 77 shows the propagation constants when the stiffness, transverse and rotational inertias of the stiffener are all considered.

8.3.5.4 The Effects of Dynamic Stiffness Coupling

Now in addition to stiffness and inertial properties, the dynamic stiffness coupling is also included in the analysis and Figure 78 shows the result. Comparison of Figures 77 and 78 reveals that the coupling reduces both bounding frequencies of a propagation zone and this is more significant at higher frequencies.

8.3.5.5 The Effects of Cross-Sectional Distortion

Finally, the cross-sectional distortion of the stiffeners is also included in the analysis and the dynamic stiffness values so obtained are used in the generation of the curves. The propagation constants of this most general case is presented in Figure 79.

Comparison of Figures 78 and 79 shows that at low frequencies (*i.e.*, first propagation zone) the cross-sectional distortion reduces the lower bounding frequency quite significantly. This is expected, because Figure C.4 shows that at low frequencies cross-sectional distortion lowers the rotational dynamic stiffness. Distortion reduces both bounding frequencies more so at higher frequencies.

The most important point to be observed is that at a certain frequency ($\cong$ 880 Hz) one of the attenuation constants takes a high value. This frequency corresponds to the natural frequency of the stiffener when its line of attachment to the plate is fully-fixed. The stiffener then behaves like a dynamic absorber resisting both transverse motion and rotation of the plate. Actually at those frequencies more than one attenuation constant may go to infinity and corresponding phase constant(s) always show a sudden change between 0 and $-\pi$.

8.4 Conclusions

This chapter has presented computed results relating to free harmonic wave motion in uniform, infinite, periodic structures. Euler-Bernoulli beams and stiffened plates as well as three-layered sandwich beams and stiffened sandwich plates have been investigated. The behaviour of phased array receptance functions and the propagation constants have been studied in detail.

It has been shown that the frequencies at which the phased array receptance functions have peaks and troughs can be identified with the natural frequencies of isolated periodic elements with either simply-supported or clamped ends.

The propagation constants of structures having various support conditions have been determined and presented. It has been found that for periodic Euler-Bernoulli beams and plates the propagation zones of structures with simple supports complement those of structures with sliding supports. In the case of three-layered sandwich structures this relation has not been observed but it has been determined that the lower bounding frequency of j^{th} propagation zone with simple supports is actually the upper bounding frequency of j^{th} propagation zone with sliding supports. It has also been verified that for periodic beams with zero transverse constraint, free wave propagation starts from zero frequency. For periodic plates of finite width and simply-supported along the infinite length, when the transverse constraint along the width is zero free wave propagation cannot begin below a certain cut-on frequency.

It has long been known that the rotational stiffness at a periodic support controls the lower bounding frequency of a propagation zone whereas the transverse stiffness controls the upper bounding frequency. Above the frequency of the complex conjugate zone the roles of the support stiffnesses are reversed.

By considering a particular stiffener/sandwich-plate configuration, the effects of the stiffnesses of the stiffener have been analysed. For the cases concerned it has been found that even

when the frequency of the Complex Conjugate Zone is very low, the stiffener rotational stiffness still controls the lower bounding frequency and the transverse stiffness controls the upper bounding frequency of the first propagation zone. This is so whether the stiffeners have any inertia or not. The introduction of stiffness coupling and stiffener inertia reduce the bounding frequencies of propagation zones, more so at higher frequencies.

It has also been found that including the effects of cross-sectional distortion of the stiffener in the calculation causes attenuation constant(s) to go to infinity at particular frequencies. At these frequencies the stiffener behaves like a dynamic absorber resisting both transverse motion and rotation of the plate. This may be useful in preventing undesirable wave propagation. The stiffener can be tuned in such a way that its natural frequency can coincide with the frequency which requires to be avoided.

CHAPTER 9

THEORY OF FORCED WAVE MOTION IN UNIFORM INFINITE PERIODIC STRUCTURES

9.1 Introduction

Very little work has been reported relating to the vibration analysis of harmonically forced, infinite, periodic structures. Munjal *et al* [18] studied the response of a railway line for point harmonic and roughness-excited forces. They modelled the structure as an infinite periodic beam. They assumed that the external excitation generates the same type of forced wave as described in Chapter 2 but their analysis used impedance and transfer matrix techniques.

This chapter follows a different approach. The infinite, periodic, uniform structures to be considered are those analyzed in Chapter 7 and are harmonically forced at a single point or along a single line in only one of their bays. Harmonic forcing has a point form $F_o e^{i\omega t}$ for beam structures. For plate structures a sinusoidally varying line force $F(y,t) = F_o \sin(m\pi y/L_y)e^{i\omega t}$ per unit length acts on the plate across the finite width L_y.

The reactions (forces and/or moments) applied on the structure by the supports at both ends of the loaded bay are under the influence of the external harmonic excitation but the remaining bays and supports respond as if the structure is undergoing free wave motion. Therefore in the field where the free motion takes place the reaction forces and/or moments exerted by the regular supports can be related through the propagation constant(s) of the structure and can be represented by sums of phased arrays of forces and moments. This concept has been developed in Chapter 7. The total forced response of the structure hence consists of components due to:

(i) the applied harmonic force
(ii) the reactions at the ends of the loaded bay
(iii) the phased arrays which constitute the remaining reactions.

This chapter purely concentrates on theoretical considerations. Applications of the method will be given in Chapter 10.

9.2 Euler-Bernoulli Beams and Plates

When a periodic Euler-Bernoulli beam or flat rectangular plate is forced in one of its bays, there are either one or two waves which travel outwards from the source in each direction. These are the waves which have been analysed in Chapter 7. Whether there are one or two waves depends on the support condition. In this section the detailed theory will be given for Euler-Bernoulli beams. The extension of the method to Euler-Bernoulli plates can be obtained by allowing the applied force and the resultant response to vary in proportion to $\sin k_y y$ in the y direction.

9.2.1 The Beam on Simple Supports

Consider Figure 80 which illustrates the model to be studied. A single transverse harmonic force $F_o e^{i\omega t}$ acts in one of the bays at $x = x_o$ measured from the left hand support of the bay. The simple supports exert unknown reaction forces on the beam at regular intervals. The reaction forces at supports Or and Oℓ are affected by the applied harmonic force whereas all the reaction forces to the left and right of these supports are affected only by the free motion. It was shown in Section 7.2.2.1 that a periodic Euler-Bernoulli beam on simple supports has only one pair of propagation constants, μ, at any frequency. Hence the reaction force at the s^{th} right hand support in the free field of the forced beam can be related to the reaction force at support 1r through

$$R_{sr} = R_{1r} e^{-\mu(s-1)} \qquad (9.1)$$

where $s = 1,\infty$.

The reaction forces at the supports to the left of support $O\ell$ are related in a similar way

$$R_{s\ell} = R_{1\ell}\, e^{-\mu(s-1)} \tag{9.2}$$

Now each of the reaction forces and the applied force F_o generate displacements given by their infinite-system point response functions (see Chapter 2). It follows that the total displacement at $x = x_r$, within the loaded bay, due to F_o, R_{or}, $R_{o\ell}$ and the infinite number of R_{sr} and $R_{s\ell}$'s is given by

$$\begin{aligned} w(x_r) &= F_o \sum_{n=1}^{2} a_n\, e^{-k_n|x_o-x_r|} \\ &+ R_{o\ell} \sum_{n=1}^{2} a_n\, e^{-k_n x_r} + R_{or} \sum_{n=1}^{2} a_n\, e^{-k_n(XL-x_r)} \\ &+ \sum_{s=1}^{\infty} R_{1r}\, e^{-\mu(s-1)} \sum_{n=1}^{2} a_n\, e^{-k_n((s+1)XL-x_r)} \\ &+ \sum_{s=1}^{\infty} R_{1\ell}\, e^{-\mu(s-1)} \sum_{n=1}^{2} a_n\, e^{-k_n(sXL+x_r)} \end{aligned} \tag{9.3}$$

where $0 \leq |x_r| \leq XL$ and x_r is measured from support number $O\ell$.

When the infinite series are summed, the above equation reduces to

$$\begin{aligned} w(x_r) &= F_o \sum_{n=1}^{2} a_n\, e^{-k_n|x_o-x_r|} \\ &+ R_{1r} \sum_{n=1}^{2} a_n\, e^{-k_n(XL-x_r)}\, f_n \\ &+ R_{or} \sum_{n=1}^{2} a_n\, e^{-k_n(XL-x_r)} + R_{o\ell} \sum_{n=1}^{2} a_n\, e^{-k_n x_r} \\ &+ R_{1\ell} \sum_{n=1}^{2} a_n\, e^{-k_n x_r}\, f_n \end{aligned} \tag{9.4}$$

where $f_n = e^{-k_n XL} / [1 - e^{-(\mu + k_n XL)}]$, $n = 1,2$ and the coefficients, a_n's, were given by equation (2.9).

Equation (9.4) has four unknowns (R_{ir}, R_{or}, $R_{o\ell}$, $R_{i\ell}$), and these can only be found provided four boundary condition equations are available. These conditions are found by considering the transverse displacements at four different support locations. Simple-supports do not deflect at all, so the boundary conditions to be satisfied are the zero transverse displacements at the supports. Two of the supports must be on the right-hand side of the loaded bay and the other two must be on the left-hand side. (Attempts to satisfy the conditions unequally at both sides (*e.g.*, all four on the right-hand side or one on the left-hand side and the other three on the right) have resulted in ill-conditioning of the final matrix equation.) In this study the boundary conditions have been satisfied at the supports 1ℓ, 0ℓ, 0r, 1r. It has been verified that the alternative case which considers the supports 1ℓ, 0ℓ, 0r, 2r also yields the same answers. This indicates that the selected supports do not have to be in corresponding pairs.

The zero displacement condition at 0r can be found from equation (9.4) by setting x_r to XL. This gives

$$R_{ir} \sum_{n=1}^{2} a_n f_n + R_{or} \sum_{n=1}^{2} a_n + R_{o\ell} \sum_{n=1}^{2} a_n e^{-k_n XL}$$

$$+ R_{i\ell} \sum_{n=1}^{2} a_n e^{-k_n XL} f_n = -P_o \sum_{n=1}^{2} a_n e^{-k_n (XL - x_o)} \qquad (9.5)$$

Similar equations can be obtained for other support locations (1ℓ,0ℓ,1r). The four simultaneous equations so obtained can be put into a fourth order matrix form and the unknowns (R_{ir}, R_{or}, $R_{o\ell}$ and $R_{i\ell}$) can be solved numerically. Appendix E gives the final matrix form of the equations. When the unknown reactions have been found, the transverse displacement at any point x_r, within the loaded bay and measured from 0ℓ, can be computed from equation (9.4).

9.2.2 The Beam on Transversely Elastic Supports

The periodic Euler-Bernoulli beam now rests on elastic supports which provide transverse constraints only. Rotation is unrestrained. It has been shown in Section 7.2.2.3 that the beam now has two pairs of propagation constants μ_1, μ_2. There are sets of support reaction components for each of these waves and for the s^{th} right-hand support, they can be written as

$$R_{s1r} = R_{i1r}\, e^{-\mu_1(s-1)}$$

$$R_{s2r} = R_{i2r}\, e^{-\mu_2(s-1)} \qquad (9.6)$$

The total reaction force at the s^{th} right hand support in the free field is the sum of the above components. In this way the total reaction forces at the s^{th} right and left-hand supports can be expressed as

$$R_{sr} = \sum_{j=1}^{2} R_{ijr}\, e^{-\mu_j(s-1)}$$

$$R_{s\ell} = \sum_{j=1}^{2} R_{ij\ell}\, e^{-\mu_j(s-1)} \qquad (9.7)$$

Now consider the total transverse displacement at any x_r within the loaded bay. The reaction forces at 0ℓ and $0r$ ($R_{o\ell}$ and R_{or}), the phased arrays of forces given by equations (9.7) and the external force F_o all produce displacement at x_r and this is given by

$$w(x_r) = F_o \sum_{n=1}^{2} a_n e^{-k_n|x_o-x_r|}$$

$$+ \sum_{j=1}^{2} \sum_{s=1}^{\infty} R_{ijr} e^{-\mu_j(s-1)} \sum_{n=1}^{2} a_n e^{-k_n((s+1)XL-x_r)}$$

$$+ R_{or} \sum_{n=1}^{2} a_n e^{-k_n(XL-x_r)} + R_{o\ell} \sum_{n=1}^{2} a_n e^{-k_n x_r}$$

$$+ \sum_{j=1}^{2} \sum_{s=1}^{\infty} R_{ij\ell} e^{-\mu_j(s-1)} \sum_{n=1}^{2} a_n e^{-k_n(sXL+x_r)} \qquad (9.8)$$

where x_r is measured from support number 0ℓ.

After the infinite series has been summed, $w(x_r)$ can be rewritten as

$$w(x_r) = F_o \sum_{n=1}^{2} a_n e^{-k_n|x_o-x_r|}$$

$$+ \sum_{j=1}^{2} R_{ijr} \sum_{n=1}^{2} a_n e^{-k_n(XL-x_r)} f_{jn}$$

$$+ R_{or} \sum_{n=1}^{2} a_n e^{-k_n(XL-x_r)} + R_{o\ell} \sum_{n=1}^{2} a_n e^{-k_n x_r}$$

$$+ \sum_{j=1}^{2} R_{ij\ell} \sum_{n=1}^{2} a_n e^{-k_n x_r} f_{jn} \qquad (9.9)$$

where $f_{jn} = e^{-k_n XL} / [1 - e^{-(\mu_j + k_n XL)}]$ $\quad j = 1,2$ and $n = 1,2$.

This equation has six unknowns (R_{i2r}, R_{i1r}, R_{or}, $R_{o\ell}$, $R_{i1\ell}$, $R_{i2\ell}$), so six boundary conditions are necessary at appropriate support locations. Since the supports now deflect, one must satisfy both compatibility and equilibrium conditions. The force applied on the beam by the j^{th} support at x_j is given by $R_j = -K_t w(x_j)$ where K_t

is the transverse stiffness of the support. $w(x_j)$ is the transverse displacement of the j^{th} support and this is equal to that of the beam.

Consider the special case at support number Or. The transverse displacement of the beam can be found from equation (9.9) by setting x_r to XL. If this displacement is now substituted into the above equilibrium equation, one obtains the following relationship between the reactions and F_o:

$$\sum_{j=1}^{2} R_{ijr} \sum_{n=1}^{2} a_n f_{jn} + R_{or}\left(\sum_{n=1}^{2} a_n + \frac{1}{K_t} \right)$$

$$+ R_{o\ell} \sum_{n=1}^{2} a_n e^{-k_n XL} + \sum_{j=1}^{2} R_{ij\ell} \sum_{n=1}^{2} a_n e^{-k_n XL} f_{jn}$$

$$= -F_o \sum_{n=1}^{2} a_n e^{-k_n(XL-x_o)} \qquad (9.10)$$

The compatibility and equilibrium conditions written for five other support locations yield another five equations of similar form. In this study the displacement boundary conditions are written for the support locations 2r, 1r, Or, 0ℓ, 1ℓ, 2ℓ. The total of six simultaneous equations can be cast into a matrix form and solved numerically for the unknown reactions. Appendix F outlines the steps and gives the final matrix form. Thereafter the transverse displacement at any x_r within the loaded bay can be found from equation (9.9).

9.2.3 The Beam on General Elastic Supports

Now consider Figure 81. It shows the total reaction forces and moments applied on the Euler-Bernoulli beam by general supports and the externally applied force F_o. It was shown in Section 7.2.2.4 that a periodic Euler-Bernoulli beam or plate on general supports has two pairs of propagation constants μ_1 and μ_2. Two sets of support reaction components corresponding to these two waves act

simultaneously. (These have been explained in the previous section.) The total reaction forces at the s^{th} right and s^{th} left hand support in the free wave field have been given by equation (9.7). Rotational elastic constraints now also exist and the total reaction moments at the s^{th} right and s^{th} left-hand support take the forms

$$M_{sr} = \sum_{j=1}^{2} M_{ijr}\, e^{-\mu_j(s-1)}$$

$$M_{s\ell} = \sum_{j=1}^{2} M_{ij\ell}\, e^{-\mu_j(s-1)} \qquad (9.11)$$

Now, the beam total transverse displacement at any point is the sum of the infinite-system point response functions of:

(i) The reaction forces and moments at two ends of the loaded bay (R_{or}, M_{or}, $R_{o\ell}$ and $M_{o\ell}$).

(ii) The phased arrays of the remaining reaction forces and moments (R_{sr}, M_{sr}, $R_{s\ell}$ and $M_{s\ell}$).

(iii) The externally applied force F_o.

Hence the transverse displacement at any x_r, within the loaded bay, can be shown to be:

$$
\begin{aligned}
w(x_r) = {} & F_o \sum_{n=1}^{2} a_n \, e^{-k_n |x_o - x_r|} \\
& + \sum_{j=1}^{2} \sum_{s=1}^{\infty} R_{ijr} \, e^{-\mu_j (s-1)} \sum_{n=1}^{2} a_n \, e^{-k_n ((s+1)XL - x_r)} \\
& - \sum_{j=1}^{2} \sum_{s=1}^{\infty} M_{ijr} \, e^{-\mu_j (s-1)} \sum_{n=1}^{2} b_n \, e^{-k_n ((s+1)XL - x_r)} \\
& + R_{or} \sum_{n=1}^{2} a_n \, e^{-k_n (XL - x_r)} - M_{or} \sum_{n=1}^{2} b_n \, e^{-k_n (XL - x_r)} \\
& + M_{o\ell} \sum_{n=1}^{2} b_n \, e^{-k_n x_r} + R_{o\ell} \sum_{n=1}^{2} a_n \, e^{-k_n x_r} \\
& + \sum_{j=1}^{2} \sum_{s=1}^{\infty} M_{ij\ell} \, e^{-\mu_j (s-1)} \sum_{n=1}^{2} b_n \, e^{-k_n (sXL + x_r)} \\
& + \sum_{j=1}^{2} \sum_{s=1}^{\infty} R_{ij\ell} \, e^{-\mu_j (s-1)} \sum_{n=1}^{2} a_n \, e^{-k_n (sXL + x_r)}
\end{aligned}
\qquad (9.12)
$$

In this, account has been taken of the fact that the transvese displacement due to moment excitation is antisymmetric with respect to the point of application of the moment.

Now the moment component $M_{ij\ \ell,r}$ is related to the force component $R_{ij\ \ell,r}$ through equation (7.22) which states

$$
\begin{bmatrix} K_t \alpha_{FF} + K_C \alpha_{MF} + 1 & K_t \alpha_{FM} + K_C \alpha_{MM} \\ K_C \alpha_{FF} + K_r \alpha_{MF} & K_C \alpha_{FM} + K_r \alpha_{MM} + 1 \end{bmatrix} \begin{Bmatrix} R_{ij\ell,r} \\ M_{ij\ell,r} \end{Bmatrix} = 0
$$

Inserting into this the expressions for the phased array receptance functions α_{FF}, α_{MF}, α_{FM} and α_{MM} from equations (7.5), (7.7), (7.8) and (7.9) respectively and carrying out the algebraic manipulations one finds the ratio of the reaction moment component to the reaction force component at the s^{th} support to be

$$\frac{M_{sj\ell,r}}{R_{sj\ell,r}} = -\frac{-K_t \sum_{n=1}^{2} \frac{a_n \sinh k_n XL}{\cosh \mu - \cosh k_n XL} + K_c \sum_{n=1}^{2} \frac{c_n \sinh \mu}{\cosh \mu - \cosh k_n XL} + 1}{K_t \sum_{n=1}^{2} \frac{b_n \sinh \mu}{\cosh \mu - \cosh k_n XL} - K_c \sum_{n=1}^{2} \frac{d_n \sinh k_n XL}{\cosh \mu - \cosh k_n XL}}$$

$$= f(\mu_j) \qquad (9.13)$$

This equation defines $f(\mu_j)$ and is valid for each component wave provided that the corresponding propagation constant μ_j is used. The moment terms M_{ijr} and $M_{ij\ell}$ in equation (9.12) can now be replaced by $R_{ijr}f(\mu_j)$ and $R_{ij\ell}f(\mu_j)$ so the number of unknowns in that equation can be reduced. Furthermore the infinite series can be summed and equation (9.12) becomes

$$w(x_r) = F_o \sum_{n=1}^{2} a_n e^{-k_n|x_o - x_r|}$$

$$+ \sum_{j=1}^{2} R_{ijr} \left\{ \sum_{n=1}^{2} a_n e^{-k_n(XL-x_r)} f_{jn} - f(-\mu_j) \sum_{n=1}^{2} b_n e^{-k_n(XL-x_r)} f_{jn} \right\}$$

$$+ R_{or} \sum_{n=1}^{2} a_n e^{-k_n(XL-x_r)} - M_{or} \sum_{n=1}^{2} b_n e^{-k_n(XL-x_r)}$$

$$+ M_{o\ell} \sum_{n=1}^{2} b_n e^{-k_n x_r} + R_{o\ell} \sum_{n=1}^{2} a_n e^{-k_n x_r}$$

$$+ \sum_{j=1}^{2} R_{ij\ell} \left\{ \sum_{n=1}^{2} a_n e^{-k_n x_r} f_{jn} + f(\mu_j) \sum_{n=1}^{2} b_n e^{-k_n x_r} f_{jn} \right\} \qquad (9.14)$$

where f_{jn} has been defined in Section 9.2.2.

Notice that equation (9.14) contains $f(-\mu_j)$ and $f(\mu_j)$. The different signs in these stem from the fact that the positive going waves (*i.e.*, waves travelling from left to right) correspond to $-\mu_j$ whereas negative going waves (*i.e.*, travelling to the left) correspond to μ_j.

There are now eight unknown reactions (R_{i2r}, R_{i1r}, R_{or}, M_{or}, $M_{o\ell}$, $R_{o\ell}$, $R_{i1\ell}$, $R_{i2\ell}$). Eight boundary conditions are required to set up eight simultaneous equations for the solution of these reactions.

Since the supports can deflect both compatibility and equilibrium conditions must be satisfied at appropriate support locations.

The transverse displacement of the periodic beam at Or can be found from equation (9.14) by setting x_r to XL. This must be equal to the transverse displacement of the support at Or. This is a statement of compatibility. The support displacement at any $x = x_j$ was given by equation (4.28) in terms of the support stiffnesses and the forces and moments acting on it. For equilibrium at the support Or the reactions given in equation (4.28) become $R_{x_j} = -R_{or}$ and $M_{x_j} = -M_{or}$. Satisfaction of the compatibility condition then leads to

$$\sum_{j=1}^{2} R_{ijr} \left\{ \sum_{n=1}^{2} a_n f_{jn} - f(-\mu_j) \sum_{n=1}^{2} b_n f_{jn} \right\}$$

$$+ R_{or} \left\{ \sum_{n=1}^{2} a_n + \frac{K_r}{K_{tot}^2} \right\} + M_{or} \left\{ \sum_{n=1}^{2} b_n - \frac{K_c}{K_{tot}^2} \right\}$$

$$+ M_{o\ell} \sum_{n=1}^{2} b_n e^{-k_n XL} + R_{o\ell} \sum_{n=1}^{2} a_n e^{-k_n XL}$$

$$+ \sum_{j=1}^{2} R_{ij\ell} \left\{ \sum_{n=1}^{2} a_n e^{-k_n XL} f_{jn} + f(\mu_j) \sum_{n=1}^{2} b_n e^{-k_n XL} f_{jn} \right\}$$

$$= -F_o \sum_{n=1}^{2} a_n e^{-k_n (XL - x_o)} \qquad (9.15)$$

Since two of the unknowns are moments, two of the boundary conditions required must satisfy the rotational compatibility and equilibrium. Now the reaction moments and forces in the free field are related through equation (9.13). Attempts to satisfy both transverse displacement and rotation conditions at the same support in the free field have been found to lead to ill-conditioning of the final matrix. Hence in this study boundary conditions used are the six transverse displacement conditions at 2ℓ, 1ℓ, 0ℓ, 0r, 1r, 2r and the two rotational conditions at 0ℓ and 0r. These eight boundary conditions give equations of similar form. The eight simultaneous equations so obtained can be put into a matrix form and can be numerically solved for the unknown reactions. Appendix G details the procedure and gives the final matrix form. Once the unknowns are determined the transverse displacement at any x_r, within the loaded bay, can be obtained from equation (9.14). Equation (G.18) can be used to determine the rotation at any x_r in the same bay.

9.3 Three-Layered Periodic Sandwich Beams and Plates

When a periodic three-layered sandwich beam or plate is forced in one of its bays, either two or three different outward going waves propagate from either side of the loaded bay. The number of wave pairs is determined by the support conditions. This section will extend the theory of Section 9.2 to sandwich plates. The derivation procedure can be applied to sandwich beams simply by dropping the sin $k_y y$ term and hence the y-wise dependency.

9.3.1 The Plate on Simple Supports

Suppose the periodic sandwich plate is excited by a line force $F_o \sin k_y y$ at (x_o, y) in one of its bays. It was shown in Section 7.4.2.1 and verified in Section 7.5.2 that three-layered periodic sandwich beams and plates on simple supports have two pairs of propagation constants μ_1 and μ_2 at any frequency. The support

reaction forces in the free wave field at the s^{th} right and left-hand supports then take the forms

$$R_{sr} = \sum_{j=1}^{2} R_{ijr}\, e^{-\mu_j(s-1)} \sin k_y y$$

$$R_{s\ell} = \sum_{j=1}^{2} R_{ij\ell}\, e^{-\mu_j(s-1)} \sin k_y y \qquad (9.16)$$

The transverse displacement at any (x_r,y) within the loaded bay can be found by considering the response due to all the reaction forces and F_o. Just as the infinite-system point response functions were used at this stage in Section 9.2.1, so we now use the infinite-system line response functions for the sandwich plate. These functions are explained in Chapter 3. The total response at (x_r,y) due to F_o and all the reactions is

$$\begin{aligned} w(x_r,y) = \Big\{ & F_o \sum_{n=1}^{3} a_n\, e^{-k_n|x_o-x_r|} \\ & + \sum_{j=1}^{2} \sum_{s=1}^{\infty} R_{ijr}\, e^{-\mu_j(s-1)} \sum_{n=1}^{3} a_n\, e^{-k_n((s+1)XL-x_r)} \\ & + R_{or} \sum_{n=1}^{3} a_n\, e^{-k_n(XL-x_r)} + R_{o\ell} \sum_{n=1}^{3} a_n\, e^{-k_n x_r} \\ & + \sum_{j=1}^{2} \sum_{s=1}^{\infty} R_{ij\ell}\, e^{-\mu_j(s-1)} \sum_{n=1}^{3} a_n\, e^{-k_n(sXL+x_r)} \Big\} \sin k_y y \end{aligned} \qquad (9.17)$$

The infinite series can easily be summed and the above equation becomes

$$w(x_r,y) = \Big\{F_o \sum_{n=1}^{3} a_n e^{-k_n|x_o-x_r|} + \sum_{j=1}^{2} R_{ijr} \sum_{n=1}^{3} a_n e^{-k_n(XL-x_r)} f_{jn}'$$

$$+ R_{or} \sum_{n=1}^{3} a_n e^{-k_n(XL-x_r)} + R_{o\ell} \sum_{n=1}^{3} a_n e^{-k_n x_r}$$

$$+ \sum_{j=1}^{2} R_{ij\ell} \sum_{n=1}^{3} a_n e^{-k_n x_r} f_{jn}' \Big\} \sin k_y y \qquad (9.18)$$

where $f_{jn}' = e^{-k_n XL} / [1 - e^{-(\mu_j + k_n XL)}]$ $j = 1,2$ and $n = 1,2,3$.

There are six unknowns (R_{i2r}, R_{i1r}, R_{or}, $R_{o\ell}$, $R_{i1\ell}$, $R_{i2\ell}$) which can be found from six appropriate boundary conditions equations. Since simple supports do not deflect, the conditions are expressed by equating the transverse displacements at the support locations (in this study at 0r, 1r, 2r, 0ℓ, 1ℓ, 2ℓ) to zero. The condition $w(0r, y) = 0$ leads to the equation

$$\Big\{ \sum_{j=1}^{2} R_{ijr} \sum_{n=1}^{3} a_n f_{jn}' + R_{or} \sum_{n=1}^{3} a_n + R_{o\ell} \sum_{n=1}^{3} a_n e^{-k_n XL}$$

$$+ \sum_{j=1}^{2} R_{ij\ell} \sum_{n=1}^{3} a_n e^{-k_n XL} f_{jn}' \Big\} \sin k_y y$$

$$= -F_o \sum_{n=1}^{3} a_n e^{-k_n(XL-x_o)} \sin k_y y \qquad (9.19)$$

It is a straightforward matter to write down the other five equations. They are given in Appendix H, together with the final matrix form. The sixth order matrix equation so found can be solved numerically for the unknown reactions. The transverse displacement at any point (x_r,y), within the loaded bay, can then be found from equation (9.18).

9.3.2 The Plate on General Supports

It was shown in Section 7.4.2.4 that when a periodic three-layered sandwich beam or plate structure rests on general supports, there exist three pairs of propagation constants: μ_1, μ_2 and μ_3 at any frequency. There are therefore three different waves which can propagate outwards from the loaded bay and corresponding to each is a component of a support reaction.

The total reaction forces in the free wave field at the s^{th} right and s^{th} left hand side supports therefore have three terms in the series as

$$R_{sr} = \sum_{j=1}^{3} R_{ijr}\, e^{-\mu_j(s-1)} \sin k_y y$$

$$R_{s\ell} = \sum_{j=1}^{3} R_{ij\ell}\, e^{-\mu_j(s-1)} \sin k_y y \qquad (9.20)$$

The reaction moments in the free field can be expressed in a similar way and are given by

$$M_{sr} = \sum_{j=1}^{3} M_{ijr}\, e^{-\mu_j(s-1)} \sin k_y y$$

$$M_{s\ell} = \sum_{j=1}^{3} M_{ij\ell}\, e^{-\mu_j(s-1)} \sin k_y y \qquad (9.21)$$

The total transverse displacement at any (x_r, y), within the loaded bay, can be obtained by considering displacements due to all the support line reaction forces and moments and the exciting line force F_o. By making use of the infinite-system line response functions, the displacement at (x_r, y) is found to be

$$w(x_r,y) = \Big\{F_o \sum_{n=1}^{3} a_n\, e^{-k_n|x_o-x_r|}$$

$$+ \sum_{j=1}^{3}\sum_{s=1}^{\infty} R_{ijr}\, e^{-\mu_j(s-1)} \sum_{n=1}^{3} a_n\, e^{-k_n((s+1)XL-x_r)}$$

$$- \sum_{j=1}^{3}\sum_{s=1}^{\infty} M_{ijr}\, e^{-\mu_j(s-1)} \sum_{n=1}^{3} b_n\, e^{-k_n((s+1)XL-x_r)}$$

$$+ R_{or} \sum_{n=1}^{3} a_n\, e^{-k_n(XL-x_r)} - M_{or} \sum_{n=1}^{3} b_n\, e^{-k_n(XL-x_r)}$$

$$+ M_{o\ell} \sum_{n=1}^{3} b_n\, e^{-k_n x_r} + R_{o\ell} \sum_{n=1}^{3} a_n\, e^{-k_n x_r}$$

$$+ \sum_{j=1}^{3}\sum_{s=1}^{\infty} M_{ij\ell}\, e^{-\mu_j(s-1)} \sum_{n=1}^{3} b_n\, e^{-k_n(sXL+x_r)}$$

$$+ \sum_{j=1}^{3}\sum_{s=1}^{\infty} R_{ij\ell}\, e^{-\mu_j(s-1)} \sum_{n=1}^{3} a_n\, e^{-k_n(sXL+x_r)}\Big\} \sin k_y y \qquad (9.22)$$

The infinite series within this equation are easily summed as before. Further M_{ijr} can be expressed in terms of R_{ijr} and $M_{ij\ell}$ in terms of $R_{ij\ell}$ (in the same way as equation (9.14) was derived) but the ratio $f(\mu_j)$ which is valid for each reaction component now contains series with three terms instead of two. Otherwise the form of equation (9.13) still applies. Using this relationship between M_{ijr} and R_{ijr} and also $M_{ij\ell}$ and $R_{ij\ell}$ we can eliminate M_{ijr} and $M_{ij\ell}$ from equation (9.22) to yield

$$w(x_r,y) = \Big\{F_o \sum_{n=1}^{3} a_n\, e^{-k_n|x_o-x_r|}$$

$$+ \sum_{j=1}^{3} R_{ijr}\Big[\sum_{n=1}^{3} a_n\, e^{-k_n(XL-x_r)}\, f_{jn}'' - f(-\mu_j) \sum_{n=1}^{3} b_n\, e^{-k_n(XL-x_r)} f_{jn}''\Big]$$

$$+ R_{or} \sum_{n=1}^{3} a_n\, e^{-k_n(XL-x_r)} - M_{or} \sum_{n=1}^{3} b_n\, e^{-k_n(XL-x_r)}$$

$$+ M_{o\ell} \sum_{n=1}^{3} b_n\, e^{-k_n x_r} + R_{o\ell} \sum_{n=1}^{3} a_n\, e^{-k_n x_r}$$

$$+ \sum_{j=1}^{3} R_{ij\ell}\Big[\sum_{n=1}^{3} a_n\, e^{-k_n x_r}\, f_{jn}'' + f(\mu_j) \sum_{n=1}^{3} b_n\, e^{-k_n x_r}\, f_{jn}''\Big]\Big\} \sin k_y y \qquad (9.23)$$

where $f_{jn}'' = e^{-k_n XL}/[1 - e^{-(\mu_j + k_n XL)}]$ $\quad j = 1,2,3$ and $n = 1,2,3$.

There are ten unknowns to be solved in this problem (R_{i3r}, R_{i2r}, R_{i1r}, R_{or}, $R_{o\ell}$, M_{or}, $M_{o\ell}$, $R_{i1\ell}$, $R_{i2\ell}$, $R_{i3\ell}$) and ten boundary conditions are required. These are the equilibrium and compatibility conditions between the sandwich plate and the stiffener at appropriate support locations. Following the procedure of Section 9.2.3 the displacement boundary condition at support Or, w(Or,y), can be shown to yield

$$\Big\{ \sum_{j=1}^{3} R_{ijr}\Big[\sum_{n=1}^{3} a_n f_{jn}'' - f(-\mu_j) \sum_{n=1}^{3} b_n f_{jn}''\Big]$$

$$+ R_{or} \Big[\sum_{n=1}^{3} a_n + \frac{K_r}{K_{tot}^2}\Big] + M_{or}\Big[\sum_{n=1}^{3} b_n - \frac{K_c}{K_{tot}^2}\Big]$$

$$+ M_{o\ell} \sum_{n=1}^{3} b_n e^{-k_n XL} + R_{o\ell} \sum_{n=1}^{3} a_n e^{-k_n XL}$$

$$+ \sum_{j=1}^{3} R_{ij\ell}\Big[\sum_{n=1}^{3} a_n f_{jn}'' e^{-k_n XL} + f(\mu_j) \sum_{n=1}^{3} b_n f_{jn}'' e^{-k_n XL}\Big]\Big\} \sin k_y Y$$

$$= -F_o\Big(\sum_{n=1}^{3} a_n e^{-k_n(XL-x_o)}\Big) \sin k_y Y \qquad (9.24)$$

Section 9.2.3 has mentioned the care with which one must choose the remaining boundary conditions. In the present case they are taken to be the two rotational conditions at 0ℓ and 0r and the seven transverse displacement conditions at 3ℓ, 2ℓ, 1ℓ, 0ℓ, 1r, 2r and 3r. Appendix I outlines the setting up of the corresponding equations and gives their final 10 × 10 matrix equation for the unknown reactions. Once the equations are solved for the reactions, the transverse displacement at any (x_r, y) $(0\ell \leq x_r \leq 0r)$ can be computed from equation (9.23).

9.4 Conclusions

This chapter has laid down the fundamentals of forced vibration analysis of infinite, periodic, uniform beams and plates. Euler-Bernoulli beams and plates and three-layered sandwich beams and plates have been studied. Point or line harmonic excitation has been applied in one bay of the structure.

The principle of the method has been to set up equations for the reactions (forces and/or moments) exerted by the supports. In the most general case the two supports at either end of the loaded bay each exert a transverse force and moment reaction (4 unknown reactions in total). The remaining supports to the right and left of the loaded bay (infinite in number) also each exert two reactions. By making use of the free wave propagation concepts in periodic structures, these remaining unknown reactions can be expressed in terms of just 2j unknown reaction force components where j is the number of independent waves which can propagate in one direction at any one frequency. In this way 2j + 4 non-homogeneous equations have been set up for 2j + 4 unknown reactions. When the equations are solved for the reactions, the response of the structure can be found at any point in the structure.

CHAPTER 10

CALCULATIONS RELATING TO FORCED WAVE MOTION IN UNIFORM INFINITE PERIODIC STRUCTURES

10.1 Introduction

This chapter presents calculated results for the forced vibration of infinite, uniform, periodic structures which are harmonically forced in one bay only. For beams, the force excitation takes place in point form $F_o\, e^{i\omega t}$. For plates, it takes the sinusoidally-varying line form $F(y,t) = F_o \sin(m\pi/L_y)y\, e^{i\omega t}$ per unit length between the simply-supported edges across the finite width L_y. 'm' represents the number of half-waves across the width. Chapter 9 has laid out the theoretical details of the approach.

This chapter first presents results for Euler-Bernoulli beams and then for the particular sandwich plate/stiffener configuration of Section 8.3.5. Special consideration is given to the effects of the support (or stiffener) stiffness and the beam damping on the harmonic response.

The harmonic vibration response considered in this chapter is the direct receptance of the beam or plate under the action of a single point or line force.

10.2 Response to a Point Force; Euler-Bernoulli Beam

The direct receptance considered in this section has the non-dimensional form given by

ND w/F : w/F (EI/XL^3) (Receptance = Displacement/Force)

A non-dimensional frequency is used for the beam as defined in Section 8.2.1. The non-dimensionalization procedure of the beam

support stiffness values to be considered here was given in Section 8.3.1.

10.2.1 Simple Supports

Figure 82 shows how the magnitude of non-dimensional transverse direct receptance w/F for a periodic beam on simple supports varies with frequency. The force is applied at $1/8^{th}$ of the bay length from one stiffener (x_o = XL/8). In order to observe the peaks clearly, very low damping ($\eta = 10^{-6}$) is assigned to the beam. The transverse direct receptance is computed from equation (9.4) and the reactions, R's, are found from equation (E.6). Notice that the receptance curve consists of a series of pairs of resonant peaks, adjacent pairs being separated by an anti-resonance trough. The frequencies at which any pair of peaks occur are the bounding frequencies of the propagation zones of the periodic structure.

Figure 83 shows the receptances of the same structure as that of Figure 82 but two different exciting force locations are analyzed (x_o = XL/2 and x_o = XL/3). The beam loss factor is again $\eta = 10^{-6}$.

Consider firstly the curve for x_o = XL/2. It can be seen that the number of pairs of peaks are less than Figure 82 (x_o = XL/8) and that the peaks at frequencies $\cong$ 6.3, $\cong$ 7.9, $\cong$ 12.6, $\cong$ 14 have been replaced by discontinuities in the curve. Likewise, on the curve for x_o = XL/3, peak at frequency $\cong$ 9.4 has been replaced by a discontinuity.

This phenomenon has a simple explanation. When the structure is excited at x_o = XL/2, the resonant beam response at the second and fourth pairs of peaks has a nodal point at x = XL/2 (*i.e.*, the beam elements are being excited in modes with nodes at this point). It follows that if the beam is excited at this point, that mode cannot be excited and resonant response cannot be obtained. Likewise, when the beam is excited at x_o = XL/3, a resonant mode with a node at x = XL/3 cannot be excited and this accounts for the lack of a peak at frequency $\cong$ 9.4.

10.2.2 Transversely Elastic Supports

The supports are now allowed to have finite transverse stiffnesses but zero rotational stiffness. First studied is the effect of changing the transverse stiffness. Figure 84 shows the direct receptances for non-dimensional transverse stiffness values of KT = 3000, 5000, 10000, 30000. Forcing is applied at x_o = XL/8. In order to compare the peak levels, the material loss factor is increased to η = 0.003. The curves are generated from equation (9.9) and equation (F.14) is used to obtain the reaction R's.

As can be seen each curve has pairs of peaks and these can be shown to occur at the bounding frequencies of the corresponding propagation zones. The curves for all KT values have resonant peaks at frequencies $\cong$ 3.1 and $\cong$ 6.3. These are the bounding frequencies which are governed by the rotational stiffness and not by the transverse stiffness. The remaining resonant peaks are at the bounding frequencies governed by the transverse stiffness and not at all by the rotational stiffness. As expected, the frequencies of these peaks drop as the transverse stiffness is reduced.

Figure 85 expands the frequency scale of Figure 84 over the range of 3 to 5. Curves for KT = 300, 500, 1000, 2000 are also presented on this figure. The other parameters are those utilized in Figure 84.

It is now clearly evident that the increasing KT reduces the peak levels at the bounding frequencies which are actually governed by KT. These resonance frequencies are the bounding frequencies of wave motion which is symmetric about a support. This causes transverse motion at the support and the frequencies are therefore influenced by KT. It is found that the response levels at the lower bounding frequencies (which are influenced by KR and occur at frequency of $\cong$ 3.1) are also lowered as KT increases. However, this effect is too small to be seen on Figures 84 and 85.

Figure 86 shows the effect of exciting the beam at different points in the loaded bay. The force is applied in turn at support location x_o = 0, x_o = XL/3 and at x_o = XL/2. KT has been taken to be 10000 and

the material loss factor, η, is 0.003. There is no rotational constraint at the supports. The magnitude of the direct receptance is plotted once again.

A series of pairs of resonant peaks or discontinuities is again seen for each loading condition. The peaks and discontinuities are again at the bounding frequencies of the corresponding propagation zones. The figure also demonstrates that at low freuencies, the response at the loading point increases as the loading point moves towards the centre of the bay. This is true at the resonant peaks also at off-resonance frequencies. At higher frequencies the maximum response may be obtained when the loading point is elsewhere.

10.2.3 General Elastic Supports; Effects of Changing the Support Stiffnesses

Next presented is the response of a beam which has general elastic supports. The transverse and rotational support stiffness values are systematically varied in turn. Forcing is applied at $1/8^{th}$ of the bay length (x_o = XL/8) and the beam material loss factor is taken as η = 0.003. The responses are computed from equation (9.14). The reactions, R's, M_{or} and $M_{o\ell}$, are found from equation (G.23).

Figure 87 shows the effect of varying the transverse stiffness when a small amount of the rotational stiffness is introduced (KR = 1). The transverse stiffnesses considered are the values used in Figure 85. As can be seen, each curve has a peak at the frequency $\cong$ 3.3. This is the bounding frequency influenced by KR and, because KR now exists, is higher than the bounding frequency of Figure 85 ($\cong$ 3.1) for which KR was zero.

Reducing the value of KT again reduces the upper bounding frequencies and increases the peak responses at these frequencies. Since Figures 85 and 87 have the same KT values these (upper) bounding frequencies are the same in both figures. The presence of KR slightly increases the peak levels at all bounding frequencies as compared to Figure 85.

Figure 88 shows the effect of varying the rotational stiffness while the transverse stiffness remains constant. The non-dimensional rotational stiffness values considered are KR = 0.1, 0.3, 1, 3, 10, 30, 100 and 300. The transverse stiffness is KT = 10000. Material loss factor is again $\eta = 0.003$.

It can be seen that reducing the value of KR reduces one of the resonance frequencies but has no effect on the other (at $\cong 4.7$). The resonance frequency which is reduced is at the lower bounding frequency of the corresponding propagation zones. The beam wave motion is anti-symmetric about the support and is therefore influenced by KR. When the rotational stiffness is increased, the response at the first resonance peak is first reduced and then increased at very high KR values. At the other peak the response is always increased. This unexpected result was first observed by Mead [36]. It contrasts with the expected behaviour seen in Figures 84, 85 and 87 where the peak responses decrease as the transverse stiffness increases.

10.3 Response to a Line Force; Three-Layered Sandwich Plate

Finally, the particular sandwich plate/stiffener configuration of Section 8.3.5 is considered. There are far too many parameters affecting the resonant response levels to permit a really comprehensive study. In this section, only the effects of stiffener cross-sectional distortion are considered by including and disregarding it in turn. Equation (9.23) is used in the determination of the responses and equation (I.13) is utilized for the solution of unknown reactions, R's, $M_{o\ell}$ and M_{or}. A sinusoidally- varying line forcing with m = 1 is applied at $1/8^{th}$ of the bay length from one stiffener ($x_o = XL/8$). The purpose is clearly to locate the resonance frequencies so the core loss factor is taken to be very low ($\beta = 10^{-6}$). In both cases the stiffener dynamic stiffnesses are considered and dynamic stiffness coupling is taken into account. Stiffness values are computed from Appendix C. The plate dimensions are those given in Section 6.3.2.1. The core shear modulus is taken to be frequency-dependent from Figure 7 corresponding

to a temperature of T = 18°C. Figure 89 shows the plate response both with the distortion of the stiffener cross-section and without it.

Once again resonant peaks are seen to occur in pairs and at the bounding frequencies of the propagation zones (see Figures 78 and 79). The effect of cross-sectional distortion on the bounding frequencies has already been considered in Section 8.3.5. It is therefore to be expected (as observed) that the frequencies of the peaks are less when stiffener cross-sectional distortion is included in the calculations.

The response levels at low frequencies are slightly increased by the inclusion of stiffener distortion but within the propagation zones they are slightly reduced.

10.4 Conclusions

This chapter has presented computed response curves for the forced vibrations of some infinite uniform, periodic structures. It has been confined to the applications of the concepts developed in Chapter 9. Results for an Euler-Bernoulli beam and a flat, rectangular, three-layered sandwich plate have been presented. Only single point (or line) harmonic force excitations have been considered.

The response versus frequency curves in all cases consist of successive pairs of resonance peaks (or discontinuities) which occur at the bounding frequencies of the propagation zones of the periodic structure.

It has been confirmed that when the rotational stiffness at a support is increased the response of the periodic beam increases at bounding frequencies which are actually controlled by KT. The response levels at bounding frequencies influenced by KR are first reduced as KR increases and then are increased. On the other hand, increasing KT lowers the response at every frequency within the propagation zones. This is more profound at higher frequency zones.

It has been shown that the low frequency response of a periodic beam on transversely elastic supports is higher when the exciting force is closest to a bay centre. At higher frequencies the response may be greater when the force acts at some other point.

The theory developed may find some applications on the vibration of railway lines. Present day rails are very long beams supported on wooden (or concrete) sleepers at regular intervals. Hence they can be modelled as infinite, periodic beams with flexible supports and acted upon by oscillating forces induced by the roughness of the mating surfaces of the wheel and the rail. A knowledge of driving point impedance (force/ velocity) is an important factor in the determination of the vibration levels transmitted to the wagons.

SECTION 4: EXPERIMENTAL WORK

CHAPTER 11

EXPERIMENTAL WORK

11.1 Introduction

This chapter describes various experiments which were conducted in order to verify some of the developed theories. The main aim was to correlate the measured frequency responses of eight-bay, stiffened plates (uniform and three-layered sandwich) with the responses predicted by the methods of Chapter 6.

The sandwich plate had a very heavily damped core. In consequence the frequency response curve of the plate had no sharp peaks or troughs, the peaks of individual resonances merging to form low 'humps'. Therefore, the task of experimentally determining the individual resonance frequencies of the multi-bay stiffened sandwich plate was impossible. On the other hand, the resonance frequencies of the lightly damped, uniform, stiffened plate were readily measurable. But the magnitude of forced response depended on certain parameters which could not be included in the idealized theory (*e.g.*, effects of acoustic damping, frequency dependent damping).

Hence within the limitations of equipment and chosen experimental methods the verification of the theories of Chapter 6 is done in two stages. The experiments on the eight-bay uniform plate are used to validate the resonance frequency aspects, whereas the experiments on the eight-bay three-layered sandwich plate are utilized to confirm the response magnitudes.

Experiments were also conducted on narrow strips cut out from the sandwich plate specimen. These have been treated as sandwich beams and experiments on them are used to verify the sandwich beam theories given in Chapter 5.

In each experiment, the plate or strip was excited by one or more electrodynamic exciters. This chapter first outlines the calibration

of these exciters and then describes experiments on the stiffened uniform plate. Experiments on the sandwich strips are then explained after which the eight-bay, stiffened sandwich plate is considered.

11.2 Calibration of Exciters

Three Ling 101 electrodynamic exciters were used in the course of the experiments. It was required to obtain accurate values for each of the 'Head Constants', which is the force generated by the exciter per unit current, and also of the 'Moving Mass' of the exciter coil and fittings. The latter cannot be measured (weighed) directly.

11.2.1 Determination of Head Constants

The general principle was as follows. The exciter was suspended from a bridge and was coupled to a force transducer which in turn was rigidly attached to a massive test-bed. The current to the exciter and the output from the transducer were measured in order to find the force per unit current.

11.2.1.1 The Test Apparatus and Procedure

Figure 90 gives the block-diagram of the experimental set-up and shows the equipment used.

The harmonic current to the exciter passed through a known fixed resistance to enable an accurate measure of voltage drop (and hence of current) to be made.

The exciters were driven from 100 [Hz] to 900 [Hz] at intervals of 100 [Hz]. The voltage across the resistor was measured on a digital voltmeter (DVM_1). The output from the force transducer was conditioned by a charge amplifier whose output was also measured on

another digital voltmeter (DVM_2). Measurements of DVM_1 and DVM_2 were taken at each frequency.

11.2.1.2 Experimental and Derived Results

The head constant is the force (Newton [N]) per unit current (Ampere [A]). The exact current was deduced from DVM_1 and the known fixed resistance. The magnitude of the force was measured from the output of the charge amplifier with a suitable calibration constant applied. The head constants were then computed by dividing these force values by the measured current values.

Table 7 presents the results and Figure 91 shows them plotted against frequency. As can be seen, they tend to increase slightly with frequency and to vary from exciter to exciter. For simplicity in subsequent work, the arithmetic average of these (averaged over the exciters and over the frequency band) has been found ($\cong$ 2.4 [N/A]).

11.2.2 Determination of the Moving Mass

The exciter was placed on the bridge with a known extra mass attached to it. An accelerometer was stuck on the mass. The principle of the test was to obtain the transfer function (*i.e.*, acceleration/force) of the exciter for a range of frequencies and for two different extra masses ($\cong$ 8.9 [g] and $\cong$ 12.3 [g]).

11.2.2.1 The Test Apparatus and Procedure

Figure 92 is the block-diagram of the experimental set-up and shows the equipment used.

The exciter was driven by the internal noise generator of the signal processing unit [34] which henceforth will be denoted as TFA (Transfer Function Analyser). A fixed resistor in the line between

the power amplifier and the exciter enabled the current to the exciter and hence the force from it to be measured.

The exciter was driven with a broadband random signal having a bandwidth of 800 [Hz]. The accelerometer signal from the charge amplifier was processed together with the exciter current signal to yield the inertance (acceleration/unit force). Data from 250 runs was acquired and averaged by the TFA for each value of the extra mass.

The transfer function with the smaller mass attached was also determined by using a sinusoidal input current to the exciter.

11.2.2.2 Experimental and Derived Results

Figures 93 and 94 show the moduli of the transfer functions when the masses $\cong$ 8.9 [g] and $\cong$ 12.3 [g] respectively were attached. The transfer function evidently levels out above a frequency of 400 Hz. This is a 'mass controlled' region and the constant magnitude is $1/m_t$ where m_t is the total mass [kg] (*i.e.*, the sum of the exciter moving mass, the extra mass and the accelerometer mass). The resonant peaks in each transfer function occur when the total mass resonates against the stiffness of the exciter diaphragm.

Table 8 compares the magnitudes of the transfer function for the mass $\cong$ 8.9 [g] found from the random experiment with that from the sinusoidal experiment above the resonance region. In the worst case (at 300 [Hz]) they only differ by about 3.5% and with increasing frequency the discrepancy diminishes.

Since the transfer function at high frequencies is given by $1/m_t$, the total mass 'm_t' can be obtained simply from the inverse of the high frequency value. From the first run the total mass was found to be $\cong$ 17.1 [g]. The extra mass and the mass of the accelerometer was $\cong$ 10.9 [g], so the exciter moving mass was $\cong$ 6.2 [g].

From the second run the total mass was found to be $\cong$ 20.3 [g], so the moving mass was $\cong$ 6.0 [g].

In Section 11.4 the moving mass of the exciter will be taken as the average of these two results (*i.e.*, 6.1 [g]). Only one exciter was tested, as it has been assumed that the three exciters had mechanically-identical head units.

11.3 Eight-Bay Stiffened Uniform Plate

This section describes the experiments conducted on an eight-bay, stiffened, aluminium plate. The aim was to determine the lowest group of resonance frequencies for a variety of different half-wavelengths 'm' across the width. m = 1,2 and 3 were studied.

11.3.1 Description of the Model

The dimensions and material properties of the plate have been given in Figure 39 and photographs are shown in Figures 95 and 96. The plate is stiffened along its two long edges by frames ≅ 0.32 [m] apart and across its width by seven 'Z section' stiffeners. The cross-sectional dimensions and material properties of the stiffeners are given in Appendix C. The frames and the stiffeners are rivetted to the plate. The distance between the lines of frame rivets is ≅ 0.34 [m]. There are six nominally- identical intermediate bays and two shorter overhanging-bays. Hence the plate can be approximated as a periodic structure with six bays.

For testing purposes, the plate was bolted through the frames on to two steel sections which were bolted to a massive test-bed. Hence the possibility of ground induced vibrations was kept to a minimum. In order to excite the plate, exciters were attached to it through small aluminium cylinders stuck on a line across the width. Their locations were determined by the mode to be excited. The exciters were suspended from a bridge across the plate. Figure 97 shows the overall arrangement.

11.3.2 The Test Apparatus

Figure 98 is the block-diagram of the experimental set-up and shows the equipment used. The TFA was the same as that used in Section 11.2.2. An accelerometer was used to measure the response and was placed for each excitation mode at the point where the response was expected to be greatest.

11.3.3 Experimental Procedure

The exciters were driven from the TFA with a random signal of bandwidth 200 [Hz] between 100 to 300 [Hz]. Data from 500 runs was acquired and averaged for each experiment. Forcing was applied along a line at $x = 0.36$ [m] and acceleration measurements were made at $x = 0.37$ [m] (see Figure 39).

Since the main purpose of this experiment was to locate the resonance frequencies, the calibration of forcing and response signals were not required. This implies that the obtained response levels had arbitrary scales.

If the frames provided simple supports, the motion across the width of the plate would vary sinusoidally in any of the resonant modes. In order to excite preferentially the modes with one half-wave across the width ($m = 1$), all three exciters should act in phase with another. One should be located at the centre of the plate width and the other two at $\cong w_e/6$ from the frame rivet lines ('w_e' denotes the width (*i.e.*, 0.34 [m])). If the outer two are driven with half the amount of the current of the central exciter, excitation of the $m = 3$ modes is minimised. The $m = 2$ modes cannot be excited by this arrangement.

To excite the $m = 2$ modes, two exciters were used. Each was placed at $\cong w_e/4$ from the centre line and were driven 180° out of phase with one another but with the same current amplitude.

To excite the $m = 3$ modes, one exciter was placed at the middle and the others at $\cong w_e/6$ from the frame rivet lines. Each exciter was

driven with the same current amplitude but the central exciter was 180° out of phase with the other two.

In order to ensure the repeatability of results, the experiment for m = 1 was conducted nine times under different conditions (*i.e.*, several different excitation levels were used, the set-up was dismantled and re-assembled and the exciters were interchanged).

Vibration mode shapes across the plate width were also determined for the first three resonance frequencies with m = 1. This was done using harmonic excitation. A moving accelerometer measurement was made along a line at x = 0.52 [m] and a reference accelerometer measurement (mid-way between the frames) was made simultaneously. The ratio of the magnitudes and the relative phase between the reference and moving accelerometer were thus determined.

11.3.4 Experimental Results

Figure 99 shows the random transfer function versus frequency for the excitation mode m = 1. As explained in Chapter 6, the resonance frequencies of an N_b bay periodic structure occur in bunches of N_b. Therefore the resonance frequencies of the plate should occur in bunches of six. This can be observed on Figure 99. The response at higher frequencies appears to be damped more than the response at lower frequencies, probably due to acoustic damping. The peak around 260 Hz is because of a group of frequencies with m = 3.

The resonance frequencies identified from Figure 99 are shown in Table 9. It also gives the average frequencies and the maximum deviations from nine sets of experiments with m = 1. The resolution of the TFA was 0.78 Hz, hence the accuracy of the procedure is evident.

When sinusoidal excitation was used, the first three resonance frequencies were found to be 131 [Hz], 140 [Hz], 151 [Hz]. Figure 100 shows the normalised, measured mode shapes across the width at these frequencies and Figure 101 gives the corresponding relative phases. Figure 100 clearly suggests that the test piece (or the excitation) is

not symmetric. The curves also indicate that the frames provided finite transverse and non-zero rotational constraints, rather than infinite transverse and zero rotational constraints as assumed in the theory of Chapter 6 (*i.e.*, simple supports). Nevertheless, to simplify the theoretical analysis the frames have been accepted as providing simple supports and a plate width of 0.34 [m] has been retained in the theoretical analysis.

Figure 102 shows transfer function versus frequency for excitation mode m = 2. The three small peaks between ≅ 130 to ≅ 160 [Hz] indicates that m = 1 mode resonances have also been excited.

Figure 103 shows transfer function versus frequency for excitation mode m = 3. Comparison of Figures 99 and 103 shows that excitation in either mode m = 1 or m = 3 can cause small responses in modes 3 and 1 respectively.

11.3.5 Comparison with the Theory

By using the method of Section 6.2.1 the theoretical resonance frequencies of the eight-bay, stiffened plate can be computed. The dimensions and the material properties of the plate are shown in Figure 39. The material loss factor is taken as $\eta = 0.01$, but this should not deeply influence the resonance frequencies. Details of the stiffeners are given in Appendix C. The stiffeners were assumed to possess dynamic stiffnesses, dynamic stiffness coupling and to undergo cross-sectional distortion. Sinusoidal line forcing is applied at $x_o = 0.36$ [m] and the response has been computed at $x_r = 0.37$ [m]. These locations correspond to the experimental excitation and measurement positions. Equation (6.3) has been used to calculate the frequency response curves. Resonance frequencies have been found by iterating to identify the frequencies for maximum response levels.

Table 10 compares the theoretical resonance frequencies so obtained with the average experimental frequencies for m = 1. The experimental and theoretical frequencies of modes 4, 5 and 6 agree quite well but the experimental frequencies of modes 1, 2 and 3 are substantially

lower than the theoretical values. These frequencies are heavily influenced by the rotational stiffness of the stiffeners, so it appears that the actual rotational stiffnesses are considerably less than those used in the calculations. The theoretical rotational stiffness took account of the effect of cross-sectional distortion of the stiffener and this effect was quite large in this particular case (see Section 6.2.3.3). However, there appear to be other factors which further reduce the actual stiffnesses and these include the effect of flexibility of the rivets which join the stiffener to the plate. More work is required to investigate this problem.

11.4 Free-Free Three-Layered Sandwich Beams

This section describes experiments on free-free three-layered sandwich beams having equal face-plates. The aim was to obtain frequency response curves and to compare these with values calculated from the theories of Section 5.2.

Two different experiments were conducted. In the first the calibrated exciter of Section 11.2.2 was used. The purpose was to determine the central direct transverse inertance of the beam. The purpose of the second was to determine the ratio of the tip transverse response to the central transverse response of the beam by using two laser vibrometers [35]. In both cases the forcing was applied at the middle so only the symmetric modes were excited.

11.4.1 The Models and the Test Apparatus

For the first experiment, the beam was attached at its centre to the exciter head and a 2 [g] accelerometer was fixed at the same point. The total mass of the accelerometer, exciter moving mass and the coupler was 11.63 [g]. The beam length was 238 [mm] and the width was 47 [mm].

For the second experiment, a different exciter was used. A mass of approximately 300 [g], which was 20 times that of the beam, was connected to the exciter spindle and the beam was attached to it. This arrangement served to maintain the acceleration at the excitation point at an almost constant level as the excitation frequency was varied. The beam length was 278 [mm].

Figure 104 shows a block diagram of the equipment used for the first experiment. The TFA was the same as used in the previous sections. The voltage across the fixed resistor in the exciter circuit gave a signal proportional to the exciting force, and the output from the charge amplifier gave a signal proportional to the acceleration response. These signals were processed by the TFA to give the transfer function.

Figure 105 shows the block diagram for the second experiment in which the velocity response at two points on the beam was measured by laser vibrometers. The output from these were processed by the TFA to yield the velocity transfer function: velocity close to the beam tip ÷ velocity at beam centre.

11.4.2 Experimental Procedure and Results

In each experiment the beam was excited randomly with a bandwidth of 800 [Hz]. Transfer functions were obtained through the TFA by averaging more than 250 runs. When using the accelerometer the temperature was 20°C and when using the lasers it was 18°C.

The measured transfer functions are shown by the dotted lines on Figures 106 and 107. Figure 106 shows the direct inertance at the beam centre (acceleration/force). Figure 107 shows the velocity transfer function.

11.4.3 Comparison with Theories

The theoretical inertance corresponding to the first experiment can be computed by making use of the beam response theories of Sections 4.3.2.2 and 5.2.3. It leads to a 7 × 7 matrix equation for the six unknown free wave amplitudes in the beam, and for the one unknown reaction exerted by the central point mass. For the second experiment, the velocity transfer function is independent of the central mass so the theory only leads to a 6 × 6 matrix equation for the unknown free wave amplitudes.

The core shear modulus in the calculations was taken from Figure 7 corresponding to either T = 20°C or T = 18°C. Over the frequency range f = 100 to 1000 [Hz] this is adequately represented by

$$\log (10\, G_c) = 0.54407 \log f + 6.91187 \quad [N/m^2] \quad \text{at } 20^\circ C$$
$$\log (10\, G_c) = 0.52288 \log f + 7.03342 \quad [N/m^2] \quad \text{at } 18^\circ C$$

Over the same frequency range and temperatures, Figure 7 gives the core loss factor to be approximately $\beta = 1.0$.

The theoretical inertance and velocity transfer function are superimposed upon the experimental values on Figures 106 and 107. Figure 107 shows quite good agreement between the theory and experiment although the theory underestimates the magnitudes of each of the peaks. Similar agreement (and disagreement) are seen on Figure 106 except at very low frequencies where the experimental curve has an additional resonant peak. This resonance is associated with the mass of the system resonating against the stiffness of the exciter diaphragm. This stiffness was not included in the theory as the associated resonance was expected to be well below the frequencies of interest – as it has turned out to be. The frequency range above ≅ 100 Hz is of principal interest in this investigation.

The experiments of this section also helped to verify the theoretical core data given in Figure 7. Although the peak levels were not in very good agreement, the accuracy in estimating the resonance frequencies and off-resonant response levels is a clear

indication that the theoretical G_c values closely represent the actual values.

11.5 Eight-Bay, Stiffened, Three-Layered Sandwich Plate

This section describes the experiments carried out on an eight-bay, stiffened three-layered sandwich plate. The purpose was to measure the transverse response of the plate to a simulated line exciting force and thus to verify the theory developed in Section 6.3.1. Excitation simulated a single half-wavelength across the width (m = 1).

For each excitation position, the measurements were made at more than one point. The reason stems from the fact that in the analysis of complicated structures, such as this stiffened multi-bay plate, the measured and ideal structures are not usually identical. Therefore single point measurements can yield considerable error in response level predictions. Hence the responses were obtained by measuring at different points and then averaging the whole data.

11.5.1 Description of the Model

The plate had equal face-plates and dimensions and properties as given in Section 6.3.2.1. Figure 42 shows the overall dimensions and Figures 108 and 109 show the top and bottom views of the plate. The frames and stiffeners were identical to those of the stiffened plate of Section 11.3 but were bonded (not rivetted) to the sandwich plate. The core of the plate consisted of the same viscoelastic material as already considered. Core shear modulus and loss factor characteristics are given by Figure 7.

The plate was mounted, as in Section 11.3, on steel channels on a massive test-bed and was excited by three electrodynamic exciters mounted on the same bridge (see Figure 97).

11.5.2 The Test Apparatus and Procedure

The apparatus used was exactly the same as that described in Section 11.3.2 (see Figure 98).

The exciters were arranged preferentially to excite the modes with m = 1 and were supplied with a random current having a bandwidth of 400 [Hz] (10 to 410 [Hz]). During the experiments the temperature was T = 20°C.

Six sets of experiments were conducted. These were done by exciting each intermediate bay in turn and measuring the acceleration responses within the same bay. The purpose was to examine the variation in response of the loaded bay as the line of excitation was changed from one bay to another. The excitation line selected in each bay was approximately at the bay centre (see Figure 108). Response measurements were made at six locations at both sides of the line of excitation. Response was always measured along the longitudinal line of the central exciter. Figure 110 gives the six excitation lines and the corresponding measurement points. For each exciter and accelerometer location, data from 250 runs was acquired and averaged. Therefore for each set, data from 1500 runs were analysed (*i.e.*, 250 runs at six locations).

11.5.3 Experimental Results and Comparison with Theory

Figures 111 to 116 show measured average inertances as dotted lines for each of the six intermediate bays. Although the plate is periodic with six bays, there is no evidence of six resonance peaks in the frequency range considered (which covers the first propagation zone of the structure (see Figure 79)). The peaks have been flattened by the heavy damping in the plate and have merged to form the single low 'hump' in each curve.

The measured values are seen to be almost independent of the location of the excitation. This is rather unexpected, as the theoretical considerations in Section 6.3.2.5 have indicated that the

response at the extreme end bays should be higher due to the contributions of the reflected waves from the ends.

The experimental results are to be compared with theoretical results based on Chapter 6, in which the plate is excited by a line distributed force $F_o \sin(m\pi y/w_e)$. In the experiment the plate was excited by three point forces as already described. These three forces can be represented by a Fourier series of distributed forces such that

$$\text{Actual force distribution} = \sum_{m=1}^{\infty} F_m \sin(m\pi y/w_e)$$

The actual force distribution consists effectively of three delta functions at $y = w_e/6,\ w_e/2,\ 5w_e/6$ and of magnitudes F/2, F, F/2 (see Section 11.3.3). Simple Fourier analysis shows that

$$F_1 = 2(F \sin \pi/2 + F/2 \sin \pi/6 + F/2 \sin 5\pi/6)/w_e$$

Since w_e is 0.34 [m], the equivalent force per unit width of the plate corresponding to the Fourier component m = 1 is

$$F_1 \cong (9\ F) \qquad [N/m]$$

The theoretical values of inertances have been calculated using the method developed in Section 6.3.1. With a given frequency, line force location and m = 1 inertance values were computed for the same points on the panel as used in the experiment. These inertances were then averaged in the same way as the experimental data. The G_C value used in the calculations was found from the 20°C expression of Section 11.4.3. The core loss factor was taken to be $\beta = 1.0$ over the whole frequency range.

The theoretical average inertances so obtained have been superimposed on Figures 111 to 116. The general shapes and magnitudes of the experimental and theoretical curves are similar. The experimental peak frequencies are always quite close to but less than the theoretical values. The reason, as suggested in Section 11.3.5, may be attributed to the imperfect representation of the stiffener

dynamic stiffnesses in the theory. The resonant magnitudes of the experimental and theoretical inertances are nearly identical. This shows that the developed analytical method is capable of analysing such a complicated structure and can provide accurate results.

CHAPTER 12

CONCLUSIONS

This study has developed analytical methods for the analysis of harmonically forced vibrations of beams and plates. Infinite and uninterrupted, finite, infinite and periodic structures have been considered. The structures were uniform in thickness. The beams considered were straight and the plates were flat. The plates had two opposite edges along the length as simply-supported.

Detailed conclusions related to individual chapters have been included at the end of each chapter. This chapter concentrates on the points which are thought to be most important and also tries to set the guidelines for any future work necessary for the better understanding of the phenomena involved.

12.1 General Conclusions

The method developed for the solution of forced vibrations of finite structures is an exact approach. The bays of multi-bay structures may be of different length and each support may have different characteristics. The support dynamic features can easily be included in the analysis. The method also can allow stiffness coupling to exist between the transverse and rotational motions of the support. Multi-point and/or convected loading can conveniently be analyzed. The free vibration characteristics such as natural frequencies and mode shapes of finite structures can readily be deduced from the forced analysis. Any response quantity such as slope, acceleration, bending moment or shear force can easily be obtained.

In the analysis of free vibrations of infinite and periodic structures, the method conveniently incorporates the effects of the infinite number of reactions imposed on the structure by the supports and combines them into the 'Phased Array Receptance Functions' of the structure. These functions have a finite number of parameters. By

considering these together with the support characteristics, the method enables the propagation constants to be obtained simply by satisfying the necessary equilibrium and compatibility conditions at a single support location.

In the case of forced vibrations of infinite and periodic structures, the method reduces the problem from an infinite number of unknowns to a finite number of unknowns and provides an exact analysis.

The study of stiffener dynamic response has revealed that when it is properly included in the analysis, cross-sectional distortion of the stiffener basically reduces the magnitude of rotational stiffness at low frequencies. Furthermore at frequencies which are the natural frequencies of the stiffener when it is fully-fixed along the line of attachment to the plate, the stiffener acts like a dynamic absorber and resists motions in both transverse direction and rotation. Also demonstrated have been the effects of dynamic stiffness coupling of the stiffeners. Its inclusion only slightly reduces the natural frequencies of finite multi-bay structures but the effect on the mode shapes can be drastic.

In the experimental studies measured transverse responses of sandwich beams have shown good agreement with the theory. The slight discrepancies encountered in stiffened plate measurements have been attributed to the deficiencies in the modelling of the stiffener characteristics.

12.2 Recommendations for Future Work

Since the analysis has been based on the Euler-Bernoulli Theory of beams and plates or the Mead-Markus Theory of sandwich beams and plates, it ignores the shear deformation of the elastic layers and rotatory inertias. The inclusion of these features will make the models applicable to a wider range of frequencies. The method also excludes in-plane longitudinal displacements.

The inclusion of longitudinal plate displacement in the analysis will mean that the stiffness (and inertia) of the stiffeners in that direction must also be included. So far this has been disregarded on the grounds that the skin provides infinite resistance along the line of attachment against movement in this direction. For the completeness of the problem, consideration of this aspect might provide more realistic approach.

Inclusion of cross-sectional distortion effects has led to a more accurate representation of the stiffener characteristics than hitherto. However, the experimental findings suggest that the model is not yet complete. It appears that the theoretical rotational stiffness of the stiffener is still higher than the actual value. Further research into the complicated nature of stiffener behaviour is therefore essential.

The method is capable of being applied to more complicated cases such as the vibrations of uniform single or multi-layered shell structures under convected loading. Although this task has not been currently undertaken it certainly deserves attention.

Another phenomenon which can be analysed through the developed method is the vibrations of open channel sections where the motions are coupled. Initial studies in this field are under way.

REFERENCES

REFERENCES

1. D.J. GORMAN 1975 John Wiley and Sons Inc. 'Free Vibration Analysis of Beams and Shafts'. Chapter 6.

2. C.L. KIRK 1960 Journal of Mechanical Engineering Science 2(3), 242-253. 'Vibration Characteristics of Stiffened Plates'.

3. C.L. KIRK 1970 Journal of Sound and Vibration 13(4), 375-388. 'Natural Frequencies of Stiffened Rectangular Plates'.

4. Y.K. LIN 1960 Journal of Applied Mechanics, 669-676. 'Free Vibrations of Continuous Skin-Stringer Panels'.

5. Y.K. LIN 1960 Journal of Applied Mechanics, 739-740. 'Coupled Bending and Torsional Vibrations of Restrained Thin-Walled Beams'.

6. Y.K. LIN, I.D. BROWN and P.C. DEUTSCHLE 1964 Journal of Sound and Vibration 1, 14-27. 'Free Vibration of a Finite Row of Continuous Skin-Stringer Panels'.

7. C.A. MERCER and C. SEAVEY 1967 Journal of Sound and Vibration 6(1), 149-162. 'Prediction of Natural Frequencies and Normal Modes of Skin-Stringer Panel Rows'.

8. L. BRILLOUIN 1946 Dover Publications Inc., New York. 'Wave Propagation in Periodic Structures'.

9. M.A. HECKL 1964 Journal of the Acoustical Society of America 36, 1335-1343. 'Investigations on to Vibrations of Grillages and Other Simple Beam Structures'.

10. D.J. MEAD and E.F. WILBY 1966 Shock and Vibration Bulletin 35(3), 45-54. 'The Random Vibrations of Multi Supported Heavily Damped Beam'.

11. G. SEN GUPTA 1970 Journal of Sound and Vibration 13(1), 89-101. 'Natural Flexural Waves and Normal Modes of Periodically Supported Beams and Plates'.

12. G. SEN GUPTA 1971 Journal of Sound and Vibration 16(4), 567-580. 'Natural Frequencies of Periodic Skin-Stringer Structures Using a Wave Approach'.

13. D.J. MEAD 1971 Trans. ASME Journal of Engineering for Industry 93(B), 783-792. 'Vibration Response and Wave Propagation of Periodic Structures'.

14. D.J. MEAD 1975 Journal of Sound and Vibration 40(1), 1-18. 'Wave Propagation and Natural Modes in Periodic Systems: 1. Mono Coupled Systems'.

15. D.J. MEAD 1975 Journal of Sound and Vibration 40(1), 19–39. 'Wave Propagation and Natural Modes in Periodic Systems: 2. Multi-Coupled Systems, With or Without Damping'.

16. A.Y.A. ABDEL-RAHMAN and M. PETYT 1980 Proceedings of International Conference on Recent Advances in Structural Dynamics, University of Southampton. 'Free and Forced Wave Propagation in Two Dimensional Periodic Systems Using Matrix Techniques'.

17. D.J. MEAD 1986 Journal of Sound and Vibration 104(1), 9–27. 'A New Method of Analyzing Wave Propagation in Periodic Structures; Applications to Periodic Timoshenko Beams and Stiffened Plates'.

18. M.L. MUNJAL and M. HECKL 1982 Journal of Sound and Vibration 81(4), 491–500. 'Vibration of a Periodic Rail-Sleeper System Excited by an Oscillating Stationary Transverse Force'.

19. G. SEN GUPTA 1980 Shock and Vibration Digest 12(3), 17–31. 'Vibration of Periodic Structures'.

20. D.J. MEAD 1965 Acoustical Fatigue in Aerospace Structures, Syracuse University Press, Syracuse, New York. 'The Damping of Stiffened Plate Structures'.

21. E.M. KERWIN 1959 Journal of the Acoustical Society of America 31, 952–962. 'Damping of Flexural Waves by a Constrained Visco-Elastic Layer'.

22. D.J. MEAD 1965 USAF Report no. AFML-TR-65-824. 'The Effect of Certain Damping Treatments on the Response of Idealized Aeroplane Structures Excited by Noise'.

23. R.A. DiTARANTO 1965 Trans. ASME Journal of Applied Mechanics 87, 881–886. 'Theory of Vibratory Bending for Elastic and Visco-Elastic Layered Finite Length Beams'.

24. D.J. MEAD and S. MARKUS 1969 Journal of Sound and Vibration 10(2), 163–175. 'The Forced Vibration of a Three-Layer Damped Sandwich Beam with Arbitrary Boundary Conditions'.

25. D.J. MEAD and S. MARKUS 1970 Journal of Sound and Vibration 12(1), 99–112. 'Loss Factors and Resonant Frequencies of Encastre Damped Sandwich Beams'.

26. D.J. MEAD 1972 Journal of Sound and Vibration 24(3), 275–295. 'The Damping Properties of Elastically Supported Sandwich Plates'.

27. D.J. MEAD 1976 Trans. ASME Journal of Engineering for Industry, 75–80. 'Loss Factors and Resonant Frequencies of Periodic Damped Sandwich Plates'.

28. D.J. MEAD 1967 Proceedings of the International Symposium on the Damping of Vibrations of Plates by Means of a Layer, Louvain, Belgium. 'The Use of Stiffened Sandwich Plates on Aircraft'.

29. B.C. NAKRA 1976 Shock and Vibration Digest 8(6), 3-12. 'Vibration Control with Viscoelastic Materials'.

30. L. CREMER, M. HECKL and E.E. UNGAR 1973 Springer-Verlag. 'Structure Borne Sound', Chapter 4.

31. R.D. BLEVINS 1979 Van Nostrand Reinhold. 'Formulas for Natural Frequency and Mode Shape', Chapter 8.

32. D.J. MEAD 1970 Journal of Sound and Vibration 11, 181-197. 'Free Wave Propagation in Periodically Supported Infinite Beam'.

33. A.K. ROY and R. PLUNKETT 1986 Journal of Sound and Vibration 104(3), 395-410. 'Wave Attenuation in Periodic Structures'.

34. Hewlett-Packard 5420 Digital Signal Analyzer User's Guide 1979 Hewlett-Packard Company, USA.

35. C.J.D. PICKERING, N.A. HALLIWELL and T.H. WILMSHURST 1986 Journal of Sound and Vibration 107(3), 471-485. 'The Laser Vibrometer: A Portable Instrument'.

36. D.J. MEAD 'Unpublished work'.

37. R.F. BERESFORD and D.J. MEAD 1966 Journal of Sound and Vibration 3(3), 315-334. 'The Free Vibrations of an Angle Section Involving Cross-Sectional Distortion'.

APPENDICES

APPENDIX A

DETERMINATION OF THE COEFFICIENTS OF INFINITE-SYSTEM LINE RESPONSE FUNCTIONS OF THREE-LAYERED SANDWICH PLATES HAVING EQUAL FACE-PLATES

Consider Figure 15. Total bending moment M_x per unit length on the whole sandwich cross-section derives from the total bending moments of the face plates M_{fp} per unit length and the bending moment due to axial forces M_{af} per unit length. Hence it can be shown to be

$$M_x = M_{fp} + M_{af} = (M_1 + M_3) + \sigma hd \qquad (A.1)$$

where M_1 and M_3 are the bending moments of the equal top and bottom face-plates respectively. σ is the direct stress on the bottom face plate and $d = h + h_c$.

Using elementary plate theory, the above equation can be written as

$$M_x = D_t\left(\frac{\partial^2 w}{\partial x^2} + \nu \frac{\partial^2 w}{\partial y^2}\right) + \left(\frac{E}{(1 - \nu^2)}\left(\frac{\partial u}{\partial x} + \nu \frac{\partial v}{\partial y}\right)\right)hd \qquad (A.2)$$

where $D_t = 2Eh^3/(12(1 - \nu^2))$. u and v are the mid-plane axial displacements of bottom face-plate in x and y directions respectively.

The total twisting moment M_{xy} per unit length on the whole sandwich cross-section is due to the twisting moments of the face-plates plus the moment due to the face-plate shear forces τ_{xy}. In this way it can be written as

$$M_{xy} = -D_t(1 - \nu) \frac{\partial^2 w}{\partial x \partial y} - \frac{Ehd}{2(1 + \nu)}\left(\frac{\partial u}{\partial y} + \frac{\partial v}{\partial x}\right) \qquad (A.3)$$

The total transverse shear force S_x per unit length on the whole section can be found to be

$$S_x = -\frac{\partial M_x}{\partial x} + \frac{\partial M_{xy}}{\partial y} \qquad (A.4)$$

The effective transverse shear force S_{eff} per unit length on the whole sandwich plate cross-section can be obtained as

$$S_{eff} = S_x + \frac{\partial M_{xy}}{\partial y} \tag{A.5}$$

Using equations (A.2), (A.3), (A.4) the above equation can be expressed as

$$S_{eff} = -\{D_t[\frac{\partial^3 w}{\partial x^3} + (2 - \nu)\frac{\partial^3 w}{\partial x \partial y^2}]$$

$$+ \frac{Ehd}{(1 - \nu^2)}[\frac{\partial^2 u}{\partial x^2} + (1 - \nu)\frac{\partial^2 u}{\partial y^2} + \frac{\partial^2 v}{\partial x \partial y}]\} \tag{A.6}$$

Equation (3.14) gives the forms of the transverse displacement w, and the face-plate mid-plane axial displacements u and v of the bottom face-plate. By substituting it together with equation (3.15) into equation (A.6) and carrying out the necessary manipulations the effective shear force can be expressed in terms of w, as

$$S_{eff} = -\{D_t k_n\{[k_n^2 - (2 - \nu)k_y^2][1 + \frac{g^* Y}{(k_n^2 - k_y^2 - g^*)}]\}\}w \tag{A.7}$$

where the parameters have been defined in Chapter 3.

Similarly, the total face-plate bending moment and the bending moment due to the face-plate axial forces can also be expressed in terms of w, as

$$M_{fp} = \{D_t(k_n^2 - \nu k_y^2)\}w \tag{A.8}$$

$$M_{af} = -\left\{\frac{Ehd^2 g^*(k_n^2 - \nu k_y^2)}{2(1 - \nu^2)(k_n^2 - k_y^2 - g^*)}\right\}w \tag{A.9}$$

Suppose that a single transverse line force $F_o \sin k_y y$ per unit length acts on the infinite sandwich plate at $(0,y)$. The transverse

displacement and rotation of the uniform, infinite, uninterrupted sandwich plate in the positive x region are given by

$$w(x,y) = F_o \sum_{n=1}^{3} a_n e^{-k_n x} \sin k_y y$$

$$\theta(x,y) = F_o \sum_{n=1}^{3} c_n e^{-k_n x} \sin k_y y \qquad \text{(A.10)}$$

The boundary conditions to be satisfied at the line of application of the force are

$$S_{eff}|_{x=0} = -\frac{F_o}{2} \sin k_y y$$

$$\frac{\partial w}{\partial x}\Big|_{x=0} = 0$$

$$u|_{x=0} = 0 \qquad \text{(A.11)}$$

Since the sandwich plate section moves as a whole $\partial w/\partial x = -k_n w$ where $n = 1$ to 3 and u is given by equations (3.14) and (3.15). The three boundary conditions of equation (A.11) can be expressed in the matrix form as

$$\begin{bmatrix} \Lambda_1 & \Lambda_2 & \Lambda_3 \\ -k_1 & -k_2 & -k_3 \\ \Gamma_1 & \Gamma_2 & \Gamma_3 \end{bmatrix} \begin{Bmatrix} a_1 \\ a_2 \\ a_3 \end{Bmatrix} = \begin{Bmatrix} -F_o/2 \\ 0 \\ 0 \end{Bmatrix} \qquad \text{(A.12)}$$

where $\Lambda_n = D_t k_n \{[k_n^2 - (2 - \nu)k_y^2]\,[1 + (g^*Y)/(k_n^2 - k_y^2 - g^*)]\}$

$\Gamma_n = (g^* d k_n)/[2(k_n^2 - k_y^2 - g^*)]$

a_1, a_2 and a_3 can be found from this matrix equation. As can be seen Λ_n is the negative of the coefficient of equation (A.7). This stems from the fact that equation (A.7) is derived by retaining all six terms of the transverse displacement expression given by equation (3.14), whereas Λ_n is obtained from equation (A.10) which only considers three terms.

Once the a_n's are found, the coefficients which represent the rotation due to a transverse force can be obtained as

$$c_n = -k_n a_n \qquad (n = 1,2,3) \tag{A.13}$$

Now, assume that a single harmonic line moment $M_o \sin k_y y$ per unit length acts on the sandwich plate at (0,y). The transverse displacement and the rotation in the positive x region can now be expressed as

$$w(x,y) = M_o \sum_{n=1}^{3} b_n e^{-k_n x} \sin k_y y$$

$$\theta(x,y) = M_o \sum_{n=1}^{3} d_n e^{-k_n x} \sin k_y y \tag{A.14}$$

and the boundary conditions at the line of application become

$$M_{fp}|_{x=0} = -\frac{M_o}{2} \sin k_y y$$

$$w|_{x=0} = 0$$

$$M_{af}|_{x=0} = 0 \tag{A.15}$$

In this, it has been assumed that the externally applied moment crates no axial forces at its line of application on the sandwich cross-section. The contribution of the axial forces to the total bending moment is therefore zero. So all the applied moment is balanced by the face-plates bending moment M_{fp}.

The three boundary conditions of equation (A.15) can be expressed in the matrix form as

$$\begin{bmatrix} \Psi_1 & \Psi_2 & \Psi_3 \\ 1 & 1 & 1 \\ \Upsilon_1 & \Upsilon_2 & \Upsilon_3 \end{bmatrix} \begin{Bmatrix} b_1 \\ b_2 \\ b_3 \end{Bmatrix} = \begin{Bmatrix} -M_o/2 \\ 0 \\ 0 \end{Bmatrix} \qquad (A.16)$$

where $\Psi_n = \{D_t(k_n^2 - \nu k_y^2)\}$

$\Upsilon_n = -[(Ehd^2g^*)/(2(1 - \nu^2))][(k_n^2 - \nu k_y^2)/(k_n^2 - k_y^2 - g^*)]$

b_1, b_2 and b_3 can now be found from equation (A.16). The rotational coefficients, d_n's, can be obtained from b_n's as

$$d_n = -k_n\, b_n \qquad (n = 1,2,3) \qquad (A.17)$$

Due to the great complexity involved in algebra, all the coefficients are computed numerically. In their calculations, unit external excitation ($F_o = M_o = 1$) is assumed.

APPENDIX B

THE RESPONSE OF AN UNDAMPED FINITE BEAM TO A POINT HARMONIC FORCE

Consider equation (4.7). It was shown in Chapter 2 that for a uniform Euler-Bernoulli beam $k_1 = k$, $k_2 = ik$ and $a_2 = ia_1$. It was also shown in the same chapter that for undamped beams k and a_1 are purely real. Equation (4.7) can therefore be rewritten as

$$\begin{bmatrix} 1 & 1 & 1 & 1 \\ 1 & -1 & 1 & -1 \\ e^{kL} & e^{ikL} & e^{-kL} & e^{-ikL} \\ e^{kL} & -e^{ikL} & e^{-kL} & -e^{-ikL} \end{bmatrix} \begin{Bmatrix} A_1 \\ A_2 \\ A_3 \\ A_4 \end{Bmatrix} = -F_o a_1 \begin{Bmatrix} e^{-kx_o} + ie^{-ikx_o} \\ e^{-kx_o} - ie^{-ikx_o} \\ e^{-k(L-x_o)} + ie^{-ik(L-x_o)} \\ e^{-k(L-x_o)} - ie^{-ik(L-x_o)} \end{Bmatrix} \quad (B.1)$$

Now add the second row to the first and the fourth row to the third in this matrix equation. Then add -1/2 of the new first row to the second and -1/2 of the new third row to the fourth. Equation (B.1) then reduces to

$$\begin{bmatrix} 2 & 0 & 2 & 0 \\ 0 & -1 & 0 & -1 \\ 2e^{kL} & 0 & 2e^{-kL} & 0 \\ 0 & -e^{ikL} & 0 & -e^{-ikL} \end{bmatrix} \begin{Bmatrix} A_1 \\ A_2 \\ A_3 \\ A_4 \end{Bmatrix} = -F_o a_1 \begin{Bmatrix} 2e^{-kx_o} \\ -ie^{-ikx_o} \\ 2e^{-k(L-x_o)} \\ -ie^{-ik(L-x_o)} \end{Bmatrix} \quad (B.2)$$

The A_n's can then be found to be

$$A_1 = - \frac{e^{-kL} \sinh kx_o}{\sinh kL} (F_o a_1)$$

$$A_2 = - \frac{ie^{-ikL} \sin kx_o}{\sin kL} (F_o a_1)$$

$$A_3 = \frac{\sinh (k(x_o - L))}{\sinh kL} (F_o a_1)$$

$$A_4 = \frac{i \sin(k(x_o - L))}{\sin kL} (F_o a_1) \qquad (B.3)$$

Using these in equation (4.1a) the transverse displacement at any x_r is given by

$$w(x_r) = F_o a_1 \left\{ - \frac{e^{-kL} \sinh kx_o}{\sinh kL} e^{kx_r} - \frac{ie^{-ikL} \sin kx_o}{\sin kL} e^{ikx_r} \right.$$

$$+ \frac{\sinh (k(x_o - L))}{\sinh kL} e^{-kx_r} + \frac{i \sin(k(x_o - L))}{\sin kL} e^{-ikx_r}$$

$$\left. + e^{-k|x_o - x_r|} + ie^{-ik|x_o - x_r|} \right\} \qquad (B.4)$$

Long algebraic manipulations show that the imaginary terms in this cancel out and the final form of the transverse displacement becomes

$$\frac{w(x_r)}{F_o} = a_1 \left\{ \frac{\sinh (k(x_o - L))}{\sinh kL} (\cosh kx_r - \sinh kx_r) \right.$$

$$- \frac{\sinh kx_o}{\sinh kL} (\cosh(k(x_r - L)) + \sinh(k(x_r - L)))$$

$$+ \cosh k(x_o - x_r) - \sinh k|x_o - x_r|$$

$$+ 2 \sin kx_o \sin kx_r \cot kL - \sin kx_o \cos kx_r$$

$$\left. - \sin kx_r \cos kx_o + \sin k|x_o - x_r| \right\} \qquad (B.5)$$

As can be seen, all the terms are purely real. It therefore proves that in the absence of damping the dynamic response of finite, uniform Euler-Bernoulli beam is purely real.

APPENDIX C

DETERMINATION OF THE DYNAMIC STIFFNESSES OF A Z-SECTION STIFFENER INCLUDING BEAM BENDING AND TORSION AND CROSS-SECTIONAL DEFORMATION

C.1 Specification of the Stiffener Displacements and Applied Forcing

Consider Figure C.1. It gives the coordinate system to be used, the dimensional parameters, the external harmonic forcing and the total deflection of the Z-section stiffener. The cross-section has a constant thickness t and is allowed to deflect transversely by w. Web BC and flange AB rotate by θ with respect to point C and the web further distorts by $u_r(z)$ relative to the tangent drawn at C. The distortion of the flange is ignored. Section CD is the effective width of the plate skin at which the stiffener is attached. The length of the stiffener in the y direction is L_y and it is simply-supported at the ends $y = 0$ and $y = L_y$. All the displacements and the rotation are sinusoidally varying along the length and harmonically varying in time, so

$$
\begin{aligned}
w(y,t) &= w \sin k_y y \, e^{i\omega t} \\
\theta(y,t) &= \theta \sin k_y y \, e^{i\omega t} \\
u_r(y,z,t) &= u_r(z) \sin k_y y \, e^{i\omega t} \\
F(y,t) &= F_o \sin k_y y \, e^{i\omega t} \quad \text{per unit length} \\
M(y,t) &= M_o \sin k_y y \, e^{i\omega t} \quad \text{per unit length}
\end{aligned}
\qquad (C.1)
$$

where $k_y = m\pi/L_y$ and m is the number of half-wavelengths along the length.

Let us denote the web distortion relative to the tangent drawn at C by

$$u_r(z) = (Az^2 + Bz^3) \qquad (C.2)$$

where A and B are the coefficients yet to be determined.

The total motion of the web in the x direction, u(z), therefore becomes

$$u(z) = (\theta z + Az^2 + Bz^3) \qquad (C.3)$$

C.2 The Kinetic Energy of the Vibrating Beam

The approach utilized in this section [36] makes use of energy principles. By considering the displacements of the web in the x and z directions and by using the elementary theory, the kinetic energy of the web can be shown to be

$$T_{web} = \frac{1}{2}\int_o^h\int_o^{L_y} \rho t(\dot{u}(z))^2 dy\, dz + \frac{1}{2}\int_o^h\int_o^{L_y} \rho t\, \dot{w}^2\, dy\, dz \qquad (C.4)$$

where '·' denotes $\partial/\partial t$.

Insert the values of u(z) from Equations (C.1), (C.2) and (C.3) and w from (C.1). Hence the kinetic energy of the web turns out to be

$$T_{web} = \frac{1}{2}\int_o^h\int_o^{L_y} \rho t(\dot{\theta}z + \dot{A}z^2 + \dot{B}z^3)^2 \sin^2 k_y y\, dydz + \frac{1}{2}\int_o^h\int_o^{L_y} \rho t\, \dot{w}^2 \sin^2 k_y y\, dy\, dz \qquad (C.5)$$

By carrying out the necessary algebra, the kinetic energy of the web becomes

$$T_{web} = \frac{\rho t L_y}{4}\left\{\dot{\theta}^2\frac{h^3}{3} + \dot{A}^2\frac{h^5}{5} + \dot{B}^2\frac{h^7}{7} + \ddot{\theta}\dot{A}\frac{h^4}{2} + 2\ddot{\theta}\dot{B}\frac{h^5}{5} + \ddot{A}\dot{B}\frac{h^6}{3} + \dot{w}^2 h\right\} \qquad (C.6)$$

Now consider Figure C.2. It gives the deflections of the flange AB. The total transverse displacement of the flange can be found to be

$$w_{tot} = w + s\,\frac{\partial u_B}{\partial z} \tag{C.7}$$

where 's' is the positional coordinate along the flange, measured from B'.

Using equation (C.3) it can be found that

$$\frac{\partial u_B}{\partial z} = \frac{\partial u(z)}{\partial z}\bigg|_{z=h} = \theta + 2Ah + 3Bh^2 \tag{C.8}$$

Hence by considering the total flange displacements in x and z directions, the kinetic energy of the flange can be expressed as

$$T_{flange} = \frac{1}{2}\int_o^d\int_o^{L_y} \rho t[\dot{w} + (\dot{\theta} + 2\dot{A}h + 3\dot{B}h^2)s]^2 \sin^2 k_y y \, dy \, ds$$

$$+ \frac{1}{2}\,\rho dt(\dot{\theta}h + \dot{A}h^2 + \dot{B}h^3)^2 \int_o^{L_y} \sin^2 k_y y \, dy \tag{C.9}$$

which reduces to

$$\begin{aligned} T_{flange} = \frac{\rho t L_y}{4}\{&\dot{w}^2 d + \dot{w}\dot{\theta}d^2 + 2\dot{w}\dot{A}hd^2 + 3\dot{w}\dot{B}d^2h^2 \\ &+ \dot{\theta}^2\frac{d^3}{3} + \frac{4}{3}\dot{A}^2h^2d^3 + 3\dot{B}^2h^4d^3 + \frac{4}{3}\dot{\theta}\dot{A}hd^3 + 2\dot{\theta}\dot{B}h^2d^3 \\ &+ 4\dot{A}\dot{B}h^3d^3 + \dot{\theta}^2h^2d + \dot{A}^2h^4d + \dot{B}^2h^6d + 2\dot{\theta}\dot{A}h^3d + 2\dot{A}\dot{B}h^5d \\ &+ 2\dot{\theta}\dot{B}h^4d\} \end{aligned} \tag{C.10}$$

The total kinetic energy of the cross-section is the sum of the kinetic energies of the web and the flange. By using equations (C.6) and (C.10) it can be shown to be

$$T = \frac{\rho t L_y}{4} \{\dot{w}^2(h + d) + \dot{w}\dot{\theta}d^2 + 2\dot{w}\dot{A}hd^2$$

$$+ 3\dot{w}\dot{B}h^2d^2 + \dot{\theta}^2 (\frac{d^3}{3} + \frac{h^3}{3} + h^2d) + \dot{A}^2 (\frac{h^5}{5} + h^4d + \frac{4}{3} h^2d^3)$$

$$+ \dot{B}^2(3h^4d^3 + h^6d + \frac{h^7}{7}) + \dot{\theta}\dot{A}(\frac{4}{3} hd^3 + \frac{h^4}{2} + 2h^3d)$$

$$+ \dot{\theta}\dot{B}(2h^2d^3 + 2h^4d + \frac{2h^5}{5}) + \dot{A}\dot{B}(4h^3d^3 + \frac{h^6}{3} + 2h^5d)\} \qquad (C.11)$$

which can be put into the form

$$T = \frac{1}{2} \lfloor \dot{q} \rfloor [M_{nd}]\{\dot{q}\} (\rho t d L_y/2) \qquad (C.12)$$

where $\lfloor \dot{q} \rfloor = \lfloor \dot{w}, \dot{\theta}h, \dot{A}h^2, \dot{B}h^3 \rfloor$ and the matrix of non-dimensional parameters $[M_{nd}]$ is given by

$$[M_{nd}] = \begin{bmatrix} 1 + \frac{h}{d} & \frac{d}{2h} & \frac{d}{h} & \frac{3}{2}\frac{d}{h} \\ \frac{d}{2h} & \frac{1}{h^2}(\frac{d^2}{3}+hd+\frac{h^3}{3d}) & \frac{1}{h^3}(\frac{2hd^2}{3}+h^3+\frac{h^4}{4d}) & \frac{1}{h^4}(h^2d^2+h^4+\frac{h^5}{5d}) \\ \frac{d}{h} & \frac{1}{h^3}(\frac{2hd^2}{3}+h^3+\frac{h^4}{4d}) & \frac{1}{h^4}(\frac{4}{3}h^2d^2+h^4+\frac{h^5}{5d}) & \frac{1}{h^5}(2h^3d^2+h^5+\frac{h^6}{6d}) \\ \frac{3}{2}\frac{d}{h} & \frac{1}{h^4}(h^2d^2+h^4+\frac{h^5}{5d}) & \frac{1}{h^5}(2h^3d^2+h^5+\frac{h^6}{6d}) & \frac{1}{h^6}(3h^4d^2+h^6+\frac{h^7}{7d}) \end{bmatrix} \qquad (C.13)$$

When the generalized coordinates are transformed to a new set as $\lfloor \dot{q}_t \rfloor = \lfloor \dot{w}, \dot{u}_B, \dot{A}h^2, \dot{B}h^3 \rfloor$, the subsequent algebra considerably simplifies. Hence replace θh by $u_B - Ah^2 - Bh^3$ (see equation (C.3) with $z = h$) and also let $d/h = \alpha$. After rearranging the new form of equation (C.12) becomes

$$T = \frac{1}{2} \lfloor \dot{q}_t \rfloor [M_{nd,t}] \{\dot{q}_t\} (\rho th\, L_y/2) \qquad (C.14)$$

where the transformed non-dimensional matrix $[M_{nd,t}]$ can be shown to be

$$[M_{nd,t}] = \begin{vmatrix} (\alpha + 1) & \frac{\alpha^2}{2} & \frac{\alpha^2}{2} & \alpha^2 \\ \frac{\alpha^2}{2} & (\frac{\alpha^3}{3} + \alpha + \frac{1}{3}) & (\frac{\alpha^3}{3} - \frac{1}{12}) & (\frac{2\alpha^3}{3} - \frac{2}{15}) \\ \frac{\alpha^2}{2} & (\frac{\alpha^3}{3} - \frac{1}{12}) & (\frac{\alpha^3}{3} + \frac{1}{30}) & (\frac{2\alpha^3}{3} + \frac{1}{20}) \\ \alpha^2 & (\frac{2\alpha^3}{3} - \frac{2}{15}) & (\frac{2\alpha^3}{3} + \frac{1}{20}) & (\frac{4\alpha^3}{3} + \frac{8}{105}) \end{vmatrix} \qquad (C.15)$$

C.3 The Potential Energy of Cross-Sectional Distortion

Consider Figure C.3. The general expression of plate potential energy per unit area is given by

$$V = \frac{D}{2} \int_0^{L_\eta} \int_0^{L_\xi} \{(\frac{\partial^2 w}{\partial \eta^2} + \frac{\partial^2 w}{\partial \xi^2})^2 - 2(1 - \nu)(\frac{\partial^2 w}{\partial \eta^2} \frac{\partial^2 w}{\partial \xi^2} - (\frac{\partial^2 w}{\partial \eta \partial \xi})^2)\} d\eta d\xi \qquad (C.16)$$

Assume that the ends of the plate at $\xi = 0$ and $\xi = L_\xi$ are simply supported. The transverse displacement w can then be given by $w = f(\eta) \sin k_\xi \xi$ and equation (C.16) becomes

$$V = \frac{DL_\xi}{4} \int_0^{L_\eta} \{(\frac{\partial^2 f(\eta)}{\partial \eta^2})^2 - 2\nu k_\xi^2 \frac{\partial^2 f(\eta)}{\partial \eta^2} f(\eta) + 2(1 - \nu) k_\xi^2 (\frac{\partial f(\eta)}{\partial \eta})^2 + k_\xi^4 f^2(\eta)\} d\eta \qquad (C.17)$$

Now consider the flange AB of Figure C.1. The total transverse displacement of the flange is given by equation (C.7) and is a function of s. Hence

$$f(s) = (w + s\,\frac{\partial u_B}{\partial z}) = (w + \theta_B s)$$

$$\frac{\partial f(s)}{\partial s} = \theta_B = \frac{\partial u(z)}{\partial z}\Big|_{z=h} = \theta + 2Ah + 3Bh^2$$

$$\frac{\partial^2 f(s)}{\partial s^2} = 0 \qquad (C.18)$$

Substitute these together with the values $\eta = s$, $L_\xi = L_y$, $L_\eta = d$, $k_\xi = k_y$ to equation (C.17). Also put $D = Et^3/(12(1 - \nu^2))$. After evaluating the integrals it becomes

$$V_{flange} = \frac{EL_y}{4}\left\{\frac{dt^3}{12(1-\nu^2)}\,k_y^4 w^2 + \frac{d^2t^3}{12(1-\nu^2)}\,k_y^4\,\theta w\right.$$

$$+ \frac{2d^2t^3h}{12(1-\nu^2)}\,k_y^4\,Aw + \frac{3d^2t^3h^2}{12(1-\nu^2)}\,k_y^4\,Bw$$

$$+ \left[\frac{2(1-\nu)dt^3}{12(1-\nu^2)}\,k_y^2 + \frac{d^3t^3}{36(1-\nu^2)}\,k_y^4\right]$$

$$\left.\cdot(\theta^2 + 4h^2A^2 + 9h^4B^2 + 4h\theta A + 6h^2\theta B + 12h^3AB)\right\} \qquad (C.19)$$

Now consider the web CB of Figure C.1. The motion perpendicular to the plane of the web is given by equation (C.3), so

$$f(z) = \theta z + Az^2 + Bz^3$$

$$\frac{\partial f(z)}{\partial z} = \theta + 2Az + 3Bz^2$$

$$\frac{\partial^2 f(z)}{\partial z^2} = 2A + 6Bz \qquad (C.20)$$

By substituting these into equation (C.17) together with $\eta = z$, $L_\xi = L_y$, $k_\xi = k_y$, $L_\eta = h$, $D = Et^3/(12(1 - \nu^2))$ and carrying out the necessary manipulations it can be shown that

$$V_{web} = \frac{EL_y}{4}\left\{\left[\frac{ht^3}{12(1-\nu^2)}\left(4 + \frac{4}{3}(2-3\nu)k_y^2h^2 + \frac{k_y^4h^4}{5}\right)\right]A^2\right.$$

$$+ \left[\frac{h^3t^3}{12(1-\nu^2)}\left(12 + \frac{1}{5}(18-30\nu)k_y^2h^2 + \frac{k_y^4h^4}{7}\right)\right]B^2$$

$$+ \left[\frac{ht^3}{12(1-\nu^2)}\left(2(1-\nu)k_y^2 + \frac{h^2k_y^4}{3}\right)\right]\theta^2$$

$$+ \left[\frac{h^2t^3}{12(1-\nu^2)}\left(12 + (6-10\nu)k_y^2h^2 + \frac{k_y^4h^4}{3}\right)\right]AB$$

$$+ \left[\frac{t^3k_y^2h^2}{12(1-\nu^2)}\left(2(2-3\nu) + \frac{k_y^2h^2}{2}\right)\right]\theta A$$

$$\left. + \left[\frac{2t^3k_y^2h^3}{12(1-\nu^2)}\left((2-4\nu) + \frac{k_y^2h^2}{5}\right)\right]\theta B\right\} \qquad (C.21)$$

C.4 The Potential Energy of a Beam in Bending and Torsion

Consider Figure C.1 again. The lower flange CD and the x-wise forces on it make the principal bending axis of the cross-section virtually parallel to CD. Let this axis be XX. Hence, the bending stresses in the section due to w are

$$\sigma_b = -Ez' \frac{\partial^2 w}{\partial y^2} \qquad (C.22)$$

where z' is the distance measured from the neutral axis XX.

The effective rotation of the section giving rise to torsion-bending stresses is $u_B/h = \theta_{eff} = \theta + Ah + Bh^2$. The direct stresses associated with this are

$$\sigma_r = -\frac{E}{h}\frac{2A_s}{\partial y^2}\frac{\partial^2 u_B}{\partial y^2} \qquad (C.23)$$

where A_s is the swept area, as defined in the conventional torsion-bending theory and is taken with respect to the centre of rotation at C.

Hence the total direct stress is

$$\sigma_t = -E\left\{\frac{2A_s}{h}\frac{\partial^2 u_B}{\partial y^2} + z'\frac{\partial^2 w}{\partial y^2}\right\} \qquad (C.24)$$

The associated potential energy of the section then becomes

$$\int_o^s \frac{\sigma_t^2}{2E}\, t\, ds = \frac{E}{2}\left\{(\frac{\partial^2 u_B}{\partial y^2})^2 \frac{1}{h^2}\int_o^s 4A_s^2\, t\, ds + (\frac{\partial^2 w}{\partial y^2})^2 \int_o^s z'^2\, t\, ds\right.$$

$$\left. + (\frac{\partial^2 u_B}{\partial y^2})(\frac{\partial^2 w}{\partial y^2})\frac{1}{h}\int_o^s 2\, A_s\, z't\, ds\right\} \qquad (C.25)$$

Now evaluate the integrals of the above equation. Let $1/h \int_o^s 2\, A_s\, z't\, ds = I$. From the elementary torsion-bending theory, it is known that

$$2A_s = \int_o^s p_e\, ds + A_o \qquad \text{and} \qquad \int_o^s 2A_s\, t\, ds = 0 \qquad (C.26)$$

Therefore

$$I = \frac{1}{h}\int_o^s [\int_o^s p_e\, ds + A_o]\, z't\, ds \qquad (C.27)$$

But since z' is measured from the neutral axis XX

$$\int_o^s z't\, ds = 0 \qquad (C.28)$$

Hence Equation (C.27) becomes

$$I = \frac{1}{h}\int_o^s\int_o^s p_e\, z'\, t\, ds\, ds \qquad (C.29)$$

Evaluate the double integral

$$I = [\int_o^s z't\, ds \int_o^s p_e\, ds\, |_o^s] - \frac{1}{h}\int_o^s p_e \int_o^s z't\, ds\, ds \qquad (C.30)$$

Because of Equation (C.28), the first part becomes zero. Now $p_e = h$ from A to B and $p_e = 0$ from B to D. Hence the above equation becomes

$$I = -\frac{1}{h}\int_o^d h \int_o^s z't \, ds \, ds = -z'_{AB}\,\frac{d^2t}{2} = -I_{XZAB} \qquad (C.31)$$

where z'_{AB} is the distance between the neutral axis XX and the flange AB.

The value of the integral $\int_o^s 4A_s^2 t \, ds$ for the whole section can be found as

$$\int_o^s 4\,A_s^2 t \, ds = \frac{h^2 d^3 t}{12}\left\{\frac{4h + 4b_{eff} + d}{h + b_{eff} + d}\right\} = I_C \qquad (C.32)$$

Finally, since z' is measured from the neutral axis, it can be shown that

$$\int_o^s z'^2 t \, ds = I_{XX} \qquad (C.33)$$

Evaluation of the integral over the whole section yields

$$I_{XX} = t\left(\frac{h^3}{3} + (d - \frac{z_o}{2})h^2 - hdz_o\right) \qquad (C.34)$$

where z_o is the distance between the flange CD and the neutral axis and is given by

$$z_o = \frac{(hd + h^2/2)}{(h + d + b_{eff})} \qquad (C.35)$$

Hence Equation (C.31) can be rewritten as

$$I_{XZAB} = \frac{d^2 t(h - z_o)}{2} \qquad (C.36)$$

The potential energy of the whole length, L_y, of the section associated with bending and torsion can then be found as

$$V_{section} = \frac{EL_y}{4} \{k_y^4 I_{XX} w^2 - k_y^4 I_{XZAB} h \theta w$$

$$- k_y^4 I_{XZAB} h^2 Aw - k_y^4 I_{XZAB} h^3 Bw + k_y^4 \Gamma_C \theta^2 + k_y^4 \Gamma_C h^2 A^2$$

$$+ k_y^4 \Gamma_C h^4 B^2 + 2k_y^4 \Gamma_C h \theta A + 2k_y^4 \Gamma_C h^2 \theta B + 2k_y^4 \Gamma_C h^3 AB\} \quad (C.37)$$

C.5 The Total Potential Energy

The total potential energy is the sum of the section energy due to bending and torsion and the distortional energies of the flange and web. Using Equations (C.19), (C.21), (C.37) it can be expressed as

$$V = \frac{EL_y}{4} \left\{ \left(I_{XX} + \frac{dt^3}{12(1-\nu^2)}\right) k_y^4 w^2 \right.$$

$$+ \left[k_y^4 \Gamma_C h^2 + \frac{dt^3h^2}{12(1-\nu^2)} \left(8(1-\nu)k_y^2 + \frac{4}{3} d^2k_y^4\right)\right.$$

$$\left. + \frac{ht^3}{12(1-\nu^2)} \left(4 + \frac{4}{3}(2-3\nu)k_y^2h^2 + \frac{k_y^4h^4}{5}\right)\right]A^2$$

$$+ \left[k_y^4\Gamma_C h^4 + \frac{h^3t^3}{12(1-\nu^2)} \left(12 + 18(1-\nu)dh\, k_y^2\right.\right.$$

$$\left.\left. + \frac{1}{5}(18-30\nu)k_y^2h^2 + \frac{k_y^4h^4}{7} + 3k_y^4hd^3\right)\right]B^2$$

$$+ \left[k_y^4\Gamma_C + \frac{t^3k_y^2}{12(1-\nu^2)}\left(2(1-\nu)d + \frac{d^3k_y^2}{3} + \frac{h^3k_y^2}{3} + 2(1-\nu)h\right)\right]\theta^2$$

$$+ \left[-k_y^4 I_{XZAB} h + \frac{d^2t^3}{12(1-\nu^2)} k_y^4\right]\theta w$$

$$+ \left[-k_y^4 I_{XZAB} h^2 + \frac{2d^2t^3h}{12(1-\nu^2)} k_y^4\right]Aw$$

$$+ \left[-k_y^4 I_{XZAB} h^3 + \frac{3d^2t^3h^2}{12(1-\nu^2)} k_y^4\right]Bw$$

$$+ \left[2k_y^4\Gamma_C h + \frac{t^3hk_y^2}{12(1-\nu^2)} \left(8(1-\nu)d + \frac{h^3k_y^2}{2}\right.\right.$$

$$\left.\left. + 2(2-3\nu)h + \frac{4}{3} d^3k_y^2\right)\right]\theta A \qquad \text{(cont.....)}$$

$$+ [2k_y^4 \Gamma_C h^2 + \frac{t^3h^2k_y^2}{12(1-\nu^2)} (12(1 - \nu)d + 2d^3k_y^2 + \frac{2}{5}h^3k_y^2$$

$$+ 2(2 - 4\nu)h)]\Theta B$$

$$+ [2k_y^4 \Gamma_C h^3 + \frac{t^3h^2}{12(1-\nu^2)} (24(1 - \nu)dhk_y^2 + 4d^3hk_y^4$$

$$+ 12 + \frac{h^4k_y^4}{3} + (6 - 10\nu)h^2k_y^2)]AB\Big\} \qquad (C.38)$$

This can be put into a matrix quadratic form as

$$V = \frac{1}{2} \lfloor q \rfloor [\tilde{I}] \{q\} (EL_yk_y^4) \qquad (C.39)$$

where $\lfloor q \rfloor = \lfloor w, \Theta h, Ah^2, Bh^3 \rfloor$ and the elements of $[\tilde{I}]$ are given by

$$\tilde{I}_{11} = I_{XX} + I_f$$

$$\tilde{I}_{12} = \tilde{I}_{21} = (-\frac{1}{2} I_{XZ} + I_f \frac{\alpha}{2})$$

$$\tilde{I}_{13} = \tilde{I}_{31} = (-\frac{1}{2} I_{XZ} + I_f \alpha)$$

$$\tilde{I}_{14} = \tilde{I}_{41} = (-\frac{1}{2} I_{XZ} + I_f \frac{3\alpha}{2})$$

$$\tilde{I}_{22} = \Big\{\frac{\Gamma_C}{h^2} + I_f [\frac{2(1 - \nu)}{\beta^2} + \frac{(2 - 2\nu)}{\delta\beta} + \frac{1}{3\alpha} + \frac{\alpha^2}{3}]\Big\}$$

$$\tilde{I}_{23} = I_{32} = \Big\{\frac{\Gamma_C}{h^2} + I_f [\frac{4(1 - \nu)}{\beta^2} + \frac{(2 - 3\nu)}{\delta\beta} + \frac{1}{4\alpha} + \frac{2\alpha^2}{3}]\Big\}$$

$$\tilde{I}_{24} = \tilde{I}_{42} = \Big\{\frac{\Gamma_C}{h^2} + I_f [\frac{6(1 - \nu)}{\beta^2} + \frac{(2 - 4\nu)}{\delta\beta} + \frac{1}{5\alpha} + \frac{3\alpha^2}{3}]\Big\}$$

$$\tilde{I}_{33} = \Big\{\frac{\Gamma_C}{h^2} + I_f [\frac{8(1 - \nu)}{\beta^2} + \frac{4}{3} \frac{(2 - 3\nu)}{\delta\beta} + \frac{1}{5\alpha} + \frac{4}{3} \alpha^2 + \frac{4}{\beta^3\delta}]\Big\}$$

$$\tilde{I}_{34} = \tilde{I}_{43} = \Big\{\frac{\Gamma_C}{h^2} + I_f [\frac{12(1 - \nu)}{\beta^2} + \frac{(3 - 5\nu)}{\delta\beta} + \frac{1}{6\alpha} + \frac{6}{3} \alpha^2 + \frac{6}{\beta^3\delta}]\Big\}$$

$$\tilde{I}_{44} = \Big\{\frac{\Gamma_C}{h^2} + I_f [\frac{18(1 - \nu)}{\beta^2} + \frac{6}{5} \frac{(3 - 5\nu)}{\delta\beta} + \frac{1}{7\alpha} + \frac{9}{3} \alpha^2 + \frac{12}{\beta^3\delta}]\Big\} \qquad (C.40)$$

where $I_f = dt^3/((12(1 - \nu^2))$, $\alpha = d/h$, $\beta = k_y h$, $\delta = k_y d$, $I_{XZ} = I_{XZAB}$.

As before, transform from the $\lfloor\ q\ \rfloor$ coordinate system to the $\lfloor\ q_t\ \rfloor = \lfloor\ w,\ u_B,\ Ah^2,\ Bh^3\ \rfloor$ coordinate system. The quadratic form for the potential energy then becomes

$$V = \frac{1}{2} \lfloor\ q_t\ \rfloor [\tilde{\tilde{I}}_t] \{q_t\}\ (EL_y k_y^4) \qquad (C.41)$$

where the elements of $[\tilde{\tilde{I}}_t]$ can be found to be

$$\tilde{\tilde{I}}_{t,11} = I_{XX} + I_f$$

$$\tilde{\tilde{I}}_{t,12} = \tilde{\tilde{I}}_{t,21} = -\frac{1}{2} I_{XZ} + I_f \frac{\alpha}{2}$$

$$\tilde{\tilde{I}}_{t,13} = \tilde{\tilde{I}}_{t,31} = I_f \frac{\alpha}{2}$$

$$\tilde{\tilde{I}}_{t,14} = \tilde{\tilde{I}}_{t,41} = I_f\, \alpha$$

$$\tilde{\tilde{I}}_{t,22} = \left\{\frac{I_C}{h^2} + I_f \left[\frac{2(1 - \nu)}{\beta^2} + \frac{2(1 - \nu)}{\delta\beta} + \frac{1}{3\alpha} + \frac{\alpha^2}{3}\right]\right\}$$

$$\tilde{\tilde{I}}_{t,23} = \tilde{\tilde{I}}_{t,32} = I_f \left[\frac{2(1 - \nu)}{\beta^2} - \frac{\nu}{\delta\beta} - \frac{1}{12\alpha} + \frac{\alpha^2}{3}\right]$$

$$\tilde{\tilde{I}}_{t,24} = \tilde{\tilde{I}}_{t,42} = I_f \left[\frac{4(1 - \nu)}{\beta^2} - \frac{2\nu}{\delta\beta} - \frac{2}{15\alpha} + \frac{2\alpha^2}{3}\right]$$

$$\tilde{\tilde{I}}_{t,33} = I_f \left[\frac{2(1 - \nu)}{\beta^2} + \frac{2}{3\delta\beta} + \frac{1}{30\alpha} + \frac{\alpha^2}{3} + \frac{4}{\beta^3\delta}\right]$$

$$\tilde{\tilde{I}}_{t,34} = \tilde{\tilde{I}}_{t,43} = I_f \left[\frac{4(1 - \nu)}{\beta^2} + \frac{1}{\delta\beta} + \frac{1}{20\alpha} + \frac{2}{3}\alpha^2 + \frac{6}{\beta^3\delta}\right]$$

$$\tilde{\tilde{I}}_{t,44} = I_f \left[\frac{8(1 - \nu)}{\beta^2} + \frac{8}{5\delta\beta} + \frac{8}{105\alpha} + \frac{4}{3}\alpha^2 + \frac{12}{\beta^3\delta}\right] \qquad (C.42)$$

C.6 The Generalized Forces

Suppose that the distributed transverse force $F_o \sin k_y y$ per unit length moves through the virtual transverse displacement $\delta w \sin k_y y$. The virtual work done becomes

$$\delta W = \int_o^{L_y} F_o \, \delta w \sin^2 k_y y \, dy = \frac{L_y}{2} F_o \, \delta w \qquad (C.43)$$

Therefore the generalized force corresponding to 'w' turns out to be

$$\frac{\delta W}{\delta w} = F_o \frac{L_y}{2} \qquad (C.44)$$

In this case the generalized forces corresponding to the other three transformed generalized coordinates become

$$\frac{\delta W}{\delta u_B} = \frac{\delta W}{\delta A h^2} = \frac{\delta W}{\delta B h^3} = 0 \qquad (C.45)$$

Now assume that the distributed moment $M_o \sin k_y y$ per unit length moves through the virtual rotation $\delta\theta \sin k_y y$. The virtual work due to this becomes

$$\delta W = \int_o^{L_y} M_o \, \delta\theta \sin^2 k_y y \, dy = \frac{L_y}{2} M_o \, \delta\theta \qquad (C.46)$$

Now

$$\theta = \frac{1}{h} (u_B - A h^2 - B h^3) \qquad (C.47)$$

Then

$$\delta\theta = \frac{1}{h} (\delta u_B - \delta A h^2 - \delta B h^3)$$

$$\delta W = \frac{L_y}{2h} M_o \, (\delta u_B - \delta A h^2 - \delta B h^3) \qquad (C.48)$$

Hence the generalized forces, corresponding to the transformed generalized coordinates can be shown to be

$$\frac{\delta W}{\delta w} = 0 \qquad \frac{\delta W}{\delta Ah^2} = -\frac{M_Q}{h}\frac{L_y}{2}$$

$$\frac{\delta W}{\delta u_B} = \frac{M_Q}{h}\frac{L_y}{2} \qquad \frac{\delta W}{\delta Bh^3} = -\frac{M_Q}{h}\frac{L_y}{2} \qquad \text{(C.49)}$$

C.7 Equations of Motion

The expressions for total kinetic energy T and the total potential energy V can now be used in Lagrange's equations of motion

$$\frac{d}{dt}\left(\frac{\partial T}{\partial \dot{q}_t}\right) + \frac{\partial V}{\partial q_t} = Q_r \qquad \text{(C.50)}$$

For harmonic motion $\ddot{q}_t$ is $-\omega^2 q_t$. Hence the left-hand side of the equation (C.50) becomes

$$[[K] - \omega^2[M]] \begin{Bmatrix} w \\ u_B \\ Ah^2 \\ Bh^3 \end{Bmatrix} \qquad \text{(C.51)}$$

It can be shown that

$$[K] = Ek_y^4 \frac{L_y}{2} [\tilde{I}_t]$$

$$[M] = \rho th \frac{L_y}{2} [M_{nd,t}] \qquad \text{(C.52)}$$

The total equation of motion can then be written as

$$[[K] - \omega^2[M]] \begin{Bmatrix} w \\ u_B \\ Ah^2 \\ Bh^3 \end{Bmatrix} = \begin{Bmatrix} F_o \\ M_o/h \\ -M_o/h \\ -M_o/h \end{Bmatrix} L_y/2 \qquad (C.53)$$

Now divide everything by $EI_f k_y^4 L_y/2$. Equation (C.53) then takes the form

$$[[K'] - \frac{\omega^2}{EI_f k_y^4} [M']] \begin{Bmatrix} w \\ u_B \\ Ah^2 \\ Bh^3 \end{Bmatrix} = \begin{Bmatrix} \text{Forcing} \end{Bmatrix} \qquad (C.54)$$

where $[K'] = (1/I_f)\,[\tilde{I}_t]$.

The forcing vector has different forms depending on the type of external loading. For the alternative cases of unit force and unit moment they are

$$\begin{Bmatrix} \text{Forcing} \\ F_o \end{Bmatrix} = \begin{Bmatrix} 1/EI_f k_y^4 \\ 0 \\ 0 \\ 0 \end{Bmatrix} \qquad \begin{Bmatrix} \text{Forcing} \\ M_o \end{Bmatrix} = \begin{Bmatrix} 0 \\ 1/EI_f k_y^4 h \\ -1/EI_f k_y^4 h \\ -1/EI_f k_y^4 h \end{Bmatrix} \qquad (C.55)$$

C.8 The Receptances and Dynamic Stiffnesses of the Beam

Now assume that the unit force F_o alone is applied. The solution vector to be obtained from equation (C.54) yields values for $[w_F,\ u_{B_F},\ Ah_F^2,\ Bh_F^3]$. From these one can obtain the forms

$$\frac{w}{F_o} = w_F$$

$$\frac{\theta}{F_o} = (u_{B_F} - Ah_F^2 - Bh_F^3)/h$$

$$\frac{\theta_B}{F_o} = (u_{B_F} + Ah_F^2 + 2Bh_F^3)/h$$

$$\left(\frac{\partial u(z)}{\partial z}\Big|_{z=h}\right)/F_o = \frac{\theta_B}{F_o} - \frac{\theta}{F_o} = (2Ah_F^2 + 3Bh_F^3)/h \qquad (C.56)$$

Now let the unit moment M_o act alone. Using the second of equations (C.55) as the forcing vector, the obtained solution vector gives the following receptances

$$\frac{w}{M_o} = w_M$$

$$\frac{\theta}{M_o} = (u_{B_M} - Ah_M^2 - Bh_M^3)/h$$

$$\frac{\theta_B}{M_o} = (u_{B_M} + Ah_M^2 + 2Bh_M^3)/h$$

$$\left(\frac{\partial u(z)}{\partial z}\Big|_{z=h}\right)/M_o = \frac{\theta_B}{M_o} - \frac{\theta}{M_o} = (2Ah_M^2 + 3Bh_M^3)/h \qquad (C.57)$$

The transverse displacement and rotation of a structure can be related to force and moment acting on it, through the receptance matrix, as

$$\begin{Bmatrix} w \\ \theta \end{Bmatrix} = \begin{bmatrix} w/F & w/M \\ \theta/F & \theta/M \end{bmatrix} \begin{Bmatrix} F \\ M \end{Bmatrix} \qquad (C.58)$$

Hence the force and the moment can be expressed as

$$F = \frac{(\theta/M)}{\phi} w - \frac{(\theta/F)}{\phi} \theta$$

$$M = -\frac{(w/M)}{\phi} w + \frac{(w/F)}{\phi} \theta \qquad (C.59)$$

where $\phi = (w/F)(\theta/M) - (w/M)(\theta/F)$.

Now $F = F_o$, $M = M_o$ and also $\theta/F_o = w/M_o$. The required dynamic stiffnesses then become

$$K_t = \frac{F_o}{w} = \frac{\theta/M_o}{\psi}$$

$$K_r = \frac{M_o}{\theta} = \frac{w/F_o}{\psi}$$

$$K_c = \frac{F_o}{\theta} = \frac{M_o}{w} = -\frac{\theta/F_o}{\psi} \qquad (C.60)$$

where $\psi = (w/F_o)(\theta/M_o) - (\theta/F_o)^2$ and the receptance expressions are given by equations (C.56) and (C.57).

C.9 Dynamic Stiffnesses without the Cross-Sectional Distortion

Now assume that there is no cross-sectional distortion of the web taking place. Therefore $Ah^2 = 0$ and $Bh^3 = 0$. Hence by using equations (C.54) and (C.55) together with equations (C.15), (C.42) and (C.52) one obtains

$$\left[\begin{bmatrix} \frac{I_{XX}}{I_f} + 1 & -\frac{I_{XZ}}{2I_f} + \frac{\alpha}{2} \\ -\frac{I_{XZ}}{2I_f} + \frac{\alpha}{2} & \frac{\Gamma_c}{I_f h^2} + \frac{\alpha^2}{3} + \frac{1.4}{\beta^2} + \frac{1}{3\alpha} + \frac{1.4}{\delta\beta} \end{bmatrix}\right.$$

$$\left. - \frac{\omega^2 \rho t h}{EI_f k_y^4} \begin{bmatrix} 1 + \alpha & \frac{\alpha^2}{2} \\ \frac{\alpha^2}{2} & (\frac{\alpha^3}{3} + \alpha + \frac{1}{3}) \end{bmatrix}\right] \begin{Bmatrix} w \\ u_B \end{Bmatrix} = \begin{Bmatrix} F_o/EI_f k_y^4 \\ M_o/EI_f k_y^4 h \end{Bmatrix} \qquad (C.61)$$

In this case $u_B = \theta h$. Hence the required dynamic stiffnesses can be found to be

$$K_{t,ndt} = \frac{F_o}{w} = \left\{(\frac{I_{XX}}{I_f} + 1) - \frac{\omega^2 \rho t h}{EI_f k_y^4}(1 + \alpha)\right\} EI_f k_y^4$$

$$K_{r,ndt} = \frac{M_o}{\theta} = \left\{[\frac{\Gamma_c}{I_f h^2} + \frac{\alpha^2}{3} + \frac{1.4}{\beta^2} + \frac{1}{3\alpha} + \frac{1.4}{\delta\beta}] - \frac{\omega^2 \rho t h}{EI_f k_y^4} (\frac{\alpha^3}{3} + \alpha + \frac{1}{3})\right\} EI_f k_y^4 h^2$$

$$K_{c,ndt} = \frac{M_o}{w} = \frac{F_o}{\theta} = \left\{(-\frac{I_{XZ}}{2I_f} + \frac{\alpha}{2}) - \frac{\omega^2 \rho t h}{EI_f k_y^4}(\frac{\alpha^2}{2})\right\} EI_f k_y^4 h \qquad (C.62)$$

where subscript $_{ndt}$ stands for no-distortion.

C.10 Calculated Values of the Dynamic Stiffnesses

Throughout this thesis, one specific stringer is used. The dimensions and the material properties are as follows:

t = 0.0012 [m]
h = 0.0318 [m]
d = 0.0254 [m]

b_{eff} = 0.085 [m]

E = 7.E10 [N/m^2]

ρ = 2700 [kg/m^3]

ν = 0.3

L_y is equal to the width of the plates concerned.

The effect of cross-sectional distortion on the stiffness values is seen in Figure C.4. This compares the stiffnesses of a beam whose cross-section distorts with those of a beam with a non-distorting cross-section. The stiffeners are taken as 0.34 [m] long. Up to 700 Hz the distortion reduces the stiffness values, very significantly in the cases of K_r and K_c. The next interesting feature reflects itself around 895 Hz where the stiffnesses of the beam with distortion go to infinity. The work of Beresford *et al* [37] shows that the corresponding frequency is the natural frequency of the section when its root (point C) is fully-fixed. The section then behaves like a dynamic absorber resisting w and θ motions.

C.10.1 The Influence of the Plate Effective Width

The effect of changing the effective width on the transverse, rotational and coupling dynamic stiffnesses is shown in Figures C.5 to C.7 respectively. Cross-sectional deformation of the web is included in the computations and the stiffnesses have been computed using equation (C.60).

Figures C.5 to C.7 show that increasing the effective width generally increases the frequencies of the peaks and troughs of all stiffnesses. The magnitudes of the transverse and coupling stiffnesses are also increased at low frequencies but that of the rotational stiffness is hardly affected.

APPENDIX D

PROPAGATION CONSTANTS OF PERIODIC, UNIFORM THREE-LAYERED SANDWICH BEAMS ON GENERAL SUPPORTS

This section deals with sandwich beams and so assumes that the excitation forces act at points along the beam. The results obtained are valid also for the x-wise variation of sandwich plates.

Consider an infinite, uniform, three-layered sandwich beam subjected to phased arrays of forces and moments. As explained in Chapter 7, the transverse displacement w, rotation w' (= θ) and the mid-plane axial displacement u at x = 0 can be related to the applied forces and moment through the matrix

$$\begin{Bmatrix} w(0) \\ w'(0) \\ u(0) \end{Bmatrix} = \begin{bmatrix} \alpha_{FF} & \alpha_{FM} & \alpha_{FN} \\ \alpha_{MF} & \alpha_{MM} & \alpha_{MN} \\ \alpha_{NF} & \alpha_{NM} & \alpha_{NN} \end{bmatrix} \begin{Bmatrix} F_o \\ M_o \\ N_o \end{Bmatrix} \qquad (D.1)$$

where the α's are the phased array receptance functions and α_{ij} defines the i^{th} type of displacement (F = transverse displacement, M = rotation, N = axial displacement u) due to j^{th} type of excitation (F = transverse force, M = moment, N = axial force in u direction).

The forces and moments acting on the s^{th} support anywhere on the beam can be related to the resulting displacements and rotation through the general support stiffness matrix as follows

$$\begin{Bmatrix} R_s \\ M_s \\ N_s \end{Bmatrix} = \begin{bmatrix} K_{tt} & K_{tr} & K_{ta} \\ K_{rt} & K_{rr} & K_{ra} \\ K_{at} & K_{ar} & K_{aa} \end{bmatrix} \begin{Bmatrix} w_s \\ w_s' \\ u_s \end{Bmatrix} \qquad (D.2)$$

where K_{ij} defines the i^{th} type of stiffness of the support due to j^{th} type of motion (t = transverse, r = rotational, a = axial in u direction).

This study assumes that all stiffnesses related to u direction are zero (*i.e.*, $K_{at} = K_{ar} = K_{aa} = K_{ta} = K_{ra} = 0$).

Since the structure and the supports are joined, the beam and support displacements and rotations are equal. Hence, $w(0) = w_s$, $w'(0) = w_s'$, $u(0) = u_s$. The forces acting on the beam and the support are related through $F_o = -R_s$, $M_o = -M_s$, $N_o = -N_s$. Equations (D.1) and (D.2) can therefore be combined to eliminate the displacements and rotations and to yield

$$\begin{Bmatrix} F_o \\ M_o \\ N_o \end{Bmatrix} = - \begin{bmatrix} K_{tt} & K_{tr} & 0 \\ K_{rt} & K_{rr} & 0 \\ 0 & 0 & 0 \end{bmatrix} \begin{bmatrix} \alpha_{FF} & \alpha_{FM} & \alpha_{FN} \\ \alpha_{MF} & \alpha_{MM} & \alpha_{MN} \\ \alpha_{NF} & \alpha_{NM} & \alpha_{NN} \end{bmatrix} \begin{Bmatrix} F_o \\ M_o \\ N_o \end{Bmatrix} \qquad (D.3)$$

This can be arranged in the form

$$\left(\begin{bmatrix} 1 & 0 & 0 \\ 0 & 1 & 0 \\ 0 & 0 & 1 \end{bmatrix} + \begin{bmatrix} K_{tt}\alpha_{FF}+K_{tr}\alpha_{MF} & K_{tt}\alpha_{FM}+K_{tr}\alpha_{MM} & K_{tt}\alpha_{FN}+K_{tr}\alpha_{MN} \\ K_{rt}\alpha_{FF}+K_{rr}\alpha_{MF} & K_{rt}\alpha_{FM}+K_{rr}\alpha_{MM} & K_{rt}\alpha_{FN}+K_{rr}\alpha_{MN} \\ 0 & 0 & 0 \end{bmatrix} \right) \begin{Bmatrix} F_o \\ M_o \\ N_o \end{Bmatrix} = 0 \qquad (D.4)$$

which is the same as

$$\begin{bmatrix} K_{tt}\alpha_{FF}+K_{tr}\alpha_{MF}+1 & K_{tt}\alpha_{FM}+K_{tr}\alpha_{MM} & K_{tt}\alpha_{FN}+K_{tr}\alpha_{MN} \\ K_{rt}\alpha_{FF}+K_{rr}\alpha_{MF} & K_{rt}\alpha_{FM}+K_{rr}\alpha_{MM}+1 & K_{rt}\alpha_{FN}+K_{rr}\alpha_{MN} \\ 0 & 0 & 1 \end{bmatrix} \begin{Bmatrix} F_o \\ M_o \\ N_o \end{Bmatrix} = 0 \qquad (D.5)$$

Free wave motion occurs at frequencies and μ values which cause the determinant of the whole matrix to vanish. Let $K_{tt} = K_t$, $K_{rr} = K_r$, $K_{rt} = K_{tr} = K_c$. Expanding the determinant and making use of $\alpha_{FM} = -\alpha_{MF}$ one obtains

$$(K_tK_r - K_c^2)(\alpha_{FF}\alpha_{MM} - \alpha_{FM}^2) + K_t\alpha_{FF} + K_r\alpha_{MM} + 1 = 0 \qquad (D.6)$$

The forms of the phased array receptance functions (α's) are given by equation (7.28). When they are substituted into equation (D.6) it becomes

$$(K_tK_r - K_c^2)\Big\{[a_1d_1 \frac{\sinh^2 k_1XL}{(\cosh \mu - \cosh k_1XL)^2} + a_2d_2 \frac{\sinh^2 k_2XL}{(\cosh \mu - \cosh k_2XL)^2}$$

$$+ a_3d_3 \frac{\sinh^2 k_3XL}{(\cosh \mu - \cosh k_3XL)^2}$$

$$+ (a_1d_2 + a_2d_1) \frac{\sinh k_1XL \sinh k_2XL}{(\cosh \mu - \cosh k_1XL)(\cosh \mu - \cosh k_2XL)}$$

$$+ (a_1d_3 + a_3d_1) \frac{\sinh k_1XL \sinh k_3XL}{(\cosh \mu - \cosh k_1XL)(\cosh \mu - \cosh k_3XL)}$$

$$+ (a_2d_3 + a_3d_2) \frac{\sinh k_2XL \sinh k_3XL}{(\cosh \mu - \cosh k_2XL)(\cosh \mu - \cosh k_3XL)}]$$

$$- [b_1c_1 \frac{\sinh^2 \mu}{(\cosh \mu - \cosh k_1XL)^2} + b_2c_2 \frac{\sinh^2 \mu}{(\cosh \mu - \cosh k_2XL)^2}$$

$$+ b_3c_3 \frac{\sinh^2 \mu}{(\cosh \mu - \cosh k_3XL)^2}$$

$$+ (b_1c_2 + b_2c_1) \frac{\sinh^2 \mu}{(\cosh \mu - \cosh k_1XL)(\cosh \mu - \cosh k_2XL)}$$

$$+ (b_1c_3 + b_3c_1) \frac{\sinh^2 \mu}{(\cosh \mu - \cosh k_1XL)(\cosh \mu - \cosh k_3XL)}$$

$$+ (b_2c_3 + b_3c_2) \frac{\sinh^2 \mu}{(\cosh \mu - \cosh k_2XL)(\cosh \mu - \cosh k_3XL)}]\Big\}$$

$$+ K_t\Big\{- \frac{a_1 \sinh k_1XL}{(\cosh \mu - \cosh k_1XL)} - \frac{a_2 \sinh k_2XL}{(\cosh \mu - \cosh k_2XL)}$$

$$- \frac{a_3 \sinh k_3XL}{(\cosh \mu - \cosh k_3XL)}\Big\}$$

$$+ K_r\Big\{- \frac{d_1 \sinh k_1XL}{(\cosh \mu - \cosh k_1XL)} - \frac{d_2 \sinh k_2XL}{(\cosh \mu - \cosh k_2XL)}$$

$$- \frac{d_3 \sinh k_3XL}{(\cosh \mu - \cosh k_3XL)}\Big\} + 1 = 0 \qquad (D.7)$$

The left-hand side of this equation can be rearranged over the common denominator $[(\cosh \mu - \cosh k_1XL)\ (\cosh \mu - \cosh k_2XL)\ (\cosh \mu - \cosh k_3XL)]^2$. The numerator is then found to be a cubic

function of $\cosh \mu$ and this must be equated to zero. Much tedious manipulation is required in order to find the coefficients of this function, but simplification is achieved by utilizing $a_n d_n = b_n c_n$ ($n = 1,2,3$). The final form of the cubic equation is given in equation (7.32).

APPENDIX E

FORCED VIBRATIONS OF SIMPLY-SUPPORTED, INFINITE, PERIODIC, UNIFORM EULER-BERNOULLI BEAM SUBJECTED TO A SINGLE HARMONIC FORCE

Consider Figure 80. Equations (9.3) and (9.4) give the transverse displacement of the beam at any x_r within the loaded bay (*i.e.*, between Or and Oℓ) and equation (9.5) represents the zero transverse displacement condition at Or.

The transverse displacement at Oℓ can be obtained from equation (9.4) by setting x_r to O. Since simple supports do not deflect, this displacement must be set to zero and the equation yields

$$R_{ir} \sum_{n=1}^{2} a_n e^{-k_n XL} f_n + R_{or} \sum_{n=1}^{2} a_n e^{-k_n XL} + R_{o\ell} \sum_{n=1}^{2} a_n + R_{i\ell} \sum_{n=1}^{2} a_n f_n = -F_o \sum_{n=1}^{2} a_n e^{-k_n x_o} \qquad (E.1)$$

where $f_n = e^{-k_n XL}/[1 - e^{-(\mu + k_n XL)}]$ $\qquad n = 1,2.$

To find the four unknowns (R_{ir}, R_{or}, $R_{o\ell}$, $R_{i\ell}$), two more boundary conditions are required in addition to equations (9.5) and (E.1). In this study, the transverse displacement conditions at 1r and 1ℓ are considered.

The transverse displacement at 1r is found to be

$$w(1r) = F_o \sum_{n=1}^{2} a_n e^{-k_n(2XL-x_o)}$$

$$+ \sum_{s=1}^{\infty} R_{ir} e^{-\mu(s-1)} \sum_{n=1}^{2} a_n e^{-k_n(s-1)XL}$$

$$+ R_{or} \sum_{n=1}^{2} a_n e^{-k_n XL} + R_{o\ell} \sum_{n=1}^{2} a_n e^{-2k_n XL}$$

$$+ \sum_{s=1}^{\infty} R_{i\ell} e^{-\mu(s-1)} \sum_{n=1}^{2} a_n e^{-k_n(s+2)XL} \qquad (E.2)$$

Summing the infinite series and setting this to zero, it reduces to

$$R_{ir} \sum_{n=1}^{2} a_n e^{k_n XL} f_n + R_{or} \sum_{n=1}^{2} a_n e^{-k_n XL} + R_{o\ell} \sum_{n=1}^{2} a_n e^{-2k_n XL}$$

$$+ R_{i\ell} \sum_{n=1}^{2} a_n e^{-2k_n XL} f_n = - F_o \sum_{n=1}^{2} a_n e^{-k_n(2XL-x_o)} \qquad (E.3)$$

The transverse displacement at 1ℓ can be written as

$$w(1\ell) = F_o \sum_{n=1}^{2} a_n e^{-k_n(XL+x_o)}$$

$$+ \sum_{s=1}^{\infty} R_{ir} e^{-\mu(s-1)} \sum_{n=1}^{2} a_n e^{-k_n(s+2)XL}$$

$$+ R_{or} \sum_{n=1}^{2} a_n e^{-2k_n XL} + R_{o\ell} \sum_{n=1}^{2} a_n e^{-k_n XL}$$

$$+ \sum_{s=1}^{\infty} R_{i\ell} e^{-\mu(s-1)} \sum_{n=1}^{2} a_n e^{-k_n(s-1)XL} \qquad (E.4)$$

Summing the infinite series and setting this displacement to zero yields

$$R_{ir}\sum_{n=1}^{2} a_n e^{-2k_nXL}f_n + R_{or}\sum_{n=1}^{2} a_n e^{-2k_nXL} + R_{o\ell}\sum_{n=1}^{2} a_n e^{-k_nXL}$$

$$+ R_{i\ell}\sum_{n=1}^{2} a_n e^{k_nXL} f_n = -F_o\sum_{n=1}^{2} a_n e^{-k_n(XL+x_o)} \qquad (E.5)$$

Equations (9.5), (E.1), (E.3), (E.5) can be put into the following matrix form

$$\begin{bmatrix} \sum_{n=1}^{2} a_n e^{k_nXL}f_n & \sum_{n=1}^{2} a_n e^{-k_nXL} & \sum_{n=1}^{2} a_n e^{-2k_nXL} & \sum_{n=1}^{2} a_n e^{-2k_nXL}f_n \\ \sum_{n=1}^{2} a_n f_n & \sum_{n=1}^{2} a_n & \sum_{n=1}^{2} a_n e^{-k_nXL} & \sum_{n=1}^{2} a_n e^{-k_nXL}f_n \\ \sum_{n=1}^{2} a_n e^{-k_nXL}f_n & \sum_{n=1}^{2} a_n e^{-k_nXL} & \sum_{n=1}^{2} a_n & \sum_{n=1}^{2} a_n f_n \\ \sum_{n=1}^{2} a_n e^{-2k_nXL}f_n & \sum_{n=1}^{2} a_n e^{-2k_nXL} & \sum_{n=1}^{2} a_n e^{-k_nXL} & \sum_{n=1}^{2} a_n e^{k_nXL}f_n \end{bmatrix} \begin{Bmatrix} R_{ir} \\ R_{or} \\ R_{o\ell} \\ R_{i\ell} \end{Bmatrix}$$

$$= -F_o \begin{Bmatrix} \sum_{n=1}^{2} a_n e^{-k_n(2XL-x_o)} \\ \sum_{n=1}^{2} a_n e^{-k_n(XL-x_o)} \\ \sum_{n=1}^{2} a_n e^{-k_nx_o} \\ \sum_{n=1}^{2} a_n e^{-k_n(XL+x_o)} \end{Bmatrix} \qquad (E.6)$$

This equation can be solved numerically for the R's. Once they have been determined, the transvese displacement at any x_r, within the loaded bay, can be obtained from equation (9.4).

APPENDIX F

FORCED VIBRATIONS OF INFINITE, PERIODIC, UNIFORM EULER-BERNOULLI BEAM ON TRANSVERSELY ELASTIC SUPPORTS SUBJECTED TO A SINGLE HARMONIC FORCE

Consider Figure 80. Equations (9.8) and (9.9) give the transverse displacement of the beam at any x_r within the loaded bay (*i.e.*, between 0ℓ and 0r) and equation (9.10) represents the elastic boundary condition at support 0r.

This case has six unknowns (R_{i2r}, R_{i1r}, R_{or}, $R_{o\ell}$, $R_{i1\ell}$ and $R_{i2\ell}$). In order to find them, five more boundary conditions which satisfy both compatibility and equilibrium conditions are required. In this study the transverse displacements at support locations 2r, 1r, 0ℓ, 1ℓ, 2ℓ are considered.

The transverse displacement of the beam at 0ℓ can be found from equation (9.9) by substituting $x_r = 0$ into it. This should be equal to that of the support given by $w(0\ell) = -R_{o\ell}/K_t$. By considering these, the elastic boundary condition at support 0ℓ can be found to be

$$\left\{ \sum_{j=1}^{2} R_{ijr} \sum_{n=1}^{2} a_n e^{-k_n XL} f_{jn} \right.$$

$$+ R_{or} \sum_{n=1}^{2} a_n e^{-k_n XL} + R_{o\ell} \left(\sum_{n=1}^{2} a_n + \frac{1}{K_t} \right)$$

$$\left. + \sum_{j=1}^{2} R_{ij\ell} \sum_{n=1}^{2} a_n f_{jn} \right\} = -F_o \sum_{n=1}^{2} a_n e^{-k_n x_o} \qquad \text{(F.1)}$$

where $f_{jn} = e^{-k_n XL} / [1 - e^{-(\mu_j + k_n XL)}]$ $\quad j = 1,2$ and $n = 1,2$.

By using the infinite-system point response functions of all the reaction forces and the external force F_o the transverse displacement of the beam at any x_r' between 0r and 1r can be shown to be:

$$w(x_r') = F_o \sum_{n=1}^{2} a_n e^{-k_n(XL-x_o+x_r')}$$

$$+ \sum_{j=1}^{2} \sum_{s=1}^{\infty} R_{ijr} e^{-\mu_j(s-1)} \sum_{n=1}^{2} a_n e^{-k_n(sXL-x_r')}$$

$$+ R_{or} \sum_{n=1}^{2} a_n e^{-k_n x_r'} + R_{o\ell} \sum_{n=1}^{2} a_n e^{-k_n(XL+x_r')}$$

$$+ \sum_{j=1}^{2} \sum_{s=1}^{\infty} R_{ij\ell} e^{-\mu_j(s-1)} \sum_{n=1}^{2} a_n e^{-k_n((s+1)XL+x_r')} \qquad (F.2)$$

where $0 \leq |x_r'| \leq XL$ and x_r' is measured from support number Or.

After the infinite series has been summed, equation (F.2) reduces to

$$w(x_r') = F_o \sum_{n=1}^{2} a_n e^{-k_n(XL-x_o+x_r')}$$

$$+ \sum_{j=1}^{2} R_{ijr} \sum_{n=1}^{2} a_n e^{k_n x_r'} f_{jn} + R_{or} \sum_{n=1}^{2} a_n e^{-k_n x_r'}$$

$$+ R_{o\ell} \sum_{n=1}^{2} a_n e^{-k_n(XL+x_r')}$$

$$+ \sum_{j=1}^{2} R_{ij\ell} \sum_{n=1}^{2} a_n e^{-k_n(XL+x_r')} f_{jn} \qquad (F.3)$$

The beam transverse displacement at 1r can be found by setting x_r' to XL in equation (F.3) and is equal to the support transverse displacement $w(1r) = -(R_{i1r} + R_{i2r})/K_t$. Hence these conditions lead to

$$\sum_{j=1}^{2} R_{ijr}\left(\sum_{n=1}^{2} a_n e^{k_n XL} f_{jn} + \frac{1}{K_t}\right)$$

$$+ R_{or} \sum_{n=1}^{2} a_n e^{-k_n XL} + R_{o\ell} \sum_{n=1}^{2} a_n e^{-k_n(2XL)}$$

$$+ \sum_{j=1}^{2} R_{ij\ell} \sum_{n=1}^{2} a_n e^{-k_n(2XL)} f_{jn}$$

$$= -F_o \sum_{n=1}^{2} a_n e^{-k_n(2XL-x_o)} \qquad \text{(F.4)}$$

The displacement of the beam at any $x_r"$ between 1r and 2r can similarly be found as

$$w(x_r") = F_o \sum_{n=1}^{2} a_n e^{-k_n(2XL-x_o+x_r")}$$

$$+ \sum_{j=1}^{2} \left(R_{ijr} \sum_{n=1}^{2} a_n e^{-k_n x_r"} + \sum_{s=2}^{\infty} R_{ijr} e^{-\mu_j(s-1)} \sum_{n=1}^{2} a_n e^{-k_n((s-1)XL-x_r")}\right)$$

$$+ R_{or} \sum_{n=1}^{2} a_n e^{-k_n(XL+x_r")} + R_{o\ell} \sum_{n=1}^{2} a_n e^{-k_n(2XL+x_r")}$$

$$+ \sum_{j=1}^{2} \sum_{s=1}^{\infty} R_{ij\ell} e^{-\mu_j(s-1)} \sum_{n=1}^{2} a_n e^{-k_n((s+2)XL+x_r")} \qquad \text{(F.5)}$$

where $0 \leq |x_r"| \leq XL$ and $x_r"$ is measured from support number 1r.

The infinite series can easily be summed and equation (F.5) simplifies to

$$w(x_r") = F_o \sum_{n=1}^{2} a_n e^{-k_n(2XL-x_o+x_r")}$$

$$+ \sum_{j=1}^{2} R_{1jr} \left(\sum_{n=1}^{2} a_n e^{-k_n x_r"} + e^{-\mu_j} \sum_{n=1}^{2} a_n e^{k_n x_r"} f_{jn} \right)$$

$$+ R_{or} \sum_{n=1}^{2} a_n e^{-k_n(XL+x_r")} + R_{o\ell} \sum_{n=1}^{2} a_n e^{-k_n(2XL+x_r")}$$

$$+ \sum_{j=1}^{2} R_{1j\ell} \sum_{n=1}^{2} a_n e^{-k_n(2XL+x_r")} f_{jn} \qquad (F.6)$$

The beam transverse displacement at 2r is found by setting $x_r"$ to XL in the above equation. This displacement is equal to the support transverse displacement given by

$$w(2r) = -\frac{(R_{21r} + R_{22r})}{K_t} = -\frac{(R_{11r}e^{-\mu_1} + R_{12r}\, e^{-\mu_2})}{K_t} \qquad (F.7)$$

Hence the satisfaction of the compatibility and equilibrium conditions yields

$$\sum_{j=1}^{2} R_{1jr} \left[\sum_{n=1}^{2} a_n e^{-k_n XL} + e^{-\mu_j} \left(\sum_{n=1}^{2} a_n e^{k_n XL} f_{jn} + \frac{1}{K_t} \right) \right]$$

$$+ R_{or} \sum_{n=1}^{2} a_n e^{-k_n(2XL)} + R_{o\ell} \sum_{n=1}^{2} a_n e^{-k_n(3XL)}$$

$$+ \sum_{j=1}^{2} R_{1j\ell} \sum_{n=1}^{2} a_n e^{-k_n(3XL)} f_{jn}$$

$$= -F_o \sum_{n=1}^{2} a_n e^{-k_n(3XL-x_o)} \qquad (F.8)$$

The transverse displacement boundary conditions at supports 1ℓ and 2ℓ can likewise be obtained. The displacement of the beam at any x_ℓ' between 0ℓ and 1ℓ can be found to be

$$w(x_\ell') = F_o \sum_{n=1}^{2} a_n e^{-k_n(x_o+x\ell')}$$

$$+ \sum_{j=1}^{2} R_{ijr} \sum_{n=1}^{2} a_n e^{-k_n(XL+x_\ell')} f_{jn} + R_{or} \sum_{n=1}^{2} a_n e^{-k_n(XL+x_\ell')}$$

$$+ R_{o\ell} \sum_{n=1}^{2} a_n e^{-k_n x_\ell'}$$

$$+ \sum_{j=1}^{2} R_{ij\ell} \sum_{n=1}^{2} a_n e^{k_n x_\ell'} f_{jn} \qquad (F.9)$$

where $0 \leq |x_\ell'| \leq XL$ and x_ℓ' is measured from support number 0ℓ.

The beam displacement at 1ℓ can be obtained from equation (F.9) by substituting $x_\ell' = XL$ in it. This is equal to the displacement of the support given by $w(1\ell) = -(R_{i1\ell} + R_{i2\ell})/K_t$. Carrying out the necessary algebra, the elastic boundary condition at 1ℓ can be found to be

$$\sum_{j=1}^{2} R_{ijr} \sum_{n=1}^{2} a_n e^{-k_n(2XL)} f_{jn}$$

$$+ R_{or} \sum_{n=1}^{2} a_n e^{-k_n(2XL)} + R_{o\ell} \sum_{n=1}^{2} a_n e^{-k_n XL}$$

$$+ \sum_{j=1}^{2} R_{ij\ell} \left(\sum_{n=1}^{2} a_n e^{k_n XL} f_{jn} + \frac{1}{K_t} \right)$$

$$= -F_o \sum_{n=1}^{2} a_n e^{-k_n(XL+x_o)} \qquad (F.10)$$

The transverse displacement of the beam at any x_ℓ'' between 1ℓ and 2ℓ can be shown to be

$$w(x_\ell") = F_o \sum_{n=1}^{2} a_n e^{-k_n(XL+x_o+x_\ell")}$$

$$+ \sum_{j=1}^{2} R_{ijr} \sum_{n=1}^{2} a_n e^{-k_n(2XL+x_\ell")} f_{jn}$$

$$+ R_{or} \sum_{n=1}^{2} a_n e^{-k_n(2XL+x_\ell")} + R_{o\ell} \sum_{n=1}^{2} a_n e^{-k_n(XL+x_\ell")}$$

$$+ \sum_{j=1}^{2} R_{ij\ell} \left(\sum_{n=1}^{2} a_n e^{-k_n x_\ell"} + e^{-\mu_j} \sum_{n=1}^{2} a_n e^{k_n x_\ell"} f_{jn} \right) \qquad (F.11)$$

where $0 \leq |x_\ell"| \leq XL$ and $x_\ell"$ is measured from support number 1ℓ.

Substitution of $x_\ell" = XL$ into equation (F.11) gives the transverse displacement of the beam at 2ℓ which is equal to the support transverse displacement given by

$$w(2\ell) = - \frac{(R_{i,\ell} e^{-\mu_1} + R_{i2\ell} e^{-\mu_2})}{K_t} \qquad (F.12)$$

Therefore the required elastic boundary condition of support 2ℓ turns out to be

$$\sum_{j=1}^{2} R_{ijr} \sum_{n=1}^{2} a_n e^{-k_n(3XL)} f_{jn}$$

$$+ R_{or} \sum_{n=1}^{2} a_n e^{-k_n(3XL)} + R_{o\ell} \sum_{n=1}^{2} a_n e^{-k_n(2XL)}$$

$$+ \sum_{j=1}^{2} R_{ij\ell} \left[\sum_{n=1}^{2} a_n e^{-k_n XL} + e^{-\mu_j} \left(\sum_{n=1}^{2} a_n e^{k_n XL} f_{jn} + \frac{1}{K_t} \right) \right]$$

$$= -F_o \sum_{n=1}^{2} a_n e^{-k_n(2XL+x_o)} \qquad (F.13)$$

Equations (9.10), (F.1), (F.4), (F.8), (F.10) and (F.13) can be put into the following matrix form

$$\begin{bmatrix} & X_{i,j} & \end{bmatrix} \begin{Bmatrix} R_{i2r} \\ R_{i1r} \\ R_{or} \\ R_{o\ell} \\ R_{i1\ell} \\ R_{i2\ell} \end{Bmatrix} = -F_o \begin{Bmatrix} \sum_{n=1}^{2} a_n e^{-k_n(3XL-x_o)} \\ \sum_{n=1}^{2} a_n e^{-k_n(2XL-x_o)} \\ \sum_{n=1}^{2} a_n e^{-k_n(XL-x_o)} \\ \sum_{n=1}^{2} a_n e^{-k_n x_o} \\ \sum_{n=1}^{2} a_n e^{-k_n(XL+x_o)} \\ \sum_{n=1}^{2} a_n e^{-k_n(2XL+x_o)} \end{Bmatrix} \qquad \text{(F.14)}$$

where

$$X_{i,1} = \sum_{n=1}^{2} a_n e^{-k_n XL} + e^{-\mu_2}\left(\sum_{n=1}^{2} a_n e^{k_n XL} f_{2n} + \frac{1}{K_t} \right) = X_{6,6}$$

$$X_{i,2} = \sum_{n=1}^{2} a_n e^{-k_n XL} + e^{-\mu_1}\left(\sum_{n=1}^{2} a_n e^{k_n XL} f_{1n} + \frac{1}{K_t} \right) = X_{6,5}$$

$$X_{i,3} = \sum_{n=1}^{2} a_n e^{-k_n(2XL)} = X_{6,4}$$

$$X_{i,4} = \sum_{n=1}^{2} a_n e^{-k_n(3XL)} = X_{6,3}$$

$$X_{i,5} = \sum_{n=1}^{2} a_n e^{-k_n(3XL)} f_{1n} = X_{6,2}$$

$$X_{1,6} = \sum_{n=1}^{2} a_n e^{-k_n(3XL)} f_{2n} = X_{6,1}$$

$$X_{2,1} = \sum_{n=1}^{2} a_n e^{k_n XL} f_{2n} + \frac{1}{K_t} = X_{5,6}$$

$$X_{2,2} = \sum_{n=1}^{2} a_n e^{k_n XL} f_{1n} + \frac{1}{K_t} = X_{5,5}$$

$$X_{2,3} = \sum_{n=1}^{2} a_n e^{-k_n XL} = X_{5,4}$$

$$X_{2,4} = \sum_{n=1}^{2} a_n e^{-k_n(2XL)} = X_{5,3}$$

$$X_{2,5} = \sum_{n=1}^{2} a_n e^{-k_n(2XL)} f_{1n} = X_{5,2}$$

$$X_{2,6} = \sum_{n=1}^{2} a_n e^{-k_n(2XL)} f_{2n} = X_{5,1}$$

$$X_{3,1} = \sum_{n=1}^{2} a_n f_{2n} = X_{4,6}$$

$$X_{3,2} = \sum_{n=1}^{2} a_n f_{1n} = X_{4,5}$$

$$X_{3,3} = \sum_{n=1}^{2} a_n + \frac{1}{K_t} = X_{4,4}$$

$$X_{3,4} = \sum_{n=1}^{2} a_n e^{-k_n XL} = X_{4,3}$$

$$X_{3,5} = \sum_{n=1}^{2} a_n e^{-k_n XL} f_{1n} = X_{4,2}$$

$$X_{3,6} = \sum_{n=1}^{2} a_n e^{-k_n XL} f_{2n} = X_{4,1}$$

The above equation can be solved numerically. Once the unknown reactions are determined, the transverse displacement can be found anywhere in the beam.

APPENDIX G

FORCED VIBRATIONS OF INFINITE, PERIODIC, UNIFORM EULER-BERNOULLI BEAM ON GENERAL ELASTIC SUPPORTS SUBJECTED TO A SINGLE HARMONIC FORCE

Consider Figure 81. Equations (9.12) and (9.14) give the transverse displacement of the beam at any x_r within the loaded bay (*i.e.*, between 0ℓ and $0r$). This case has eight unknowns (R_{i2r}, R_{i1r}, R_{or}, M_{or}, $M_{o\ell}$, $R_{o\ell}$, $R_{i1\ell}$ and $R_{i2\ell}$). Therefore eight boundary conditions which satisfy both compatibility and equilibrium conditions are necessary. In this study they are set up as six transverse displacement conditions at 2ℓ, 1ℓ, 0ℓ, $0r$, $1r$, $2r$ and two rotational conditions at 0ℓ and $0r$. The reasons of selection of this particular set of support conditions are given in Section 9.2.3.

Equation (9.15) gives the transverse displacement condition at support $0r$. The transverse displacement of the beam at support 0ℓ can be obtained from equation (9.14) by substituting $x_r = 0$ in it and is equal to the support transverse displacement $w(0\ell) = -(K_r/K^2_{tot})R_{o\ell} + (K_c/K^2_{tot})M_{o\ell}$. The satisfaction of these equilibrium and compatibility conditions yields the displacement boundary condition at support 0ℓ as,

$$\sum_{j=1}^{2} R_{ijr}\left[\sum_{n=1}^{2} a_n e^{-k_n XL} f_{jn} - f(-\mu_j)\sum_{n=1}^{2} b_n e^{-k_n XL} f_{jn}\right]$$

$$+ R_{or}\sum_{n=1}^{2} a_n e^{-k_n XL} - M_{or}\sum_{n=1}^{2} b_n e^{-k_n XL}$$

$$+ M_{o\ell}\left(\sum_{n=1}^{2} b_n - \frac{K_c}{K^2_{tot}}\right) + R_{o\ell}\left(\sum_{n=1}^{2} a_n + \frac{K_r}{K^2_{tot}}\right)$$

$$+ \sum_{j=1}^{2} R_{ij\ell}\left[\sum_{n=1}^{2} a_n f_{jn} + f(\mu_j)\sum_{n=1}^{2} b_n f_{jn}\right]$$

$$= -F_o \sum_{n=1}^{2} a_n e^{-k_n x_o} \qquad (G.1)$$

where $f_{jn} = e^{-k_n XL} / [1 - e^{-(\mu_j + k_n XL)}]$ $j = 1,2$ and $n = 1,2$.

The beam transverse displacement at any x_r' between Or and lr can be shown to be

$$
\begin{aligned}
w(x_r') = {} & F_o \sum_{n=1}^{2} a_n e^{-k_n(XL - x_o + x_r')} \\
& + \sum_{j=1}^{2} \sum_{s=1}^{\infty} R_{ijr} e^{-\mu_j(s-1)} \sum_{n=1}^{2} a_n e^{-k_n(sXL - x_r')} \\
& - \sum_{j=1}^{2} \sum_{s=1}^{\infty} M_{ijr} e^{-\mu_j(s-1)} \sum_{n=1}^{2} b_n e^{-k_n(sXL - x_r')} \\
& + R_{or} \sum_{n=1}^{2} a_n e^{-k_n x_r'} + M_{or} \sum_{n=1}^{2} b_n e^{-k_n x_r'} \\
& + M_{o\ell} \sum_{n=1}^{2} b_n e^{-k_n(XL + x_r')} + R_{o\ell} \sum_{n=1}^{2} a_n e^{-k_n(XL + x_r')} \\
& + \sum_{j=1}^{2} \sum_{s=1}^{\infty} R_{ij\ell} e^{-\mu_j(s-1)} \sum_{n=1}^{2} a_n e^{-k_n((s+1)XL + x_r')} \\
& + \sum_{j=1}^{2} \sum_{s=1}^{\infty} M_{ij\ell} e^{-\mu_j(s-1)} \sum_{n=1}^{2} b_n e^{-k_n((s+1)XL + x_r')} \qquad \text{(G.2)}
\end{aligned}
$$

where $0 \leq |x_r'| \leq XL$ and x_r' is measured from support number Or.

Now in Chapter 9 the moment reactions in the free field have been represented in terms of forces through equation (9.13) for each of the wave motion existing on the beam. Hence by eliminating the moments from equation (G.2), and summing the infinite series it can be found that the transverse displacement of the beam is given by

$$w(x_r') = F_o \sum_{n=1}^{2} a_n e^{-k_n(XL-x_o+x_r')}$$

$$+ \sum_{j=1}^{2} R_{ijr} \left[\sum_{n=1}^{2} a_n e^{k_n x_r'} f_{jn} - f(-\mu_j) \sum_{n=1}^{2} b_n e^{k_n x_r'} f_{jn} \right]$$

$$+ R_{or} \sum_{n=1}^{2} a_n e^{-k_n x_r'} + M_{or} \sum_{n=1}^{2} b_n e^{-k_n x_r'}$$

$$+ M_{o\ell} \sum_{n=1}^{2} b_n e^{-k_n(XL+x_r')} + R_{o\ell} \sum_{n=1}^{2} a_n e^{-k_n(XL+x_r')}$$

$$+ \sum_{j=1}^{2} R_{ij\ell} \left[\sum_{n=1}^{2} a_n e^{-k_n(XL+x_r')} f_{jn} + f(\mu_j) \sum_{n=1}^{2} b_n e^{-k_n(XL+x_r')} f_{jn} \right] \qquad (G.3)$$

The beam transverse displacement at support 1r can be obtained from the above equation by setting $x_r' = XL$ in it and is equal to the support transverse displacement given by

$$w(1r) = -\frac{K_r}{K_{tot}^2} (R_{i1r} + R_{i2r}) + \frac{K_c}{K_{tot}^2} (M_{i1r} + M_{i2r}) \qquad (G.4)$$

which is equal to

$$w(1r) = -\frac{K_r}{K_{tot}^2} (R_{i1r} + R_{i2r}) + \frac{K_c}{K_{tot}^2} (f(-\mu_1)R_{i1r} + f(-\mu_2)R_{i2r}) \qquad (G.5)$$

The satisfaction of both compatibility and equilibrium conditions at support location 1r yields

$$\sum_{j=1}^{2} R_{ijr} \left[\sum_{n=1}^{2} a_n e^{k_n XL} f_{jn} + \frac{K_r}{K_{tot}^2} \right.$$

$$\left. - f(-\mu_j)\left(\sum_{n=1}^{2} b_n e^{k_n XL} f_{jn} + \frac{K_c}{K_{tot}^2} \right) \right]$$

$$+ R_{or} \sum_{n=1}^{2} a_n e^{-k_n XL} + M_{or} \sum_{n=1}^{2} b_n e^{-k_n XL}$$

$$+ M_{o\ell} \sum_{n=1}^{2} b_n e^{-k_n(2XL)} + R_{o\ell} \sum_{n=1}^{2} a_n e^{-k_n(2XL)}$$

$$+ \sum_{j=1}^{2} R_{ij\ell} \left[\sum_{n=1}^{2} a_n e^{-k_n(2XL)} f_{jn} + f(\mu_j) \sum_{n=1}^{2} b_n e^{-k_n(2XL)} f_{jn} \right]$$

$$= - F_o \sum_{n=1}^{2} a_n e^{-k_n(2XL - x_o)} \qquad (G.6)$$

The transverse displacement of the beam at any x_r" between 1r and 2r can be shown to be

$$w(x_r") = F_o \sum_{n=1}^{2} a_n e^{-k_n(2XL-x_o+x_r")}$$

$$+ \sum_{j=1}^{2} R_{ijr} \sum_{n=1}^{2} a_n e^{-k_n x_r"} + \sum_{j=1}^{2} \sum_{s=2}^{\infty} R_{ijr} e^{-\mu_j(s-1)} \sum_{n=1}^{2} a_n e^{-k_n((s-1)XL-x_r")}$$

$$+ \sum_{j=1}^{2} M_{ijr} \sum_{n=1}^{2} b_n e^{-k_n x_r"} - \sum_{j=1}^{2} \sum_{s=2}^{\infty} M_{ijr} e^{-\mu_j(s-1)} \sum_{n=1}^{2} b_n e^{-k_n((s-1)XL-x_r")}$$

$$+ R_{or} \sum_{n=1}^{2} a_n e^{-k_n(XL+x_r")} + M_{or} \sum_{n=1}^{2} b_n e^{-k_n(XL+x_r")}$$

$$+ M_{o\ell} \sum_{n=1}^{2} b_n e^{-k_n(2XL+x_r")} + R_{o\ell} \sum_{n=1}^{2} a_n e^{-k_n(2XL+x_r")}$$

$$+ \sum_{j=1}^{2} \sum_{s=1}^{\infty} R_{ij\ell} e^{-\mu_j(s-1)} \sum_{n=1}^{2} a_n e^{-k_n((s+2)XL+x_r")}$$

$$+ \sum_{j=1}^{2} \sum_{s=1}^{\infty} M_{ij\ell} e^{-\mu_j(s-1)} \sum_{n=1}^{2} b_n e^{-k_n((s+2)XL+x_r")} \qquad (G.7)$$

where $0 \leq |x_r"| \leq XL$ and $x_r"$ is measured from support number 1r.

After the infinite series has been summed, equation (G.7) can be rewritten as

$$w(x_r'') = F_o \sum_{n=1}^{2} a_n e^{-k_n(2XL-x_o+x_r'')}$$

$$+ \sum_{j=1}^{2} R_{ijr}\Big[\sum_{n=1}^{2} a_n e^{-k_n x_r''} + e^{-\mu_j} \sum_{n=1}^{2} a_n e^{k_n x_r''} f_{jn}$$

$$+ f(-\mu_j)\Big(\sum_{n=1}^{2} b_n e^{-k_n x_r''} - e^{-\mu_j} \sum_{n=1}^{2} b_n e^{k_n x_r''} f_{jn}\Big)\Big]$$

$$+ R_{or} \sum_{n=1}^{2} a_n e^{-k_n(XL+x_r'')} + M_{or} \sum_{n=1}^{2} b_n e^{-k_n(XL+x_r'')}$$

$$+ M_{o\ell} \sum_{n=1}^{2} b_n e^{-k_n(2XL+x_r'')} + R_{o\ell} \sum_{n=1}^{2} a_n e^{-k_n(2XL+x_r'')}$$

$$+ \sum_{j=1}^{2} R_{ij\ell}\Big[\sum_{n=1}^{2} a_n e^{-k_n(2XL+x_r'')} f_{jn} + f(\mu_j) \sum_{n=1}^{2} b_n e^{-k_n(2XL+x_r'')} f_{jn}\Big] \qquad (G.8)$$

The beam transverse displacement at support 2r can be found from equation (G.8) by setting $x_r'' = XL$ in it. This is equal to the support transverse displacement at 2r which can be found to be

$$w(2r) = -\frac{K_r}{K_{tot}^2}(R_{i1r} e^{-\mu_1} + R_{i2r} e^{-\mu_2})$$

$$+ \frac{K_c}{K_{tot}^2}(f(-\mu_1)R_{i1r} e^{-\mu_1} + f(-\mu_2)R_{i2r} e^{-\mu_2}) \qquad (G.9)$$

By considering the compatibility and equilibrium conditions, the displacement boundary condition at support 2r yields

$$\sum_{j=1}^{2} R_{ijr}\Big[\Big[\sum_{n=1}^{2} a_n e^{-k_n XL} + e^{-\mu_j}\Big(\sum_{n=1}^{2} a_n e^{k_n XL} f_{jn} + \frac{K_r}{K_{tot}^2}\Big)\Big]$$

$$+ f(-\mu_j)\Big[\sum_{n=1}^{2} b_n e^{-k_n XL} - e^{-\mu_j}\Big(\sum_{n=1}^{2} b_n e^{k_n XL} f_{jn} + \frac{K_c}{K_{tot}^2}\Big)\Big]\Big\}$$

$$+ R_{or} \sum_{n=1}^{2} a_n e^{-k_n(2XL)} + M_{or} \sum_{n=1}^{2} b_n e^{-k_n(2XL)}$$

$$+ M_{o\ell} \sum_{n=1}^{2} b_n e^{-k_n(3XL)} + R_{o\ell} \sum_{n=1}^{2} a_n e^{-k_n(3XL)}$$

$$+ \sum_{j=1}^{2} R_{ij\ell}\Big[\sum_{n=1}^{2} a_n e^{-k_n(3XL)} f_{jn} + f(\mu_j) \sum_{n=1}^{2} b_n e^{-k_n(3XL)} f_{jn}\Big]$$

$$= -F_o \sum_{n=1}^{2} a_n e^{-k_n(3XL - x_o)} \qquad \text{(G.10)}$$

The transverse displacement conditions at supports 1ℓ and 2ℓ can likewise be obtained.

It can be shown that the beam transverse displacement at any x_ℓ' between 0ℓ and 1ℓ is

$$w(x_{\ell}') = F_o \sum_{n=1}^{2} a_n e^{-k_n(x_o+x_{\ell}')}$$

$$+ \sum_{j=1}^{2} R_{ijr} \left[\sum_{n=1}^{2} a_n e^{-k_n(XL+x_{\ell}')} f_{jn} - f(-\mu_j) \sum_{n=1}^{2} b_n e^{-k_n(XL+x_{\ell}')} f_{jn} \right]$$

$$+ R_{or} \sum_{n=1}^{2} a_n e^{-k_n(XL+x_{\ell}')} - M_{or} \sum_{n=1}^{2} b_n e^{-k_n(XL+x_{\ell}')}$$

$$- M_{o\ell} \sum_{n=1}^{2} b_n e^{-k_n x_{\ell}'} + R_{o\ell} \sum_{n=1}^{2} a_n e^{-k_n x_{\ell}'}$$

$$+ \sum_{j=1}^{2} R_{ij\ell} \left[\sum_{n=1}^{2} a_n e^{k_n x_{\ell}'} f_{jn} + f(\mu_j) \sum_{n=1}^{2} b_n e^{k_n x_{\ell}'} f_{jn} \right] \qquad (G.11)$$

where $0 \leq |x_{\ell}'| \leq XL$ and x_{ℓ}' is mesured from support number 0ℓ.

By setting x_{ℓ}' to XL in this equation, one obtains the transverse displacement of the beam at 1ℓ. This transverse displacement must be equal to that of the support given by

$$w(1\ell) = -\frac{K_r}{K_{tot}^2}(R_{i1\ell} + R_{i2\ell}) + \frac{K_c}{K_{tot}^2}(f(\mu_1)R_{i1\ell} + f(\mu_2)R_{i2\ell}) \qquad (G.12)$$

As before, by carring out the necessary manipulations the transverse displacement condition at support 1ℓ can be found to be

$$\sum_{j=1}^{2} R_{ijr}\left[\sum_{n=1}^{2} a_n e^{-k_n(2XL)} f_{jn} - f(-\mu_j)\sum_{n=1}^{2} b_n e^{-k_n(2XL)} f_{jn}\right]$$

$$+ R_{or}\sum_{n=1}^{2} a_n e^{-k_n(2XL)} - M_{or}\sum_{n=1}^{2} b_n e^{-k_n(2XL)}$$

$$- M_{o\ell}\sum_{n=1}^{2} b_n e^{-k_n XL} + R_{o\ell}\sum_{n=1}^{2} a_n e^{-k_n XL}$$

$$+ \sum_{j=1}^{2} R_{ij\ell}\left[\sum_{n=1}^{2} a_n e^{k_n XL} f_{jn} + \frac{K_r}{K_{tot}^2}\right.$$

$$\left. + f(\mu_j)\left(\sum_{n=1}^{2} b_n e^{k_n XL} f_{jn} - \frac{K_c}{K_{tot}^2}\right)\right]$$

$$= -F_o \sum_{n=1}^{2} a_n e^{-k_n(XL+x_o)} \qquad \text{(G.13)}$$

The transverse displacement of the beam at any x_ℓ" between 1ℓ and 2ℓ can be shown to be

$$w(x_\ell") = F_o \sum_{n=1}^{2} a_n e^{-k_n(XL+x_o+x_\ell")}$$

$$+ \sum_{j=1}^{2} R_{ijr}\Big[\sum_{n=1}^{2} a_n e^{-k_n(2XL+x_\ell")} f_{jn}$$

$$-f(-\mu_j)\Big(\sum_{n=1}^{2} b_n e^{-k_n(2XL+x_\ell")} f_{jn}\Big]$$

$$+ R_{or} \sum_{n=1}^{2} a_n e^{-k_n(2XL+x_\ell")} - M_{or} \sum_{n=1}^{2} b_n e^{-k_n(2XL+x_\ell")}$$

$$- M_{o\ell} \sum_{n=1}^{2} b_n e^{-k_n(XL+x_\ell")} + R_{o\ell} \sum_{n=1}^{2} a_n e^{-k_n(XL+x_\ell")}$$

$$+ \sum_{j=1}^{2} R_{ij\ell}\Big[\sum_{n=1}^{2} a_n e^{-k_n x_\ell"} + e^{-\mu_j} \sum_{n=1}^{2} a_n e^{k_n x_\ell"} f_{jn}$$

$$- f(\mu_j)\Big(\sum_{n=1}^{2} b_n e^{-k_n x_\ell"} - e^{-\mu_j} \sum_{n=1}^{2} b_n e^{k_n x_\ell"} f_{jn}\Big)\Big] \qquad (G.14)$$

where $0 \leq |x_\ell"| \leq XL$ and $x_\ell"$ is measured from support 1ℓ.

The beam displacement at 2ℓ can be found from the above equation by setting $x_\ell"$ to XL and is equal to the support transverse displacement

$$w(2\ell) = -\frac{K_r}{K_{tot}^2}\left(R_{i1\ell} e^{-\mu_1} + R_{i2\ell} e^{-\mu_2}\right)$$

$$+ \frac{K_c}{K_{tot}^2}\left(f(\mu_1)R_{i1\ell} e^{-\mu_1} + f(\mu_2)R_{i2\ell} e^{-\mu_2}\right) \qquad (G.15)$$

Hence, the satisfaction of both compatibility and equilibrium conditions at support 2ℓ gives

$$\sum_{j=1}^{2} R_{ijr}\Big[\sum_{n=1}^{2} a_n e^{-k_n(3XL)} f_{jn}$$

$$- f(-\mu_j)\sum_{n=1}^{2} b_n e^{-k_n(3XL)} f_{jn}\Big]$$

$$+ R_{or}\sum_{n=1}^{2} a_n e^{-k_n(3XL)} - M_{or}\sum_{n=1}^{2} b_n e^{-k_n(3XL)}$$

$$- M_{o\ell}\sum_{n=1}^{2} b_n e^{-k_n(2XL)} + R_{o\ell}\sum_{n=1}^{2} a_n e^{-k_n(2XL)}$$

$$+ \sum_{j=1}^{2} R_{ij\ell}\Big[\Big[\sum_{n=1}^{2} a_n e^{-k_n XL} + e^{-\mu_j}\Big(\sum_{n=1}^{2} a_n e^{k_n XL} f_{jn} + \frac{K_r}{K_{tot}^2}\Big)\Big]$$

$$- f(\mu_j)\Big[\sum_{n=1}^{2} b_n e^{-k_n XL} - e^{-\mu_j}\Big(\sum_{n=1}^{2} b_n e^{k_n XL} f_{jn} - \frac{K_c}{K_{tot}^2}\Big)\Big]\Big]$$

$$= -F_o\sum_{n=1}^{2} a_n e^{-k_n(2XL+x_o)} \qquad (G.16)$$

In addition to these transverse displacement conditions, one must also satisfy the rotational boundary conditions at supports Or and Oℓ. Now the rotation θ_r at any x_r within the loaded bay (*i.e.*, between Oℓ and Or) can be shown to be

$$\theta(x_r) = (jk)F_o \sum_{n=1}^{2} c_n e^{-k_n|x_o-x_r|}$$

$$- \sum_{j=1}^{2} \sum_{s=1}^{\infty} R_{ijr} e^{-\mu_j(s-1)} \sum_{n=1}^{2} c_n e^{-k_n((s+1)XL-x_r)}$$

$$+ \sum_{j=1}^{2} \sum_{s=1}^{\infty} M_{ijr} e^{-\mu_j(s-1)} \sum_{n=1}^{2} d_n e^{-k_n((s+1)XL-x_r)}$$

$$- R_{or} \sum_{n=1}^{2} c_n e^{-k_n(XL-x_r)} + M_{or} \sum_{n=1}^{2} d_n e^{-k_n(XL-x_r)}$$

$$+ M_{o\ell} \sum_{n=1}^{2} d_n e^{-k_n x_r} + R_{o\ell} \sum_{n=1}^{2} c_n e^{-k_n x_r}$$

$$+ \sum_{j=1}^{2} \sum_{s=1}^{\infty} M_{ij\ell} e^{-\mu_j(s-1)} \sum_{n=1}^{2} d_n e^{-k_n(sXL+x_r)}$$

$$+ \sum_{j=1}^{2} \sum_{s=1}^{\infty} R_{ij\ell} e^{-\mu_j(s-1)} \sum_{n=1}^{2} c_n e^{-k_n(sXL+x_r)} \qquad \text{(G.17)}$$

where $jk = -1$ if $x_r < x_o$; $jk = 1$ if $x_r > x_o$. $0 \leq |x_r| \leq XL$ and x_r is measured from support number 0ℓ.

When the infinite series are summed, equation (G.17) can conveniently be expressed as

$$\theta(x_r) = (jk)\, F_o \sum_{n=1}^{2} c_n\, e^{-k_n|x_o - x_r|}$$

$$- \sum_{j=1}^{2} R_{ijr} \left[\sum_{n=1}^{2} c_n\, e^{-k_n(XL-x_r)} f_{jn} - f(-\mu_j) \sum_{n=1}^{2} d_n\, e^{-k_n(XL-x_r)} f_{jn} \right]$$

$$- R_{or} \sum_{n=1}^{2} c_n\, e^{-k_n(XL-x_r)} + M_{or} \sum_{n=1}^{2} d_n\, e^{-k_n(XL-x_r)}$$

$$+ M_{o\ell} \sum_{n=1}^{2} d_n\, e^{-k_n x_r} + R_{o\ell} \sum_{n=1}^{2} c_n\, e^{-k_n x_r}$$

$$+ \sum_{j=1}^{2} R_{ij\ell} \left[\sum_{n=1}^{2} c_n\, e^{-k_n x_r} f_{jn} + f(\mu_j) \sum_{n=1}^{2} d_n\, e^{-k_n x_r} f_{jn} \right] \qquad (G.18)$$

where the rotational coefficients c_n's and d_n's were given in Section 2.2.1.

Now by setting x_r to XL, one obtains the rotation of the beam at support Or which is equal to the support rotation given by

$$\theta(Or) = \frac{K_c}{K_{tot}^2} R_{or} - \frac{K_t}{K_{tot}^2} M_{or} \qquad (G.19)$$

Also by setting x_r to 0, the rotation of the beam at support Oℓ can be found. This is equal to the support rotation at Oℓ which is

$$\theta(O\ell) = \frac{K_c}{K_{tot}^2} R_{o\ell} - \frac{K_t}{K_{tot}^2} M_{o\ell} \qquad (G.20)$$

Hence, by considering the above arguments and equations (G.18) to (G.20), the rotational boundary conditions at supports Or and Oℓ can be obtained. The condition at Or gives

$$- \sum_{j=1}^{2} R_{ijr} \left[\sum_{n=1}^{2} c_n f_{jn} - f(-\mu_j) \sum_{n=1}^{2} d_n f_{jn} \right]$$

$$- R_{or} \left(\sum_{n=1}^{2} c_n + \frac{K_c}{K_{tot}^2} \right) + M_{or} \left(\sum_{n=1}^{2} d_n + \frac{K_t}{K_{tot}^2} \right)$$

$$+ M_{o\ell} \sum_{n=1}^{2} d_n e^{-k_n XL} + R_{o\ell} \sum_{n=1}^{2} c_n e^{-k_n XL}$$

$$+ \sum_{j=1}^{2} R_{ij\ell} \left[\sum_{n=1}^{2} c_n e^{-k_n XL} f_{jn} + f(\mu_j) \sum_{n=1}^{2} d_n e^{-k_n XL} f_{jn} \right]$$

$$= -F_o \sum_{n=1}^{2} c_n e^{-k_n (XL - x_o)} \qquad \text{(G.21)}$$

and the condition at 0ℓ results in

$$- \sum_{j=1}^{2} R_{ijr} \left[\sum_{n=1}^{2} c_n e^{-k_n XL} f_{jn} - f(-\mu_j) \sum_{n=1}^{2} d_n e^{-k_n XL} f_{jn} \right]$$

$$- R_{or} \sum_{n=1}^{2} c_n e^{-k_n XL} + M_{or} \sum_{n=1}^{2} d_n e^{-k_n XL}$$

$$+ M_{o\ell} \left(\sum_{n=1}^{2} d_n + \frac{K_t}{K_{tot}^2} \right) + R_{o\ell} \left(\sum_{n=1}^{2} c_n - \frac{K_c}{K_{tot}^2} \right)$$

$$+ \sum_{j=1}^{2} R_{ij\ell} \left[\sum_{n=1}^{2} c_n f_{jn} + f(\mu_j) \sum_{n=1}^{2} d_n f_{jn} \right]$$

$$= -(-F_o \sum_{n=1}^{2} c_n e^{-k_n x_o}) \qquad \text{(G.22)}$$

Equations (9.15), (G.1), (G.6), (G.10), (G.13), (G.16), (G.21) and (G.22) can be put into a matrix form as

$$\begin{bmatrix} \\ X_{i,j} \\ \\ \end{bmatrix} \begin{Bmatrix} R_{iir} \\ R_{iir} \\ R_{or} \\ M_{or} \\ M_{o\ell} \\ R_{o\ell} \\ R_{ii\ell} \\ R_{i2\ell} \end{Bmatrix} = -F_o \begin{Bmatrix} \sum_{n=1}^{2} a_n e^{-k_n(3XL-x_o)} \\ \sum_{n=1}^{2} a_n e^{-k_n(2XL-x_o)} \\ \sum_{n=1}^{2} a_n e^{-k_n(XL-x_o)} \\ \sum_{n=1}^{2} c_n e^{-k_n(XL-x_o)} \\ -\sum_{n=1}^{2} c_n e^{-k_n x_o} \\ \sum_{n=1}^{2} a_n e^{-k_n x_o} \\ \sum_{n=1}^{2} a_n e^{-k_n(XL+x_o)} \\ \sum_{n=1}^{2} a_n e^{-k_n(2XL+x_o)} \end{Bmatrix} \qquad (G.23)$$

This equation can be solved numerically. Once the unknowns are determined, the transverse displacement or rotation at any bay can easily be found.

APPENDIX H

FORCED VIBRATIONS OF INFINITE, PERIODIC THREE-LAYERED SANDWICH PLATE ON SIMPLE SUPPORTS SUBJECTED TO A SINGLE HARMONIC LINE FORCE

Equations (9.17) and (9.18) give the sandwich plate transverse displacement at any (x_r,y) within the loaded bay (*i.e.*, between 0ℓ and $0r$) and equation (9.19) gives the zero transverse displacement condition at $0r$.

This case has six unknowns (R_{i2r}, R_{i1r}, R_{or}, $R_{o\ell}$, $R_{i1\ell}$ and $R_{i2\ell}$). Therefore in addition to equation (9.19) five more boundary conditions which represent the zero transverse displacement are necessary. In this study they are set up at support locations $1r$, $2r$, 0ℓ, 1ℓ, 2ℓ.

If one substitutes $x_r = 0$ into equation (9.18) the transverse displacement of the sandwich plate at $(0\ell,y)$ is obtained. Equating this to zero yields

$$\left\{ \sum_{j=1}^{2} R_{ijr} \sum_{n=1}^{3} a_n e^{-k_n XL} f_{jn}' + R_{or} \sum_{n=1}^{3} a_n e^{-k_n XL} + R_{o\ell} \sum_{n=1}^{3} a_n + \sum_{j=1}^{2} R_{ij\ell} \sum_{n=1}^{3} a_n f_{jn}' \right\} \sin k_y y = -F_o \sum_{n=1}^{3} a_n e^{-k_n x_o} \sin k_y y \qquad (H.1)$$

where $f_{jn}' = e^{-k_n XL}/[1 - e^{-(\mu_j + k_n XL)}]$ $\quad j = 1,2$ and $n = 1,2,3$.

The transverse displacement of the plate at any (x_r',y) between $0r$ and $1r$ can be found by considering the infinite-system line response functions of all the reaction forces and the applied force $F_o \sin k_y y$. In this way one obtains $w(x_r',y)$ as

$$w(x_r',y) = \Big\{F_o \sum_{n=1}^{3} a_n\, e^{-k_n(XL-x_o+x_r')}$$

$$+ \sum_{j=1}^{2} \sum_{s=1}^{\infty} R_{ijr}\, e^{-\mu_j(s-1)} \sum_{n=1}^{3} a_n\, e^{-k_n(sXL-x_r')}$$

$$+ R_{or} \sum_{n=1}^{3} a_n\, e^{-k_n x_r'} + R_{o\ell} \sum_{n=1}^{3} a_n\, e^{-k_n(XL+x_r')}$$

$$+ \sum_{j=1}^{2} \sum_{s=1}^{\infty} R_{ij\ell}\, e^{-\mu_j(s-1)} \sum_{n=1}^{3} a_n\, e^{-k_n((s+1)XL+x_r')}\Big\} \sin k_y y \qquad (H.2)$$

where $0 \leq |x_r'| \leq XL$ and x_r' is measured from support number Or.

The transverse line displacements at any other bay can likewise be obtained. The procedure is the same as given in Appendix E but now three-terms infinite-system line response functions must be used instead of two-terms infinite-system point response functions.

The infinite series equation in equation (H.2) can easily be summed and it reduces to

$$w(x_r',y) = \Big\{F_o \sum_{n=1}^{3} a_n\, e^{-k_n(XL-x_o+x_r')}$$

$$+ \sum_{j=1}^{2} R_{ijr} \sum_{n=1}^{3} a_n\, e^{k_n x_r'} f_{jn}' + R_{or} \sum_{n=1}^{3} a_n\, e^{-k_n x_r'}$$

$$+ R_{o\ell} \sum_{n=1}^{3} a_n\, e^{-k_n(XL+x_r')}$$

$$+ \sum_{j=1}^{2} R_{ij\ell} \sum_{n=1}^{3} a_n\, e^{-k_n(XL+x_r')}\, f_{jn}'\Big\} \sin k_y y \qquad (H.3)$$

The transverse displacement of the plate at 1r can be found by setting $x_r' = XL$ in equation (H.3). Equating this to zero gives the required boundary condition at 1r as

$$\left\{ \sum_{j=1}^{2} R_{ijr} \sum_{n=1}^{3} a_n e^{k_n XL} f_{jn}' \right.$$

$$+ R_{or} \sum_{n=1}^{3} a_n e^{-k_n XL} + R_{o\ell} \sum_{n=1}^{3} a_n e^{-k_n(2XL)}$$

$$\left. + \sum_{j=1}^{2} R_{ij\ell} \sum_{n=1}^{3} a_n e^{-k_n(2XL)} f_{jn}' \right\} \sin k_y y$$

$$= -F_o \sum_{n=1}^{3} a_n e^{-k_n(2XL-x_o)} \sin k_y y \qquad \text{(H.4)}$$

Following similar procedures, the other boundary conditions can be found to be

$$w(2r,y) = 0 \; : \; \left\{ \sum_{j=1}^{2} R_{ijr} \left(\sum_{n=1}^{3} a_n e^{-k_n XL} + e^{-\mu_j} \sum_{n=1}^{3} a_n e^{k_n XL} f_{jn}' \right) \right.$$

$$+ R_{or} \sum_{n=1}^{3} a_n e^{-k_n(2XL)} + R_{o\ell} \sum_{n=1}^{3} a_n e^{-k_n(3XL)}$$

$$\left. + \sum_{j=1}^{2} R_{ij\ell} \sum_{n=1}^{3} a_n e^{-k_n(3XL)} f_{jn}' \right\} \sin k_y y$$

$$= -F_o \sum_{n=1}^{3} a_n e^{-k_n(3XL-x_o)} \sin k_y y \qquad \text{(H.5)}$$

$$w(1\ell,y) = 0: \left\{ \sum_{j=1}^{2} R_{ijr} \sum_{n=1}^{3} a_n e^{-k_n(2XL)} f_{jn}' \right.$$

$$+ R_{or} \sum_{n=1}^{3} a_n e^{-k_n(2XL)} + R_{o\ell} \sum_{n=1}^{3} a_n e^{-k_n XL}$$

$$\left. + \sum_{j=1}^{2} R_{ij\ell} \sum_{n=1}^{3} a_n e^{k_n XL} f_{jn}' \right] \sin k_y y$$

$$= -F_o \sum_{n=1}^{3} a_n e^{-k_n(x_o+XL)} \sin k_y y \qquad (H.6)$$

$$w(2\ell,y) = 0: \left\{ \sum_{j=1}^{2} R_{ijr} \sum_{n=1}^{3} a_n e^{-k_n(3XL)} f_{jn}' \right.$$

$$+ R_{or} \sum_{n=1}^{3} a_n e^{-k_n(3XL)} + R_{o\ell} \sum_{n=1}^{3} a_n e^{-k_n(2XL)}$$

$$\left. + \sum_{j=1}^{2} R_{ij\ell} \left(\sum_{n=1}^{3} a_n e^{-k_n XL} + e^{-\mu_j} \sum_{n=1}^{3} a_n e^{k_n XL} f_{jn}' \right) \right] \sin k_y y$$

$$= -F_o \sum_{n=1}^{3} a_n e^{-k_n(2XL+x_o)} \sin k_y y \qquad (H.7)$$

Equations (9.19), (H.1), (H.4), (H.5), (H.6) and (H.7) can be cast into a matrix form as

$$\begin{bmatrix} \\ X_{i,j} \\ \\ \end{bmatrix} \begin{Bmatrix} R_{i2r} \\ R_{i1r} \\ R_{or} \\ R_{o\ell} \\ R_{i1\ell} \\ R_{i2\ell} \end{Bmatrix} = -F_o \begin{Bmatrix} \sum_{n=1}^{3} a_n e^{-k_n(3XL-x_o)} \\ \sum_{n=1}^{3} a_n e^{-k_n(2XL-x_o)} \\ \sum_{n=1}^{3} a_n e^{-k_n(XL-x_o)} \\ \sum_{n=1}^{3} a_n e^{-k_n x_o} \\ \sum_{n=1}^{3} a_n e^{-k_n(XL+x_o)} \\ \sum_{n=1}^{3} a_n e^{-k_n(2XL+x_o)} \end{Bmatrix} \qquad (H.8)$$

This equation can be solved numerically. Once the unknowns are determined, the transverse displacement at any (x_r,y) within the loaded bay can be found from equation (9.18).

APPENDIX I

FORCED VIBRATIONS OF INFINITE PERIODIC THREE-LAYERED SANDWICH PLATE ON GENERAL SUPPORTS SUBJECTED TO A SINGLE HARMONIC LINE FORCE

Equations (9.22) and (9.23) give the transverse displacement of the plate at any (x_r, y) within the loaded bay (*i.e.*, between 0ℓ and $0r$) and equation (9.24) represents the elastic boundary condition at $0r$.

This case has ten unknowns (R_{i3r}, R_{i2r}, R_{i1r}, R_{or}, M_{or}, $M_{o\ell}$, $R_{o\ell}$, $R_{i1\ell}$, $R_{i2\ell}$, $R_{i3\ell}$). Therefore in addition to equation (9.24) nine more boundary condition equations, which satisfy both compatibility and the equilibrium conditions at required positions, are necessary. This study considers the transverse displacement conditions at support locations $3r$, $2r$, $1r$, 0ℓ, 1ℓ, 2ℓ, 3ℓ and the rotations at $0r$ and 0ℓ.

Appendix G outlines the determination of transverse displacements at the bays between 2ℓ and $2r$ and rotation within the loaded bay (between 0ℓ and $0r$) for an Euler-Bernoulli beam on general elastic supports. The corresponding sandwich plate displacements and rotations can likewise be obtained but now three-terms infinite-system line response functions must be used instead of two-terms point response functions. The plate displacements and rotations so obtained must be equal to those of supports at support locations. In this section most of the detailed derivations will not be repeated but the results of boundary conditions will be given. It can be found that the following conditions are true

$$w(0\ell,y) = 0: \left\{ \sum_{j=1}^{3} R_{ijr}\left[\sum_{n=1}^{3} a_n e^{-k_n XL} f_{jn}'' - f(-\mu_j) \sum_{n=1}^{3} b_n e^{-k_n XL} f_{jn}''\right]\right.$$

$$+ R_{or} \sum_{n=1}^{3} a_n e^{-k_n XL} - M_{or} \sum_{n=1}^{3} b_n e^{-k_n XL}$$

$$+ M_{o\ell} \left(\sum_{n=1}^{3} b_n - \frac{K_c}{K_{tot}^2} \right) + R_{o\ell} \left(\sum_{n=1}^{3} a_n + \frac{K_r}{K_{tot}^2} \right)$$

$$\left. + \sum_{j=1}^{3} R_{ij\ell}\left[\sum_{n=1}^{3} a_n f_{jn}'' + f(\mu_j) \sum_{n=1}^{3} b_n f_{jn}''\right]\right\} \sin k_y y$$

$$= -F_o \sum_{n=1}^{3} a_n e^{-k_n x_o} \sin k_y y \qquad \text{(I.1)}$$

where $f_{jn}'' = e^{-k_n XL} / [1 - e^{-(\mu_j + k_n XL)}]$ $n = 1,2,3$ and $j = 1,2,3$.

$$w(1r,y) = 0 : \left\{ \sum_{j=1}^{3} R_{ijr} \left[\sum_{n=1}^{3} a_n e^{k_n XL} f_{jn}'' + \frac{K_r}{K_{tot}^2} \right.\right.$$

$$\left. - f(-\mu_j)\left(\sum_{n=1}^{3} b_n e^{k_n XL} f_{jn}'' + \frac{K_c}{K_{tot}^2} \right)\right]$$

$$+ R_{or} \sum_{n=1}^{3} a_n e^{-k_n XL} + M_{or} \sum_{n=1}^{3} b_n e^{-k_n XL}$$

$$+ M_{o\ell} \sum_{n=1}^{3} b_n e^{-k_n (2XL)} + R_{o\ell} \sum_{n=1}^{3} a_n e^{-k_n (2XL)}$$

$$\left. + \sum_{j=1}^{3} R_{ij\ell} \left[\sum_{n=1}^{3} a_n e^{-k_n (2XL)} f_{jn}'' + f(\mu_j) \sum_{n=1}^{3} b_n e^{-k_n (2XL)} f_{jn}''\right]\right\} \sin k_y y$$

$$= -F_o \sum_{n=1}^{3} a_n e^{-k_n (2XL - x_o)} \sin k_y y \qquad \text{(I.2)}$$

$$w(2r,y) = 0 : \Big\{ \sum_{j=1}^{3} R_{ijr} \Big(\Big[\sum_{n=1}^{3} a_n e^{-k_n XL} + e^{-\mu_j} \Big(\sum_{n=1}^{3} a_n e^{k_n XL} f_{jn}''$$

$$+ \frac{K_r}{K_{tot}^2} \Big) \Big] + f(-\mu_j) \Big[\sum_{n=1}^{3} b_n e^{-k_n XL}$$

$$- e^{-\mu_j} \Big(\sum_{n=1}^{3} b_n e^{k_n XL} f_{jn}'' + \frac{K_c}{K_{tot}^2} \Big) \Big] \Big\}$$

$$+ R_{or} \sum_{n=1}^{3} a_n e^{-k_n(2XL)} + M_{or} \sum_{n=1}^{3} b_n e^{-k_n(2XL)}$$

$$+ M_{o\ell} \sum_{n=1}^{3} b_n e^{-k_n(3XL)} + R_{o\ell} \sum_{n=1}^{3} a_n e^{-k_n(3XL)}$$

$$+ \sum_{j=1}^{3} R_{ij\ell} \Big[\sum_{n=1}^{3} a_n e^{-k_n(3XL)} f_{jn}''$$

$$+ f(\mu_j) \sum_{n=1}^{3} b_n e^{-k_n(3XL)} f_{jn}'' \Big] \Big\} \sin k_y y$$

$$= -F_o \sum_{n=1}^{3} a_n e^{-k_n(3XL - x_o)} \sin k_y y \qquad \text{(I.3)}$$

$$w(1\ell,y) = 0 : \left\{ \sum_{j=1}^{3} R_{ijr} \left[\sum_{n=1}^{3} a_n e^{-k_n(2XL)} f_{jn}'' \right.\right.$$

$$\left. - f(-\mu_j) \sum_{n=1}^{3} b_n e^{-k_n(2XL)} f_{jn}'' \right]$$

$$+ R_{or} \sum_{n=1}^{3} a_n e^{-k_n(2XL)} - M_{or} \sum_{n=1}^{3} b_n e^{-k_n(2XL)}$$

$$- M_{o\ell} \sum_{n=1}^{3} b_n e^{-k_n XL} + R_{o\ell} \sum_{n=1}^{3} a_n e^{-k_n XL}$$

$$+ \sum_{j=1}^{3} R_{ij\ell} \left[\sum_{n=1}^{3} a_n e^{k_n XL} f_{jn}'' + \frac{K_r}{K_{tot}^2} \right.$$

$$\left. \left. + f(\mu_j)\left(\sum_{n=1}^{3} b_n e^{k_n XL} f_{jn}'' - \frac{K_c}{K_{tot}^2} \right) \right] \right\} \sin k_y y$$

$$= -F_o \sum_{n=1}^{3} a_n e^{-k_n(XL+x_o)} \sin k_y y \qquad (I.4)$$

$$w(2\ell,y) = 0 : \Big\{ \sum_{j=1}^{3} R_{ijr} \Big[\sum_{n=1}^{3} a_n e^{-k_n(3XL)} f_{jn}''$$

$$- f(-\mu_j) \sum_{n=1}^{3} b_n e^{-k_n(3XL)} f_{jn}'' \Big]$$

$$+ R_{or} \sum_{n=1}^{3} a_n e^{-k_n(3XL)} - M_{or} \sum_{n=1}^{3} b_n e^{-k_n(3XL)}$$

$$- M_{o\ell} \sum_{n=1}^{3} b_n e^{-k_n(2XL)} + R_{o\ell} \sum_{n=1}^{3} a_n e^{-k_n(2XL)}$$

$$+ \sum_{j=1}^{3} R_{ij\ell} \Big\{ \Big[\sum_{n=1}^{3} a_n e^{-k_n XL} + e^{-\mu_j} \Big(\sum_{n=1}^{3} a_n e^{k_n XL} f_{jn}'' + \frac{K_r}{K_{tot}^2} \Big) \Big]$$

$$- f(\mu_j) \Big[\sum_{n=1}^{3} b_n e^{-k_n XL} - e^{-\mu_j} \Big(\sum_{n=1}^{3} b_n e^{k_n XL} f_{jn}'' - \frac{K_c}{K_{tot}^2} \Big) \Big] \Big\} \Big\} \sin k_y y$$

$$= -F_o \sum_{n=1}^{3} a_n e^{-k_n(2XL+x_o)} \sin k_y y \qquad \text{(I.5)}$$

$$\theta(0\ell,y) = 0 : \Big\{ - \sum_{j=1}^{3} R_{ijr} \Big[\sum_{n=1}^{3} c_n e^{-k_n XL} f_{jn}''$$

$$- f(-\mu_j) \sum_{n=1}^{3} d_n e^{-k_n XL} f_{jn}'' \Big]$$

$$- R_{or} \sum_{n=1}^{3} c_n e^{-k_n XL} + M_{or} \sum_{n=1}^{3} d_n e^{-k_n XL}$$

$$+ M_{o\ell} \Big(\sum_{n=1}^{3} d_n + \frac{K_t}{K_{tot}^2} \Big) + R_{o\ell} \Big(\sum_{n=1}^{3} c_n - \frac{K_c}{K_{tot}^2} \Big)$$

$$+ \sum_{j=1}^{3} R_{ij\ell} \Big[\sum_{n=1}^{3} c_n f_{jn}'' + f(\mu_j) \sum_{n=1}^{3} d_n f_{jn}'' \Big] \Big\} \sin k_y y$$

$$= -(-F_o \sum_{n=1}^{3} c_n e^{-k_n x_o}) \sin k_y y \qquad \text{(I.6)}$$

$$\theta(0r,y) = 0 : \Big\{ -\sum_{j=1}^{3} R_{ijr} \Big[\sum_{n=1}^{3} c_n f_{jn}'' - f(-\mu_j) \sum_{n=1}^{3} d_n f_{jn}'' \Big]$$

$$- R_{or}\Big(\sum_{n=1}^{3} c_n + \frac{K_c}{K_{tot}^2} \Big) + M_{or}\Big(\sum_{n=1}^{3} d_n + \frac{K_t}{K_{tot}^2} \Big)$$

$$+ M_{o\ell} \sum_{n=1}^{3} d_n e^{-k_n XL} + R_{o\ell} \sum_{n=1}^{3} c_n e^{-k_n XL}$$

$$+ \sum_{j=1}^{3} R_{ij\ell} \Big[\sum_{n=1}^{3} c_n e^{-k_n XL} f_{jn}'' + f(\mu_j) \sum_{n=1}^{3} d_n e^{-k_n XL} f_{jn}'' \Big] \Big\} \sin k_y y$$

$$= -F_o \sum_{n=1}^{3} c_n e^{-k_n(XL - x_o)} \sin k_y y \qquad \text{(I.7)}$$

Now by considering the infinite-system line response functions of all the reaction forces and moments and that of the external line force $F_o \sin k_y y$, the transverse displacement of the sandwich plate at any (x_r, y) between supports 2r and 3r can be shown to be

$$w(x_r,y) = \Big\{F_o \sum_{n=1}^{3} a_n\, e^{-k_n(3XL-x_o+x_r)}$$

$$+ \sum_{j=1}^{3} R_{ijr} \sum_{n=1}^{3} a_n\, e^{-k_n(XL+x_r)} + \sum_{j=1}^{3} M_{ijr}\, b_n\, e^{-k_n(XL+x_r)}$$

$$+ \sum_{j=1}^{3} R_{ijr}\, e^{-\mu_j} \sum_{n=1}^{3} a_n\, e^{-k_n x_r} + \sum_{j=1}^{3} M_{ijr}\, e^{-\mu_j} \sum_{n=1}^{3} b_n\, e^{-k_n x_r}$$

$$+ \sum_{j=1}^{3} \sum_{s=3}^{\infty} R_{ijr}\, e^{-\mu_j(s-1)} \sum_{n=1}^{3} a_n\, e^{-k_n((s-2)XL-x_r)}$$

$$- \sum_{j=1}^{3} \sum_{s=3}^{\infty} M_{ijr}\, e^{-\mu_j(s-1)} \sum_{n=1}^{3} b_n\, e^{-k_n((s-2)XL-x_r)}$$

$$+ R_{or} \sum_{n=1}^{3} a_n\, e^{-k_n(2XL+x_r)} + M_{or} \sum_{n=1}^{3} b_n\, e^{-k_n(2XL+x_r)}$$

$$+ M_{o\ell} \sum_{n=1}^{3} b_n\, e^{-k_n(3XL+x_r)} + R_{o\ell} \sum_{n=1}^{3} a_n\, e^{-k_n(3XL+x_r)}$$

$$+ \sum_{j=1}^{3} \sum_{s=1}^{\infty} R_{ijr}\, e^{-\mu_j(s-1)} \sum_{n=1}^{3} a_n\, e^{-k_n((s+3)XL+x_r)}$$

$$+ \sum_{j=1}^{3} \sum_{s=1}^{\infty} M_{ijr}\, e^{-\mu_j(s-1)} \sum_{n=1}^{3} b_n\, e^{-k_n((s+3)XL+x_r)}\Big\} \sin k_y y \qquad (I.8)$$

where $0 \leq |x_r| \leq XL$ and x_r is measured from support number 2r.

After the infinite series has been summed, equation (I.8) can be rewritten as

$$w(x_r,y) = \Big\{F_o \sum_{n=1}^{3} a_n\, e^{-k_n(3XL-x_o+x_r)}$$

$$+ \sum_{j=1}^{3} R_{ijr}\Big[\sum_{n=1}^{3} a_n\, e^{-k_n(XL+x_r)} + f(-\mu_j) \sum_{j=1}^{3} b_n\, e^{-k_n(XL+x_r)}\Big]$$

$$+ \sum_{j=1}^{3} R_{ijr}\Big[e^{-\mu_j} \sum_{n=1}^{3} a_n\, e^{-k_n x_r} + f(-\mu_j)\, e^{-\mu_j} \sum_{n=1}^{3} b_n\, e^{-k_n x_r}\Big]$$

$$+ \sum_{j=1}^{3} R_{ijr}\Big[e^{-2\mu_j} \sum_{n=1}^{3} a_n\, e^{k_n x_r} f_{jn}''$$

$$- f(-\mu_j)\, e^{-2\mu_j} \sum_{n=1}^{3} b_n\, e^{k_n x_r} f_{jn}''\Big]$$

$$+ R_{or} \sum_{n=1}^{3} a_n\, e^{-k_n(2XL+x_r)} + M_{or} \sum_{n=1}^{3} b_n\, e^{-k_n(2XL+x_r)}$$

$$+ M_{o\ell} \sum_{n=1}^{3} b_n\, e^{-k_n(3XL+x_r)} + R_{o\ell} \sum_{n=1}^{3} a_n\, e^{-k_n(3XL+x_r)}$$

$$+ \sum_{j=1}^{3} R_{ij\ell}\Big[\sum_{n=1}^{3} a_n\, e^{-k_n(3XL+x_r)} f_{jn}''$$

$$+ f(\mu_j) \sum_{n=1}^{3} b_n\, e^{-k_n(3XL+x_r)} f_{jn}''\Big]\Big\} \sin k_y y \qquad \text{(I.9)}$$

The plate transverse displacement at support 3r can be found from equation (I.9) by setting x_r to XL in it. This is equal to the displacement of the support given by

$$w(3r) = -\frac{K_r}{K_{tot}^2}\,(R_{i1r}\, e^{-2\mu_1} + R_{i2r}\, e^{-2\mu_2} + R_{i3r}\, e^{-2\mu_3})$$

$$+ \frac{K_c}{K_{tot}^2}\,(f(-\mu_1)R_{i1r}\, e^{-2\mu_1} + f(-\mu_2)R_{i2r}\, e^{-2\mu_2} + f(-\mu_3)R_{i3r}\, e^{-2\mu_3}) \qquad \text{(I.10)}$$

Hence by considering the above arguments, the transverse displacement boundary condition at support 3r can be shown to be

$$\Bigg\{ \sum_{j=1}^{3} R_{ijr} \Bigg\{ \Big[\sum_{n=1}^{3} a_n e^{-k_n(2XL)} + e^{-\mu_j} \sum_{n=1}^{3} a_n e^{-k_n XL}$$

$$+ e^{-2\mu_j} \Big(\sum_{n=1}^{3} a_n e^{k_n XL} f_{jn}'' + \frac{K_r}{K_{tot}^2} \Big) \Big] + f(-\mu_j) \Big[\sum_{n=1}^{3} b_n e^{-k_n(2XL)}$$

$$+ e^{-\mu_j} \sum_{n=1}^{3} b_n e^{-k_n XL} - e^{-2\mu_j} \Big(\sum_{n=1}^{3} b_n e^{k_n XL} f_{jn}'' + \frac{K_c}{K_{tot}^2} \Big) \Big] \Bigg\}$$

$$+ R_{or} \sum_{n=1}^{3} a_n e^{-k_n(3XL)} + M_{or} \sum_{n=1}^{3} b_n e^{-k_n(3XL)}$$

$$+ M_{o\ell} \sum_{n=1}^{3} b_n e^{-k_n(4XL)} + R_{o\ell} \sum_{n=1}^{3} a_n e^{-k_n(4XL)}$$

$$+ \sum_{j=1}^{3} R_{ij\ell} \Big[\sum_{n=1}^{3} a_n e^{-k_n(4XL)} f_{jn}''$$

$$+ f(\mu_j) \sum_{n=1}^{3} b_n e^{-k_n(4XL)} f_{jn}'' \Big] \Bigg\} \sin k_y Y$$

$$= -F_o \sum_{n=1}^{3} a_n e^{-k_n(4XL - x_o)} \sin k_y Y \qquad \text{(I.11)}$$

The transverse displacement boundary condition at support 3ℓ can likewise be found as

$$\left\{ \sum_{j=1}^{3} R_{ijr} \left[\sum_{n=1}^{3} a_n e^{-k_n(4XL)} f_{jn}'' - f(-\mu_j) \sum_{n=1}^{3} b_n e^{-k_n(4XL)} f_{jn}'' \right] \right.$$

$$+ R_{or} \sum_{n=1}^{3} a_n e^{-k_n(4XL)} - M_{or} \sum_{n=1}^{3} b_n e^{-k_n(4XL)}$$

$$- M_{o\ell} \sum_{n=1}^{3} b_n e^{-k_n(3XL)} + R_{o\ell} \sum_{n=1}^{3} a_n e^{-k_n(3XL)}$$

$$+ \sum_{j=1}^{3} R_{ij\ell} \left\{ \sum_{n=1}^{3} a_n e^{-k_n(2XL)} + e^{-\mu_j} \sum_{n=1}^{3} a_n e^{-k_n XL} \right.$$

$$+ e^{-2\mu_j} \left(\sum_{n=1}^{3} a_n e^{k_n XL} f_{jn}'' + \frac{K_r}{K_{tot}^2} \right)$$

$$+ f(\mu_j) \left[- \sum_{n=1}^{3} b_n e^{-k_n(2XL)} - e^{-\mu_j} \sum_{n=1}^{3} b_n e^{-k_n XL} \right.$$

$$\left. \left. \left. + e^{-2\mu_j} \left(\sum_{n=1}^{3} b_n e^{k_n XL} f_{jn}'' - \frac{K_c}{K_{tot}^2} \right) \right] \right\} \sin k_y y$$

$$= -F_o \sum_{n=1}^{3} a_n e^{-k_n(3XL+x_o)} \sin k_y y \qquad \text{(I.12)}$$

Equations (9.24), (I.1), (I.2), (I.3), (I.4), (I.5), (I.6), (I.7), (I.11) and (I.12) can be put into the following matrix form

TABLES

Simply-Supported Ends		Clamped Ends		Free Ends	
Current Method	Reference [31]	Current Method	Reference [31]	Current Method	Reference [31]
9.87	9.87	12.65	12.65	1.99	1.99
12.65	12.65	18.47	18.47	2.72	2.72
18.47	18.46	22.37	22.37	12.82	12.82

TABLE 1: Comparison of Natural Frequencies of a Three Equal Bay Euler-Bernoulli Beam with Intermediate Simple Supports (Current method $\eta = 10^{-6}$, Reference [31] $\eta = 0$)

Simply-Supported Ends		Clamped Ends		Free Ends	
Current Method	Reference [31]	Current Method	Reference [31]	Current Method	Reference [31]
9.87	9.87	10.63	10.63	2.36	2.36
10.63	10.63	12.65	12.65	2.38	2.38
12.65	12.65	15.42	15.42	10.69	10.69
15.42	15.42	18.47	18.47	12.73	12.73
18.47	18.43	21.17	21.18	15.42	15.42
21.17	21.18	22.37	22.37	18.36	18.36

TABLE 2: Comparison of Natural Frequencies of a Six Equal Bay Euler-Bernoulli Beam with Intermediate Simple Supports (Current method $\eta = 10^{-6}$, Reference [31] $\eta = 0$)

$h = 0.04$ [in] $= 1.016 \times 10^{-3}$ [m]

$x_b = 8.2$ [in] $= 0.209$ [m]

$L_y = 20.0$ [in] $= 0.508$ [m]

$\rho = 0.101$ [lb.s^2/in^4] $= 2795.7$ [kg/m^3]

$E = 10.5 \times 10^6$ [lb/in^2] $= 7.24 \times 10^{10}$ [N/m^2]

$\nu = 0.3$

TABLE 3: Dimensions and Material Properties of the Six Equal-Bay Euler-Bernoulli Plate

Current Method	Reference [7]
99.9	99.9
103.04	103.1
108.2	108.2
114.9	115.0
122.1	122.1
127.9	127.9

TABLE 4: Comparison of Natural Frequencies [Hz] of a Six Equal Bay Euler-Bernoulli Plate on Stiffeners
(Current Method $\eta = 10^{-6}$, Reference [7] $\eta = 0$)

Mode	(i)	(ii)	(iii)	(iv)
1	170.05	169.70	168.41	150.19
2	171.31	170.99	169.85	153.75
3	173.93	173.69	172.78	160.04
4	175.90	175.73	175.03	166.42
5	177.95	177.86	177.43	172.96
6	179.93	179.78	179.18	176.84

TABLE 5: Effects of Stiffener Stiffnesses on the Natural Frequencies [Hz] of the Eight-Bay Euler-Bernoulli Plate

(i) No distortion, no inertia, no coupling

(ii) No distortion, inertia, no coupling

(iii) No distortion, inertia, coupling

(iv) Distortion, inertia, coupling (*i.e.*, General Support)

Current Method	Method of Reference [11]
207.96	208
213.68	214
229.73	230
252.84	253
277.84	278
297.91	298

TABLE 6: Comparison of Natural Frequencies [Hz] of a Six Equal Bay Simply-Supported, Three-Layered Sandwich Plate (Current Method $\beta = 10^{-6}$, Method of Reference [11] $\beta=0$)

f [Hz]	(i)	(ii)	(iii)
100	2.366	2.327	2.361
200	2.378	2.355	2.394
300	2.367	2.342	2.377
400	2.414	2.351	2.365
500	2.414	2.409	2.424
600	2.462	2.424	2.443
700	2.462	2.431	2.475
800	2.473	2.466	2.502
900	2.521	2.502	2.537

TABLE 7: Experimentally Determined Head Constants [N/A] of the Exciters

(i) 1.Exciter

(ii) 2.Exciter

(iii) 3.Exciter

f [Hz]	Random Transfer Function [1/kg]	Sinusoidal Transfer Function [1/kg]
200	79.37	81.62
300	64.53	66.79
400	59.74	61.54
500	57.73	58.94
600	57.34	58.19
700	57.83	58.38
800	58.02	58.30

TABLE 8: Comparison of Experimentally Determined Transfer Functions of the Exciter ($m_{extra} \cong 8.9$ [g])

Mode	Resonance Frequencies of Figure 99 [Hz]	Average Frequencies of nine sets of measurements [Hz]	Maximum Deviations of nine sets of measurements [Hz]	
1	131.75	132.15	-0.90	+1.11
2	138.28	139.35	-1.07	+1.84
3	149.46	151.41	-1.95	+2.86
4	165.63	166.81	-1.18	+1.87
5	173.73	174.15	-1.18	+1.83
6	181.25	181.82	-0.57	+0.87

TABLE 9: Experimentally Obtained Resonance Frequencies of the Eight-Bay Stiffened Plate (m = 1, h = 0.91 [mm])

Mode	Average Frequencies of Nine Sets of Experimental Measurements [Hz]	Theoretical Resonance Frequencies [Hz]
1	132.15	150.03
2	139.35	153.74
3	151.41	160.11
4	166.81	166.53
5	174.15	172.93
6	181.82	177.01

TABLE 10: Comparison of Theoretical and Average Experimental Resonance Frequencies of the Eight-Bay Stiffened Plate (m = 1, h = 0.91 [mm])

FIGURES

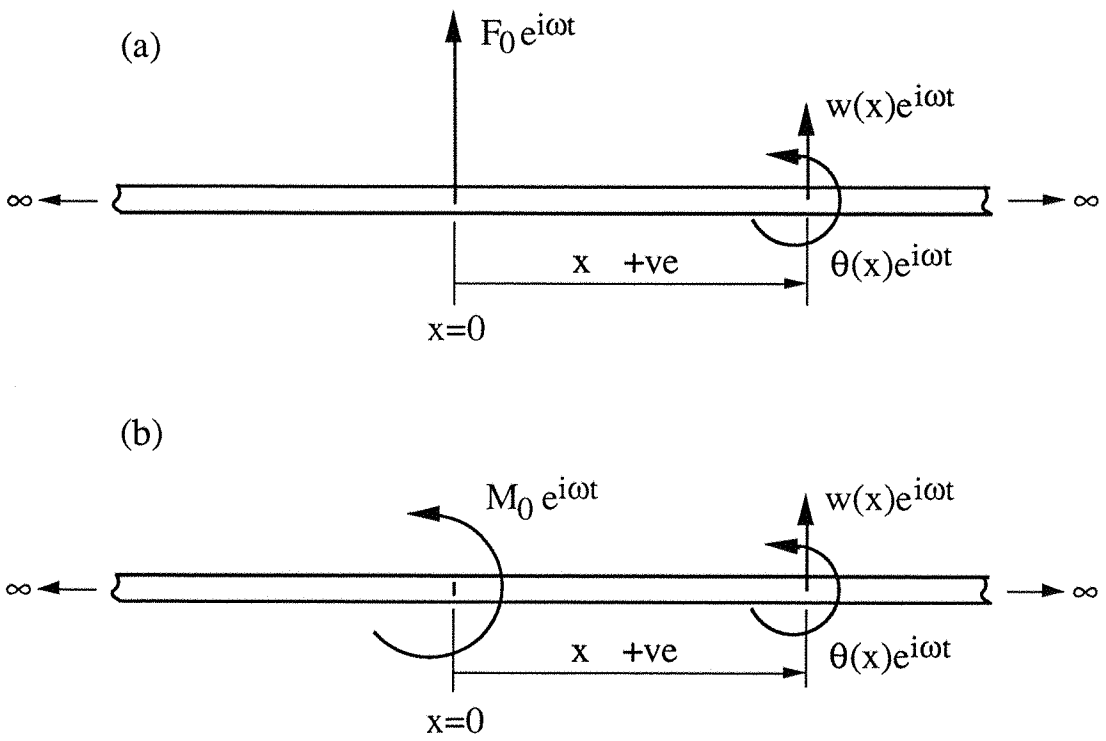

Figure 1: Diagram of Forcing, Response and Sign Conventions for Infinite, Uninterrupted Euler-Bernoulli Beams.

a) Force Excitation
b) Moment Excitation

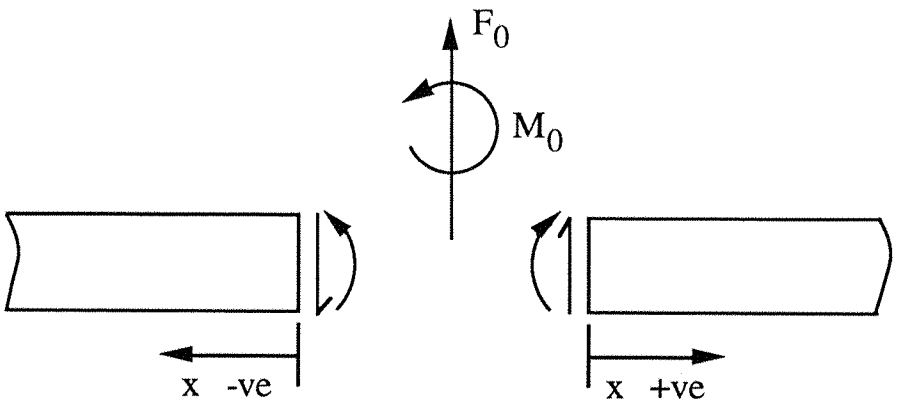

Figure 2: Positive Sign Convention of Forces and Moments for Euler-Bernoulli Beams.

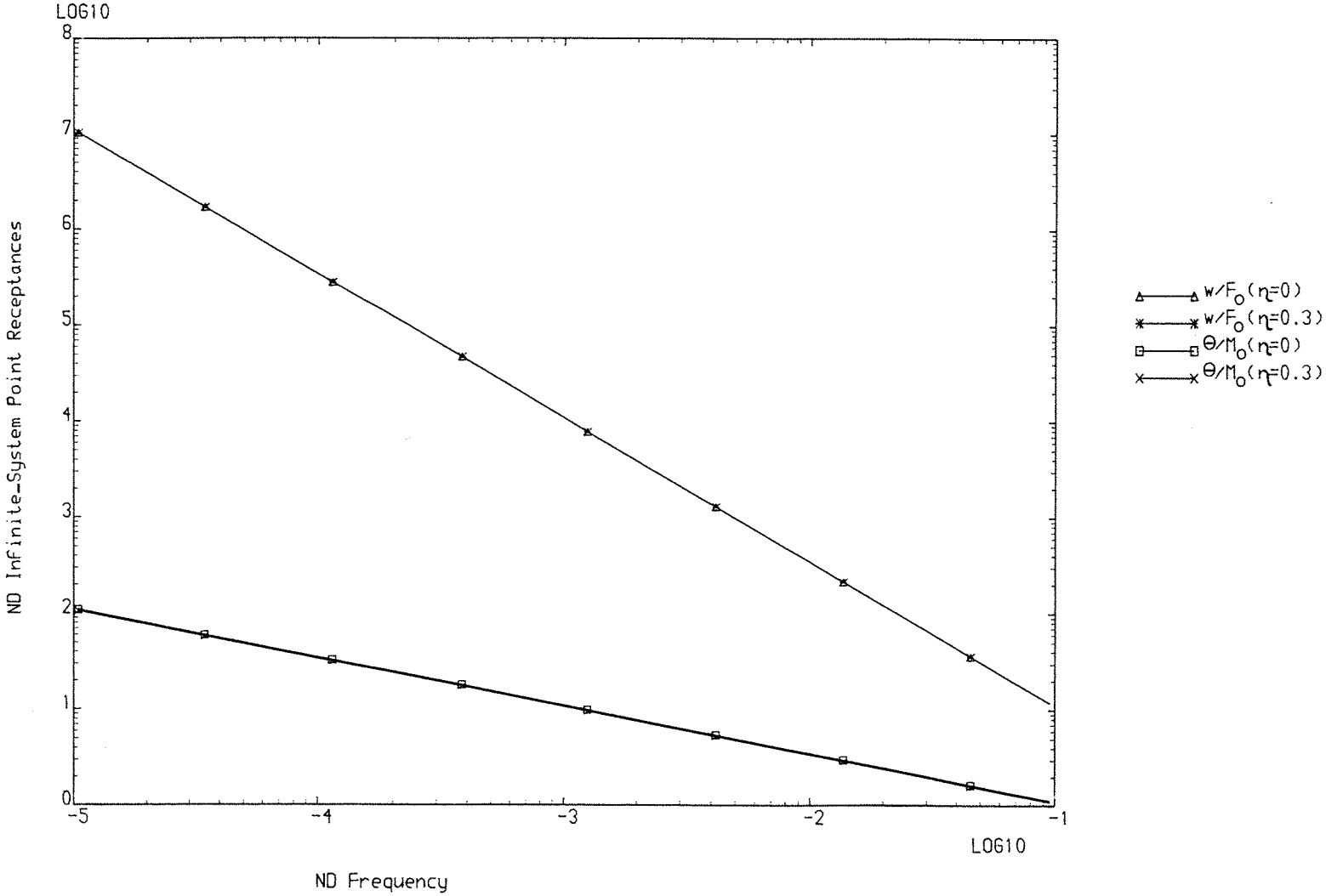

Fig. 3 Non-Dimensional Magnitudes of Infinite-System Point Receptances of Euler-Bernoulli Beams

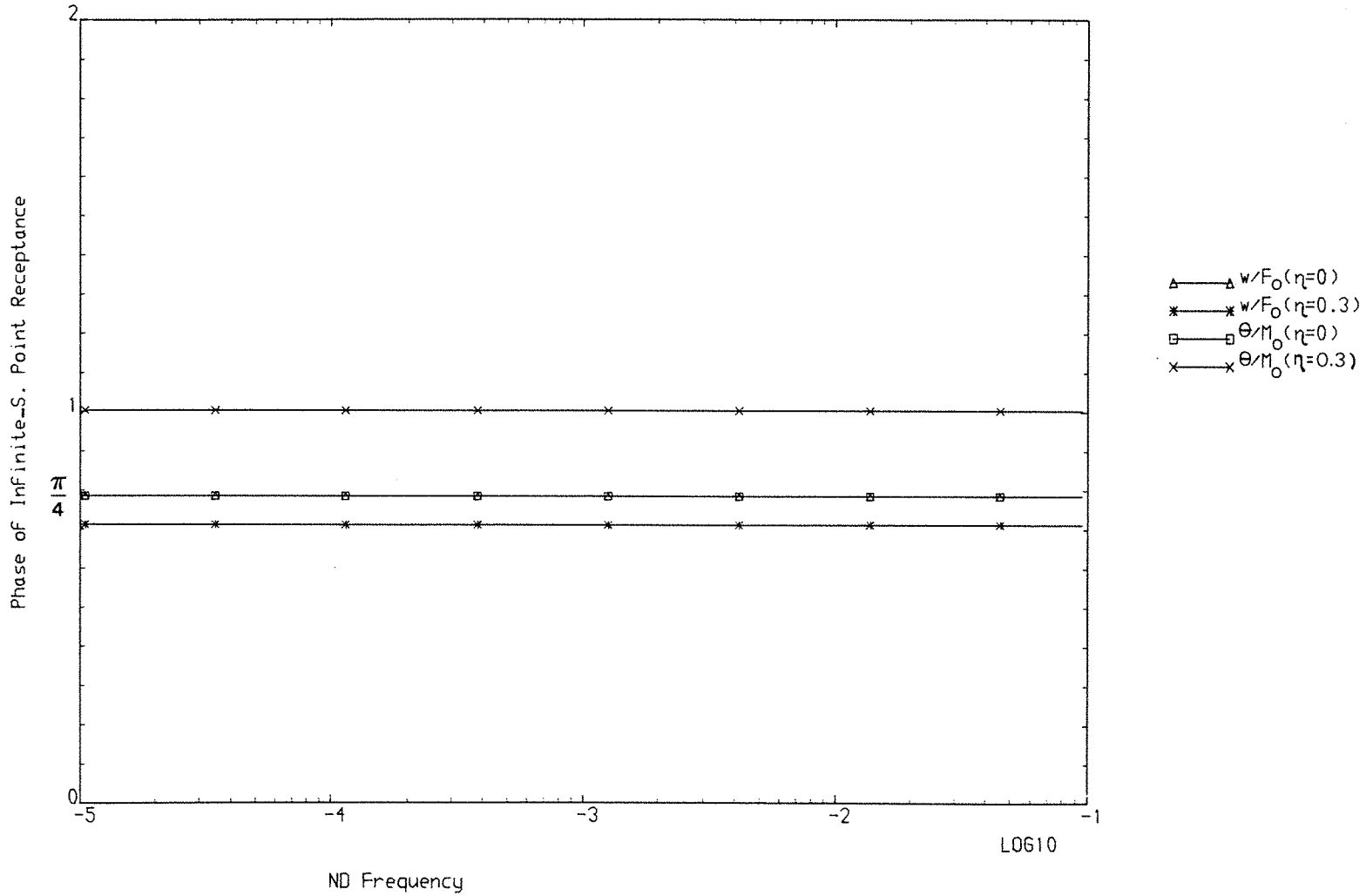

Fig. 4 Phases of Infinite-System Point Receptances of Euler-Bernoulli Beams

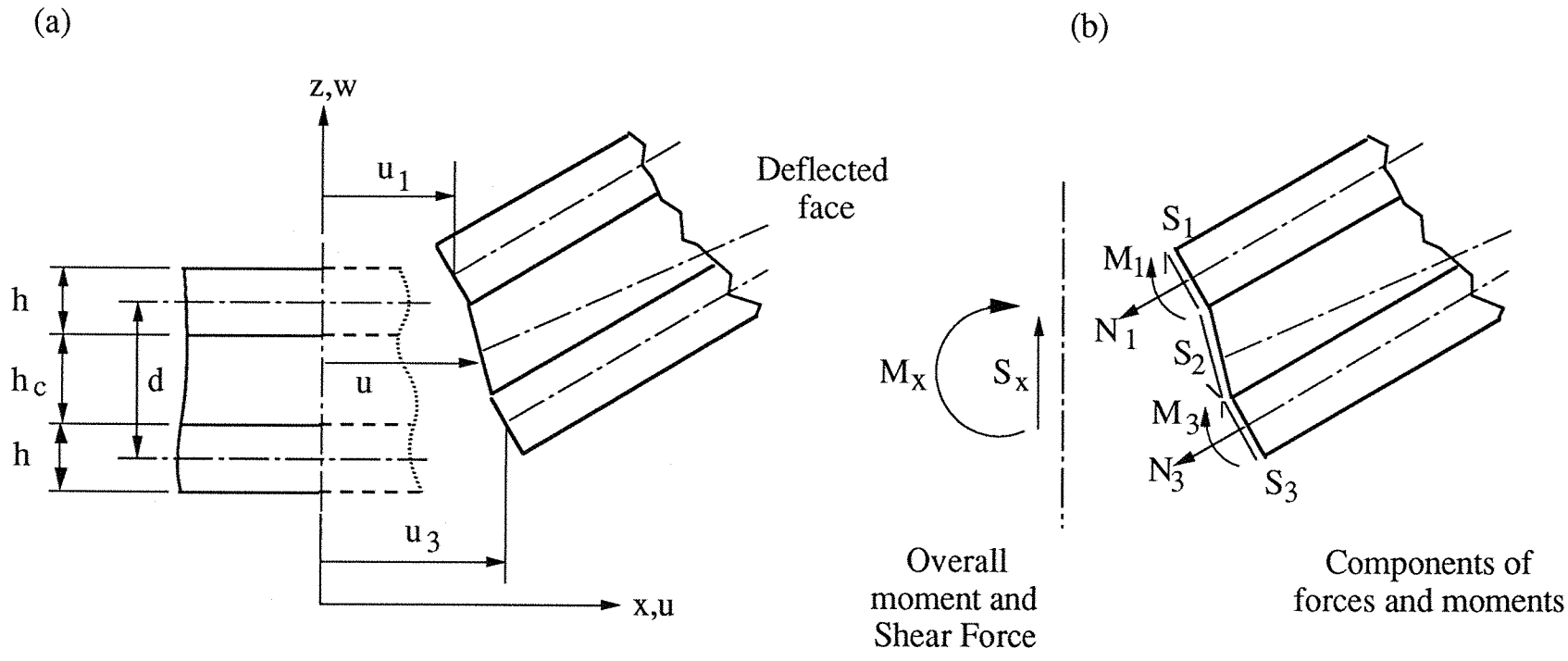

Figure 5: Cordinate, Displacement and Stress System for Three-Layered Sandwich Beams with Equal Face-Plates

a) Dimensions and Displacements
b) Forces and Moments

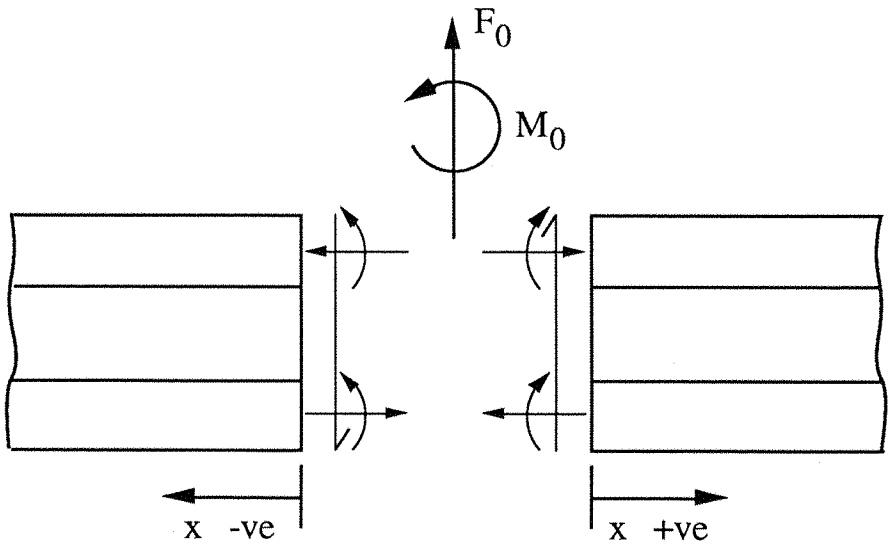

Figure 6: Positive Sign Convention of Forces and Moments for Three-Layered Sandwich Beams.

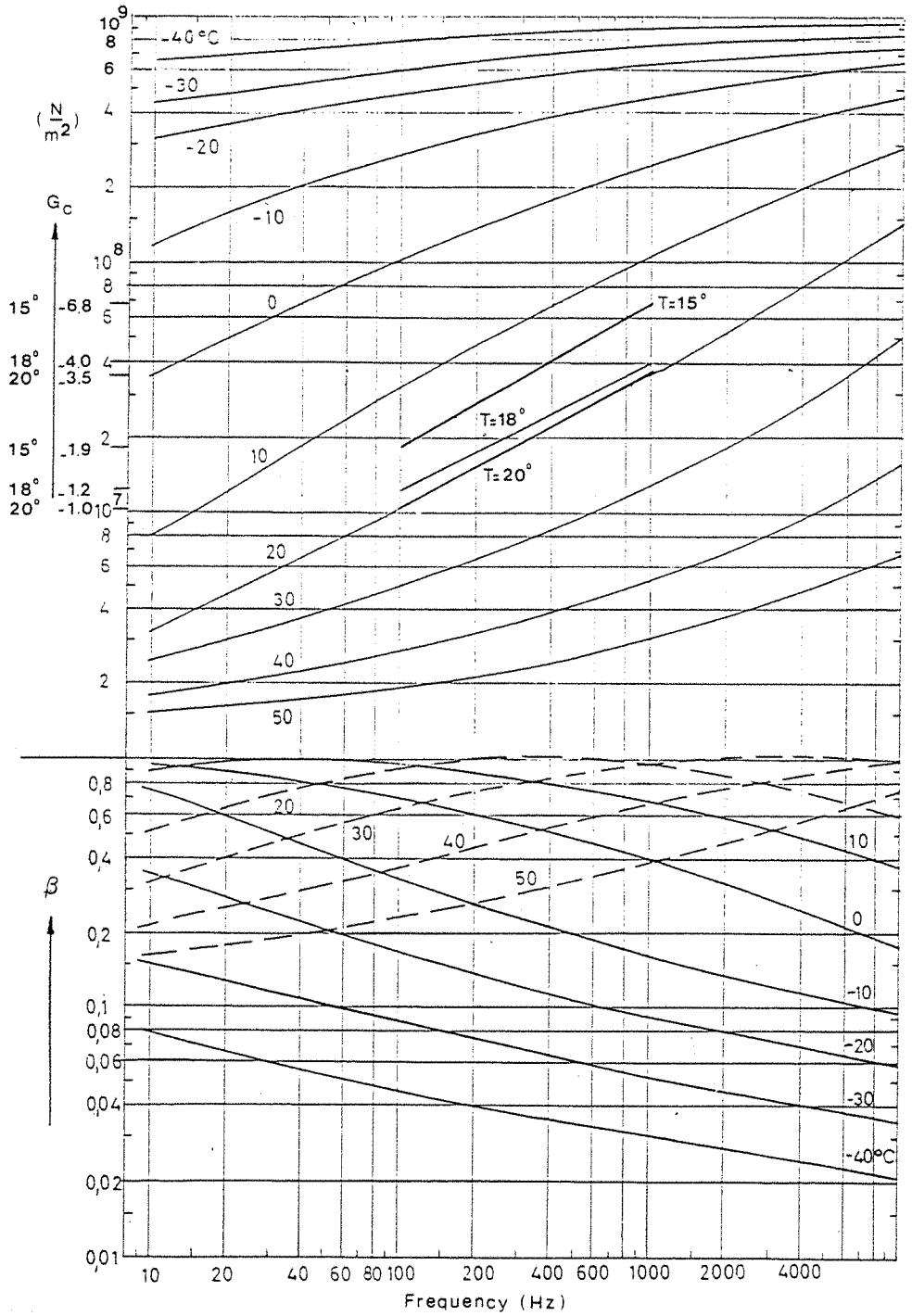

Fig. 7 Core Properties of Sandwich Structures

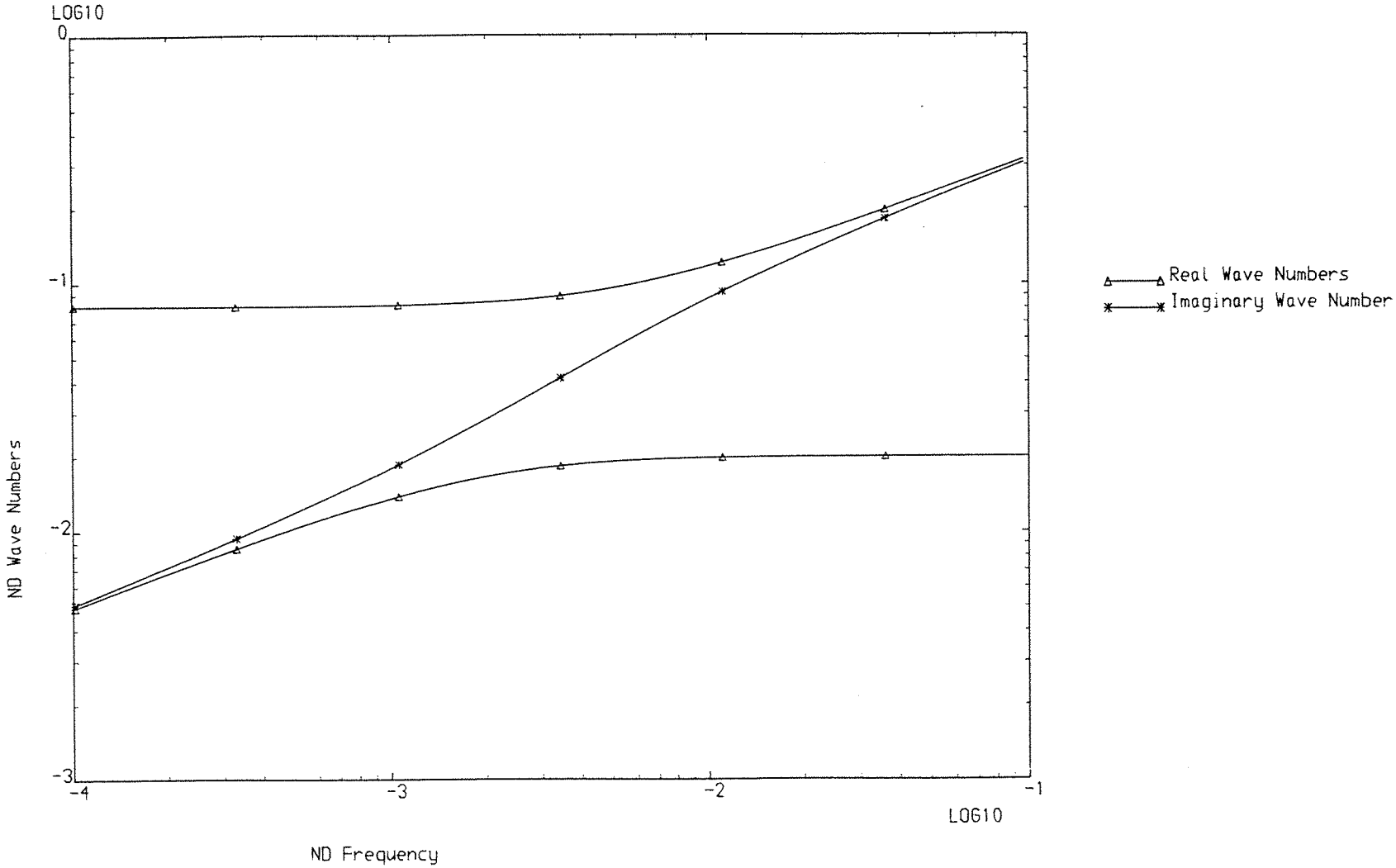

Fig. 8 Non-Dimensional Magnitudes of Wave Numbers of Three-Layered Sandwich Beam (β = 0, G_C = 1.7×10^6[N/m^2])

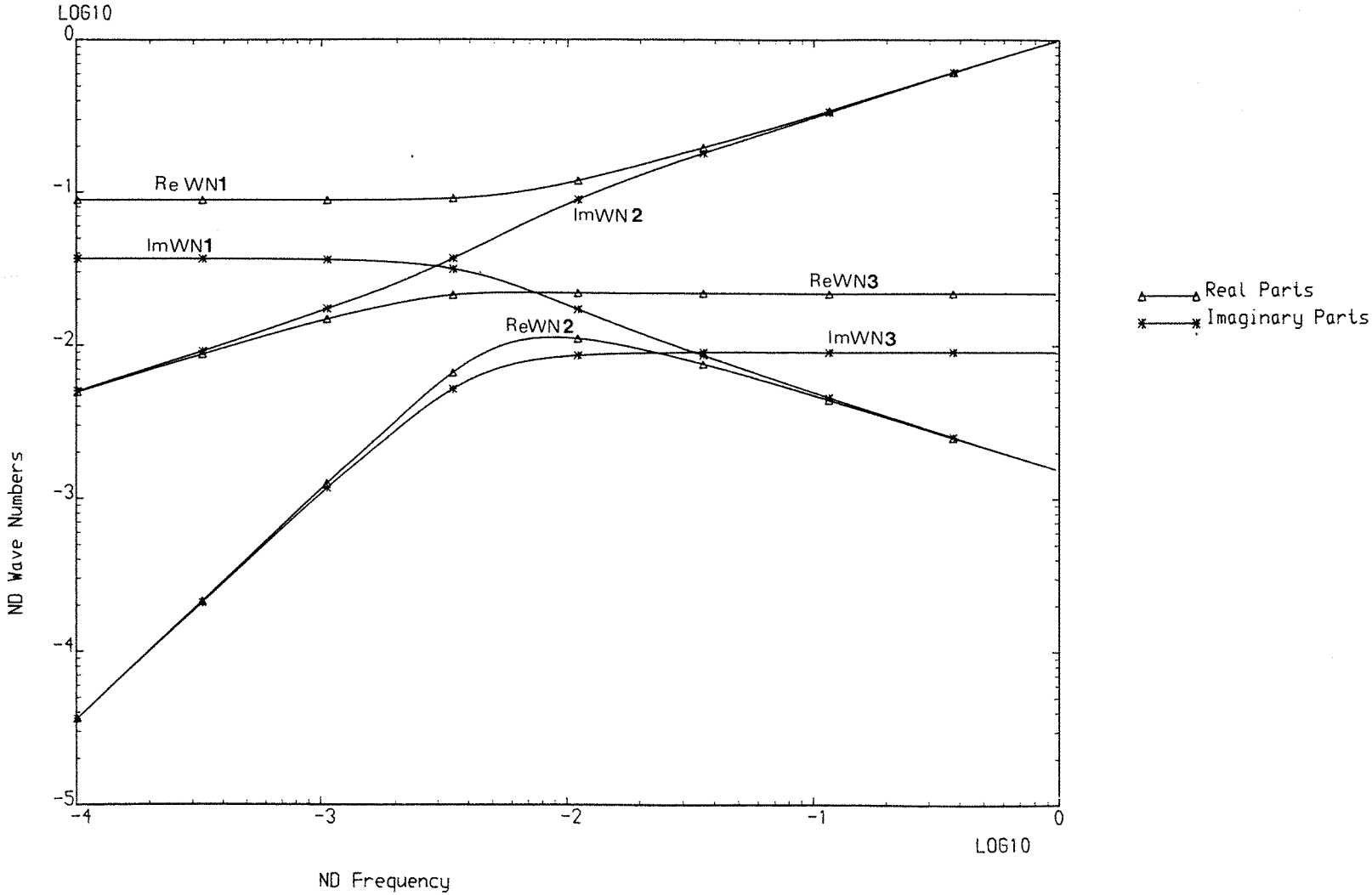

Fig. 9 Non-Dimensional Magnitudes of Wave Numbers of Three-Layered Sandwich Beam (β = 1, G_C = 1.7×10^6[N/m^2])

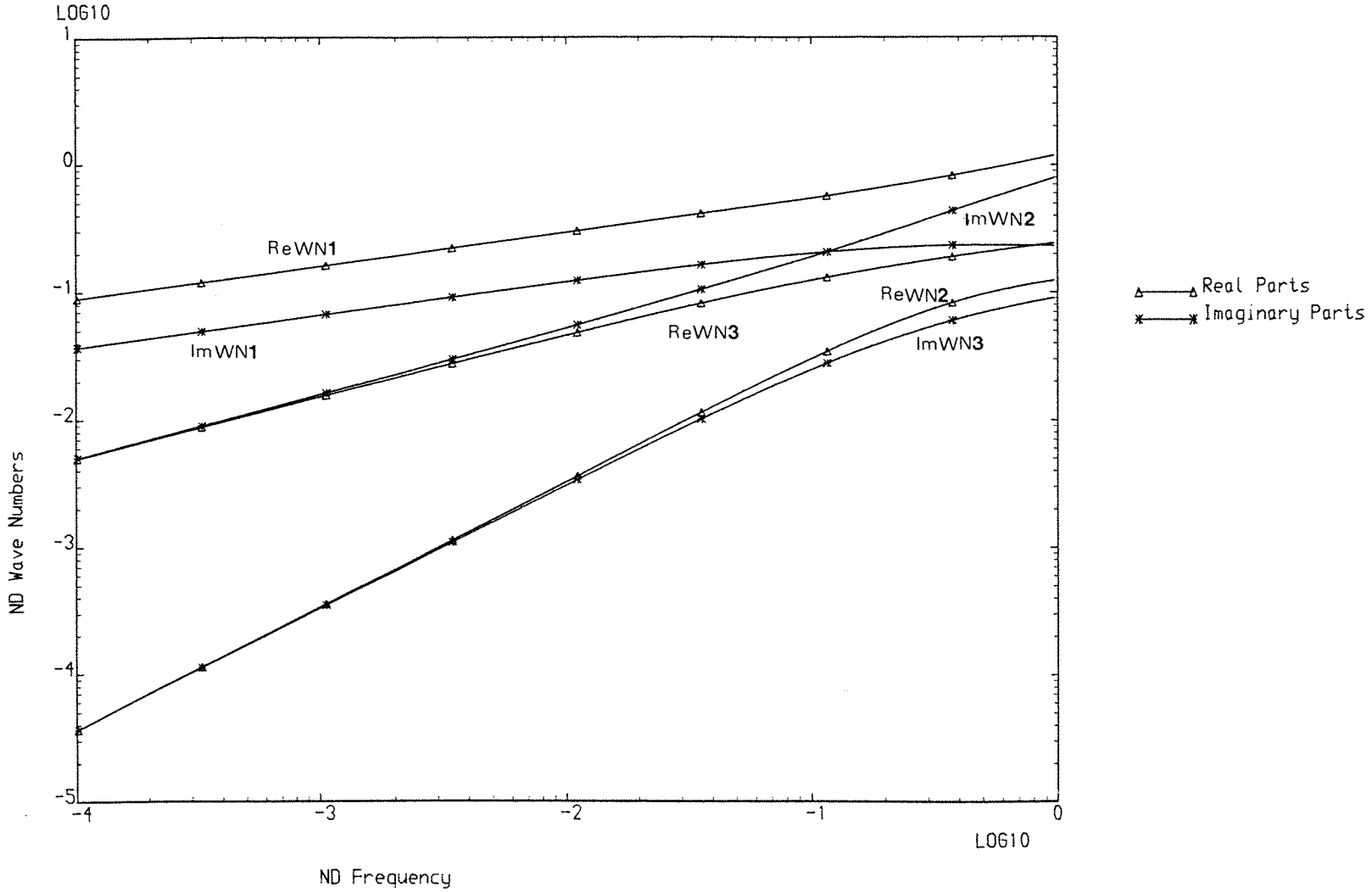

Fig. 10 Non-Dimensional Magnitudes of Wave Numbers of Three-Layered Sandwich Beam (β = 1)

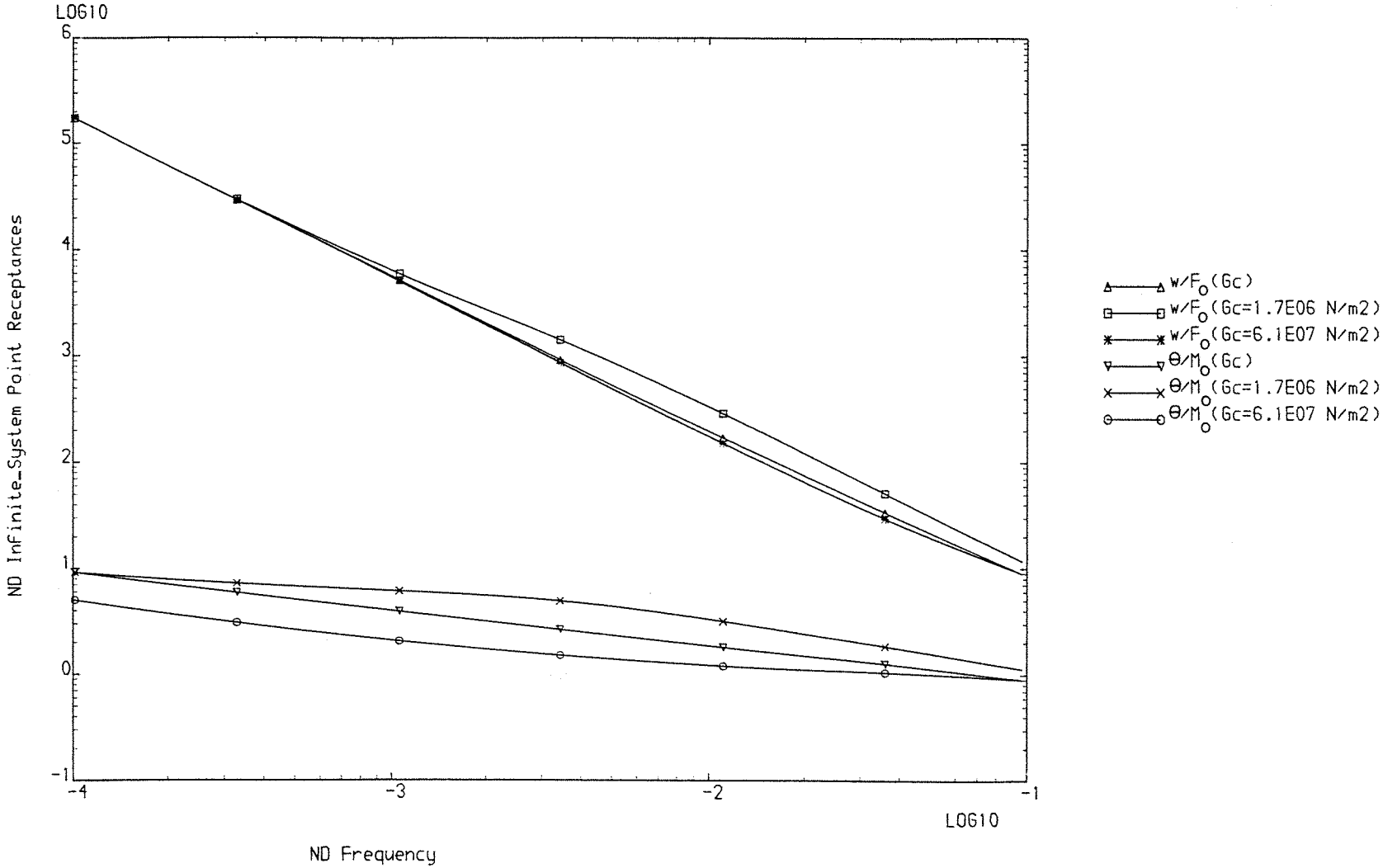

Fig. 11 Non-Dimensional Magnitudes of Infinite-System Point Receptances of Three-Layered Sandwich Beam (β = 0)

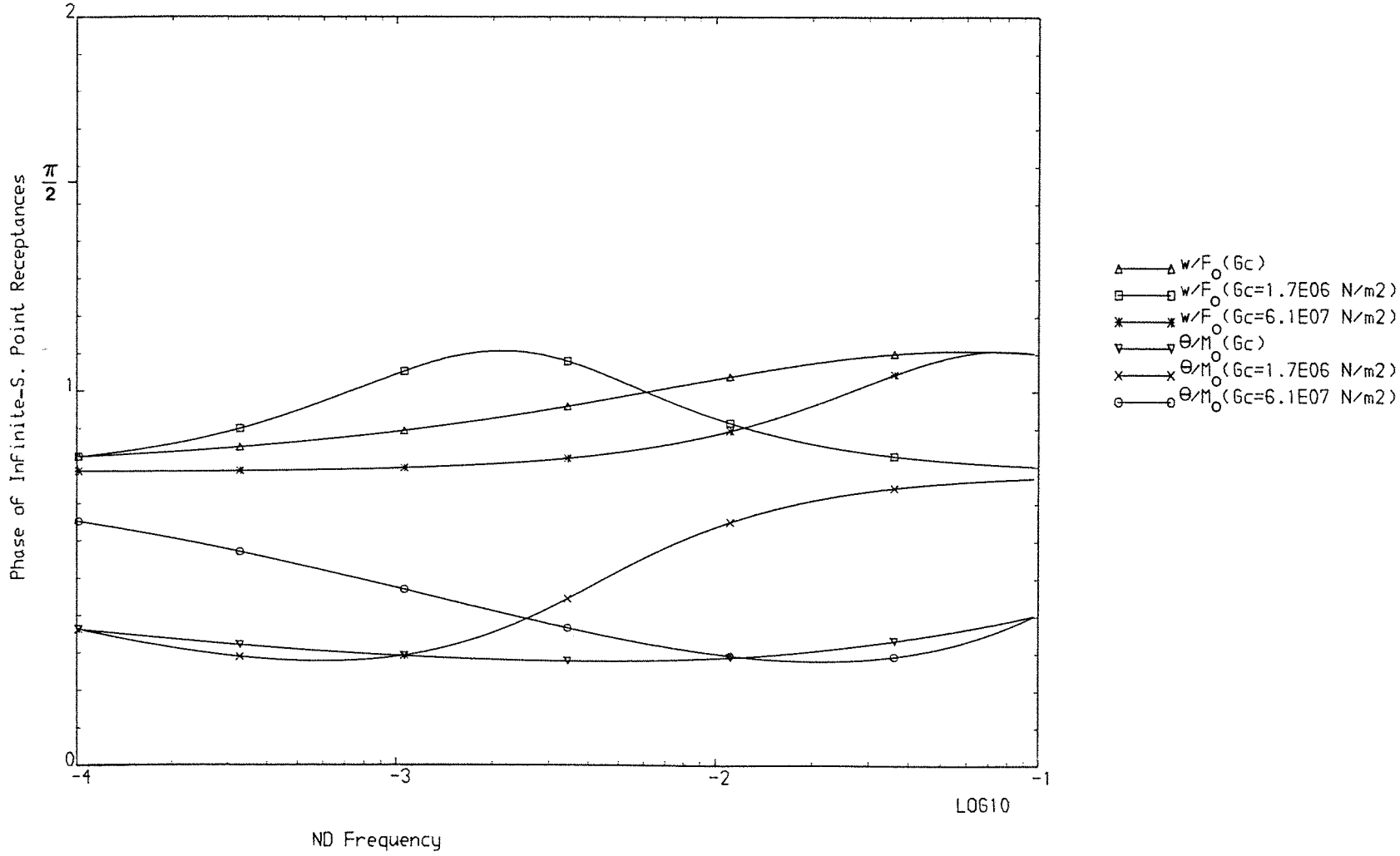

Fig. 12 Phases of Infinite-System Point Receptances of Three-Layered Sandwich Beam (β = 0)

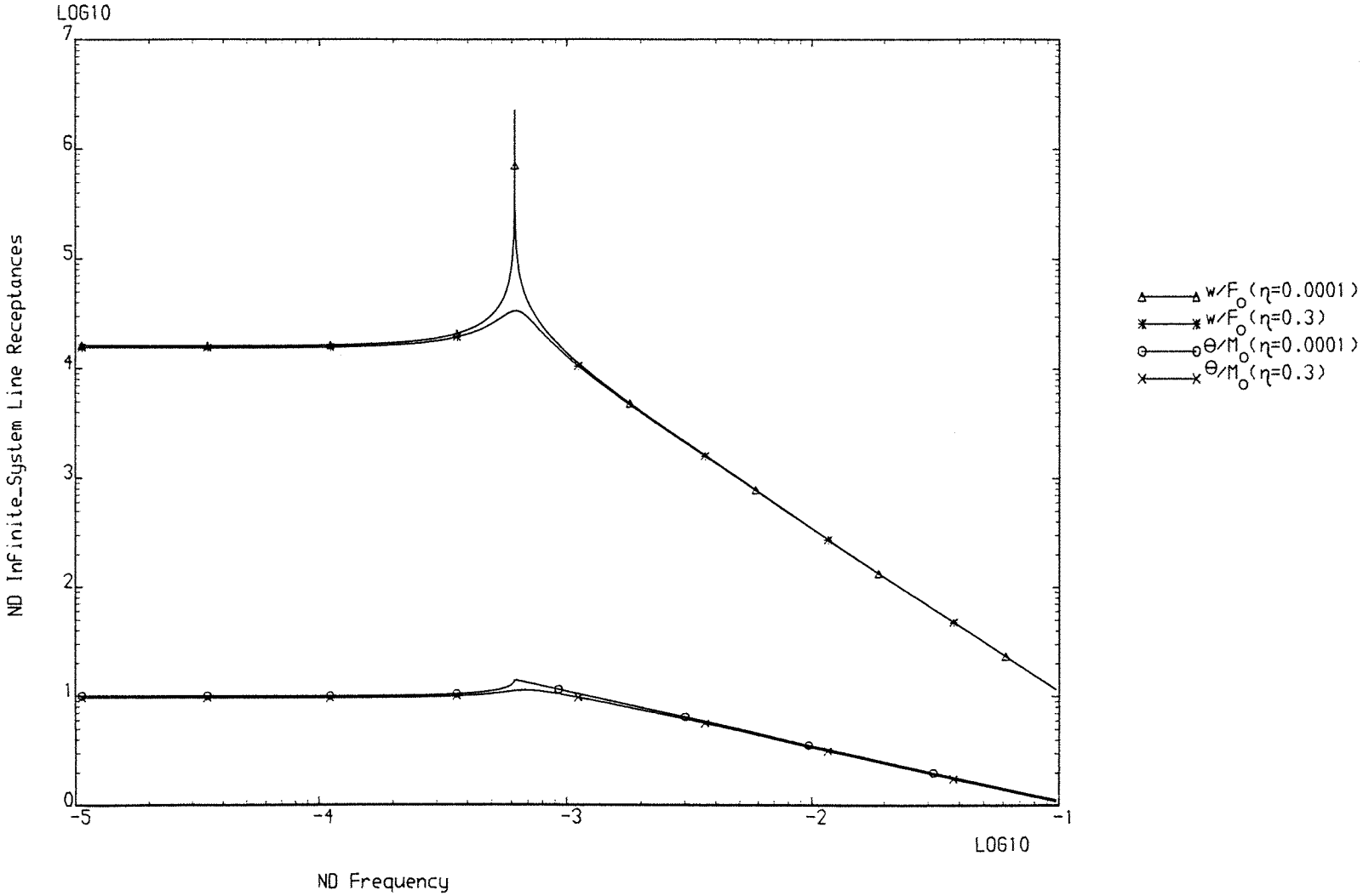

Fig. 13 Non-Dimensional Magnitudes of Infinite-System Line Receptances of Euler-Bernoulli Plate

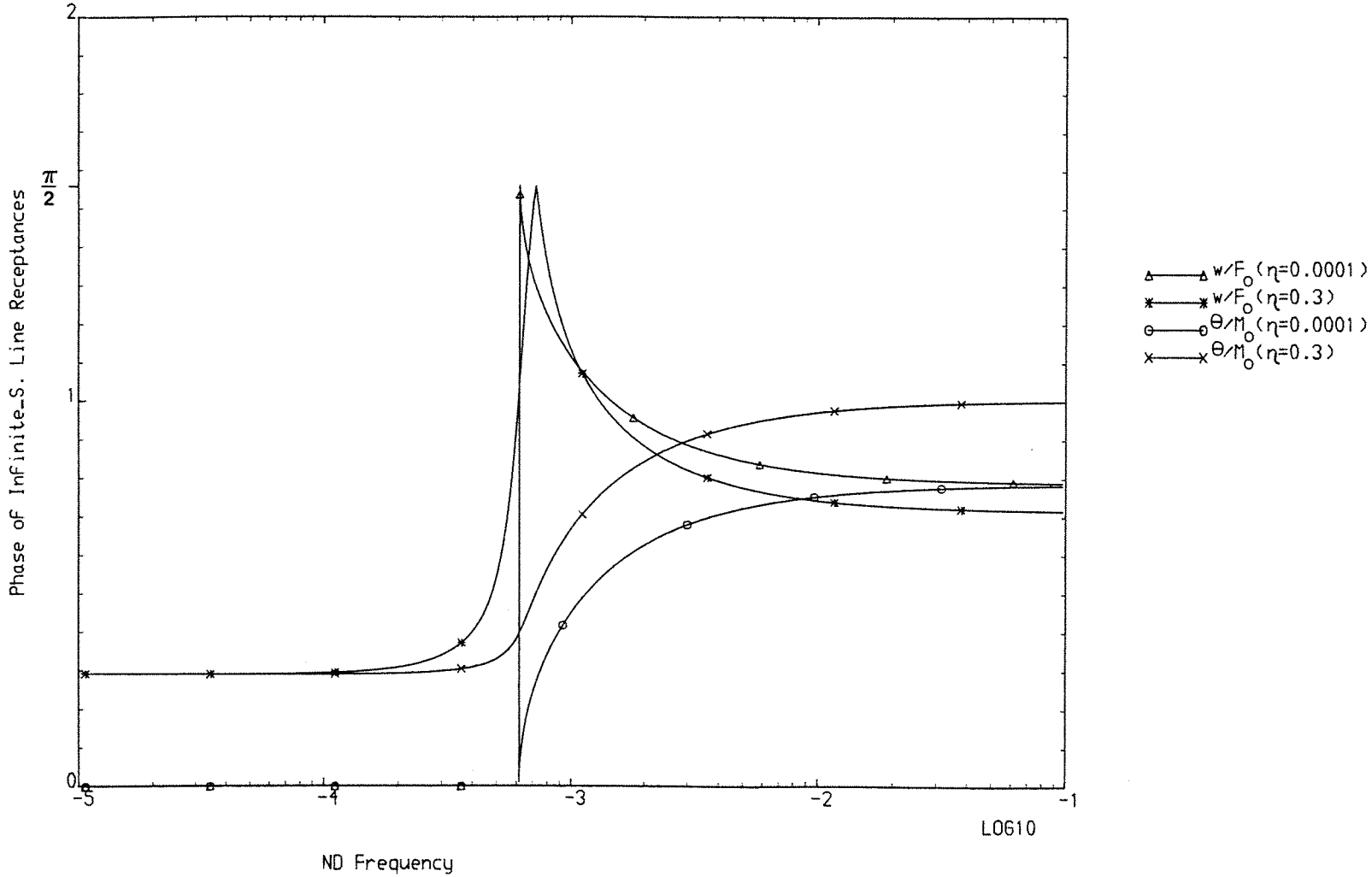

Fig. 14 Phases of Infinite-System Line Receptances of Euler-Bernoulli Plate

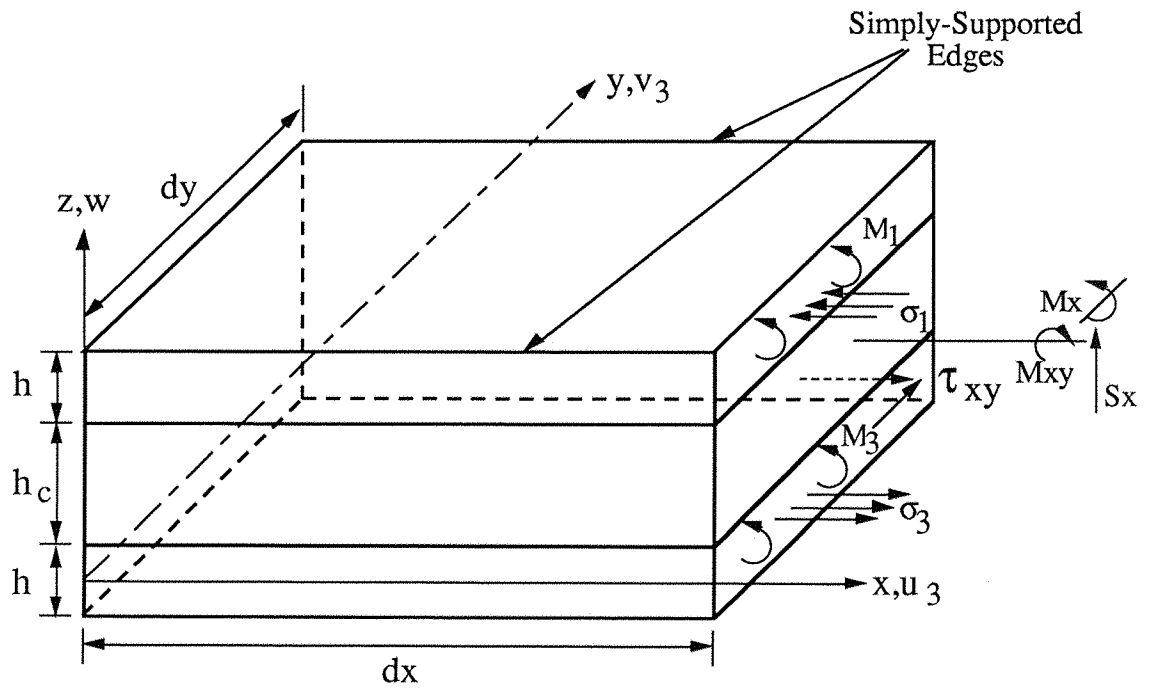

Figure 15: Coordinate Displacement and Stress System for Three-Layered Sandwich Plate with Equal Face-Plates.

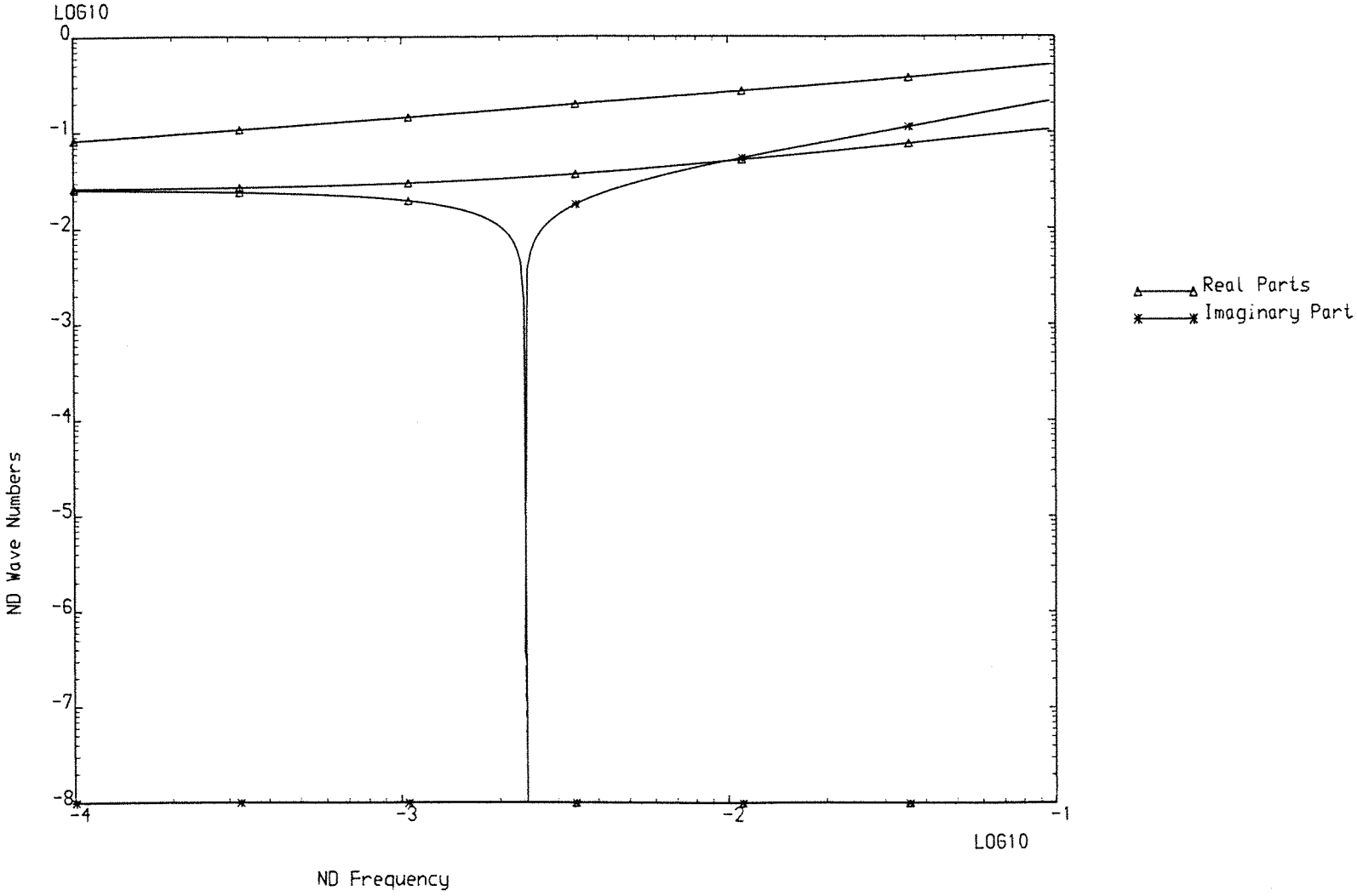

Fig. 16 Non-Dimensional Magnitudes of Wave Numbers of Three-Layered Sandwich Plate (β = 0)

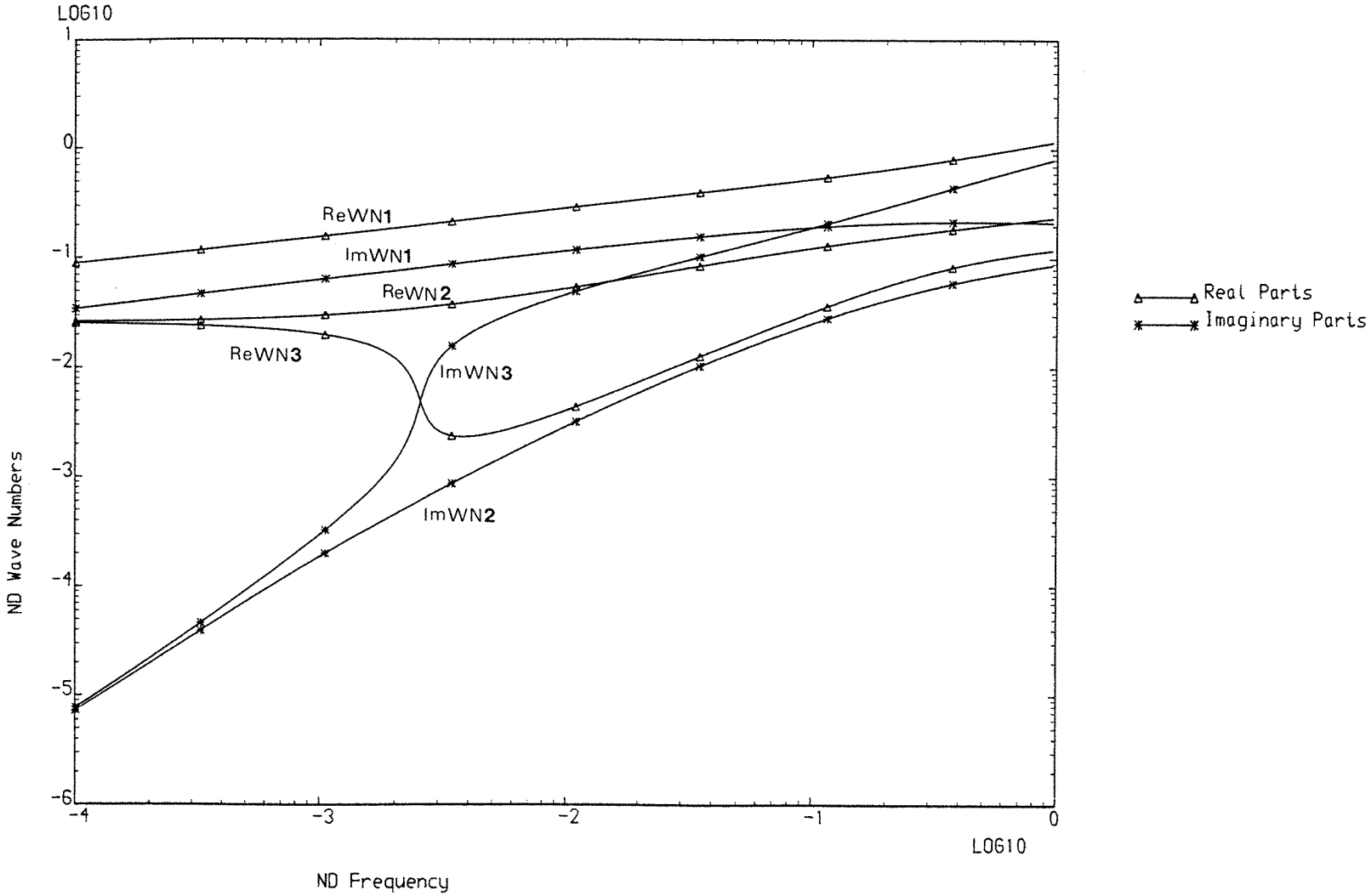

Fig. 17 Non-Dimensional Magnitudes of Wave Numbers of Three-Layered Sandwich Plate (β = 1)

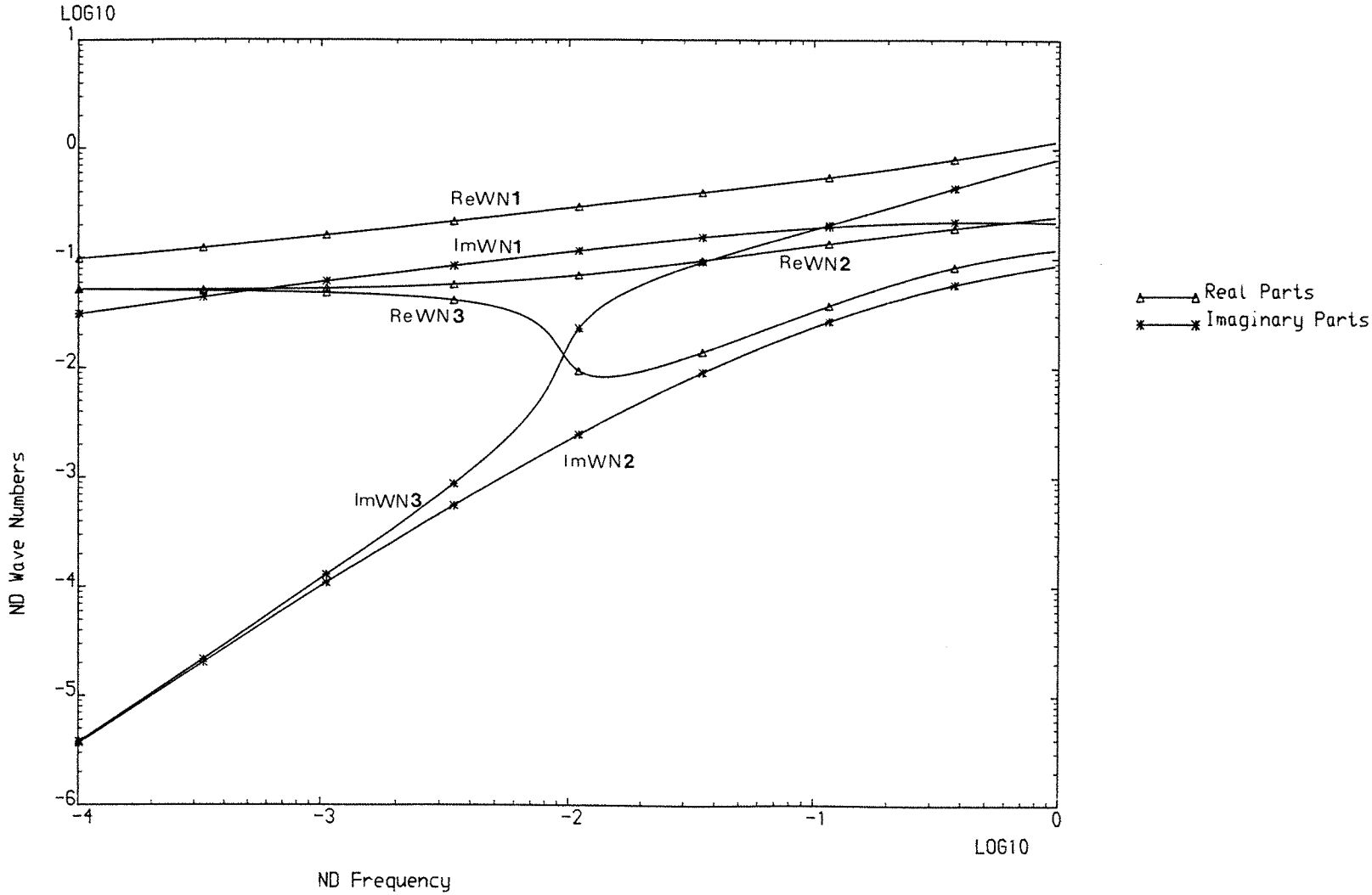

Fig. 18 Non-Dimensional Magnitudes of Wave Numbers of Three-Layered Sandwich Plate ($\beta = 1, m = 2$)

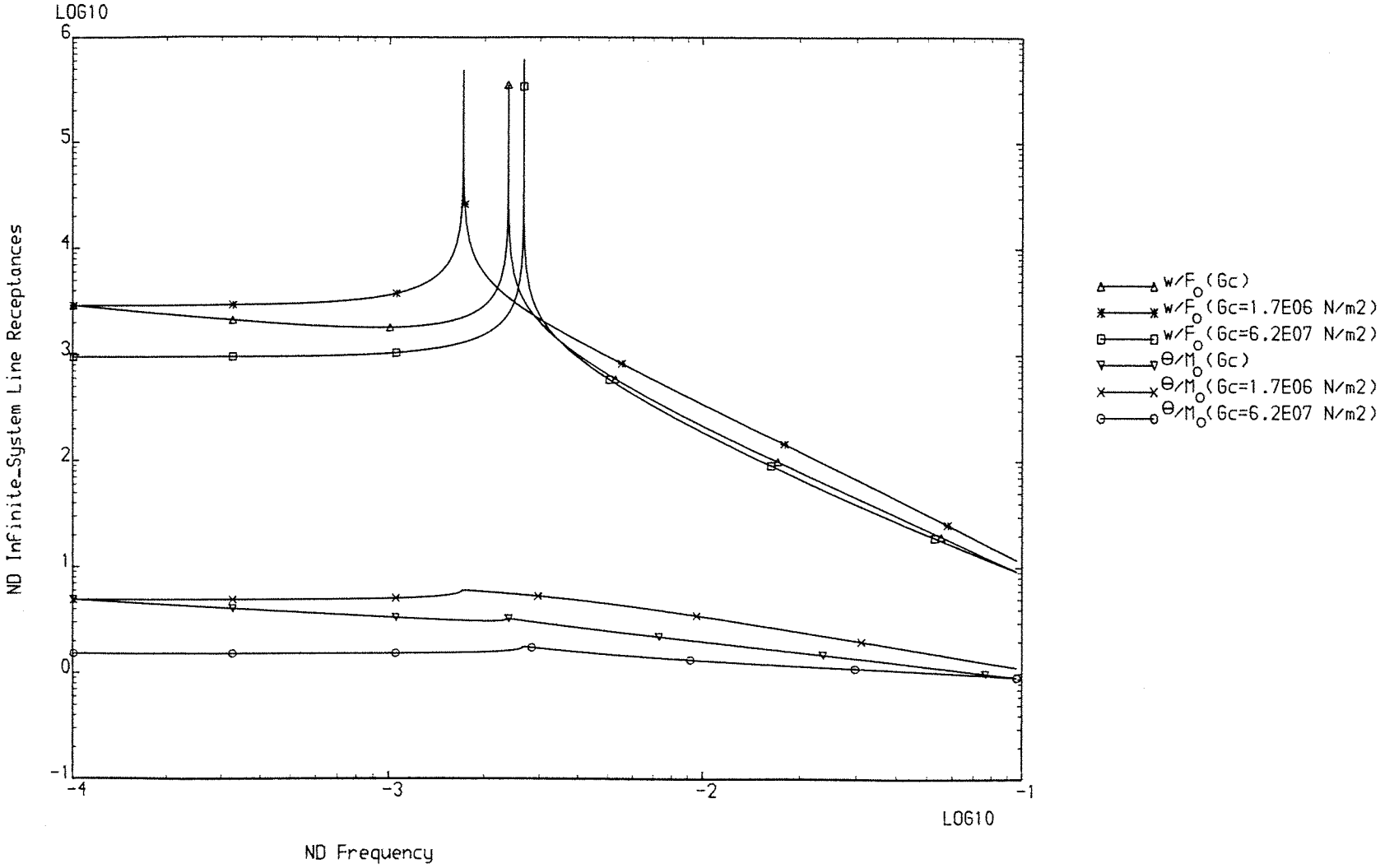

Fig. 19 Non-Dimensional Magnitudes of Infinite-System Line Receptances of Three-Layered Sandwich Plate ($\beta = 10^{-4}$)

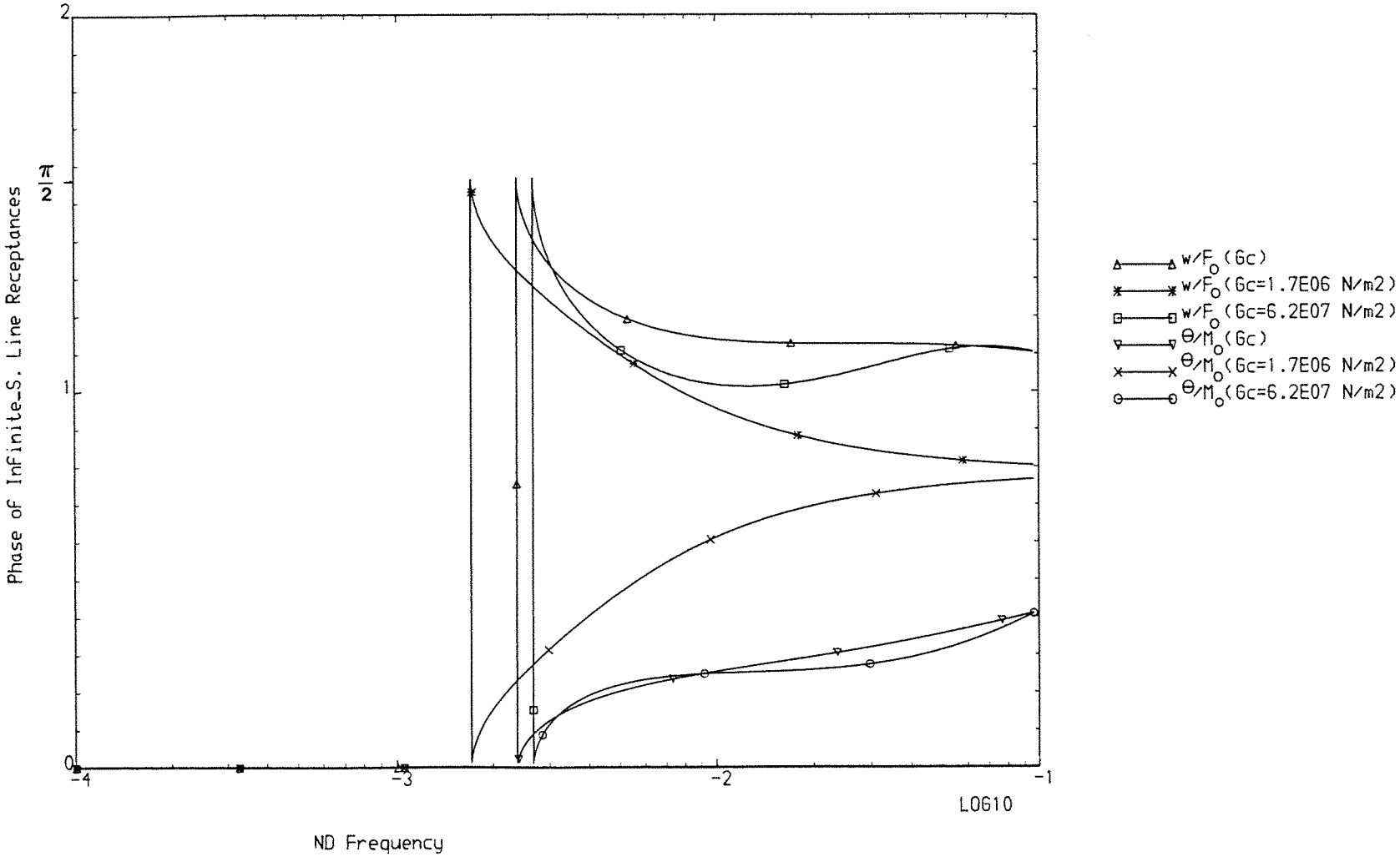

Fig. 20 Phases of Infinite-System Line Receptances of Three-Layered Sandwich Plate ($\beta = 10^{-4}$)

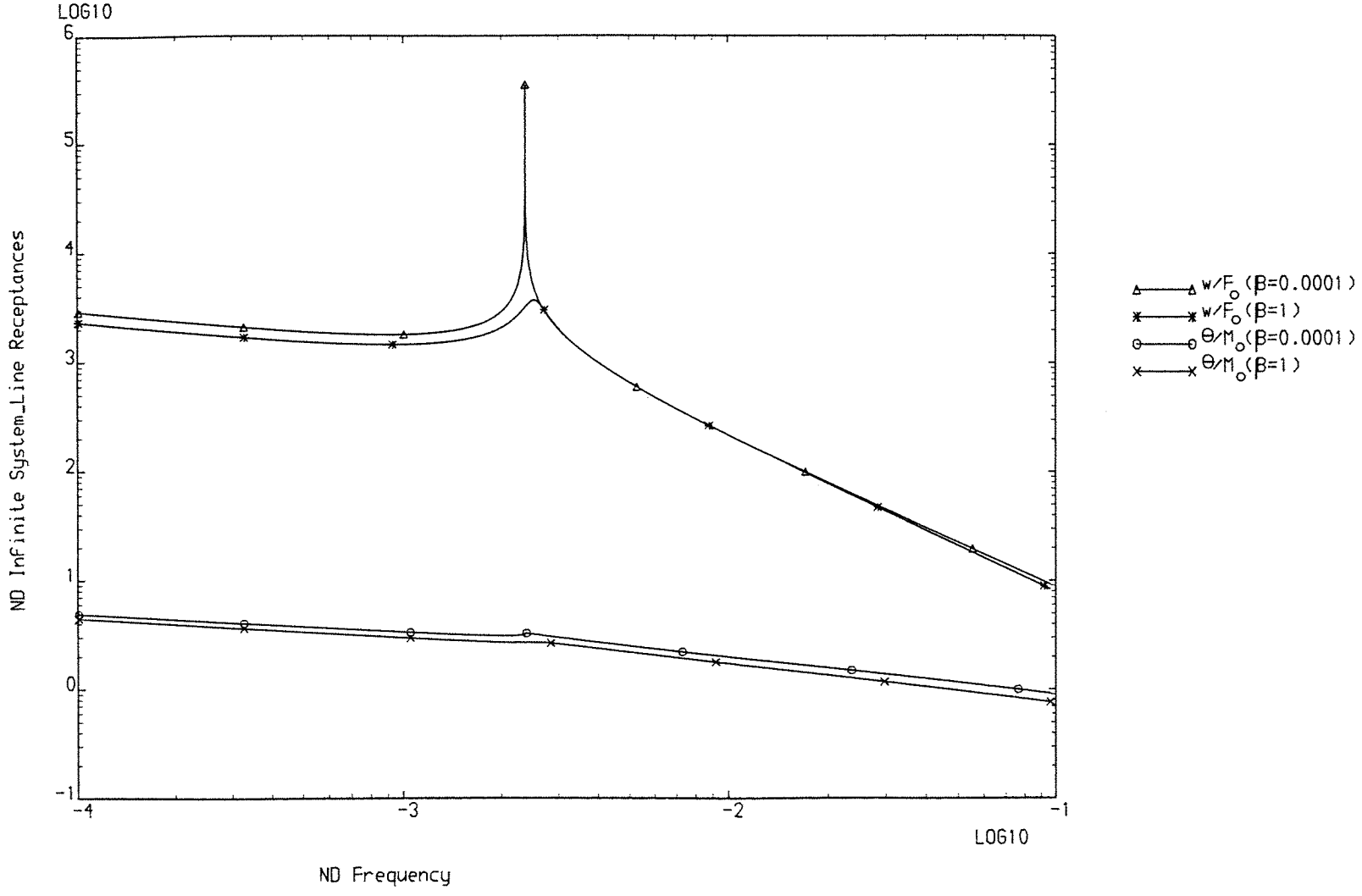

Fig. 21 Non-Dimensional Magnitudes of Infinite-System Line Receptances of Three-Layered Sandwich Plate

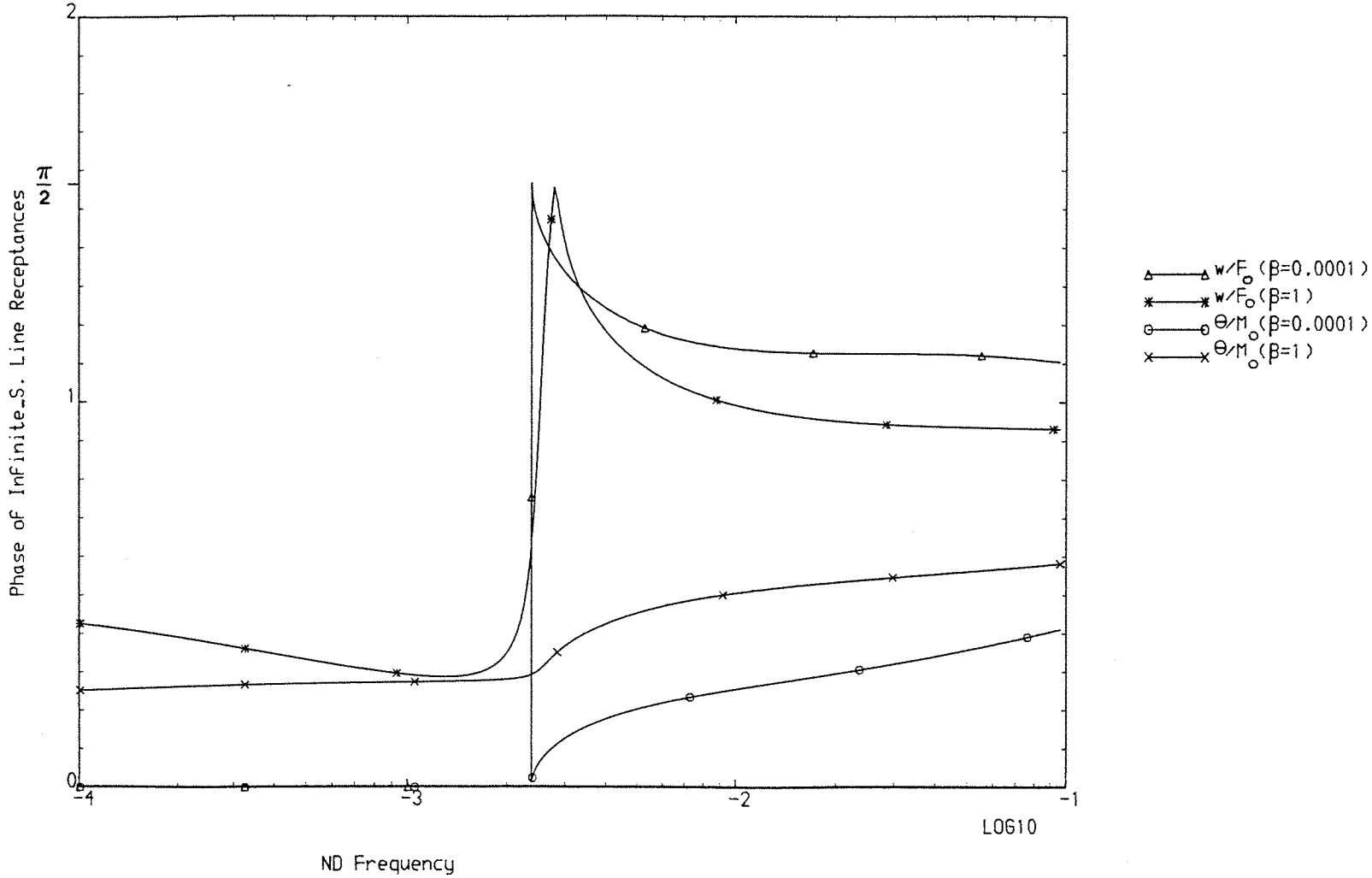

Fig. 22 **Phases of Infinite-System Line Receptances of Three-Layered Sandwich Plate**

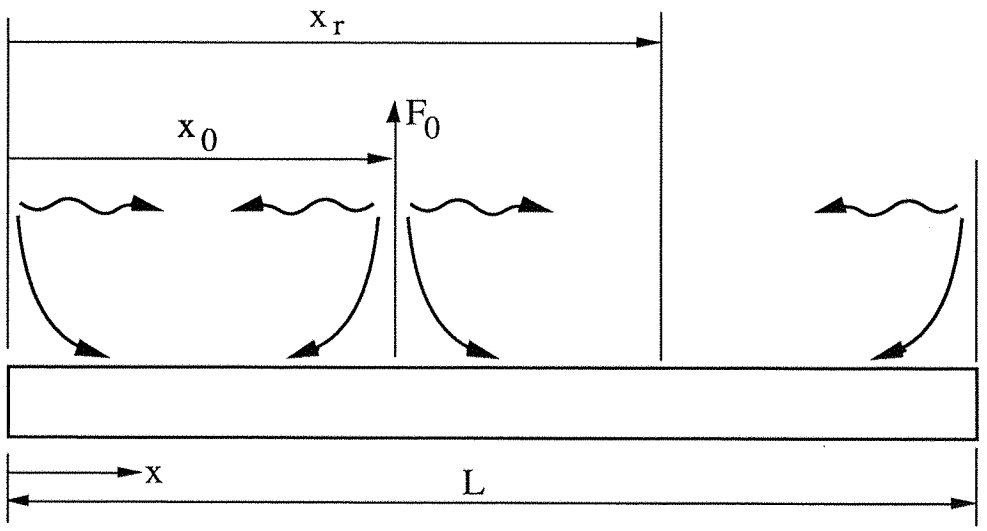

(a)

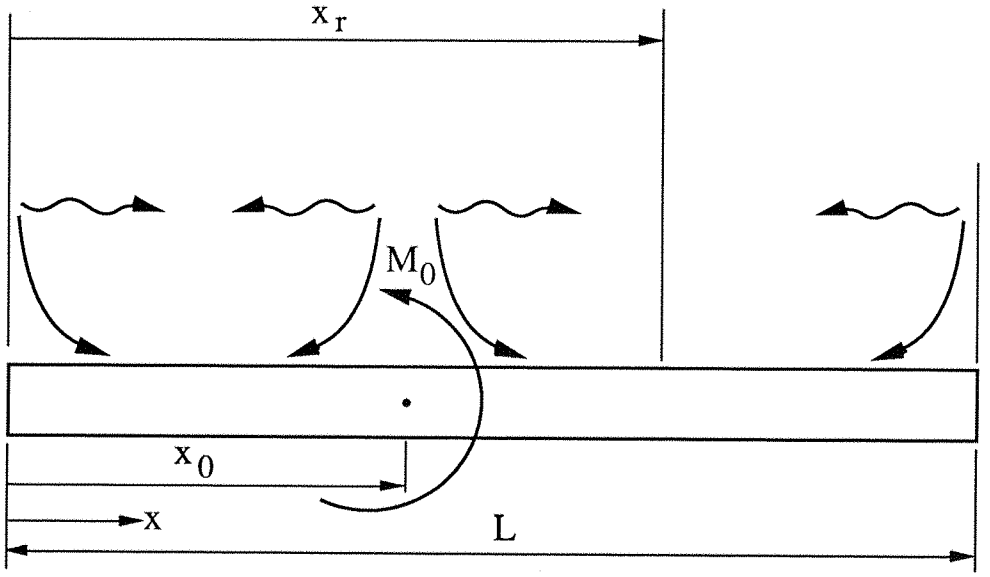

(b)

Figure 23: The Forced and Free Waves of a Single-Bay Euler-Bernoulli Beam Under the Influence of a

a) Harmonic Force
b) Harmonic Moment

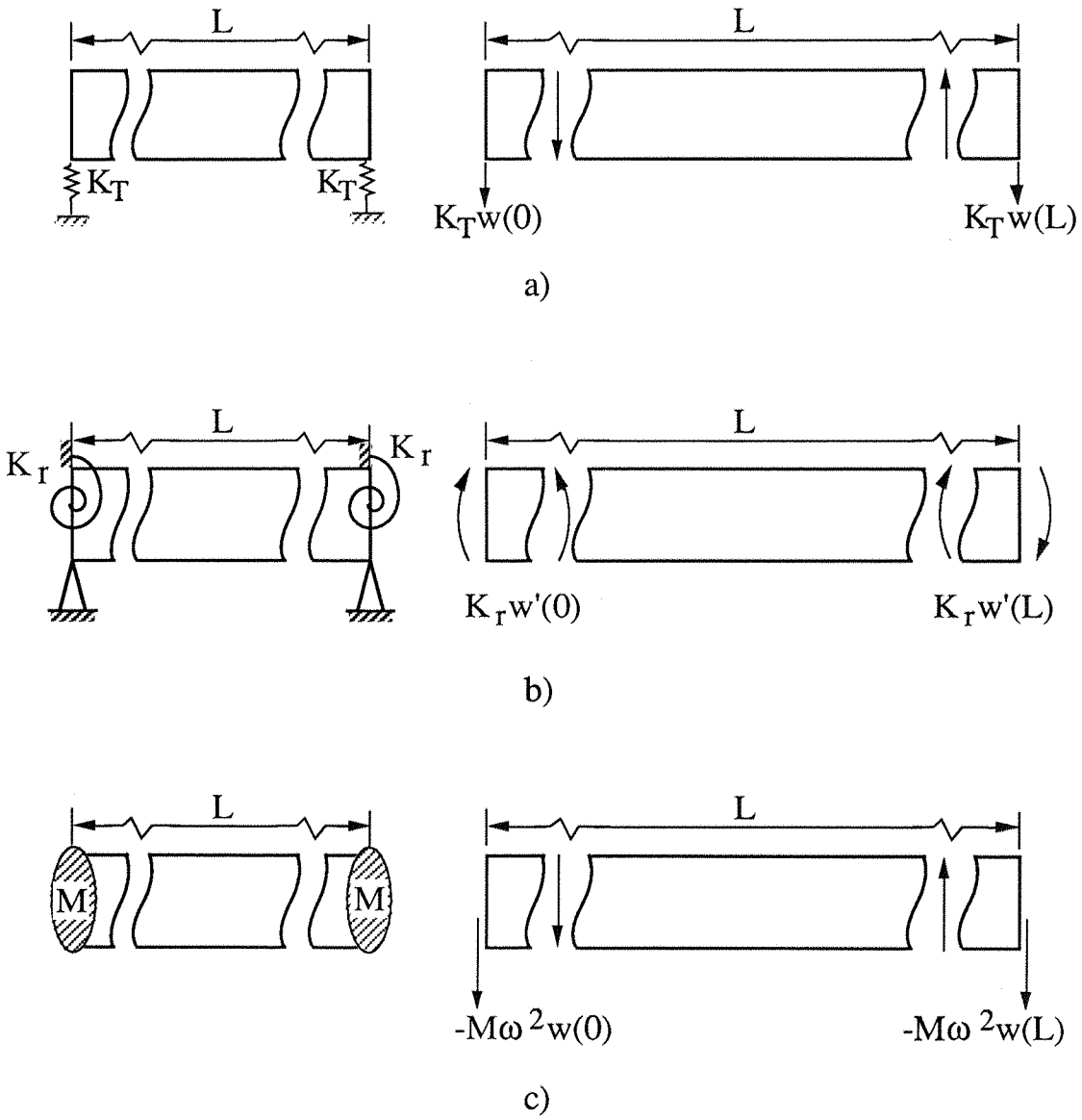

Figure 24: Non-Classical Boundary Conditions of Euler-Bernoulli Beams.

a) Transverse Spring
b) Rotational Spring
c) Point Mass

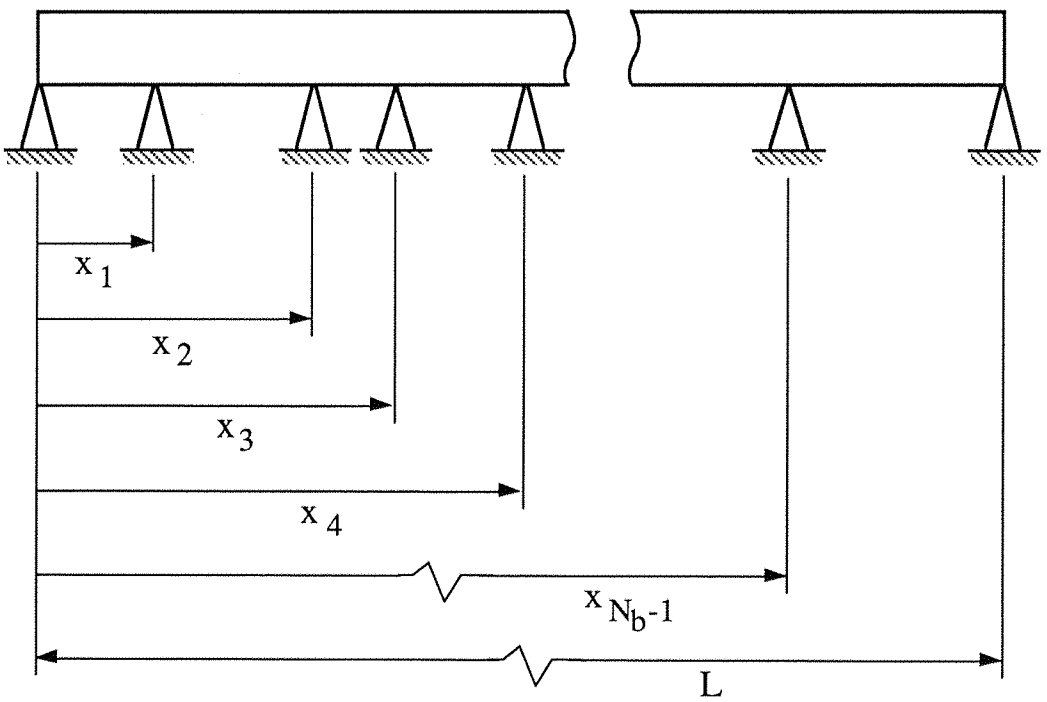

Figure 25: N_b Bay Simply-Supported Euler-Bernoulli Beam.

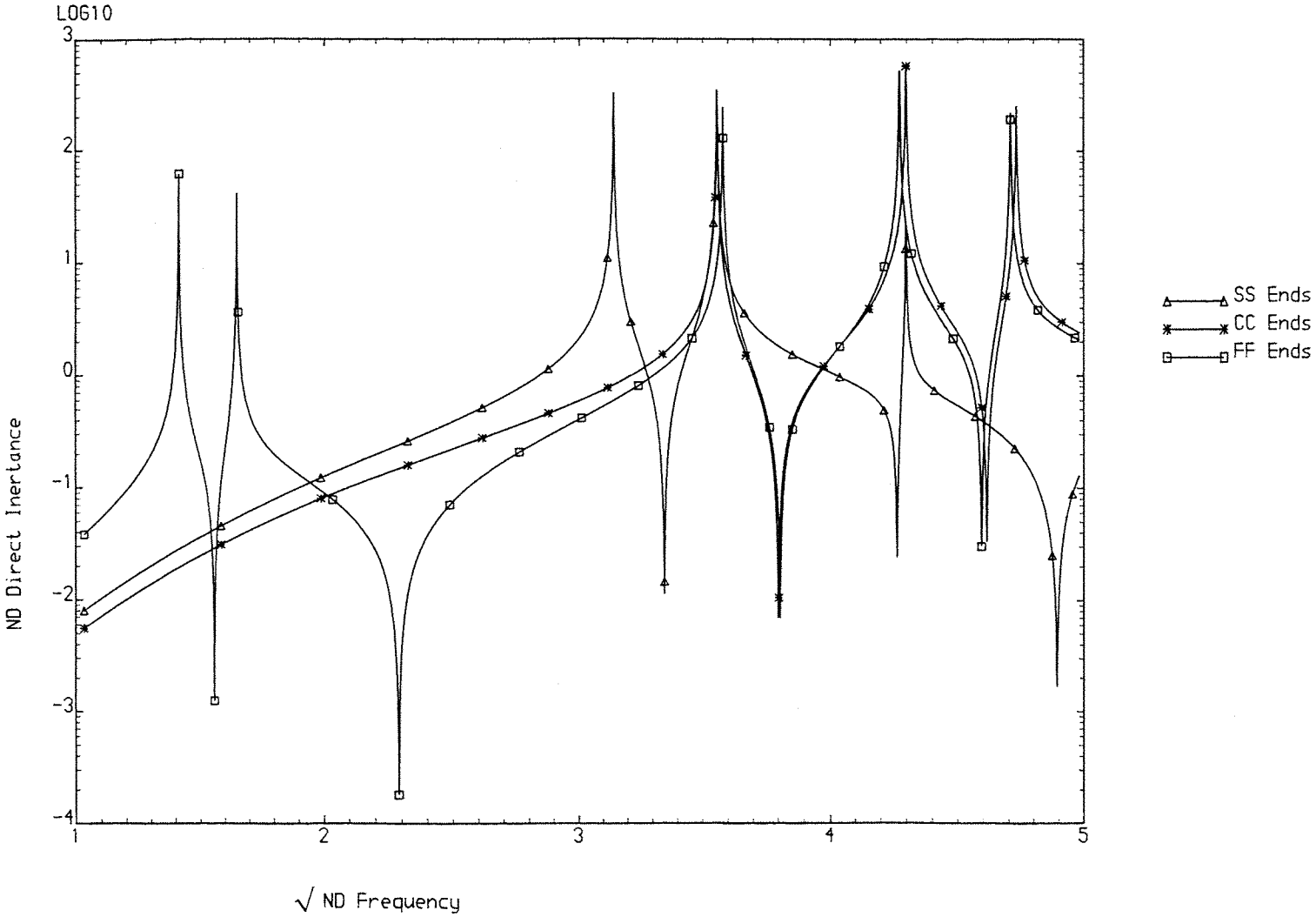

Fig. 26 Non-Dimensional Magnitudes of Transverse Responses of 3 Equal Bay Euler-Bernoulli Beam (η=0.001, Intermediate Simple Supports, x_o=L/4)

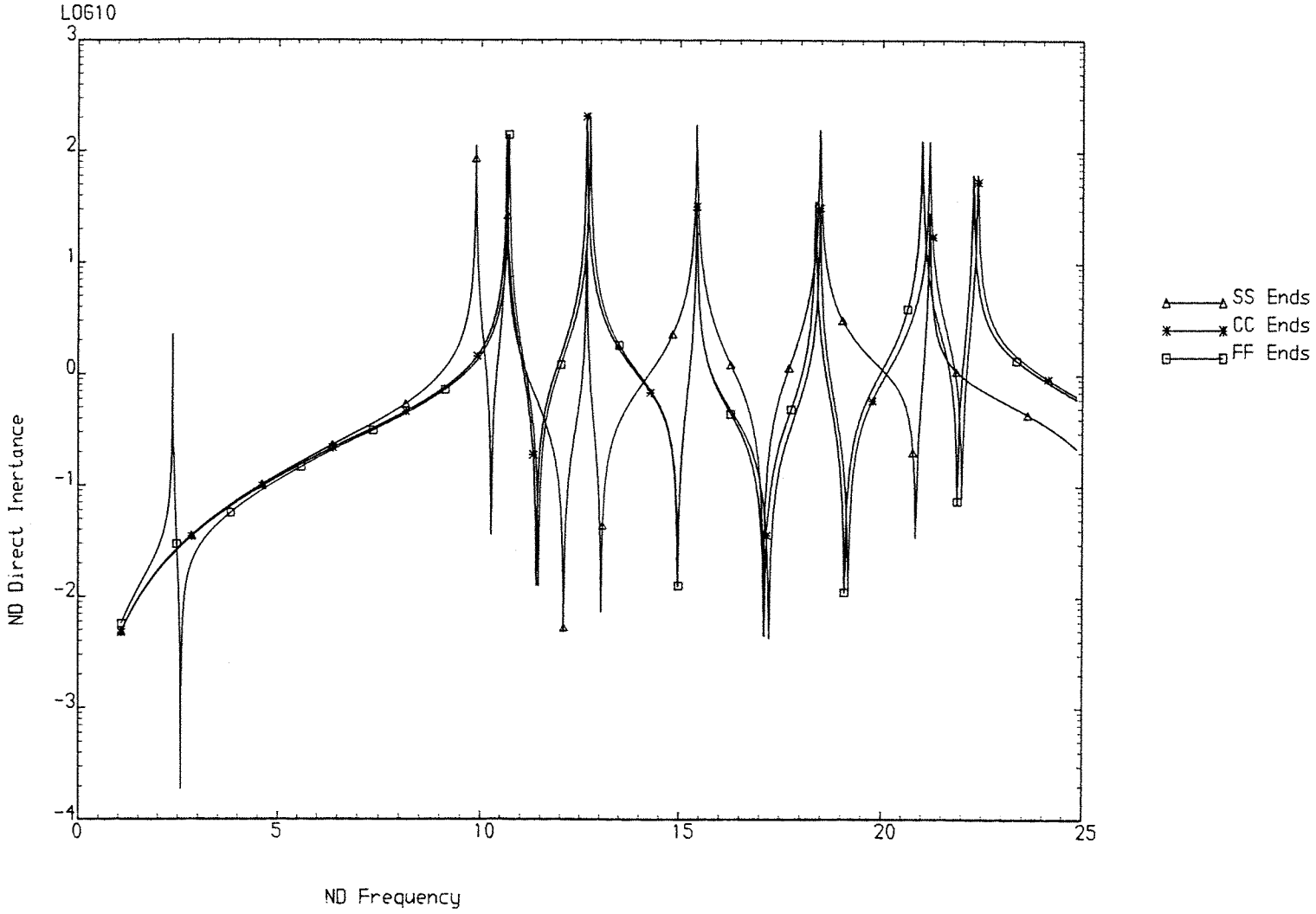

Fig. 27 Non-Dimensional Magnitudes of Transverse Responses of 6 Equal Bay Euler-Bernoulli Beam (η=0.001, Intermediate Simple Supports, x_o=L/4)

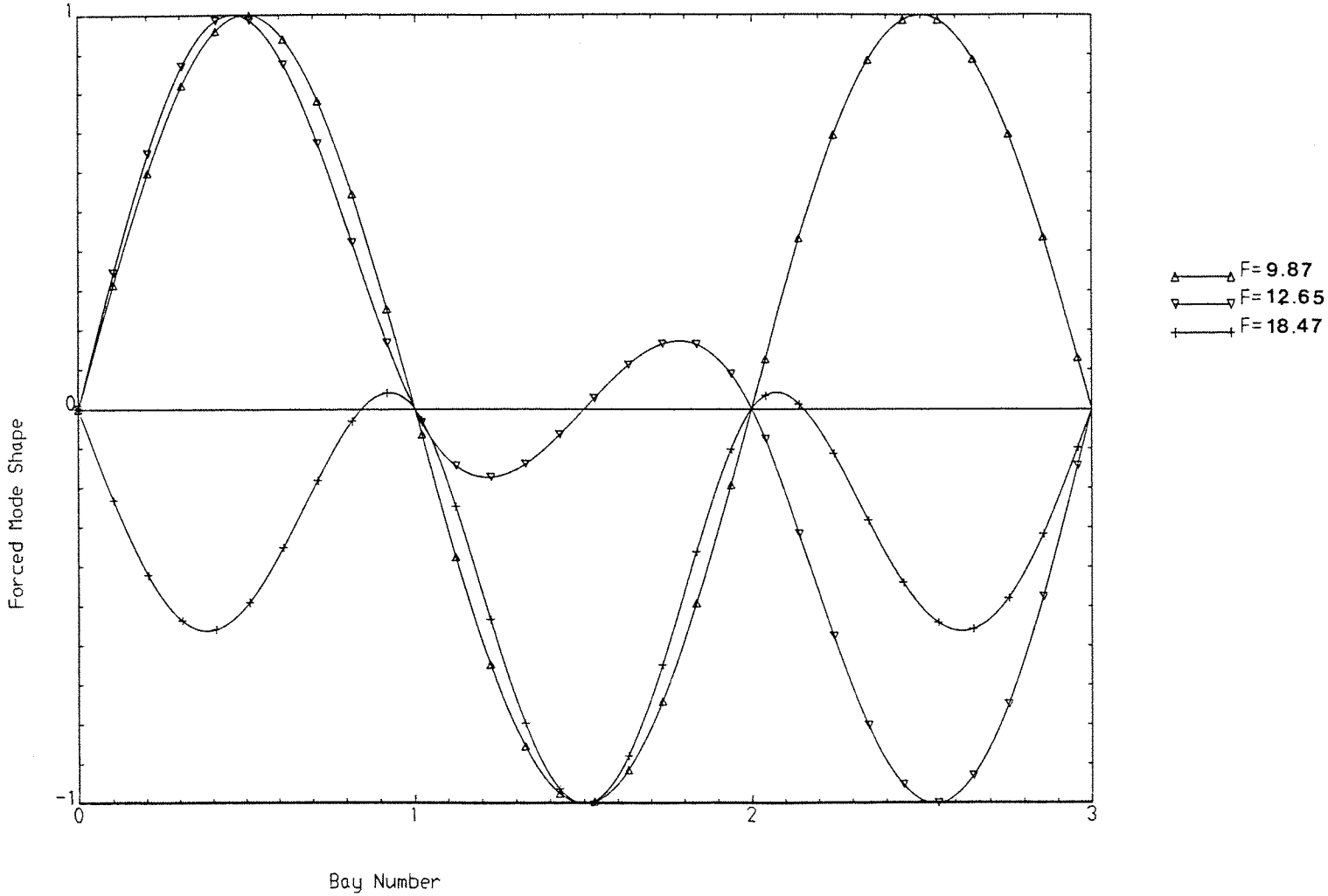

Fig. 28 Forced Mode Shapes of Three Equal Bay Euler-Bernoulli Beam (η = 0, Intermediate Simple Supports, x_o = L/6, SS Ends)

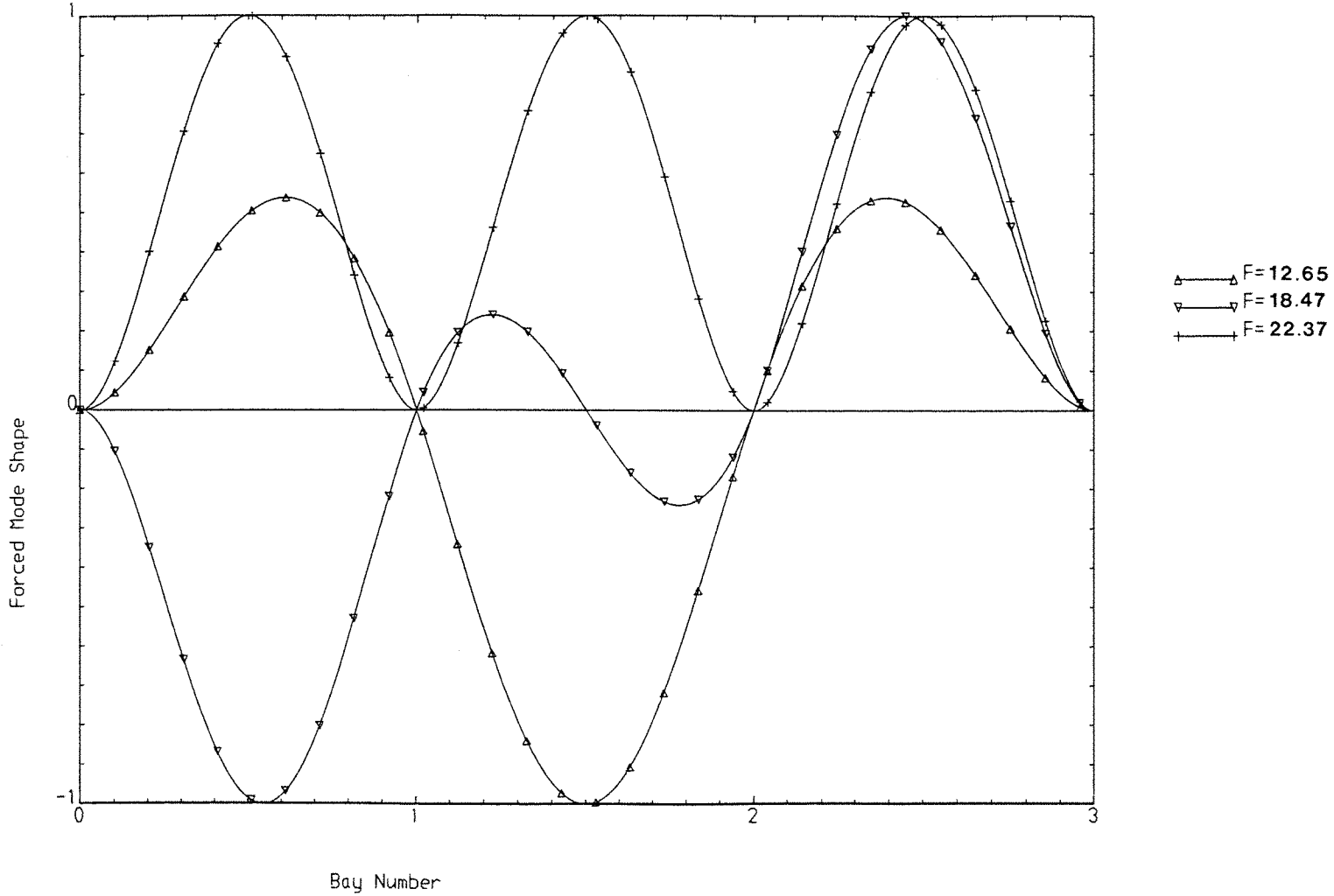

Fig. 29 **Forced Mode Shapes of Three Equal Bay Euler-Bernoulli Beam (η = 0, Intermediate Simple Supports, x_o = L/6, Clamped Ends)**

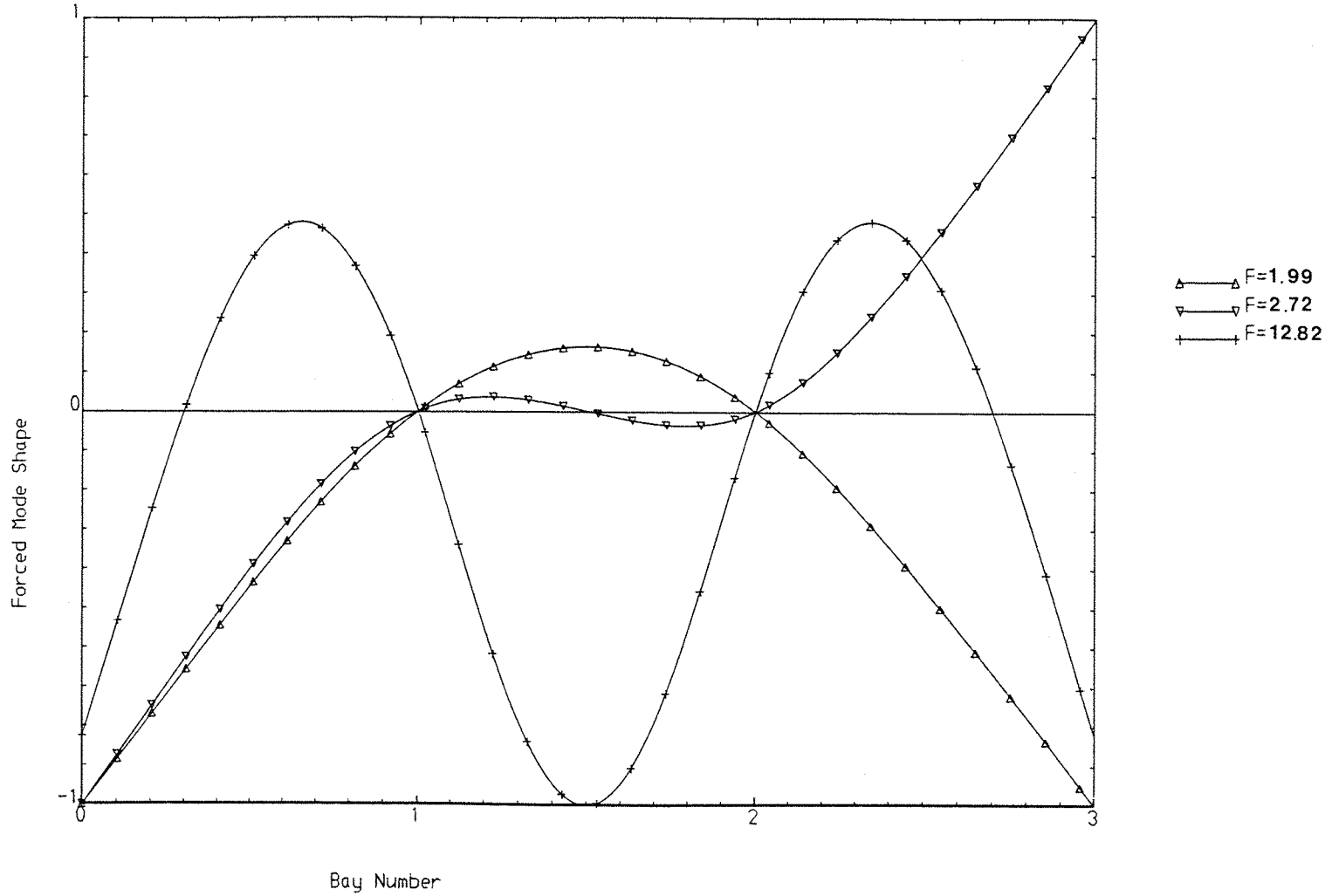

Fig. 30 Forced Mode Shapes of Three Equal Bay Euler-Bernoulli Beam (η = 0, Intermediate Simple Supports, x_o = L/6, Free Ends)

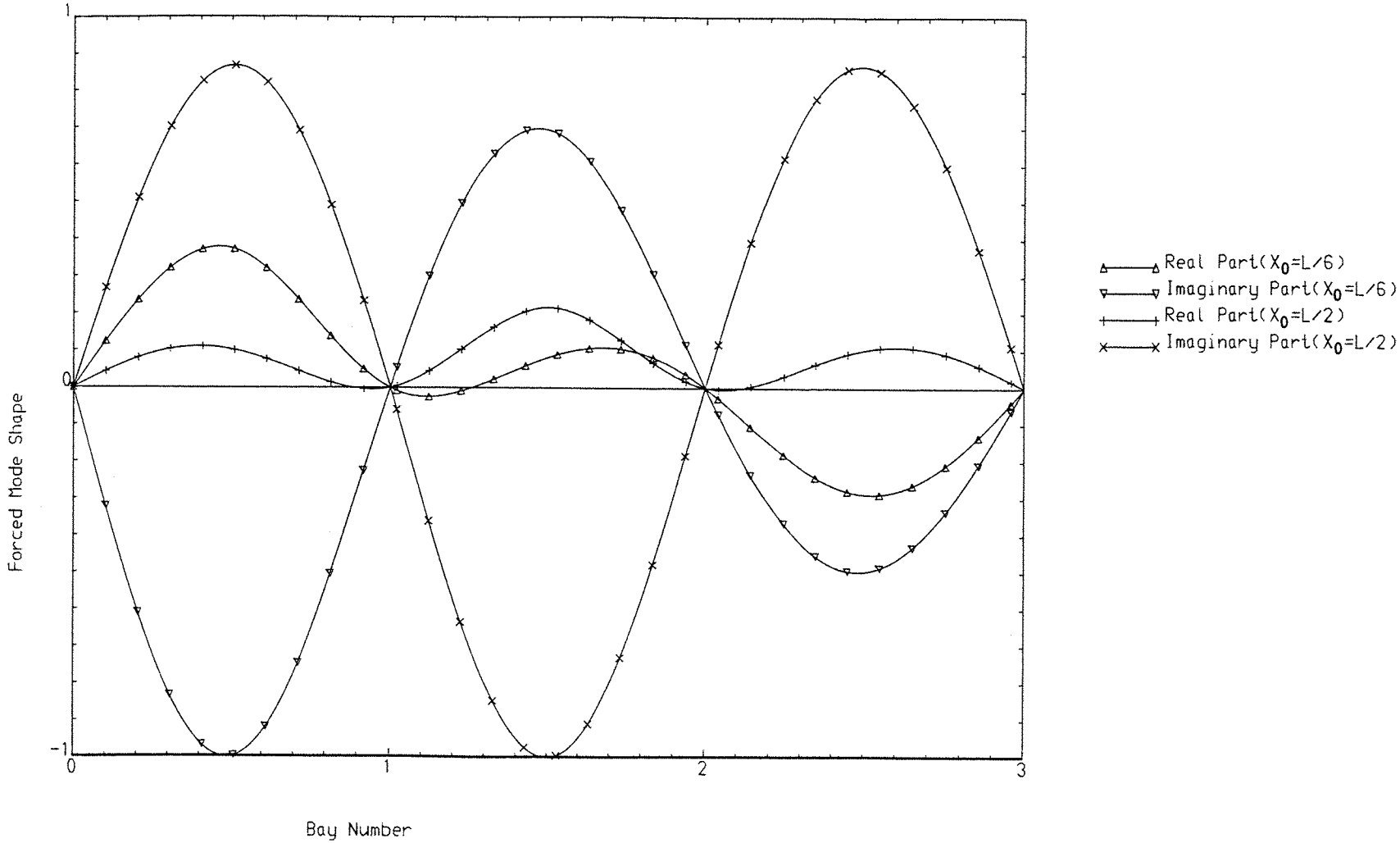

Fig. 31 Forced Mode Shapes of Three Equal Bay Euler-Bernoulli Beam (η = 0.3, Intermediate Simple Supports, ND f = 9.87, SS Ends)

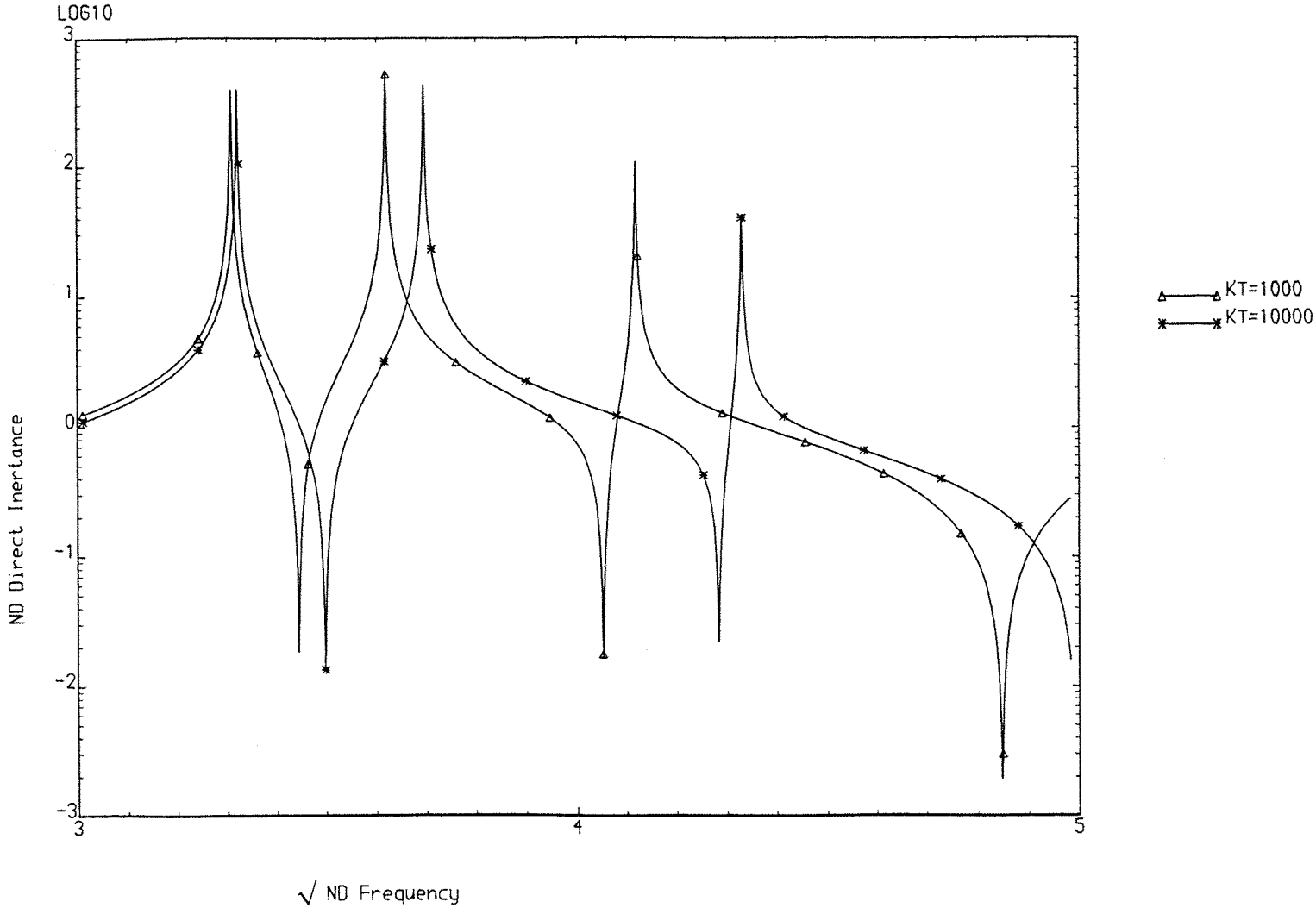

Fig. 32 Non-Dimensional Magnitudes of Transverse Responses of Three Equal Bay Euler-Bernoulli Beam (η = 0.001, KR = 1, x_o = L/4)

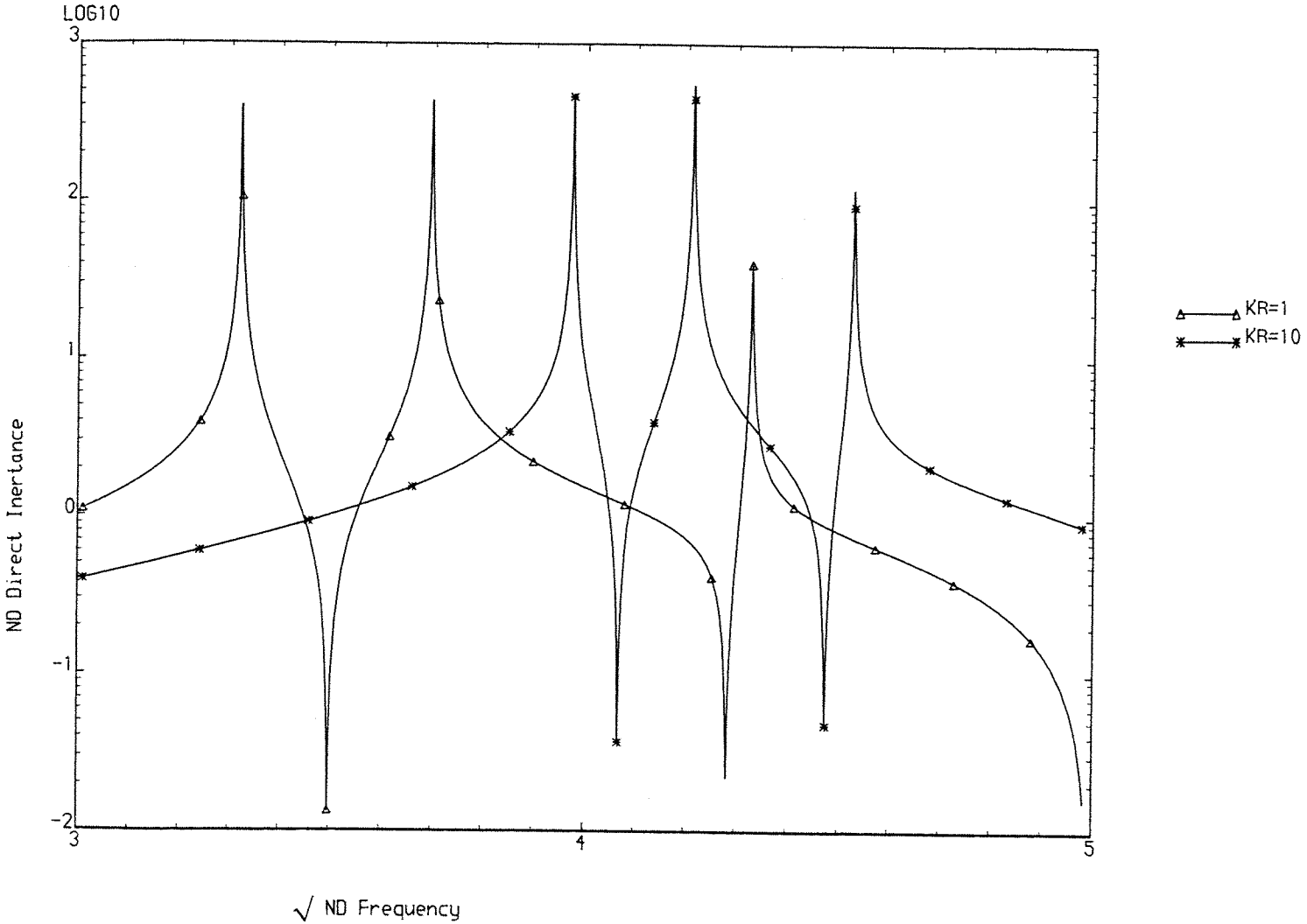

Fig. 33 Non-Dimensional Magnitudes of Transverse Responses of Three Equal Bay Euler-Bernoulli Beam (η = 0.001, KT = 10^4, x_o = L/4)

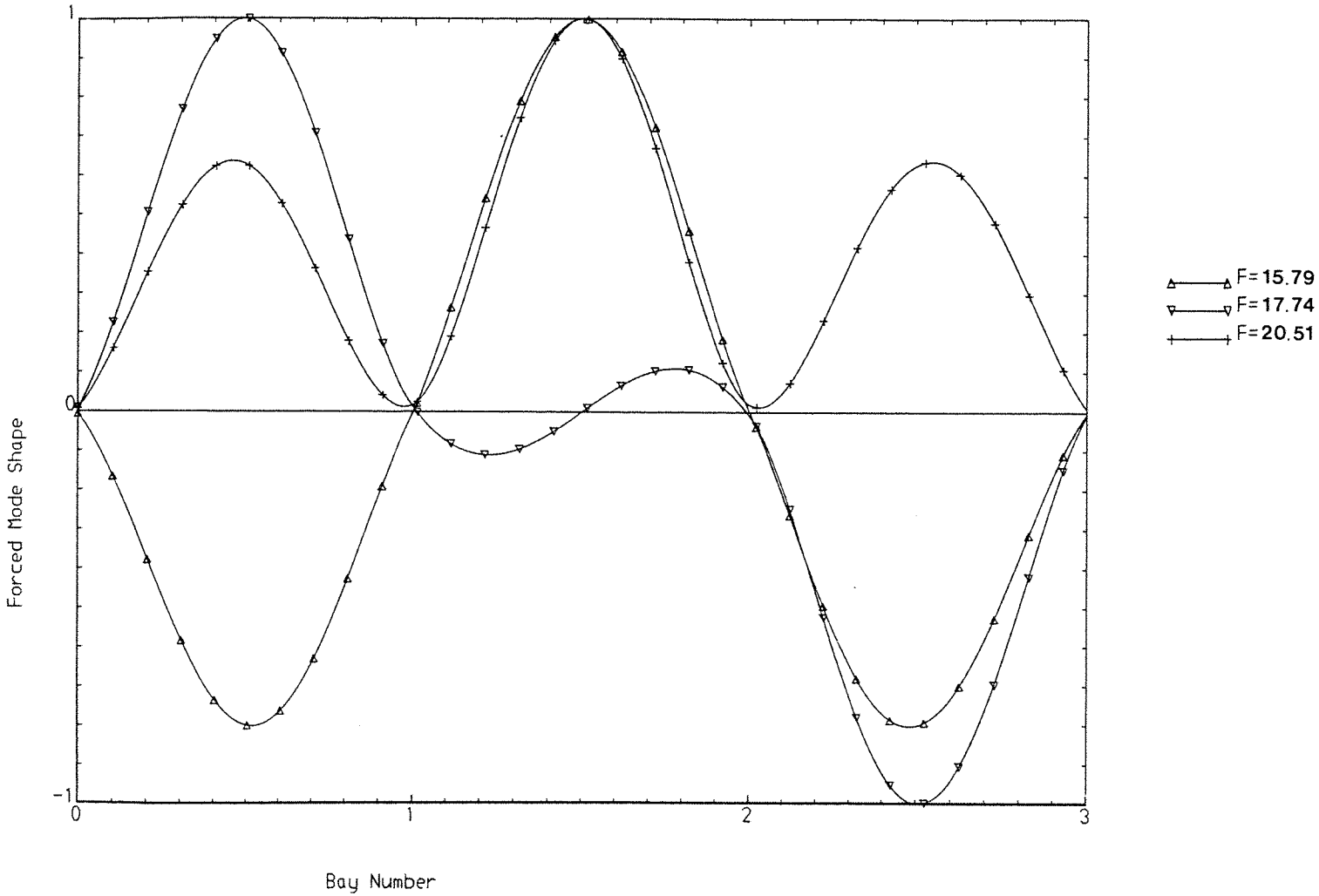

Fig. 34 Forced Mode Shapes of Three Equal Bay Euler-Bernoulli Beam (η = 0, KT = 10^4, KR = 10, x_o = L/6)

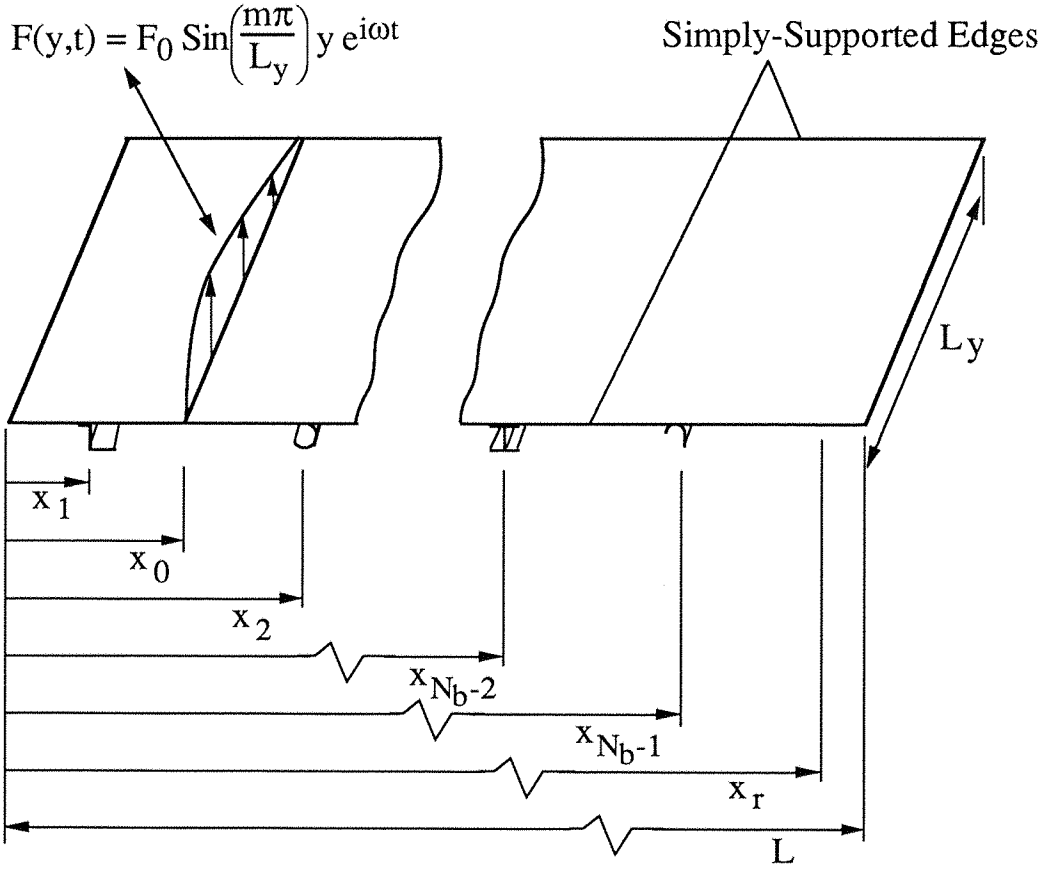

Figure 35: N_b Bay Euler-Bernoulli Plate.

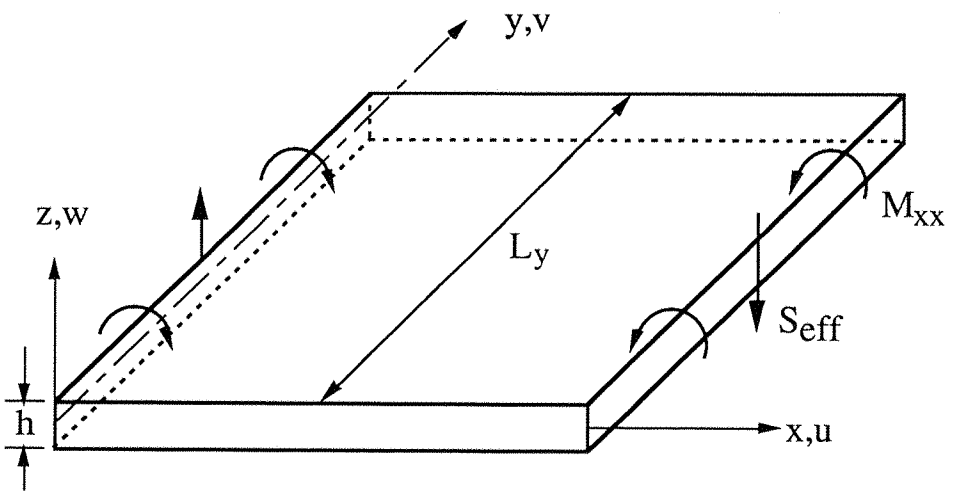

Figure 36: Coordinate, Displacement and Stress-System for Euler-Bernoulli Plates.

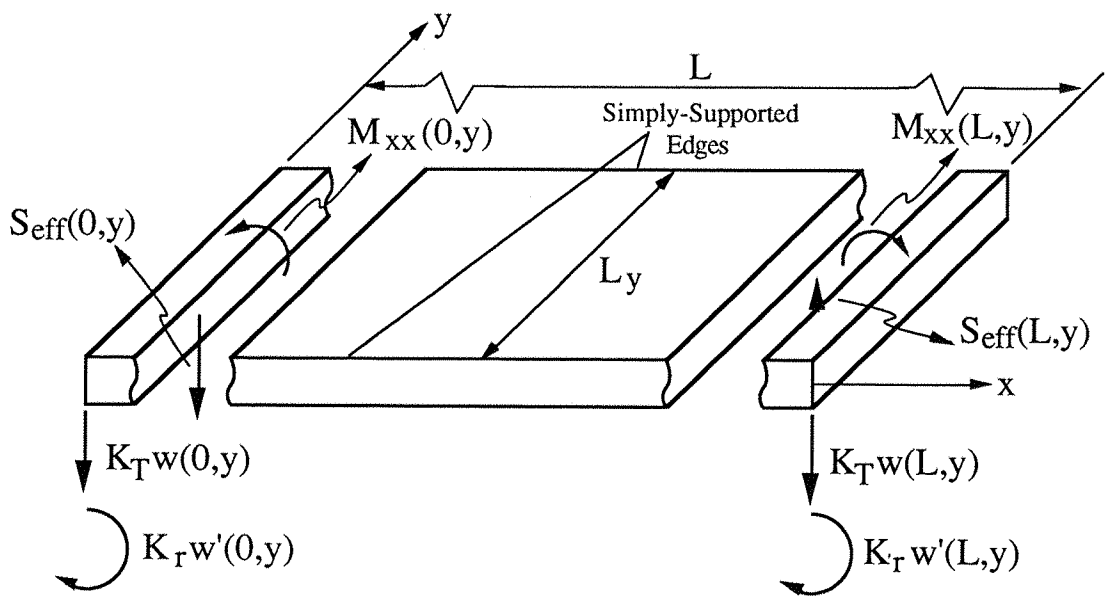

Figure 37: Positive Sign Convention for Euler-Bernoulli Plate with Elastically Supported x-wise Edges.

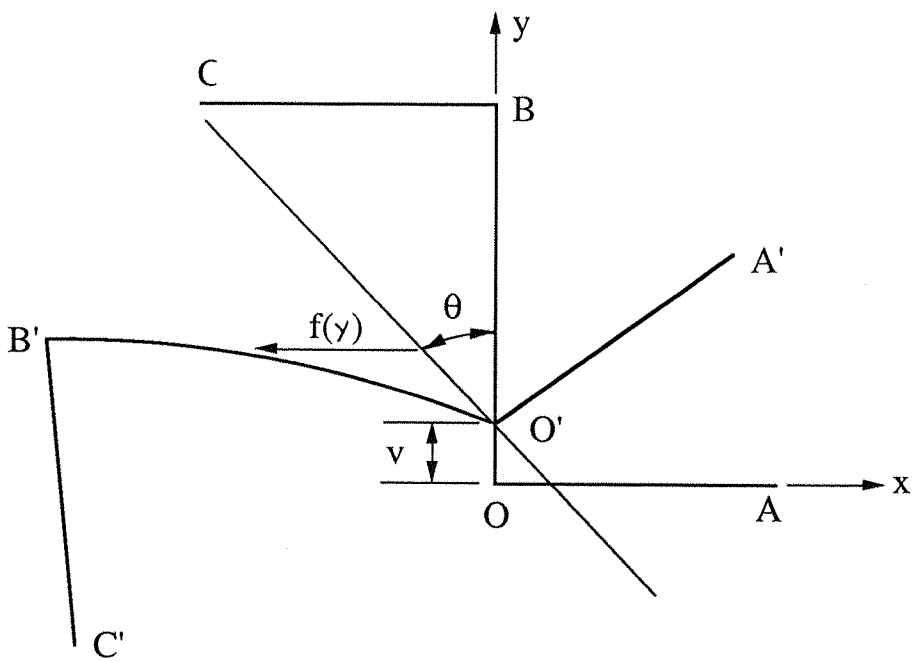

Figure 38: Static and Deformed Cross-sections of a Z-Section Stiffener.

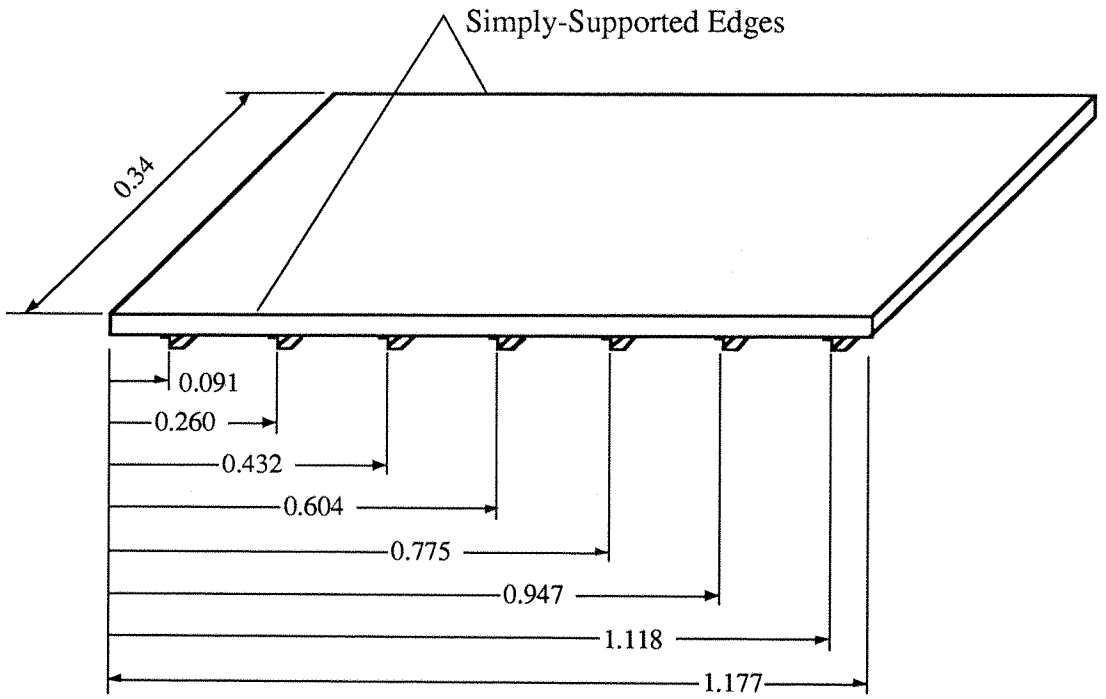

Figure 39: Dimensions [m] of Eight-Bay Euler-Bernoulli Plate (h=0.91 [mm] $E=7.10^{10}$ [N/m^2], ρ=2700 [kg/m^3] υ=0.3)

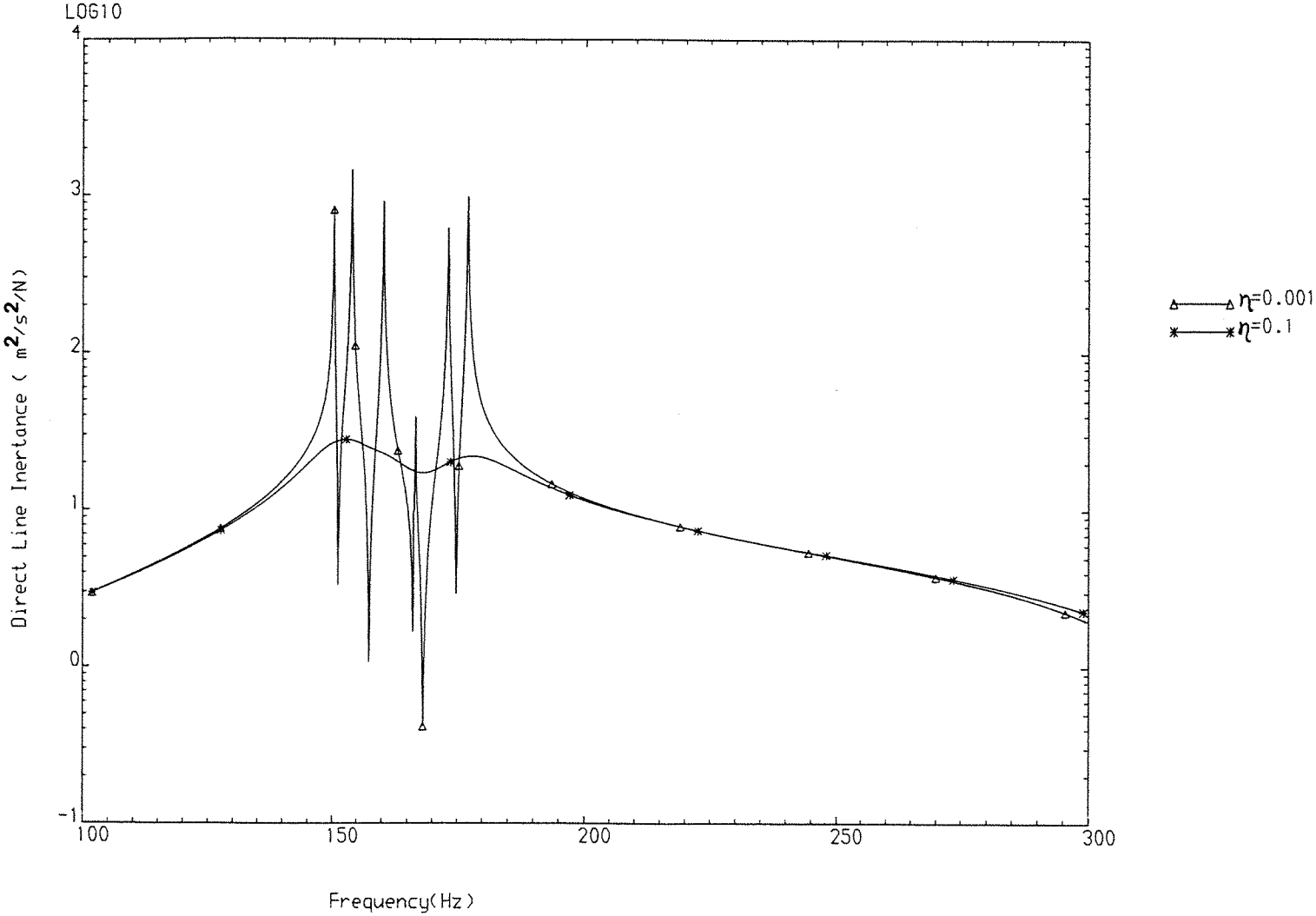

Fig. 40 Magnitudes of Transverse Responses of Eight-Bay Euler-Bernoulli Plate (x_o = 0.37[m])

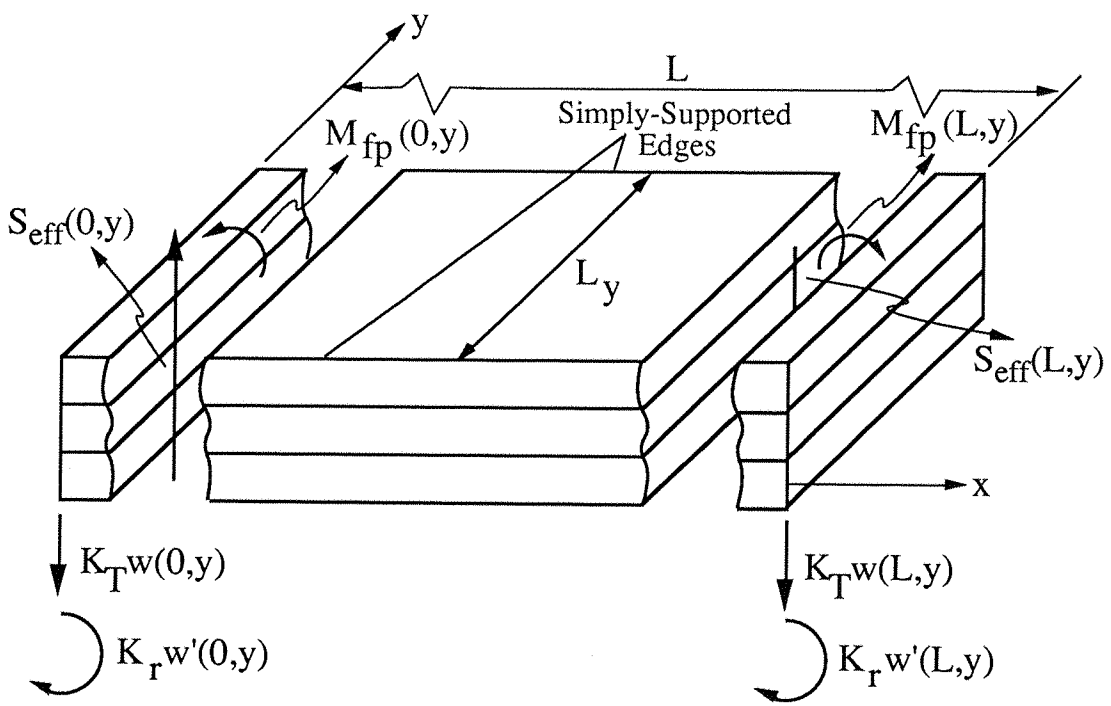

Figure 41: Positive Sign Convention for Three-Layered Sandwich Plate with Equal Face-Plates and Elastically Supported x-wise Edges.

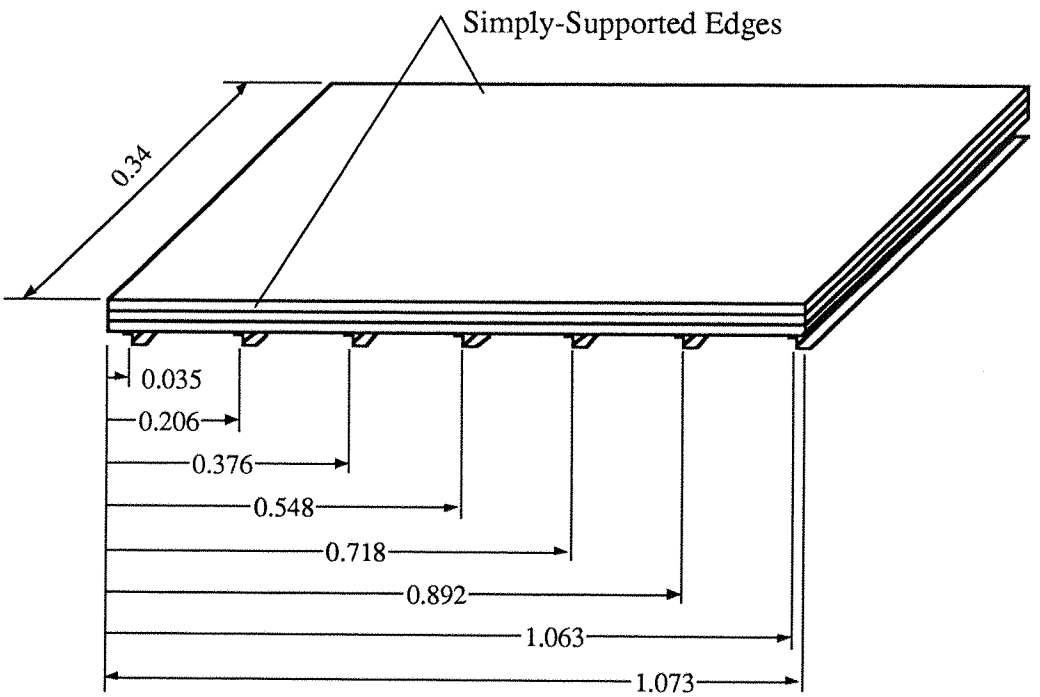

Figure 42: Dimensions [m] of Eight-Bay, Three-Layered Sandwich Plate with Equal Face-Plates.
(h=0.56 [mm], h_c=1.13 [mm], E=7.10^{10} [N/m^2], m_s=4.282 [kg/m^2], υ=0.3)

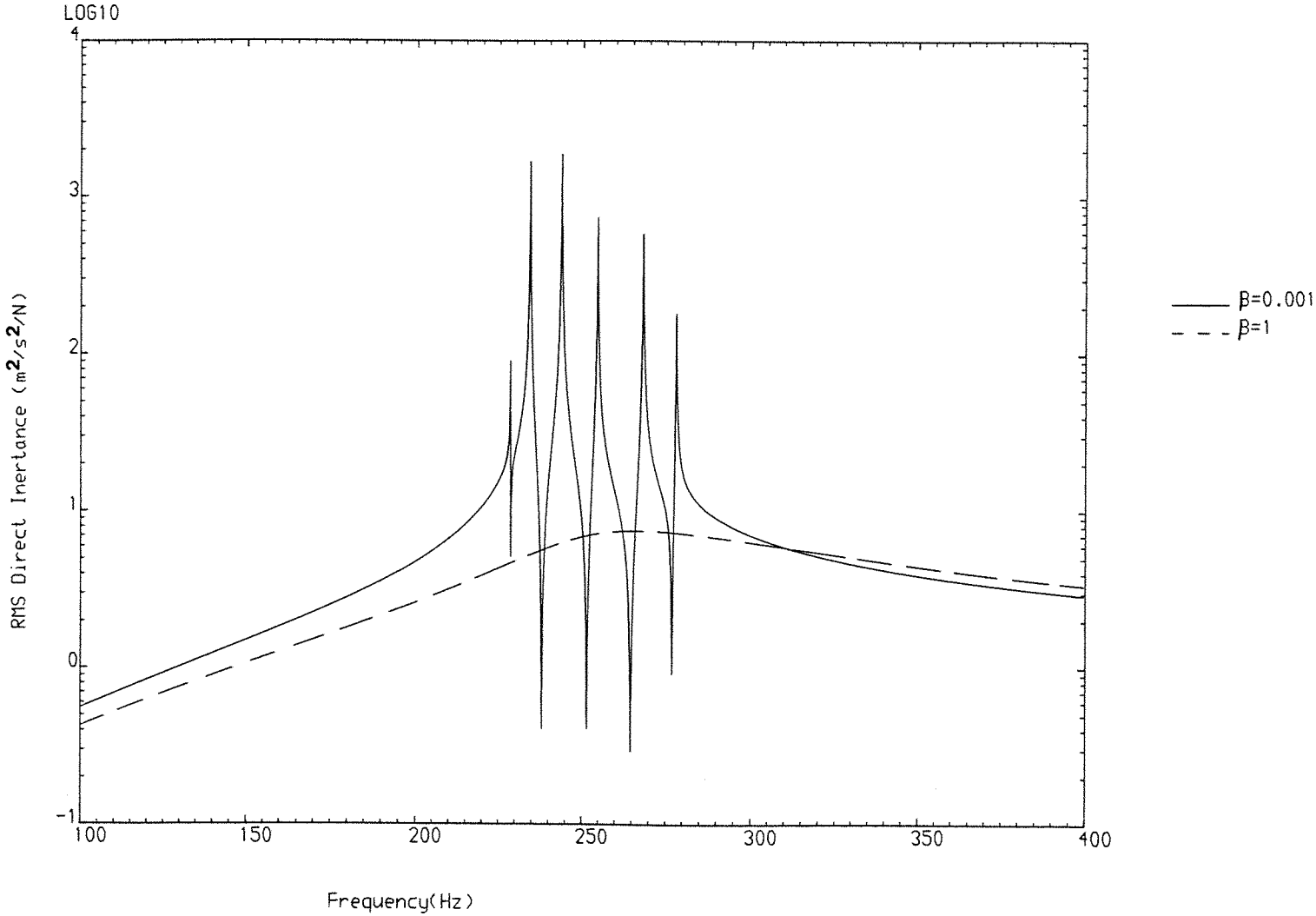

Fig. 43 Magnitudes of Transverse Responses of Eight-Bay, Three-Layered Sandwich Plate (General Supports, x_o = 0.12 [m])

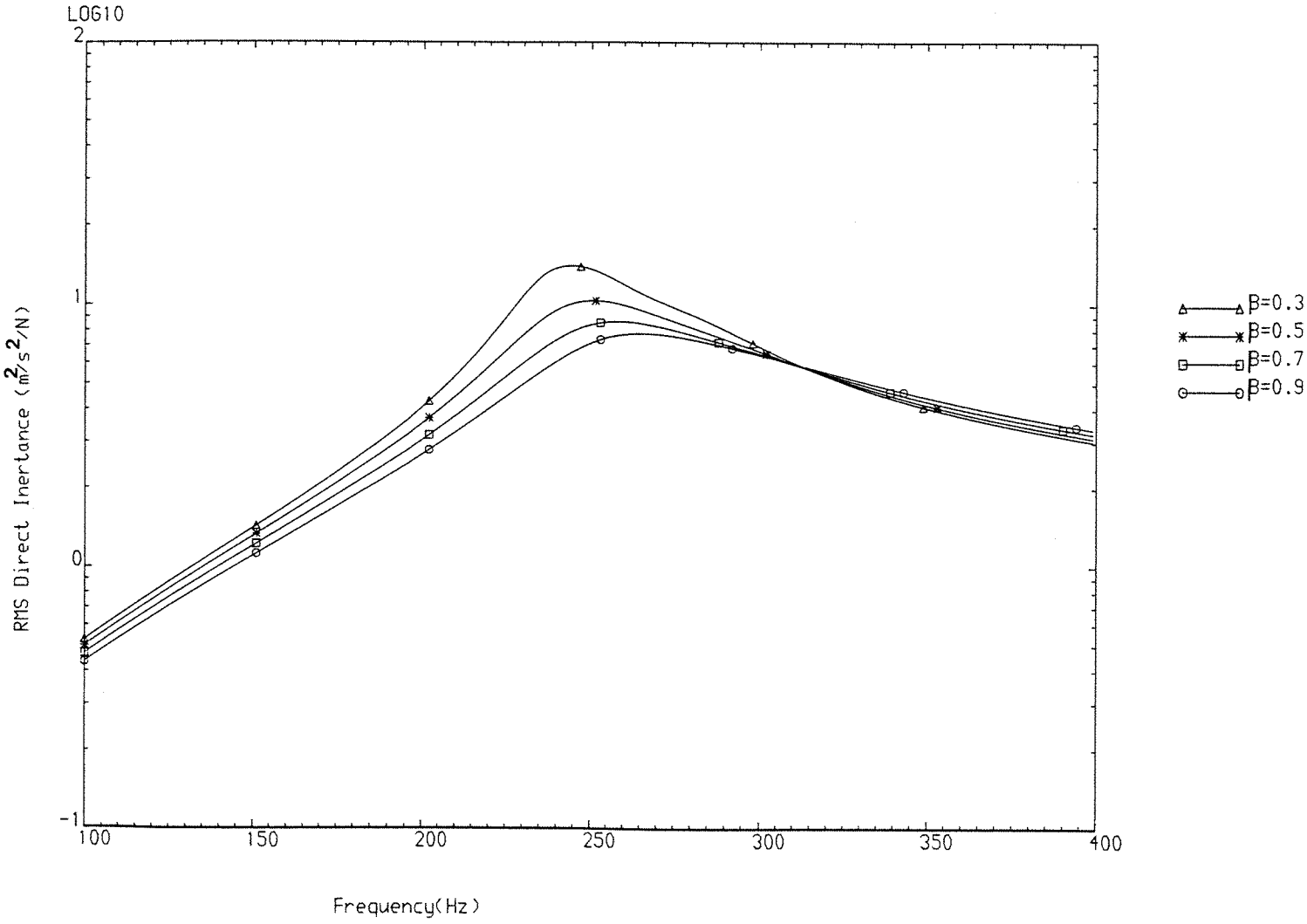

Fig. 44 **Magnitudes of Transverse Responses of Eight-Bay, Three-Layered Sandwich Plate (General Supports, x_o = 0.12 [m])**

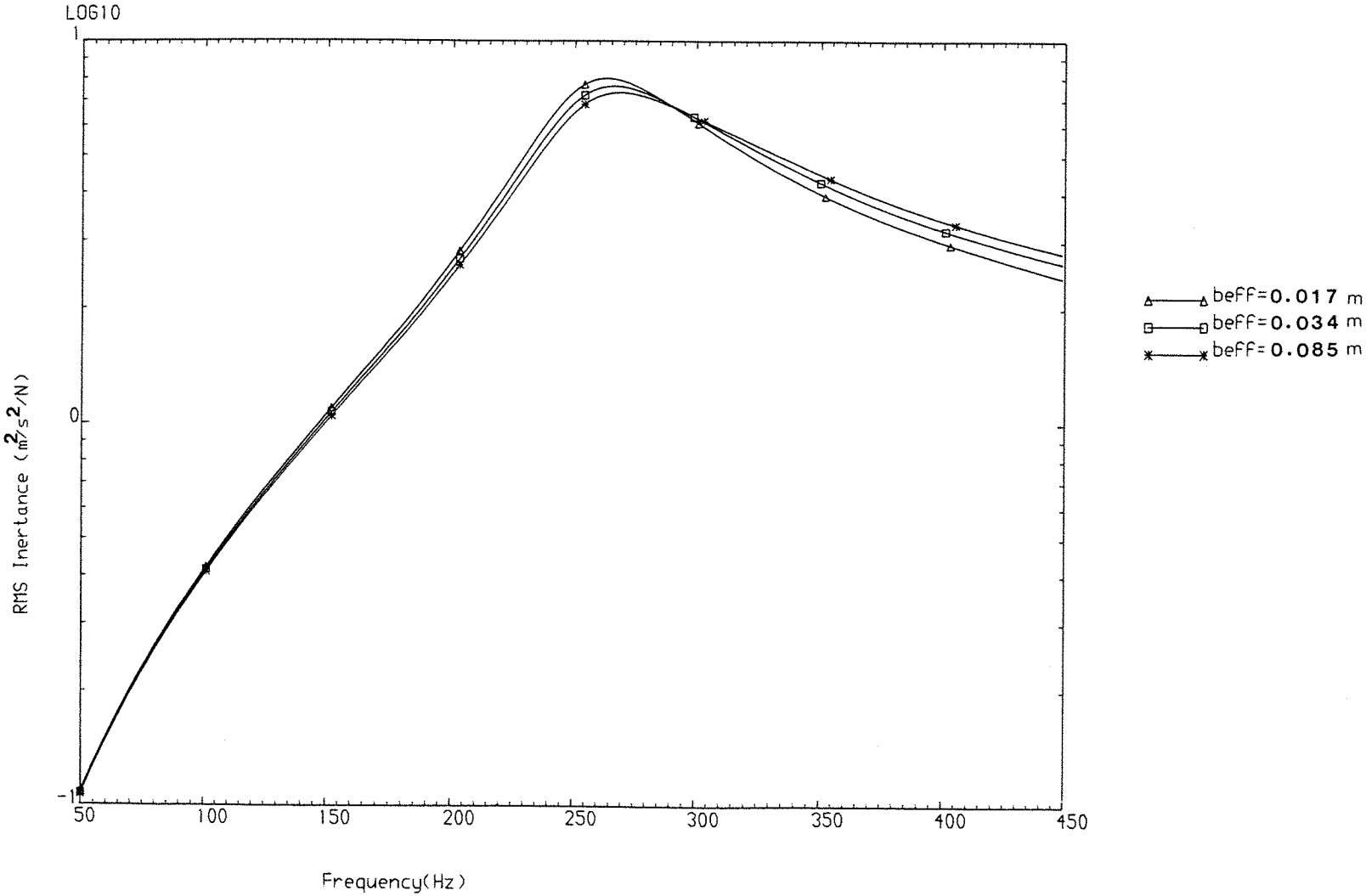

Fig. 45 Magnitudes of Transverse Responses of Eight-Bay, Three-Layered Sandwich Plate (β = 1, General Supports, x_o = 0.12 [m], x_r = 0.13 [m])

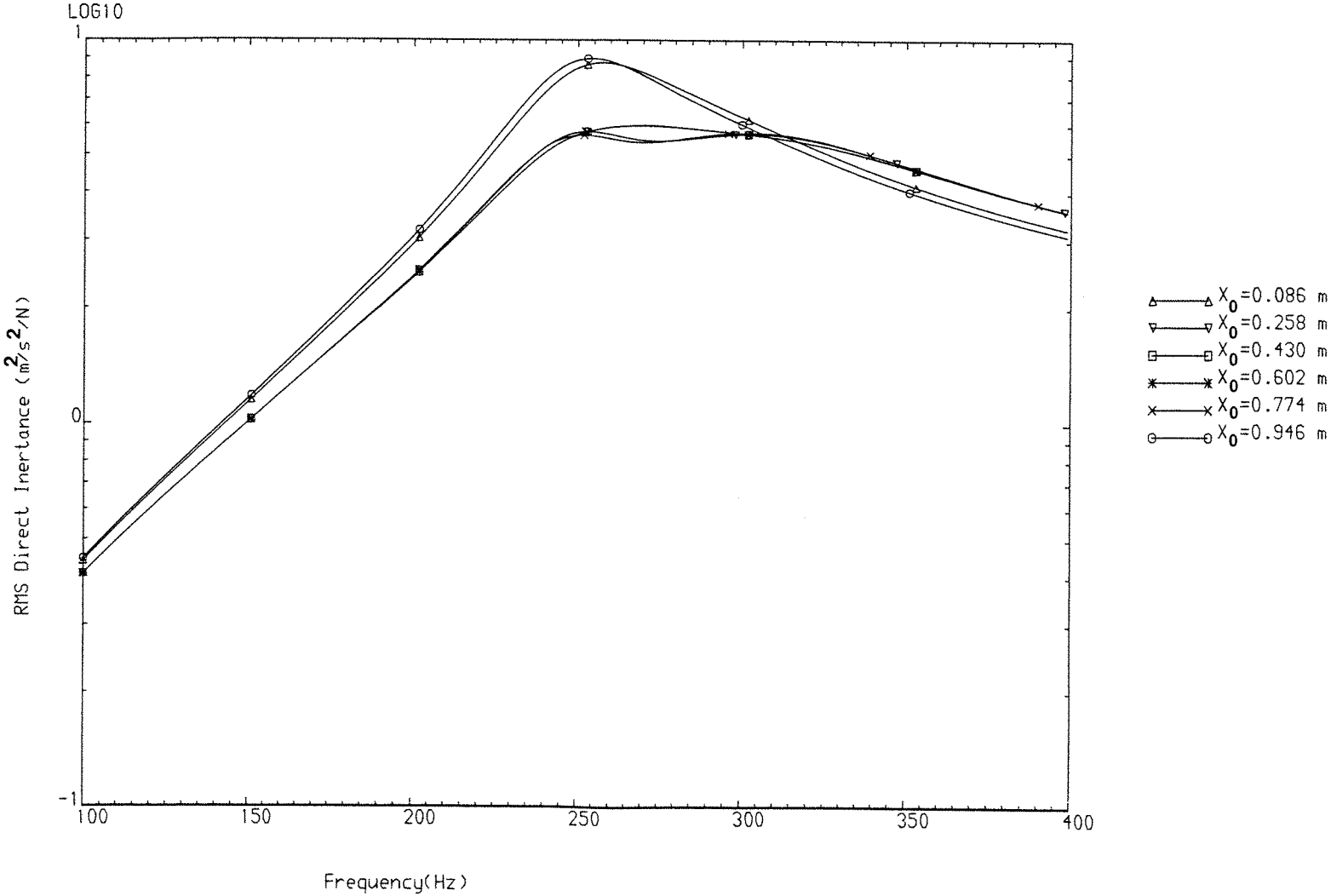

Fig. 46 **Magnitudes of Transverse Responses of Six Equal Bay, Three-Layered Sandwich Plate (β = 1, General Supports)**

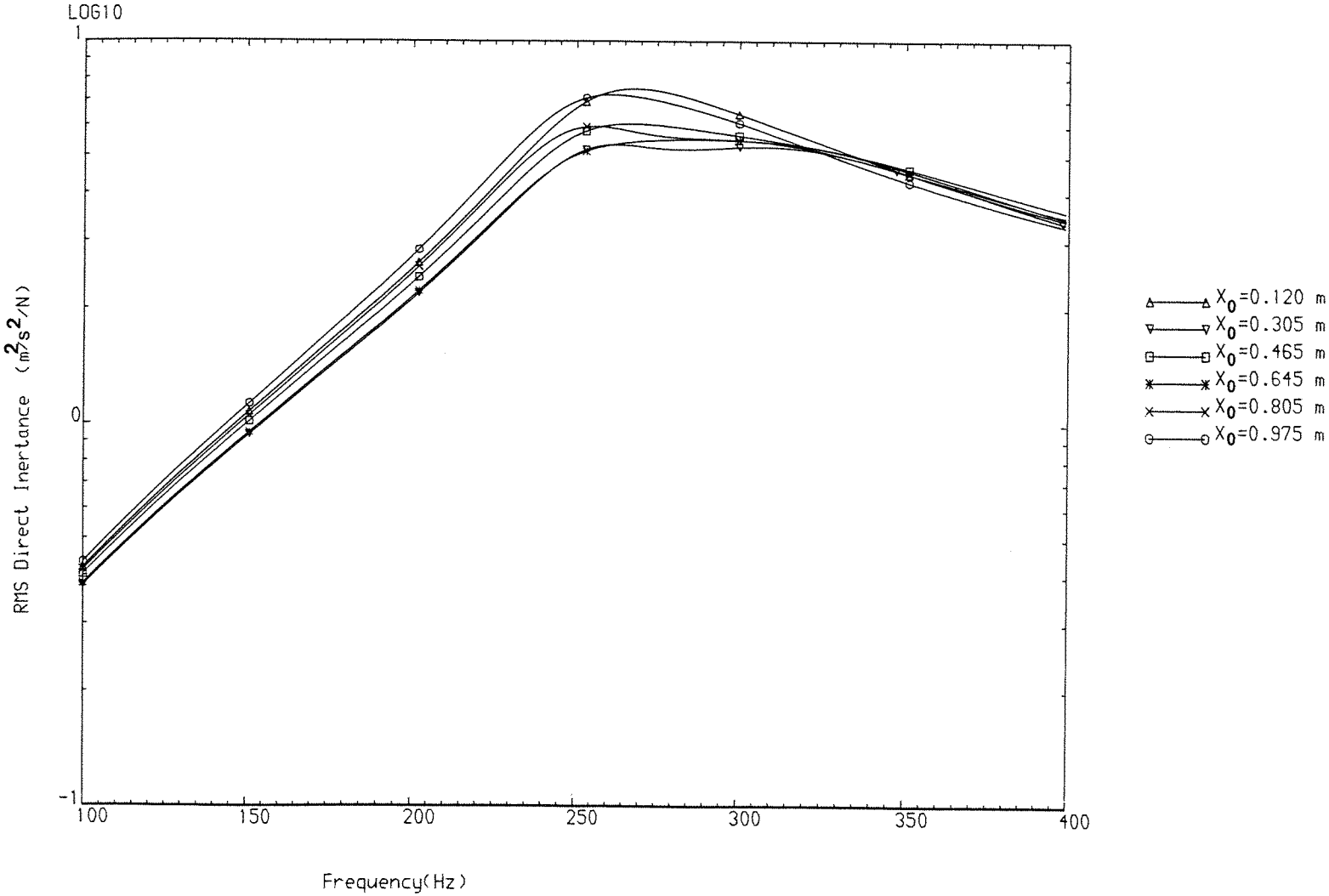

Fig. 47 **Magnitudes of Transverse Responses of Eight-Bay, Three-Layered Sandwich Plate (β = 1, General Supports)**

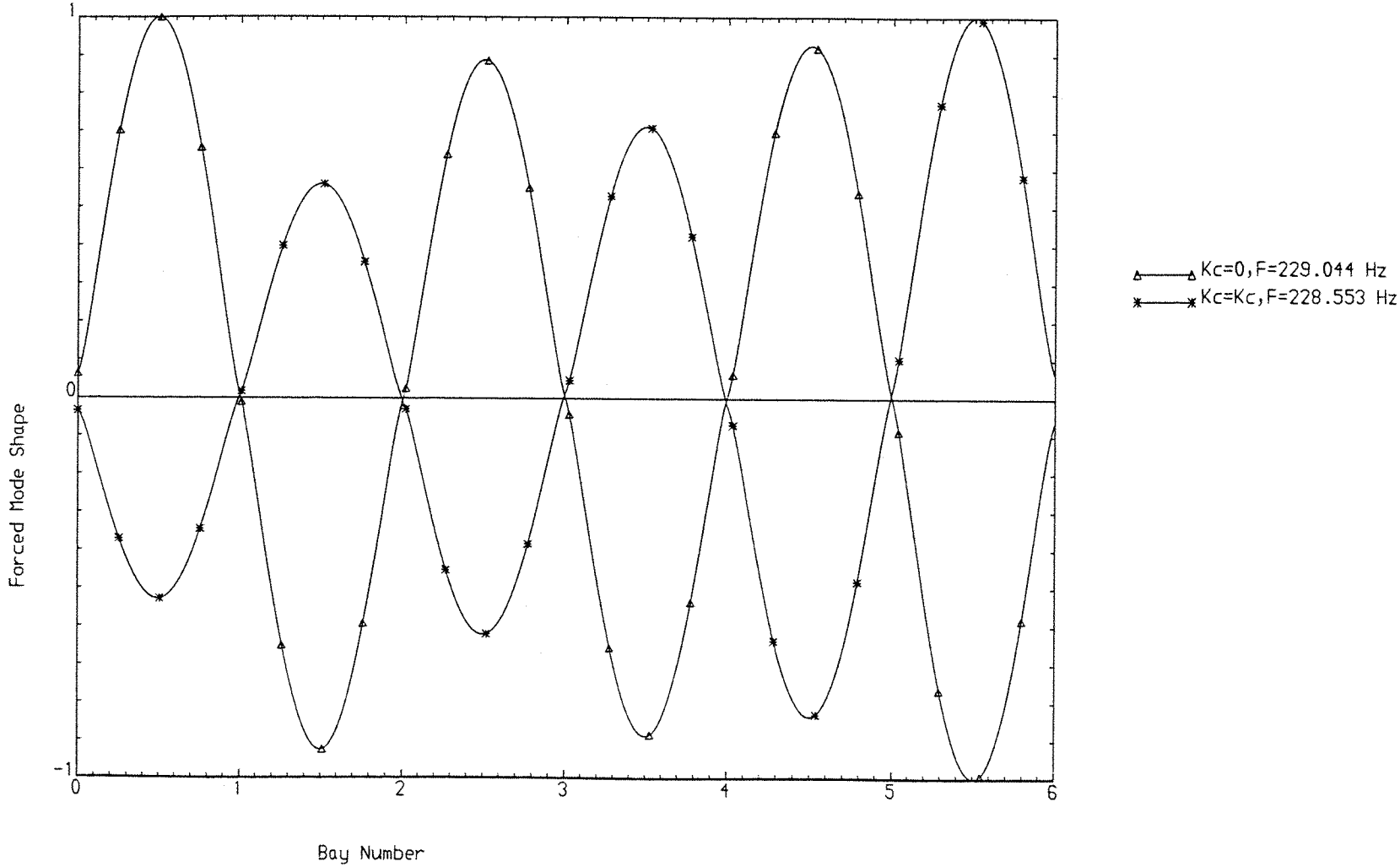

Fig. 48 First Forced Mode Shape of Six Equal Bay, Three-Layered Sandwich Plate (β = 0, General Supports, x_o = L/12)

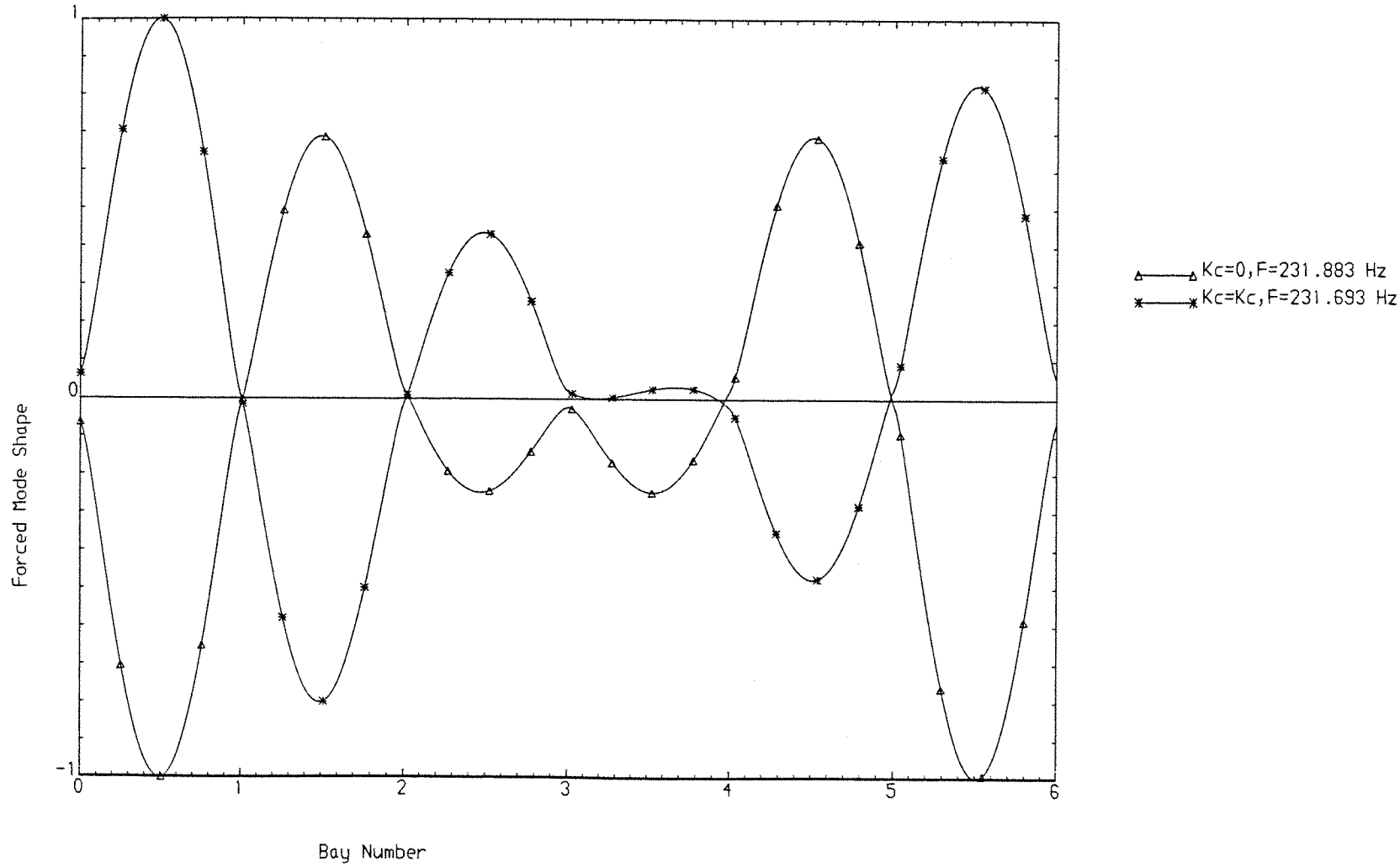

Fig. 49 Second Forced Mode Shape of Six Equal Bay, Three-Layered Sandwich Plate (β = 0, General Supports, x_o = L/12)

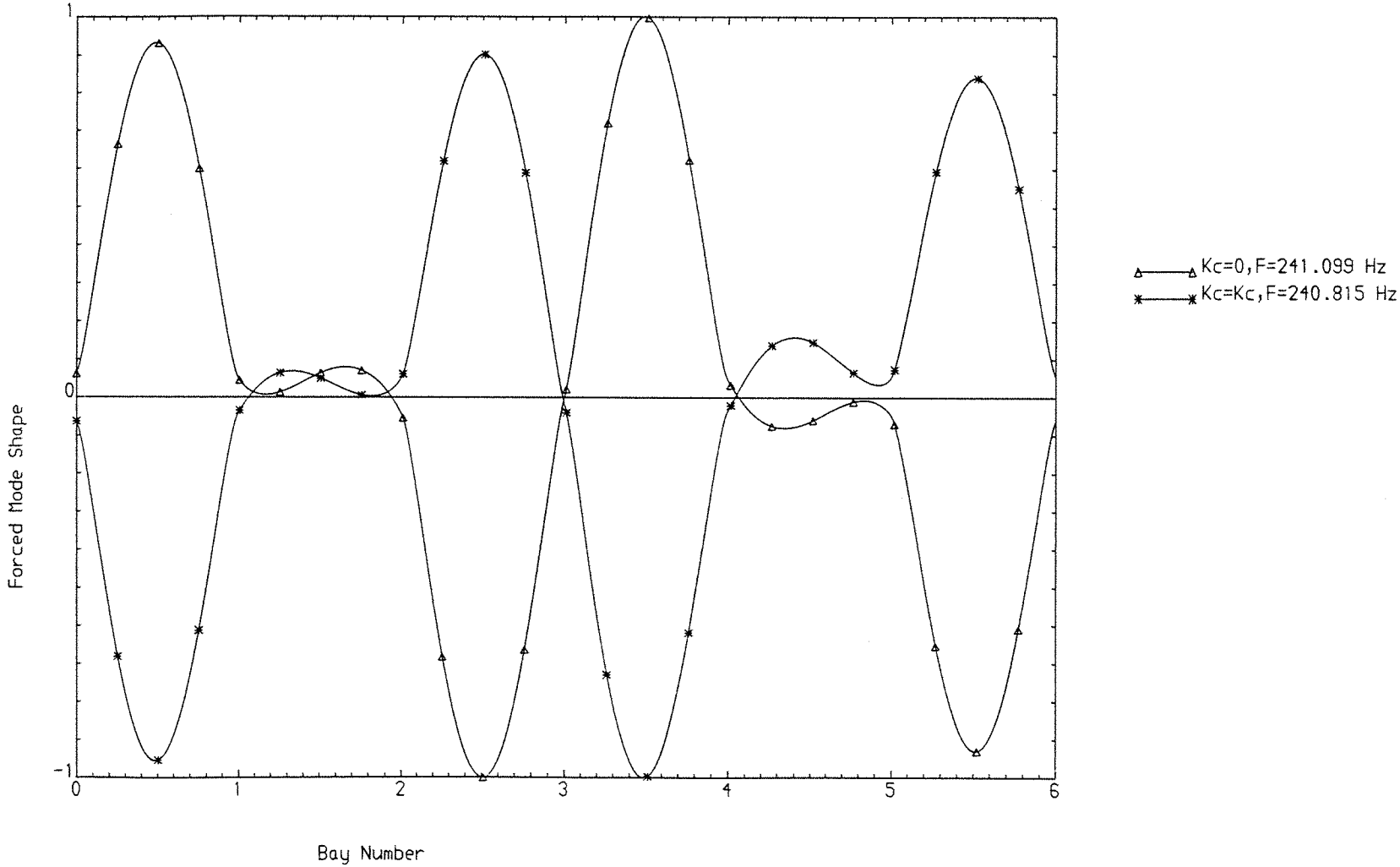

Fig. 50 Third Forced Mode Shape of Six Equal Bay, Three-Layered Sandwich Plate (β = 0, General Supports, x_o = L/12)

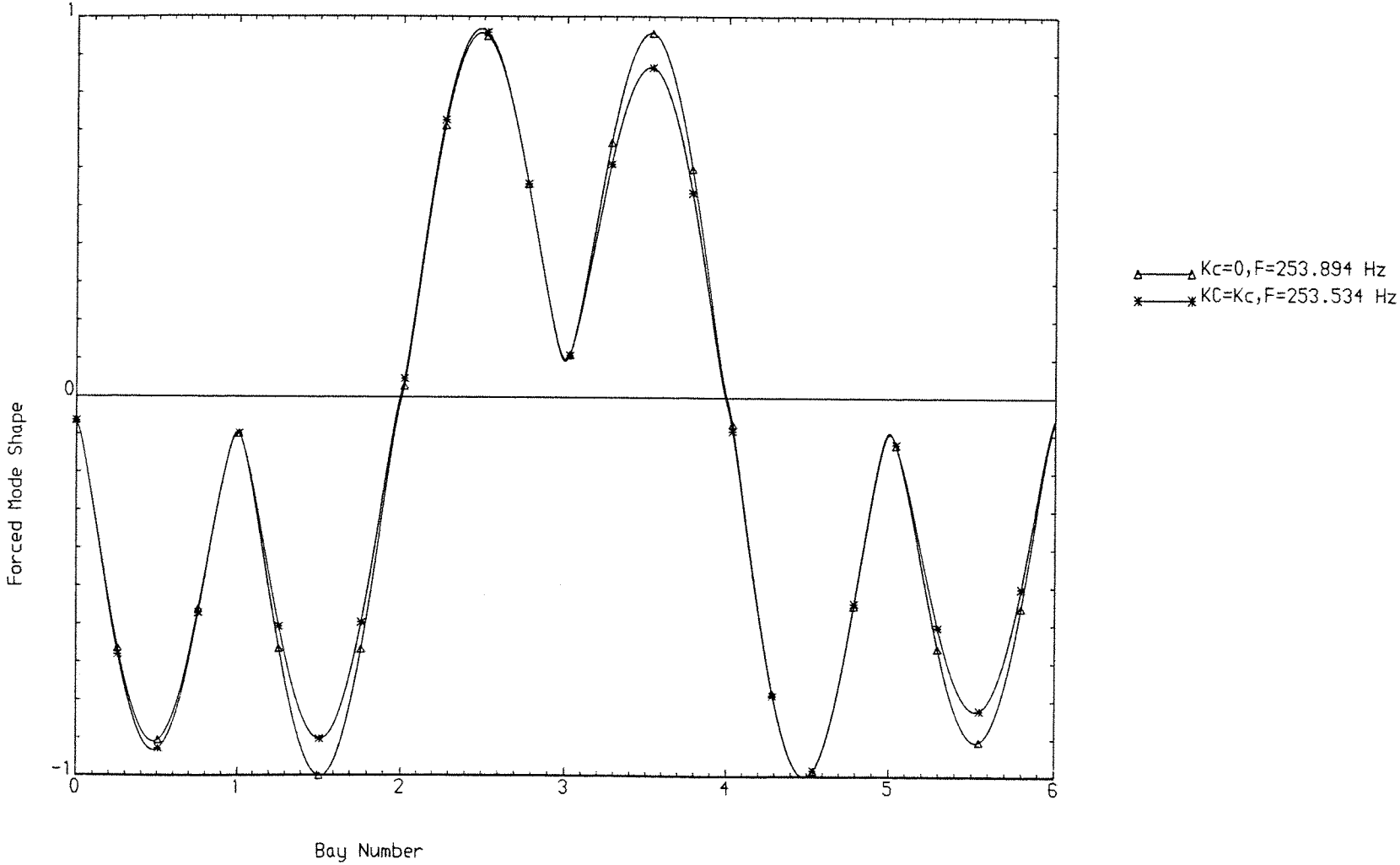

Fig. 51 Fourth Forced Mode Shape of Six Equal Bay, Three-Layered Sandwich Plate (β = 0, General Supports, x_o = L/12)

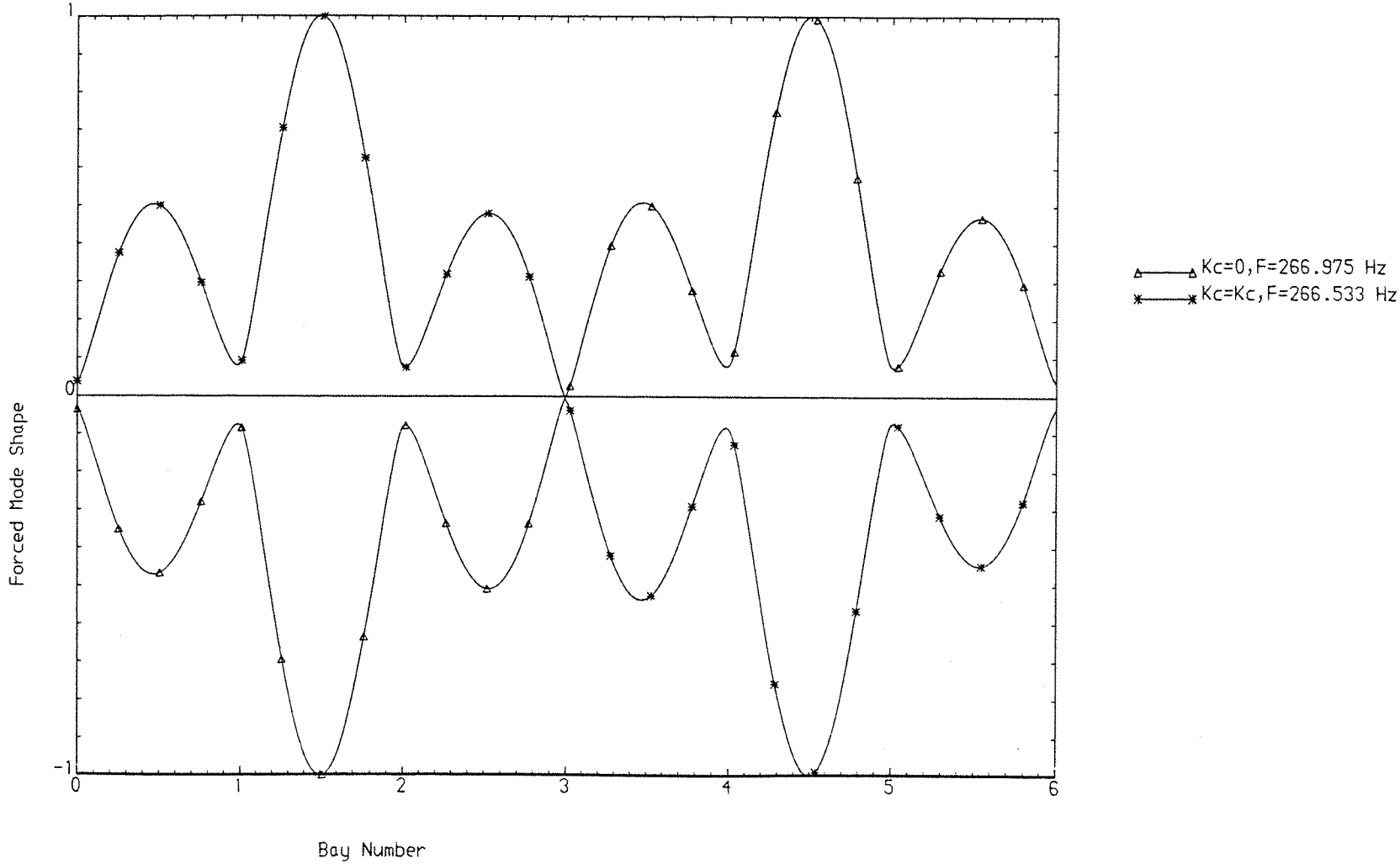

Fig. 52 Fifth Forced Mode Shape of Six Equal Bay, Three-Layered Sandwich Plate (β = 0, General Supports, x_o = L/12)

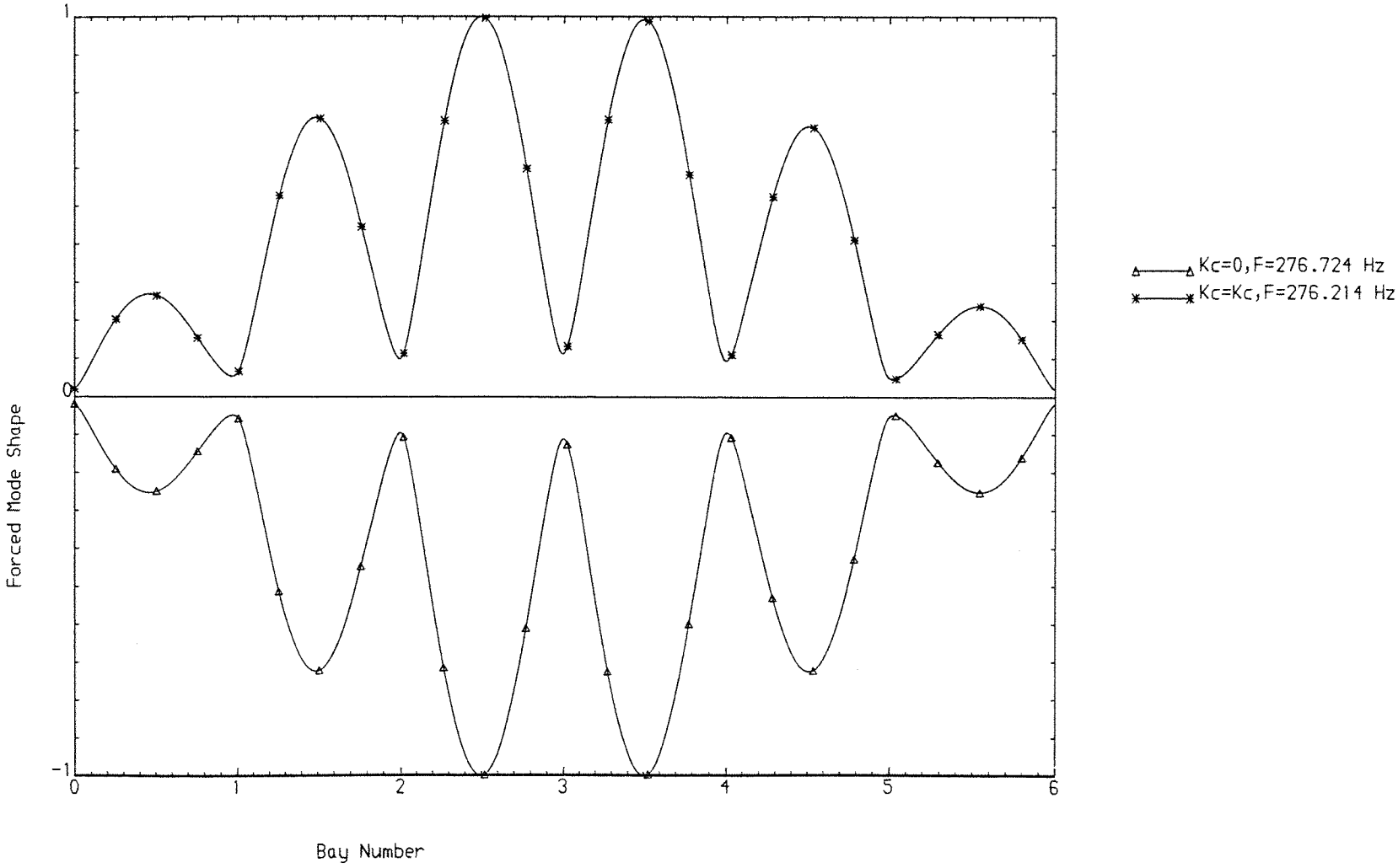

Fig. 53 Sixth Forced Mode Shape of Six Equal Bay, Three-Layered Sandwich Plate (β = 0, General Supports, x_o = L/12)

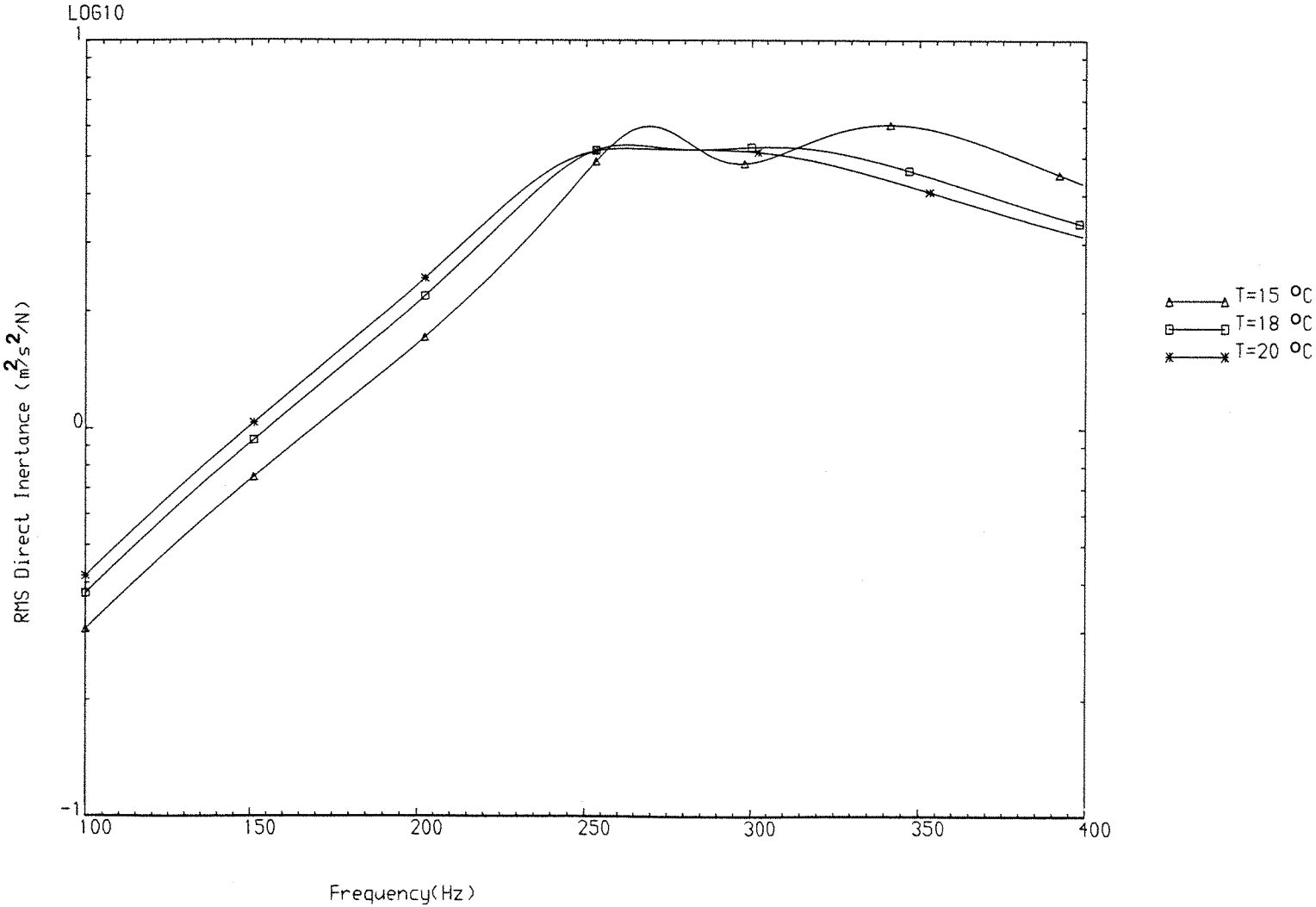

Fig. 54 Magnitudes of Transverse Responses of Eight-Bay, Three-Layered Sandwich Plate (β = 1, General Supports, x_o = 0.305 [m])

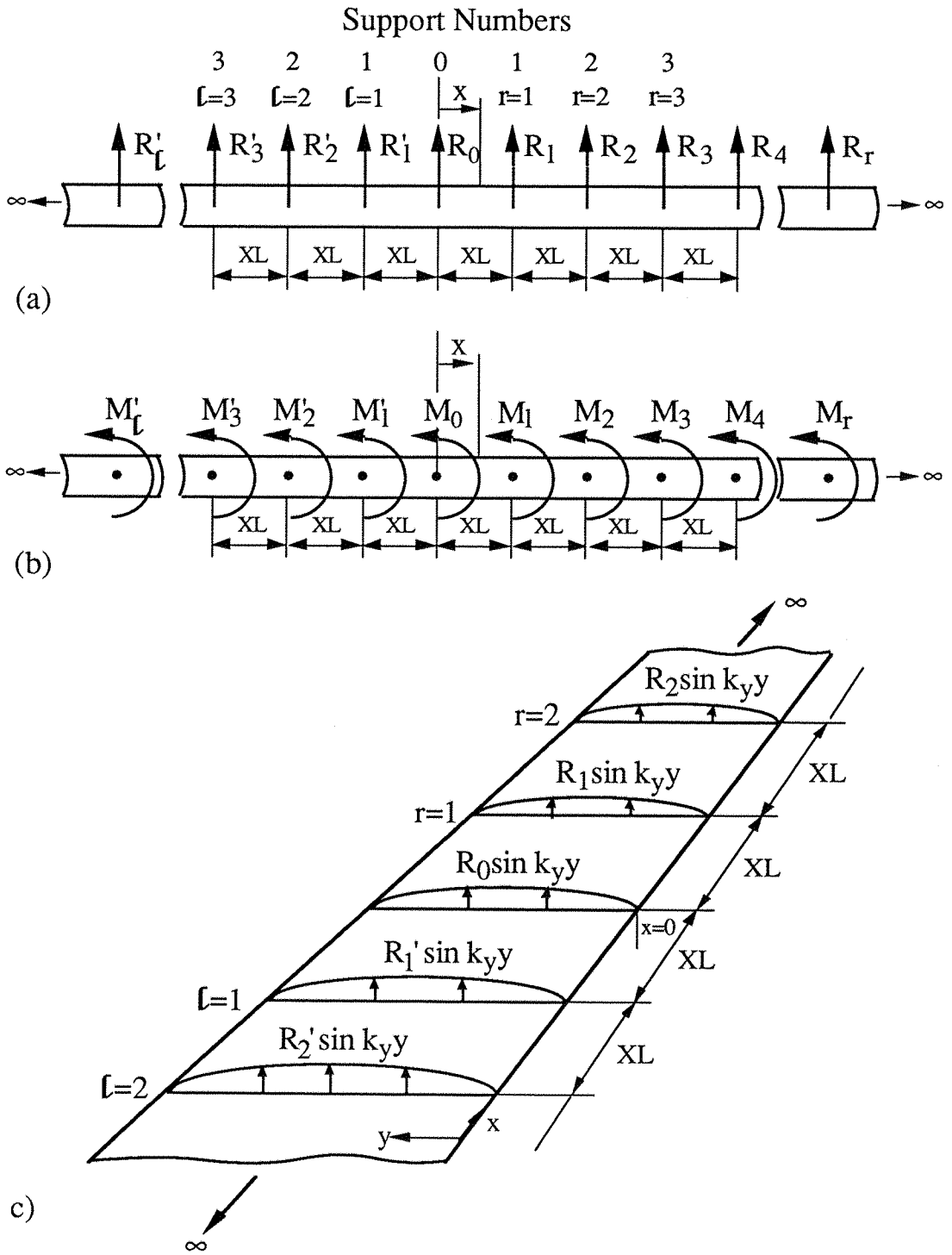

Figure 55: Infinite, Periodic Structures Under the Influence of Support Reactions

a) Array of Point Forces on Euler-Bernoulli Beam
b) Array of Point Moments on Euler-Bernoulli Beam
c) Array of Line Forces on Euler-Bernoulli Plate (m=1)

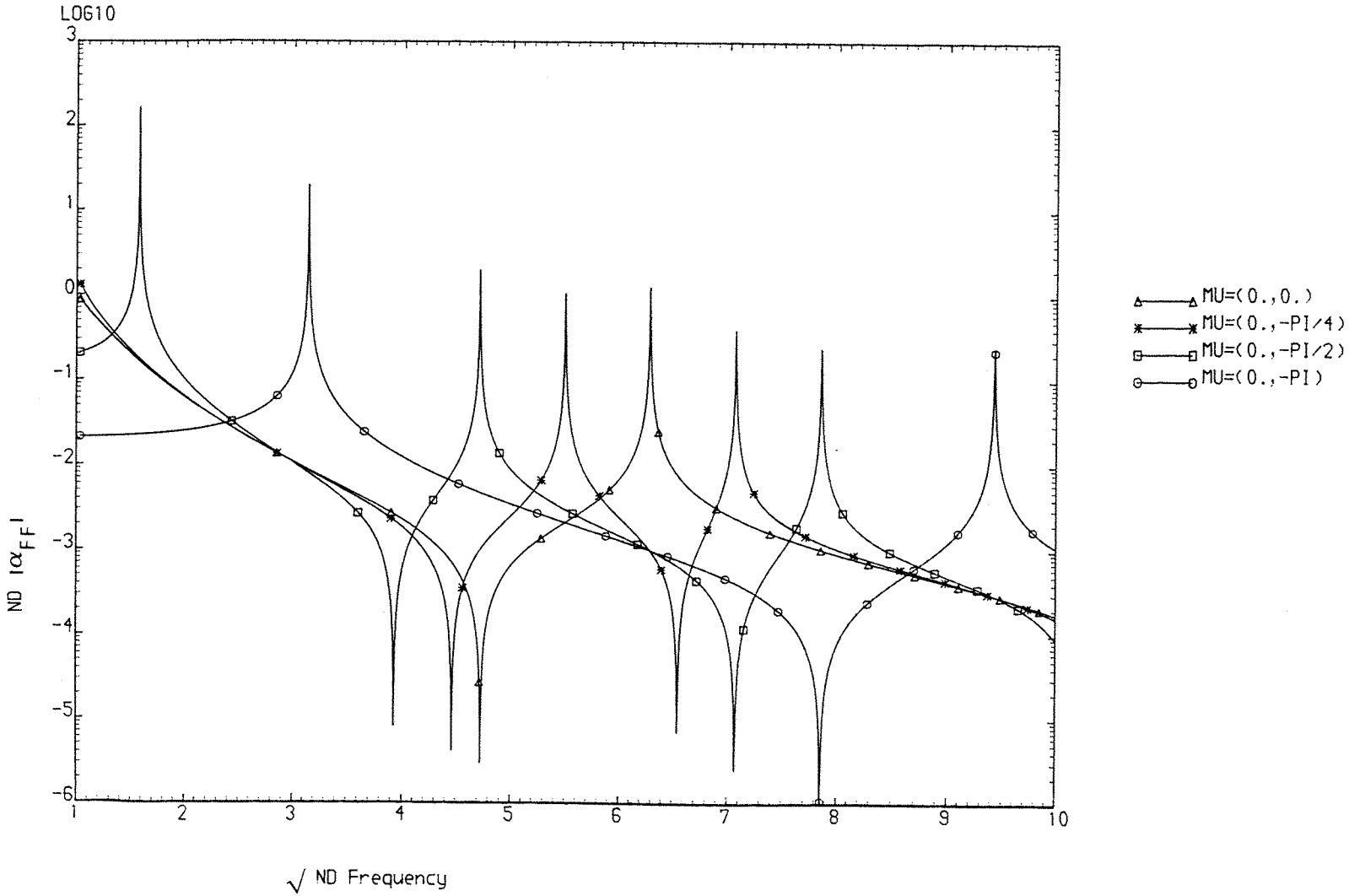

Fig. 56 Non-Dimensional Magnitudes of Phased Array Receptance Function α_{FF} of Infinite, Periodic Euler-Bernoulli Beam (η = 0.001)

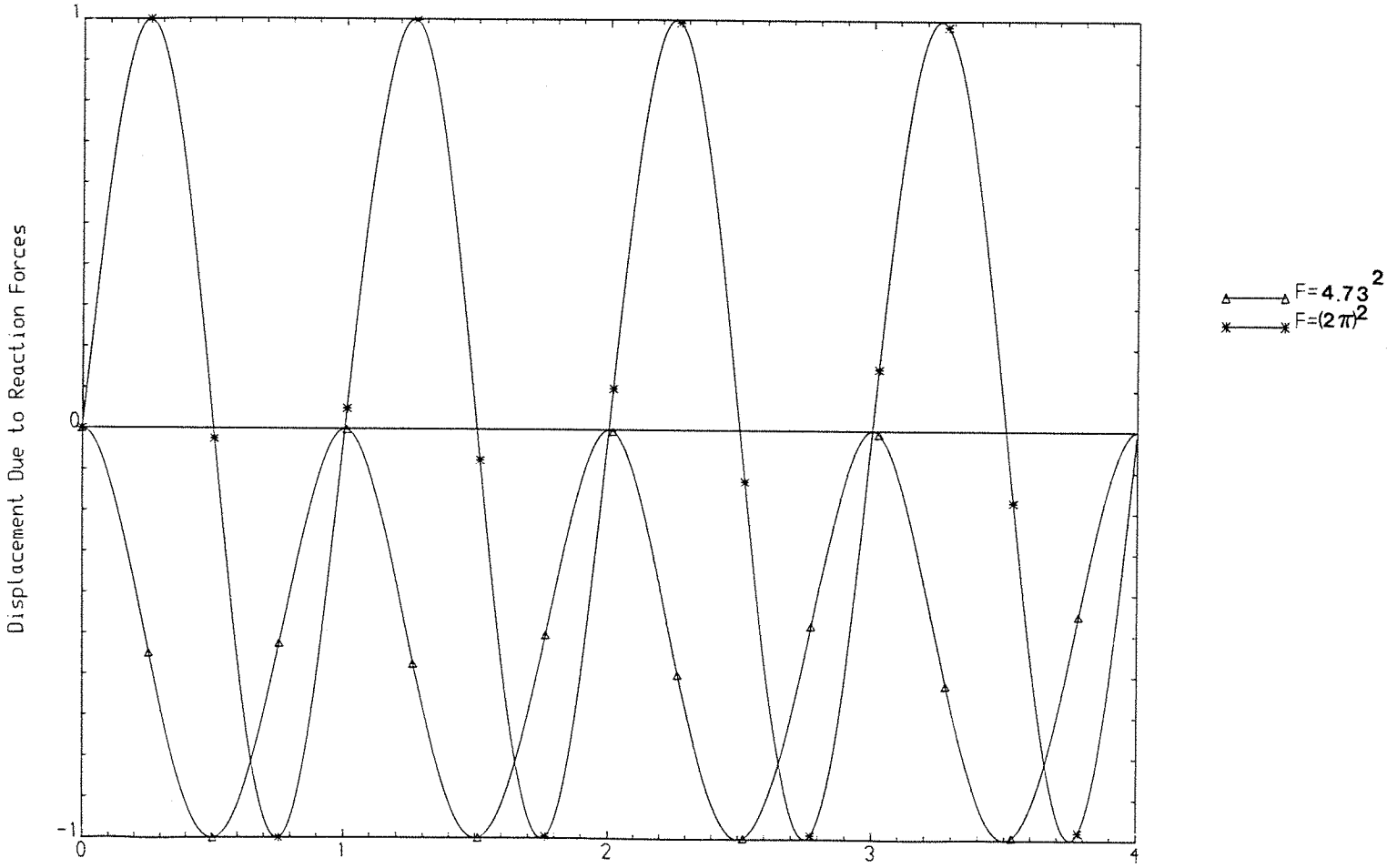

Fig. 57 Displacement of Infinite, Periodic Euler-Bernoulli Beam due to Reaction Forces (η = 0, Simple Supports, μ = (0.,0.))

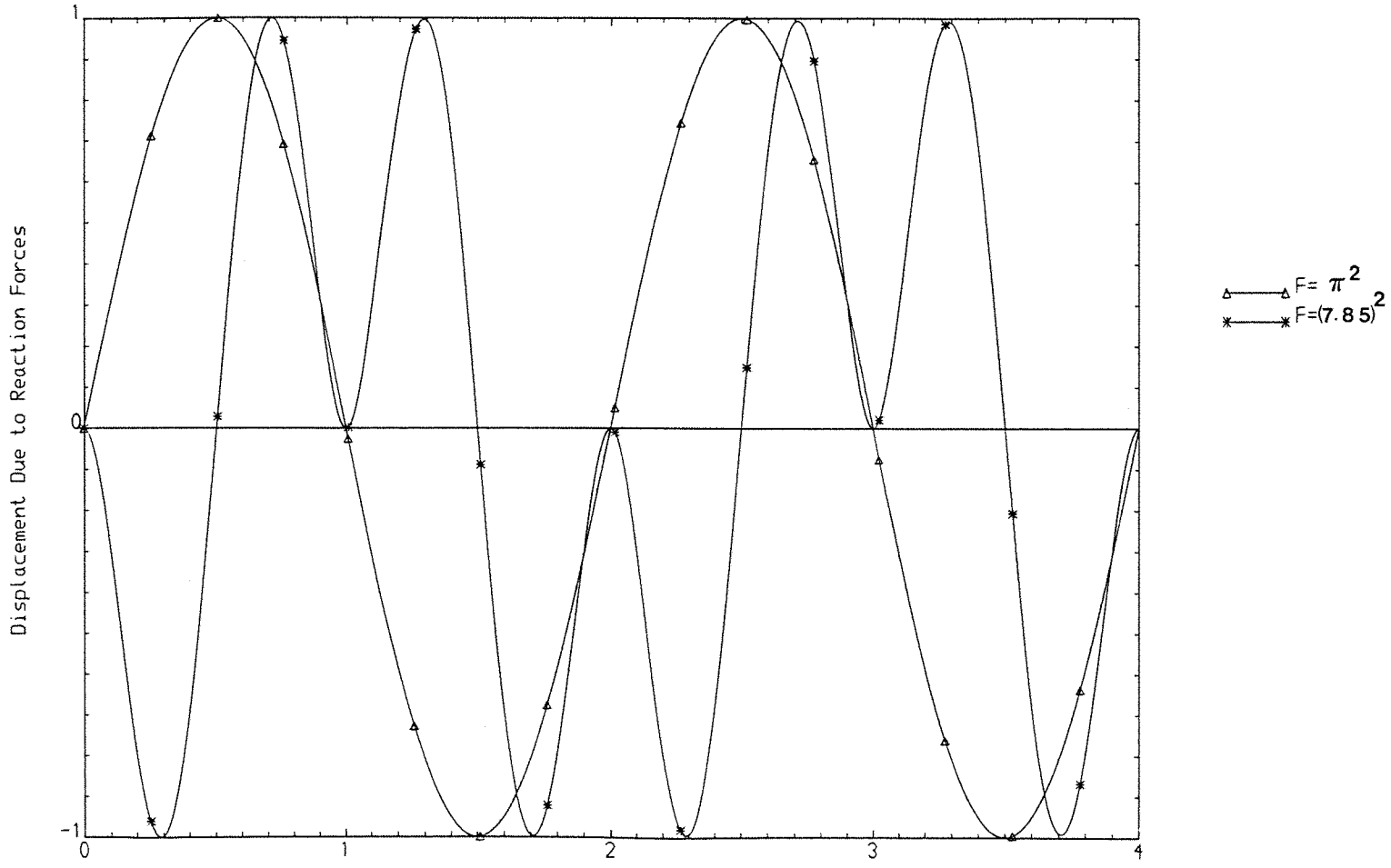

Fig. 58 Displacement of Infinite, Periodic Euler-Bernoulli Beam due to Reaction Forces (η = 0, Simple Supports, μ = (0.,$-\pi$))

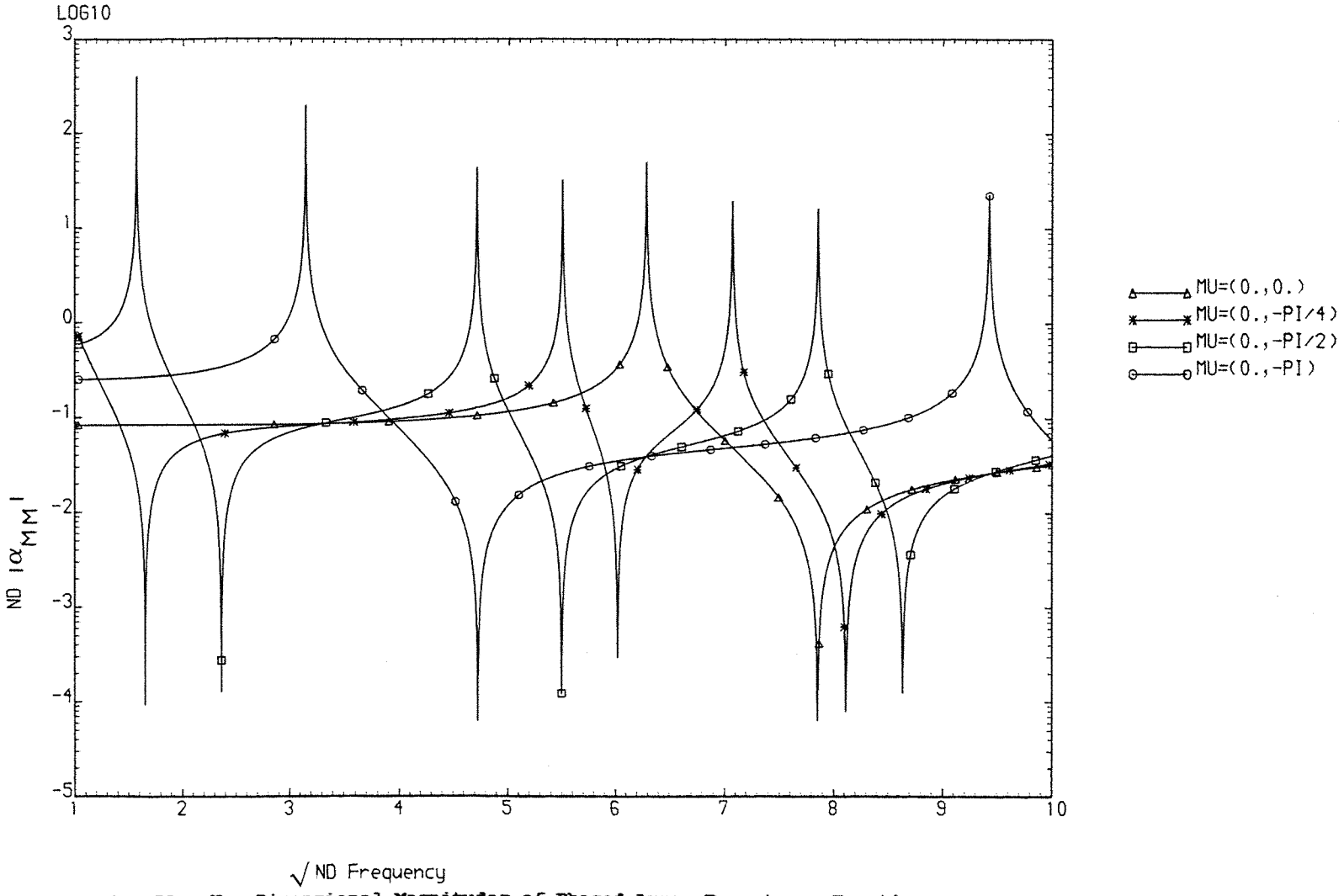

Fig. 59 **Non-Dimensional Magnitudes of Phased Array Receptance Function α_{MM} of Infinite, Periodic Euler-Bernoulli Beam (η = 0.001)**

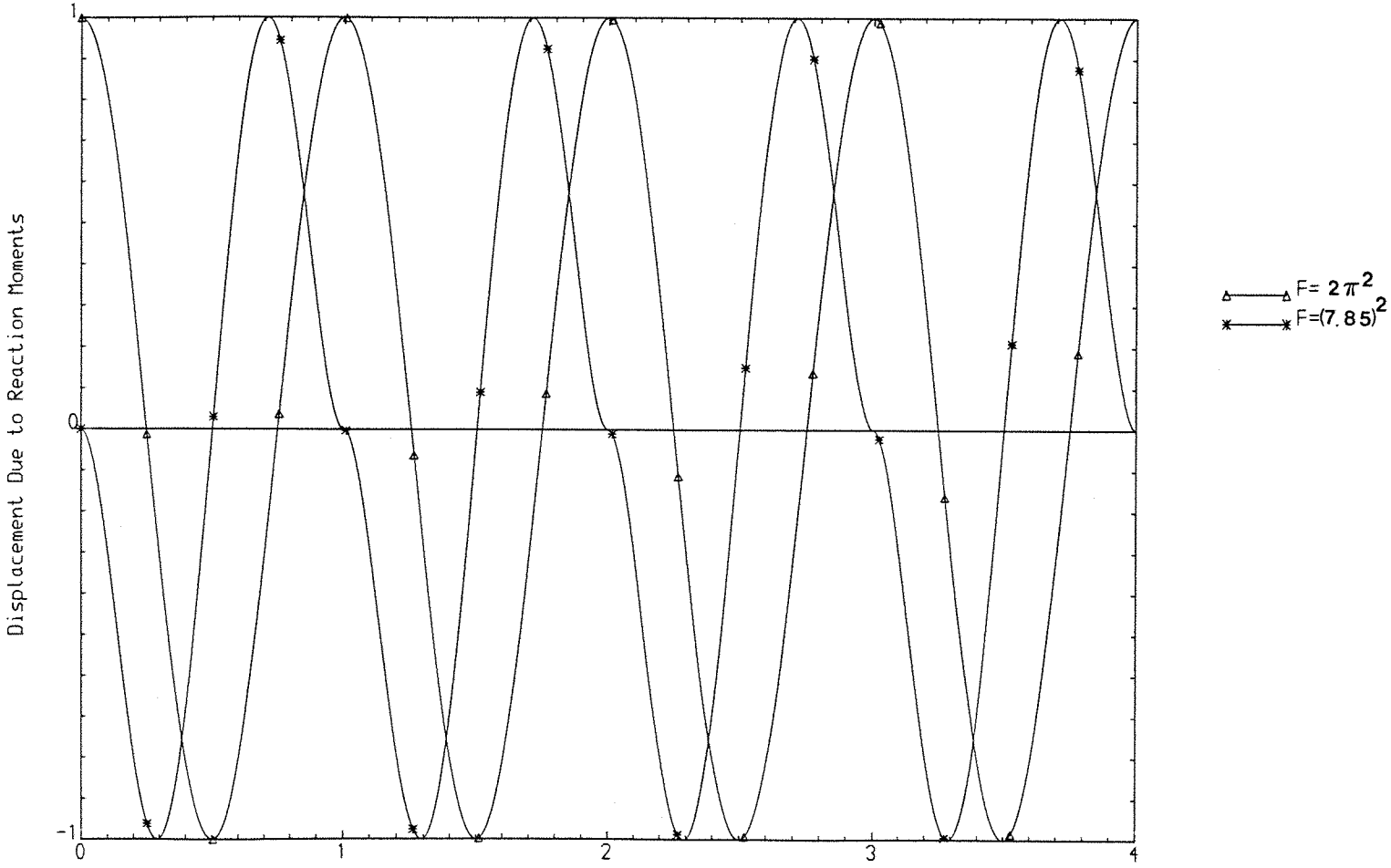

Fig. 60 Displacement of Infinite, Periodic Euler-Bernoulli Beam due to Reaction Moments (η = 0, Sliding Supports, μ = (0.,0.))

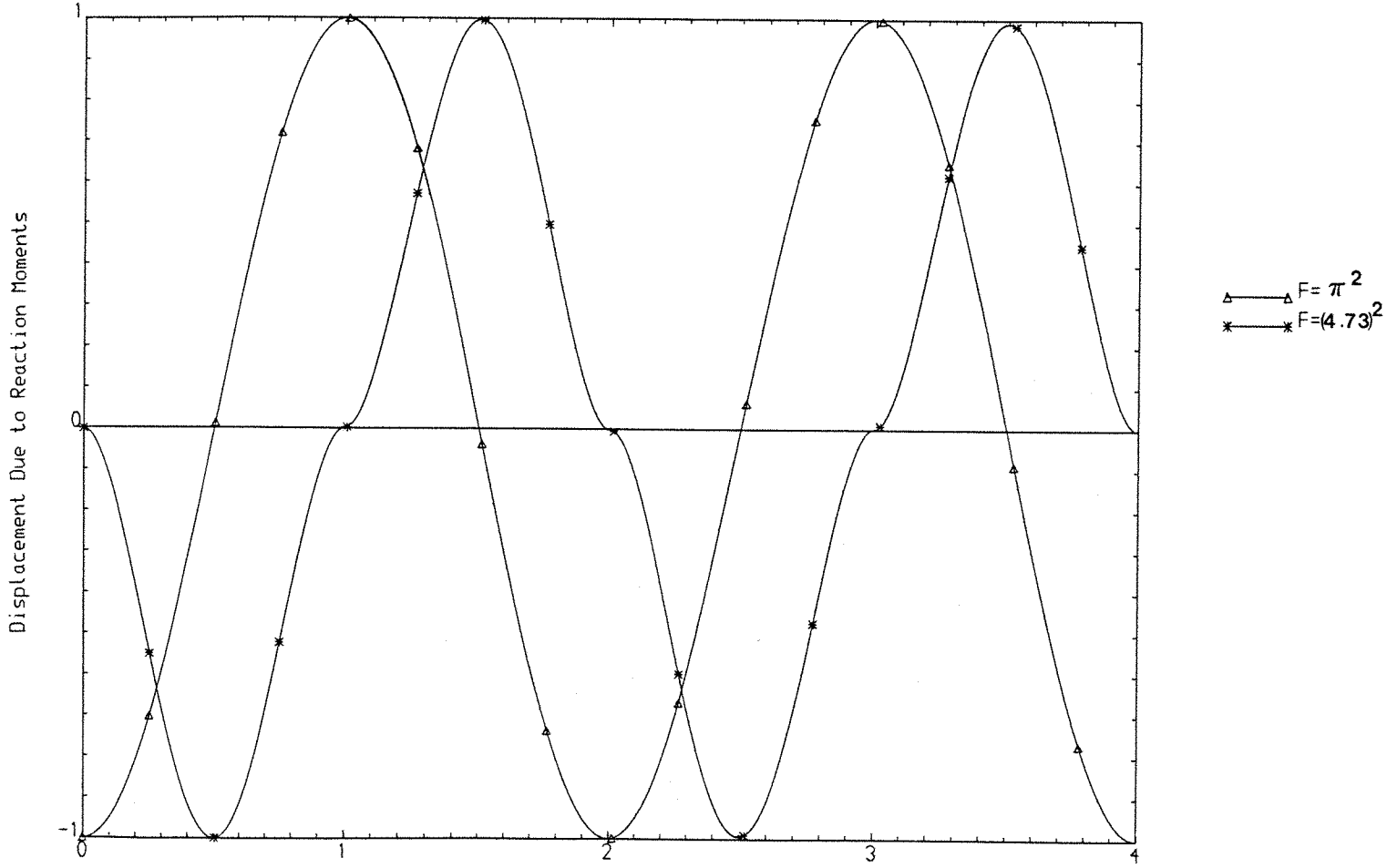

Fig. 61 Displacement of Infinite, Periodic Euler-Bernoulli Beam due to Reaction Moments (η = 0, Sliding Supports, μ = (0.,$-\pi$))

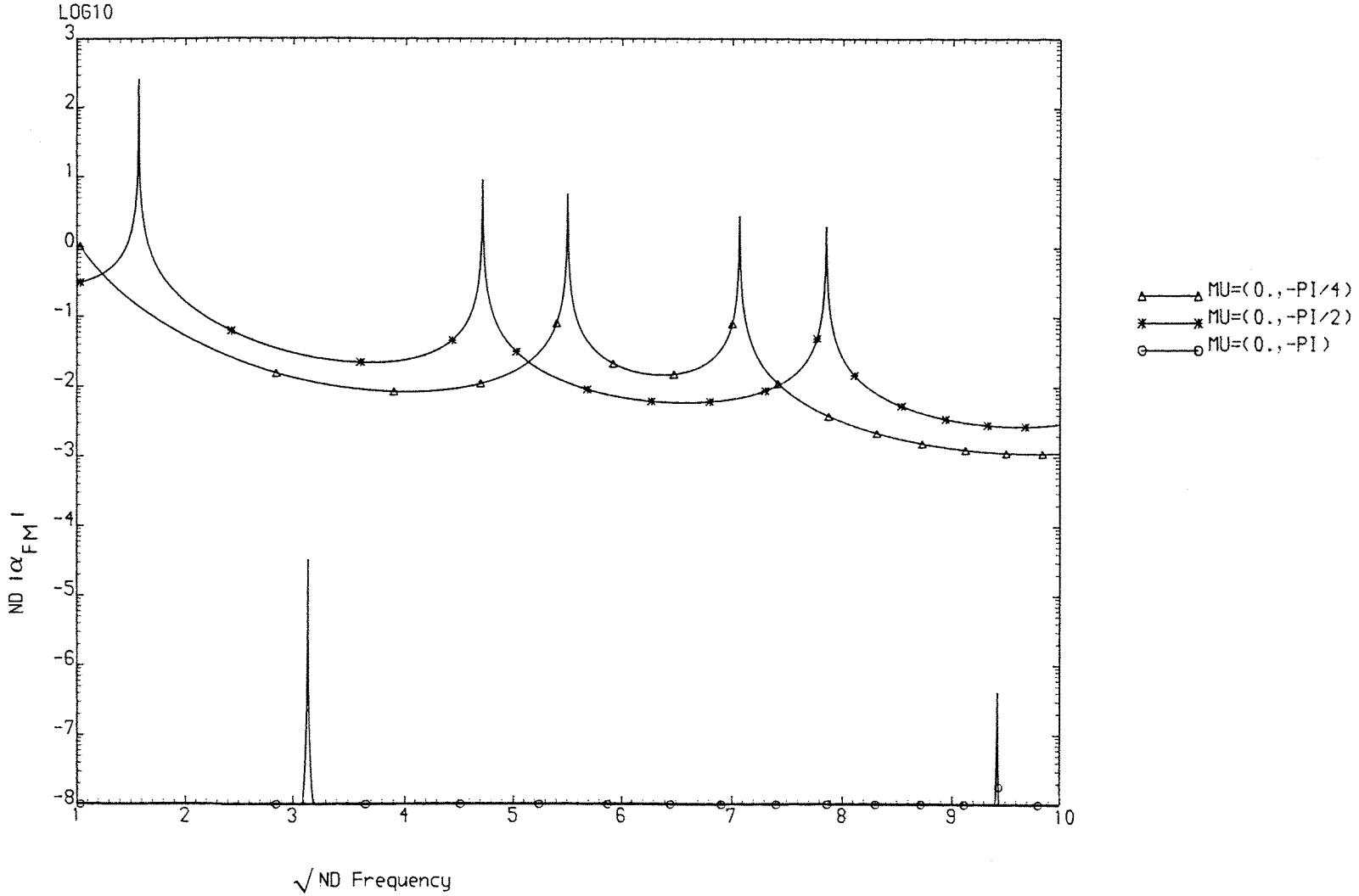

Fig. 62 Non-Dimensional Magnitudes of Phased Array Receptance Function α_{FM} of Infinite, Periodic Euler-Bernoulli Beam (η = 0.001)

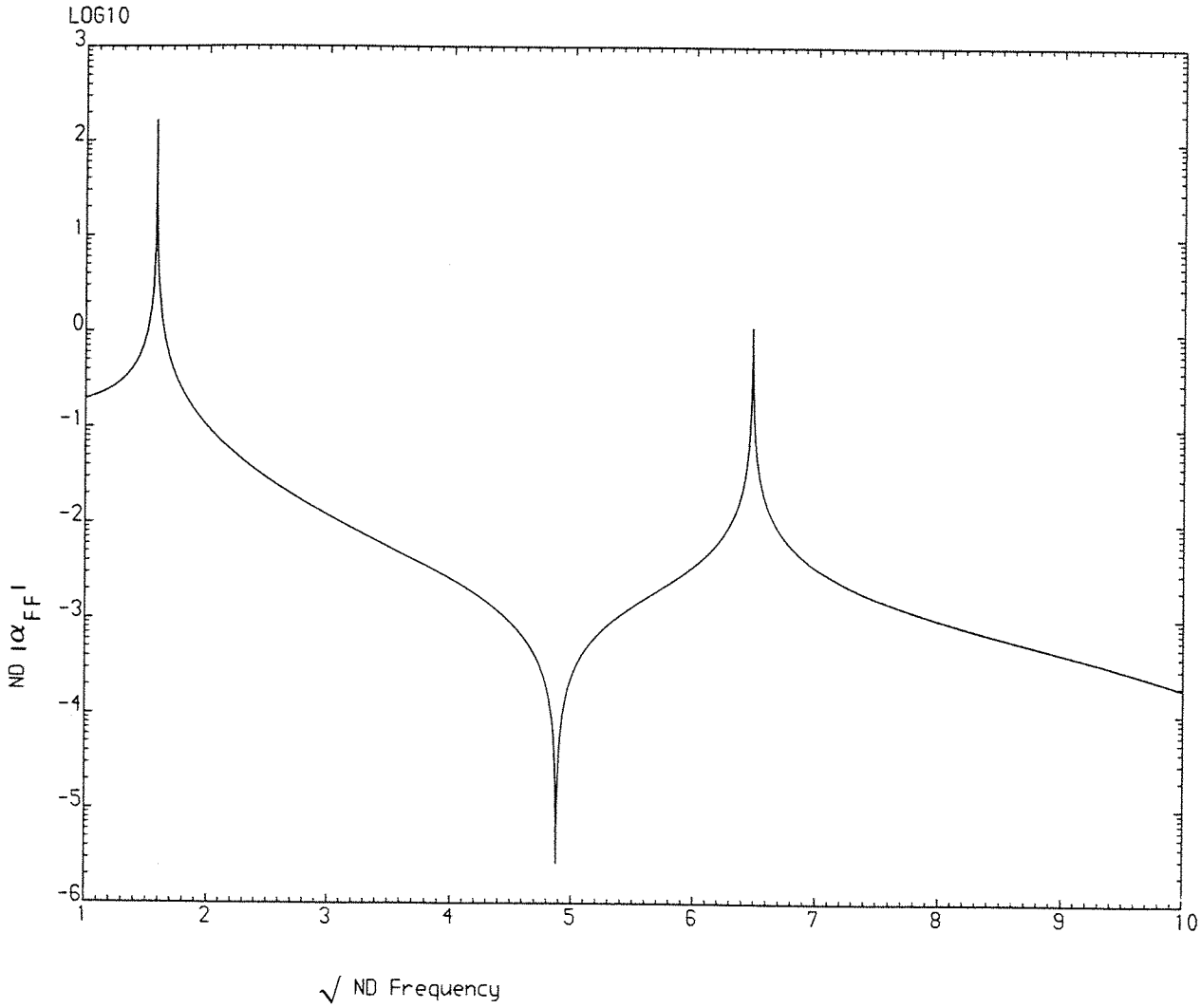

Fig. 63 Non-Dimensional Magnitude of Phased Array Receptance Function α_{FF} of Infinite, Periodic, Euler-Bernoulli Plate (η = 0.001,μ = (0.,0.))

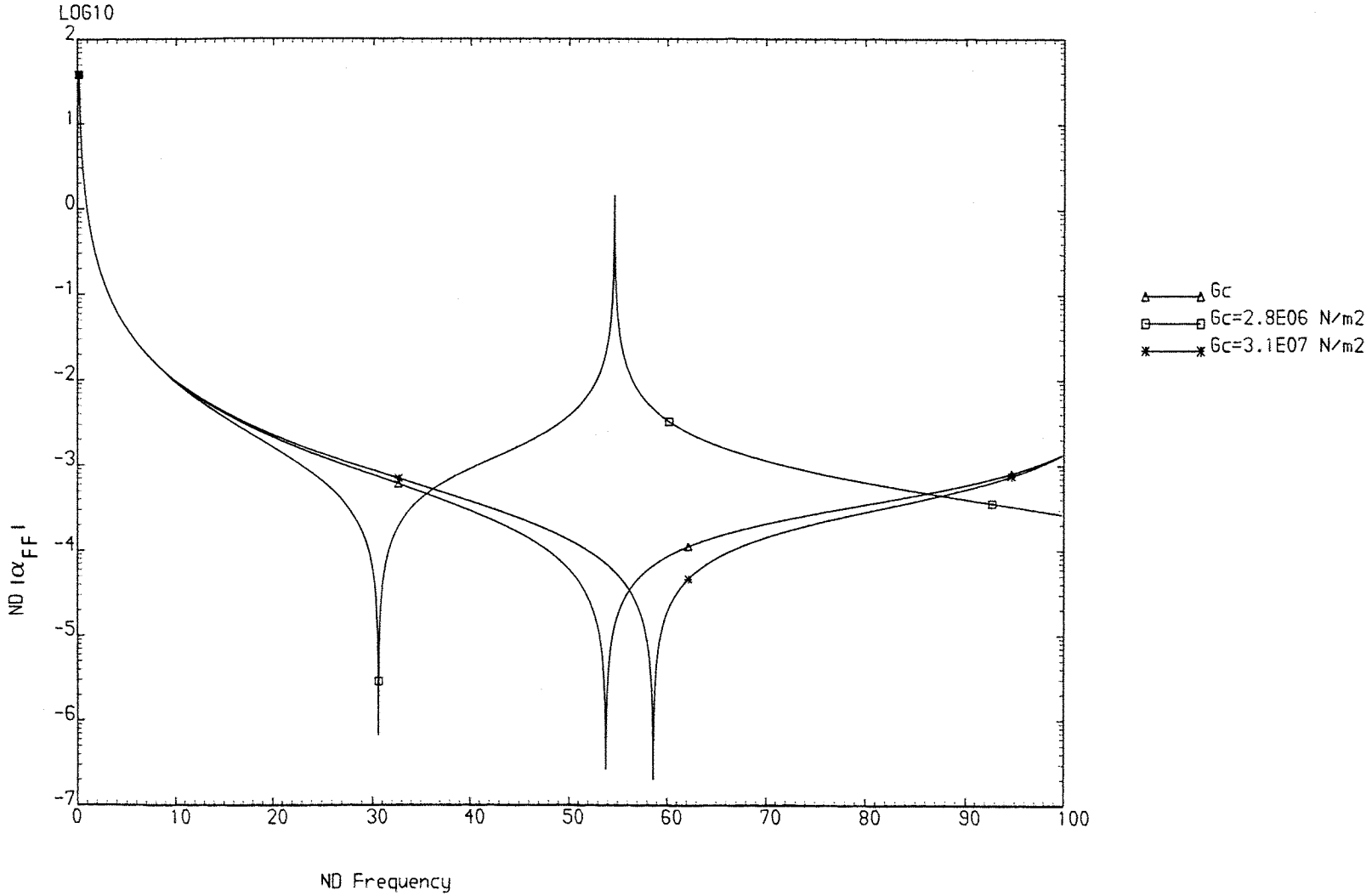

Fig. 64 Non-Dimensional Magnitudes of Phased Array Receptance Function α_{FF} of Infinite, Periodic, Three-Layered Sandwich Beam(β=0.001, μ=(0.,0.))

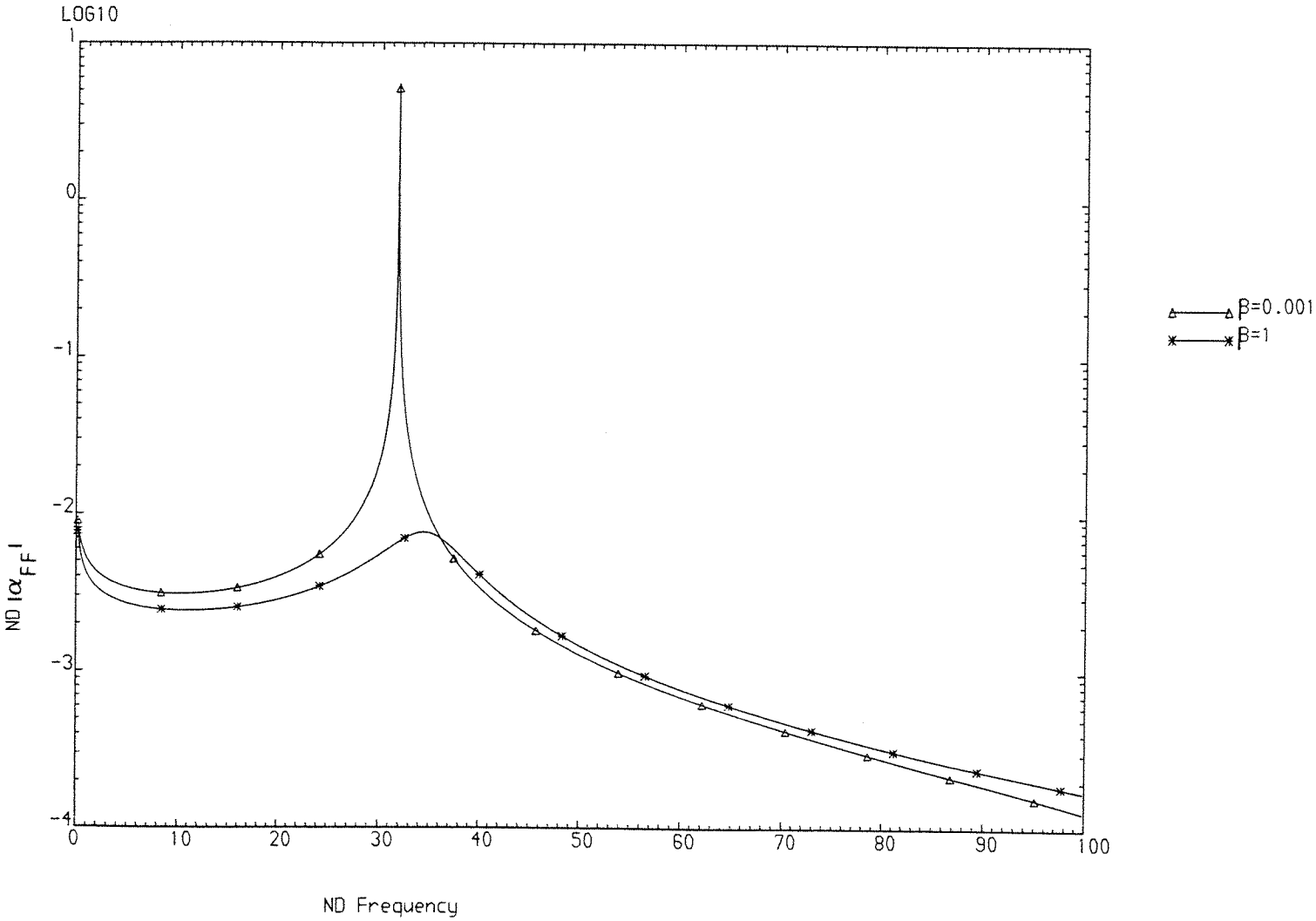

Fig. 65 Non-Dimensional Magnitudes of Phased Array Receptance Function α_{FP} of Infinite, Periodic, Three-Layered Sandwich Beam (μ = (0.,-π))

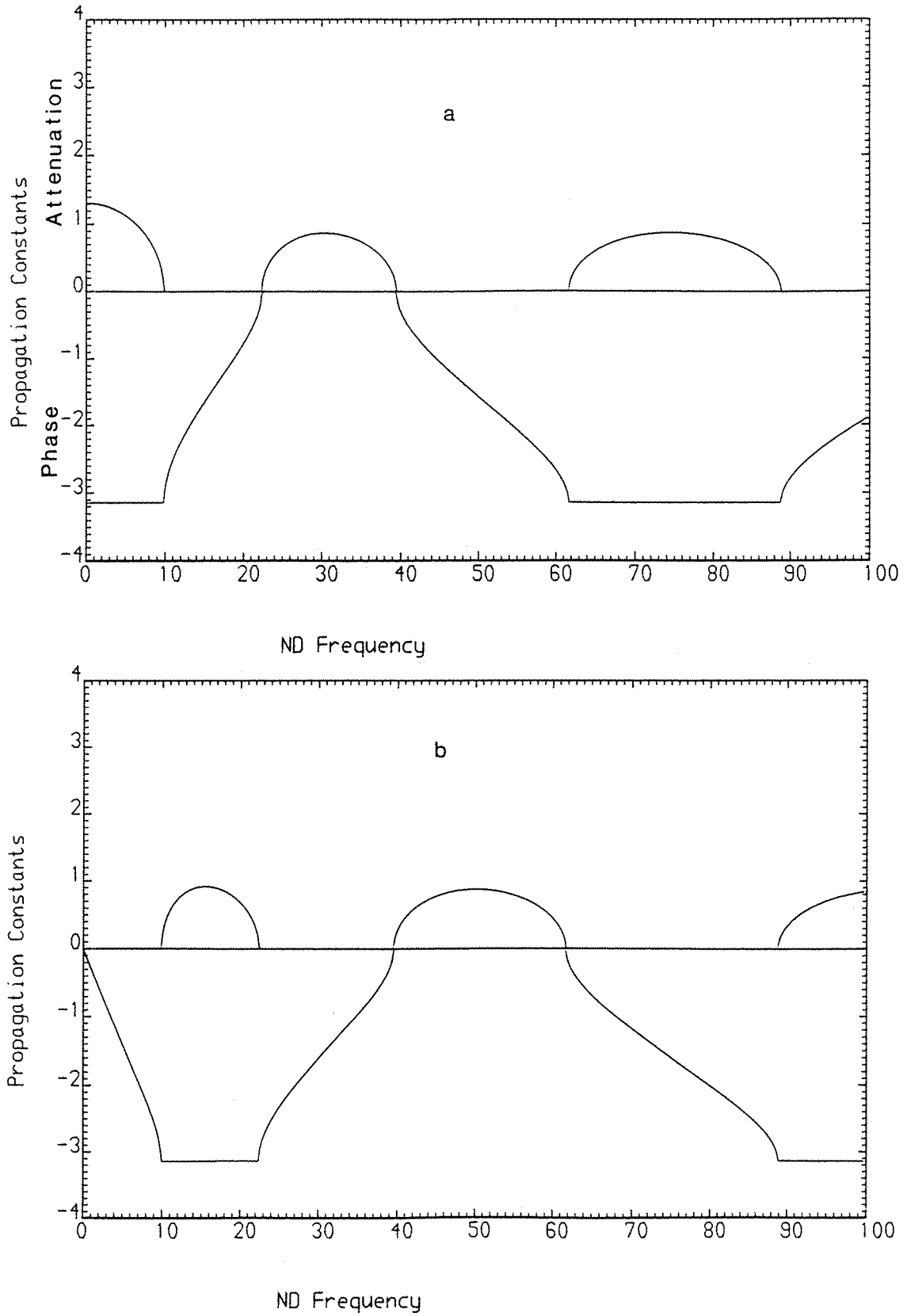

Fig. 66 Propagation Constants of Infinite, Periodic Euler-Bernoulli Beam ($\eta = 0$) (a) Simple Supports (b) Sliding Supports

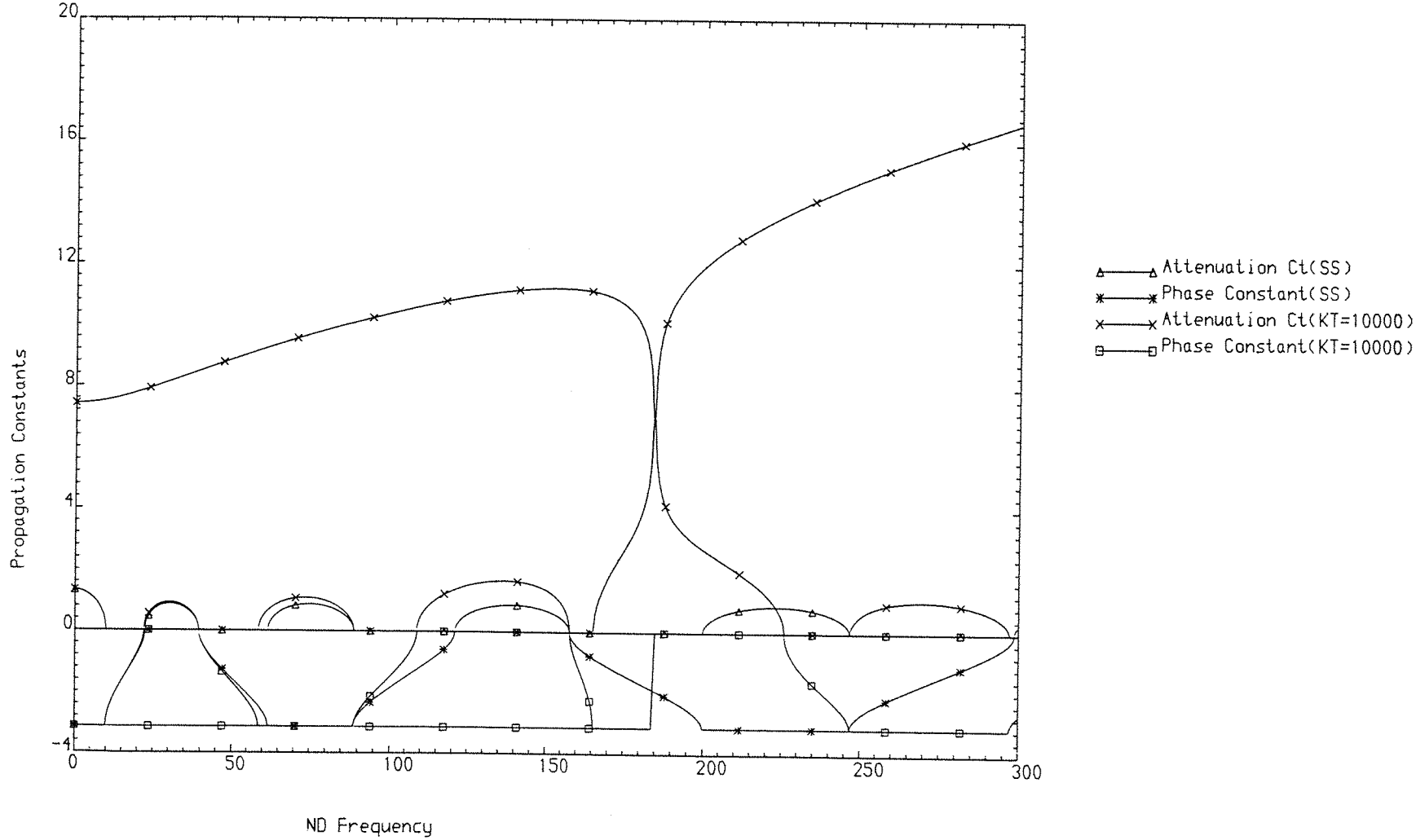

Fig. 67 Propagation Constants of Infinite, Periodic Euler-Bernoulli Beam ($\eta = 0$)

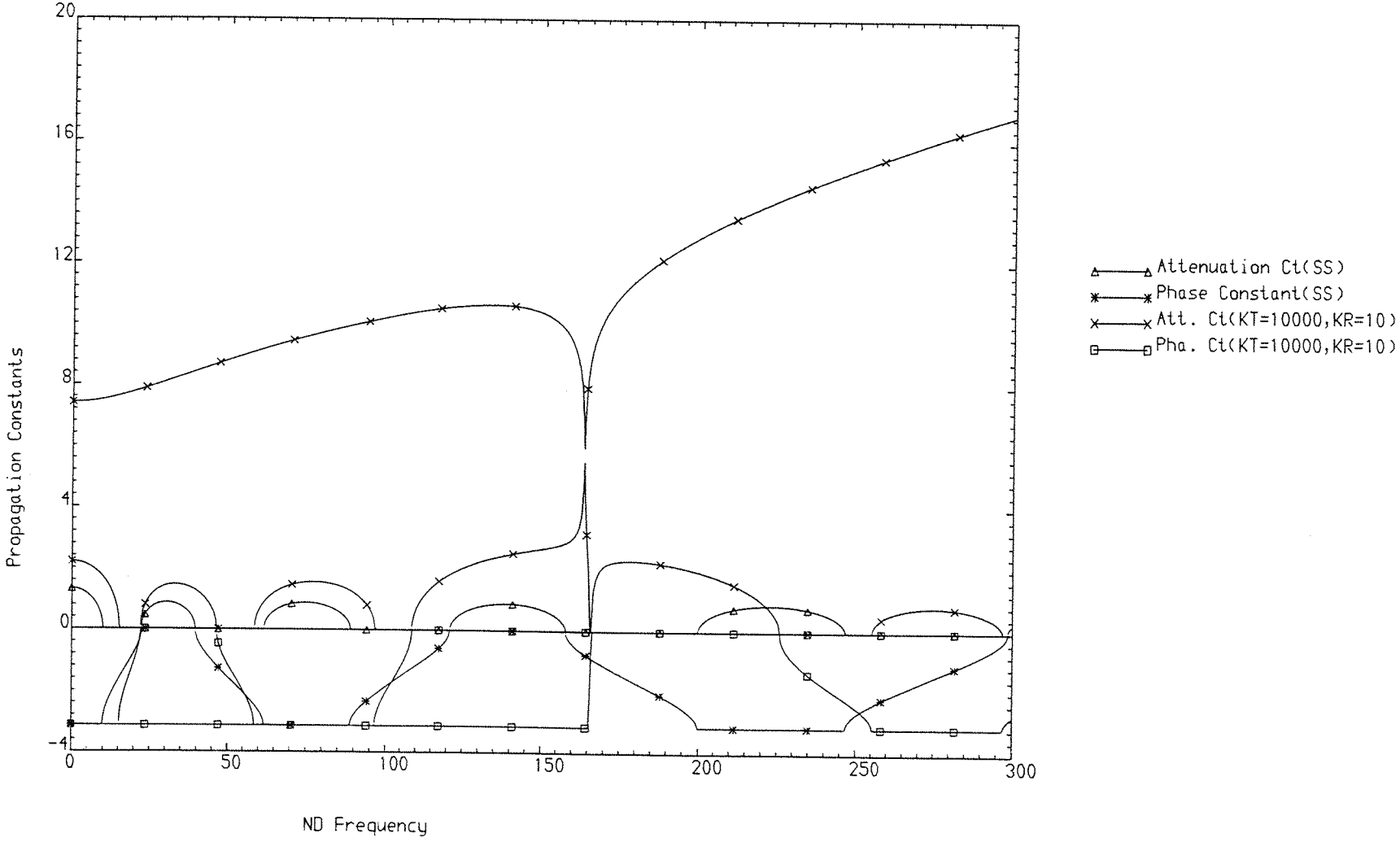

Fig. 68 **Propagation Constants of Infinite, Periodic Euler-Bernoulli Beam (η = 0)**

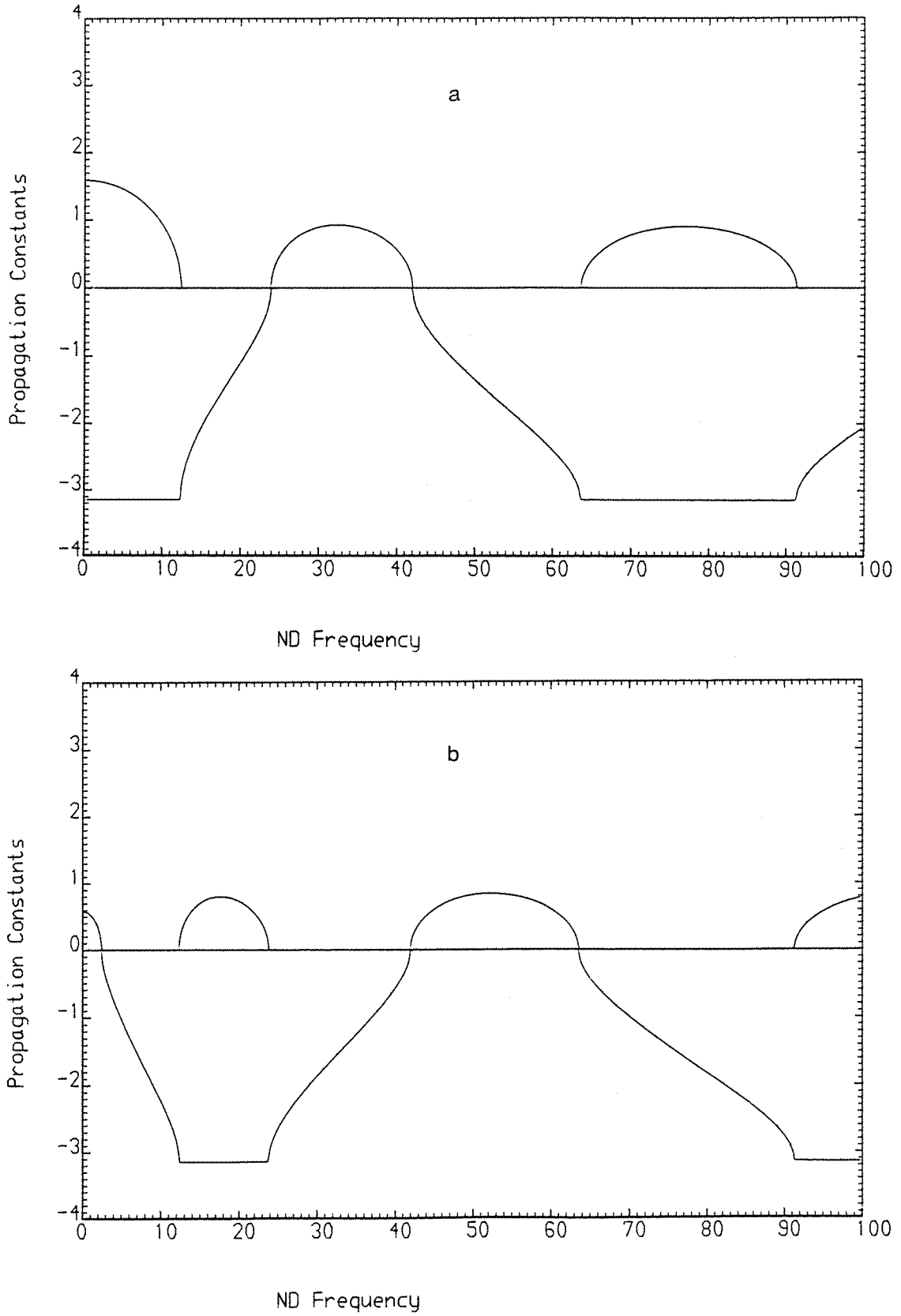

Fig. 69 Propagation Constants of Infinite, Periodic Euler-Bernoulli Plate (η = 0) (a) Simple Supports (b) Sliding Supports

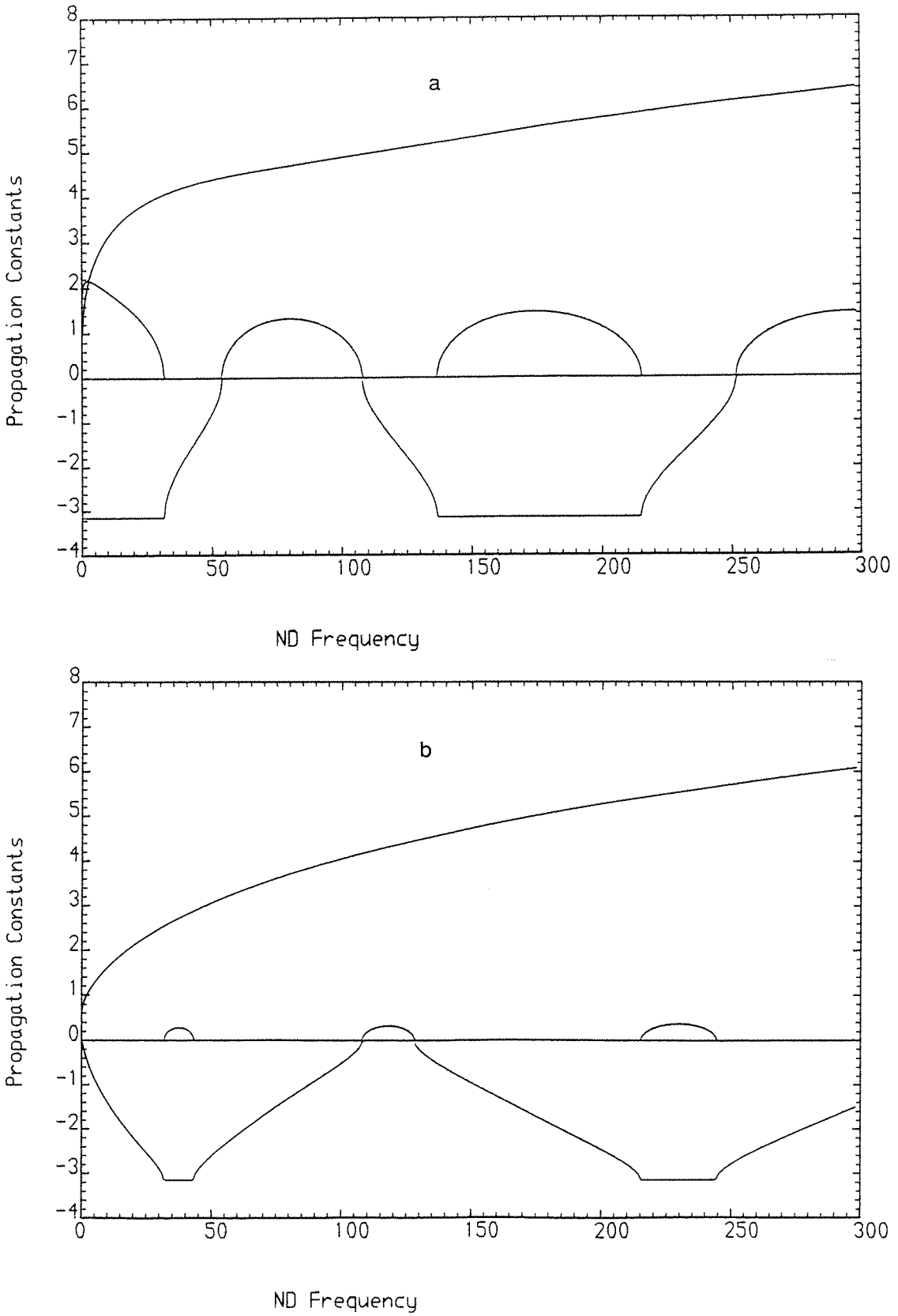

Fig. 70 Propagation Constants of Infinite, Periodic, Three-Layered Sandwich Beam (β = 0) (a) Simple Supports (b) Sliding Supports

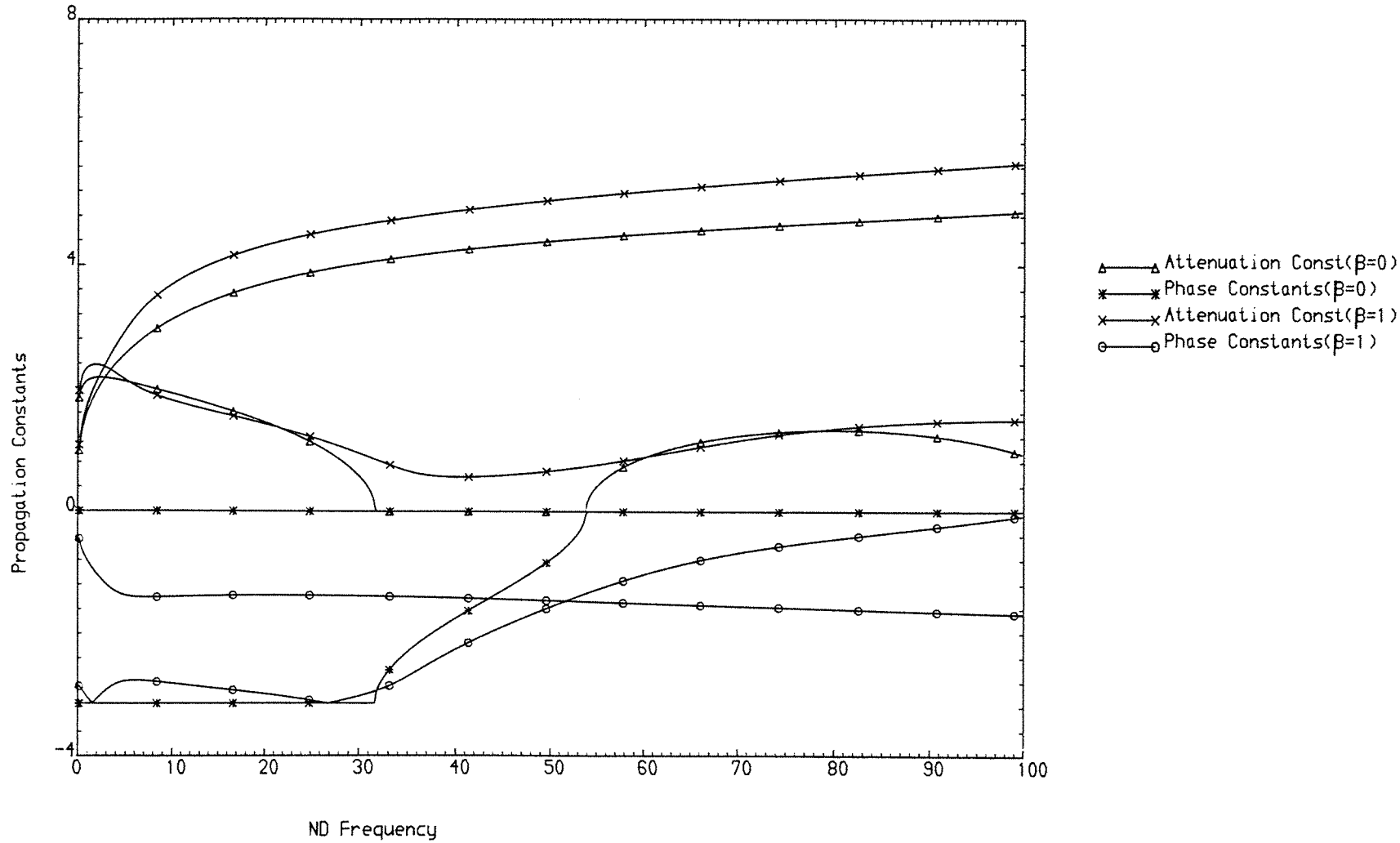

Fig. 71 Effects of Core Damping on the Propagation Constants of Infinite, Periodic, Three-Layered Sandwich Beam (Simple Supports)

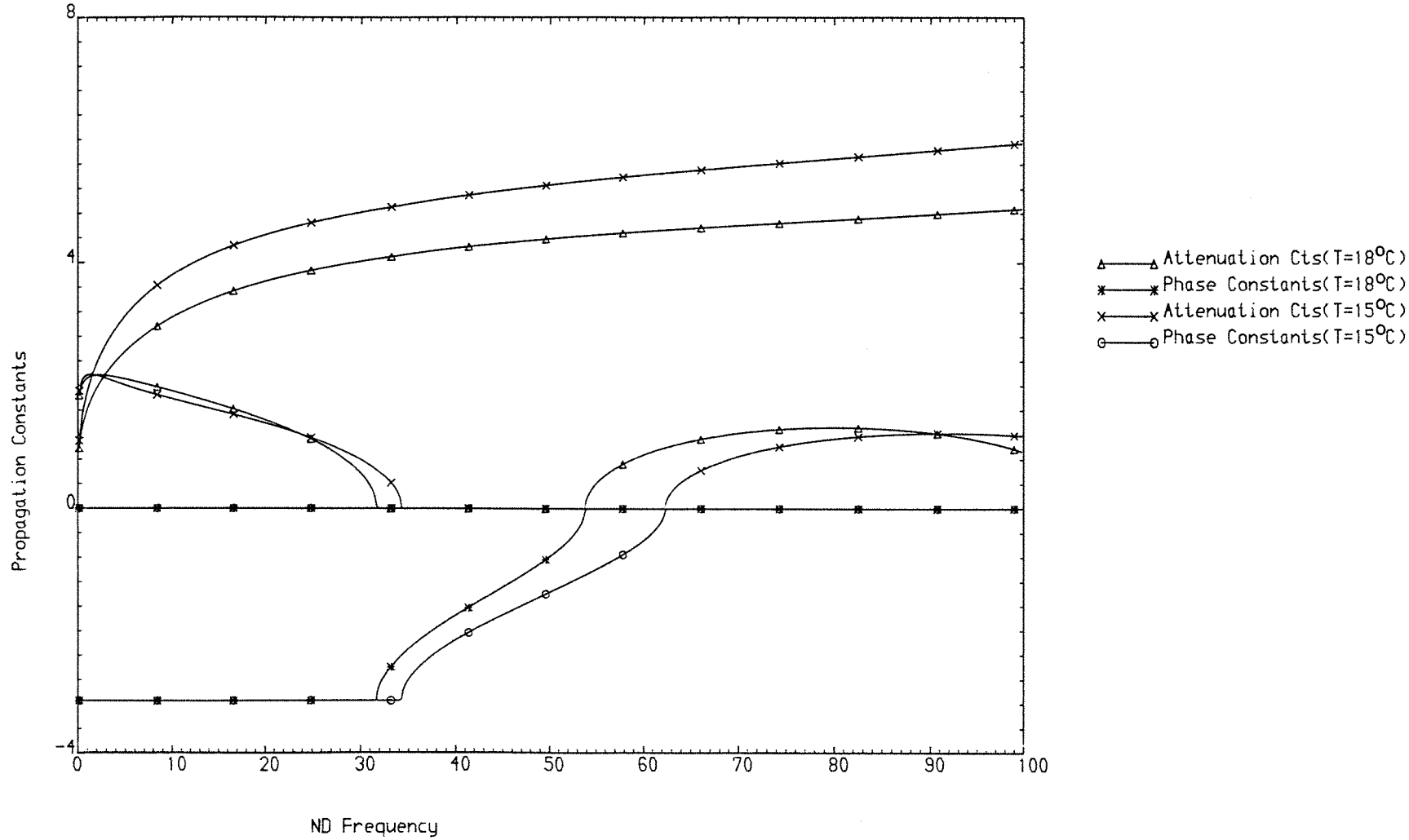

Fig. 72 Effects of Temperature on the Propagation Constants of Infinite, Periodic, Three-Layered Sandwich Beam (β = 0, Simple Supports)

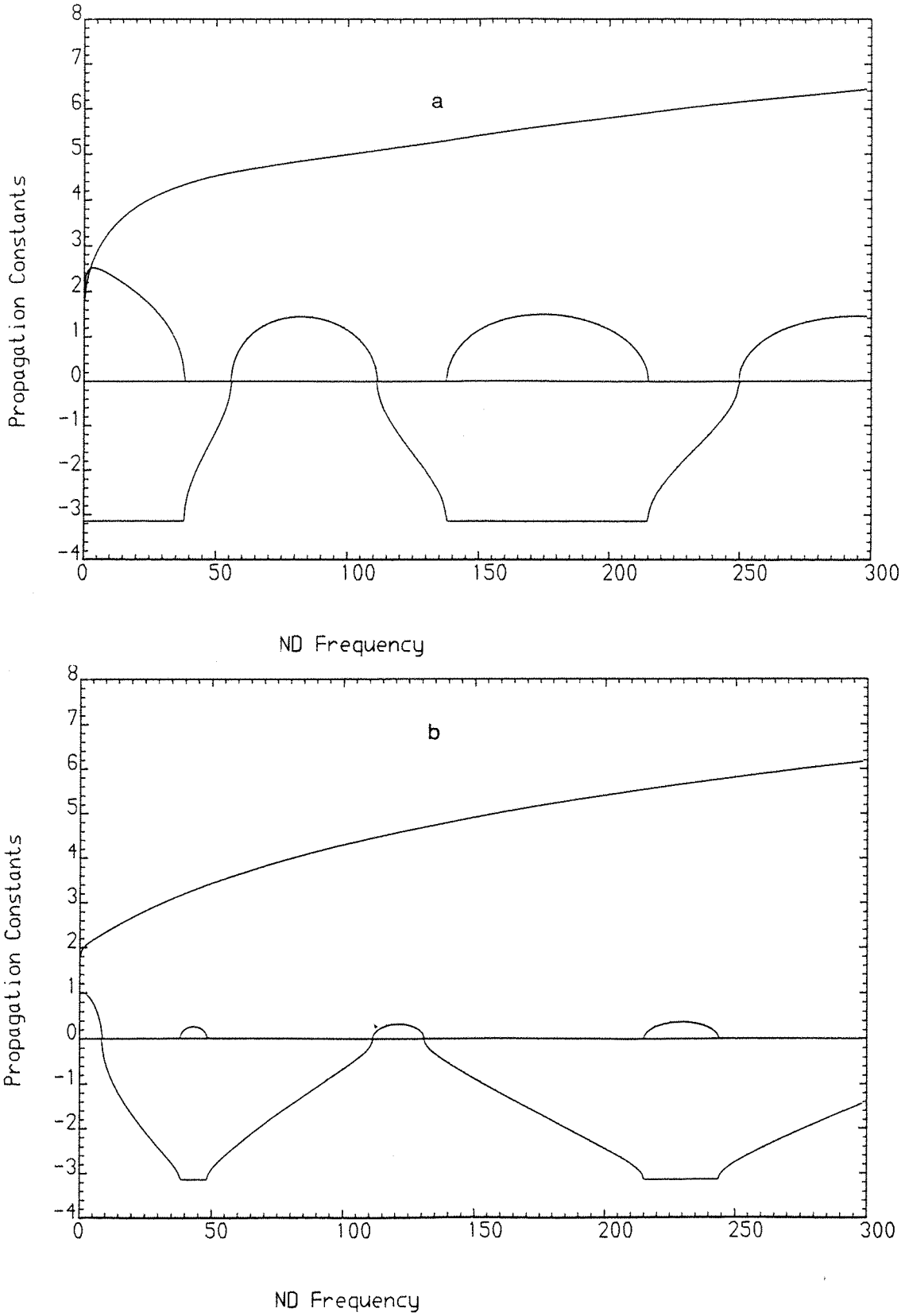

Fig. 73 Propagation Constants of Infinite, Periodic, Three-Layered Sandwich Plate (β = 0) (a) Simple Supports (b) Sliding Supports

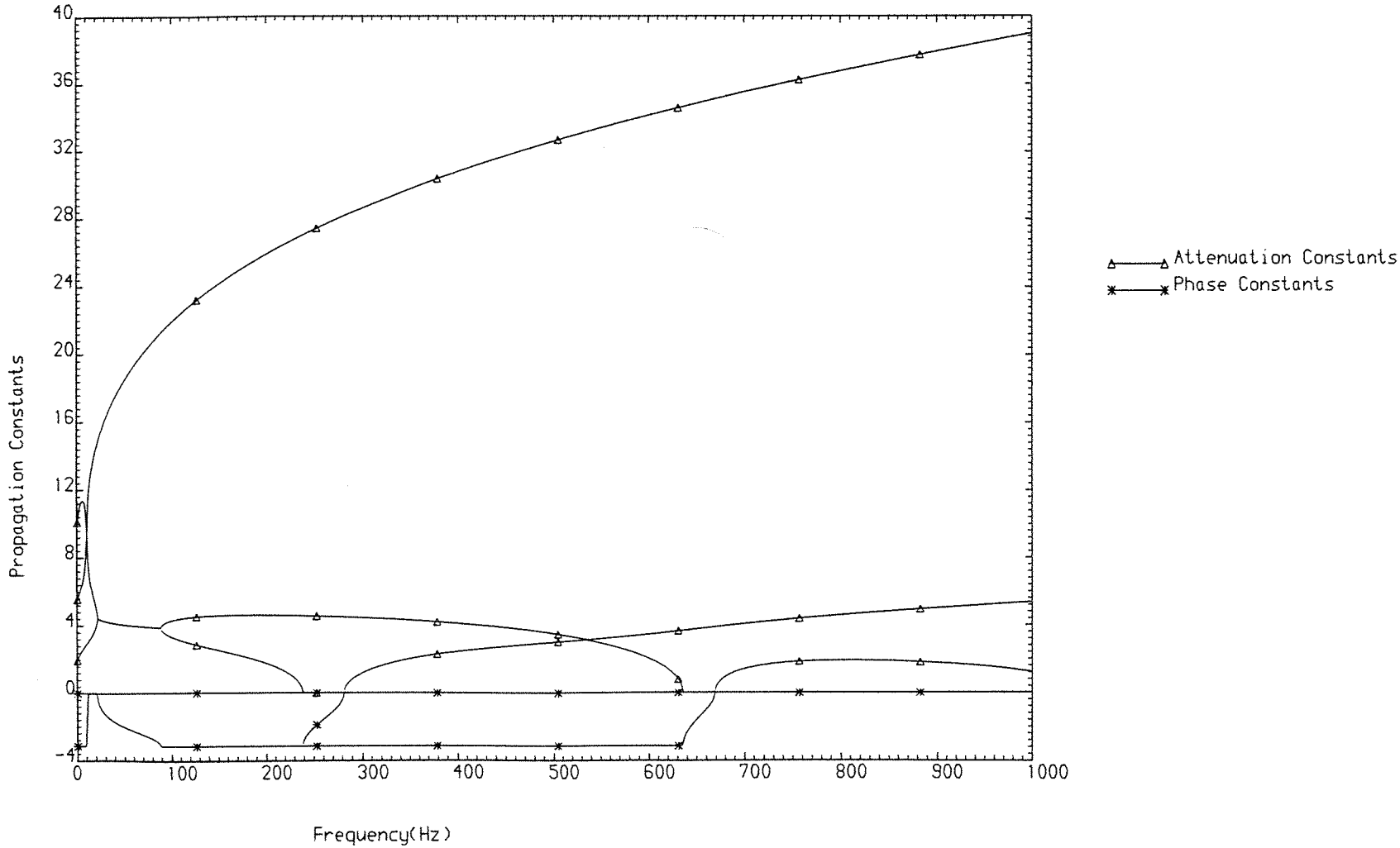

Fig. 74 Propagation Constants of Infinite, Periodic, Three-Layered Sandwich Plate (β = 0, Stiffeners without any inertia, coupling and distortion)

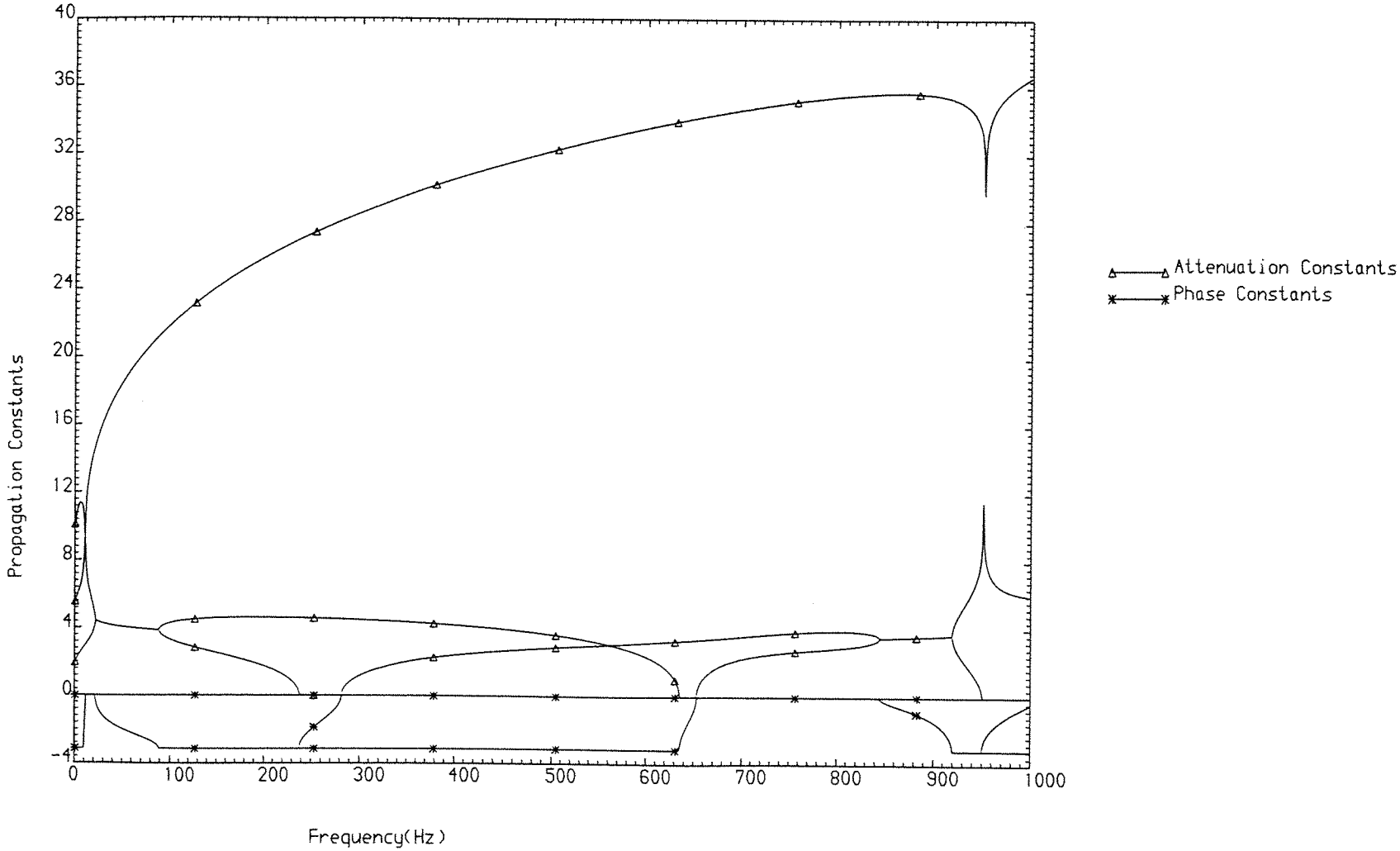

Fig. 75 Propagation Constants of Infinite, Periodic, Three-Layered Sandwich Plate (β = 0, Stiffeners without transverse inertia, coupling and distortion)

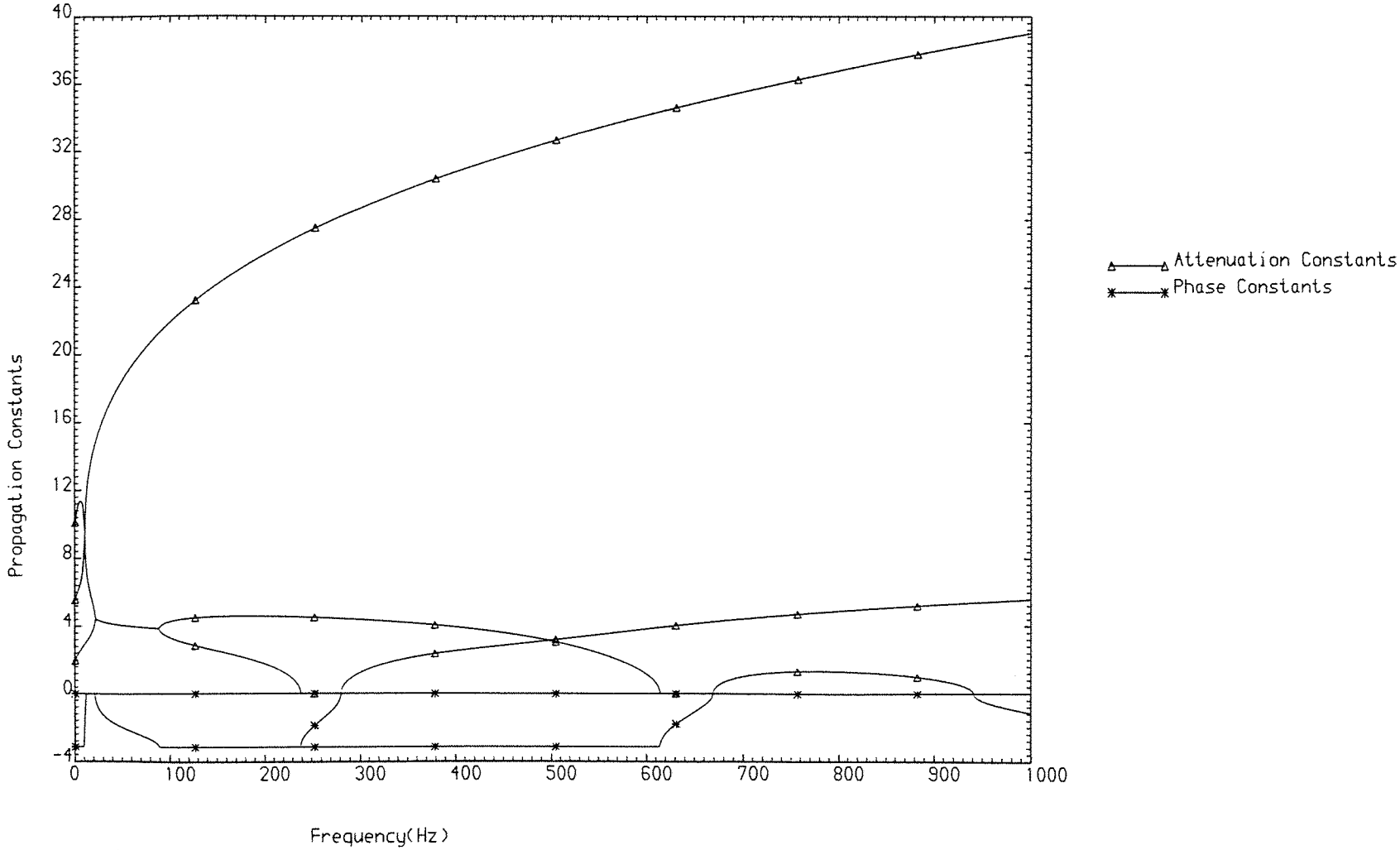

Fig. 76 Propagation Constants of Infinite, Periodic, Three-Layered Sandwich Plate (β = 0, Stiffeners without rotational inertia, coupling and distortion)

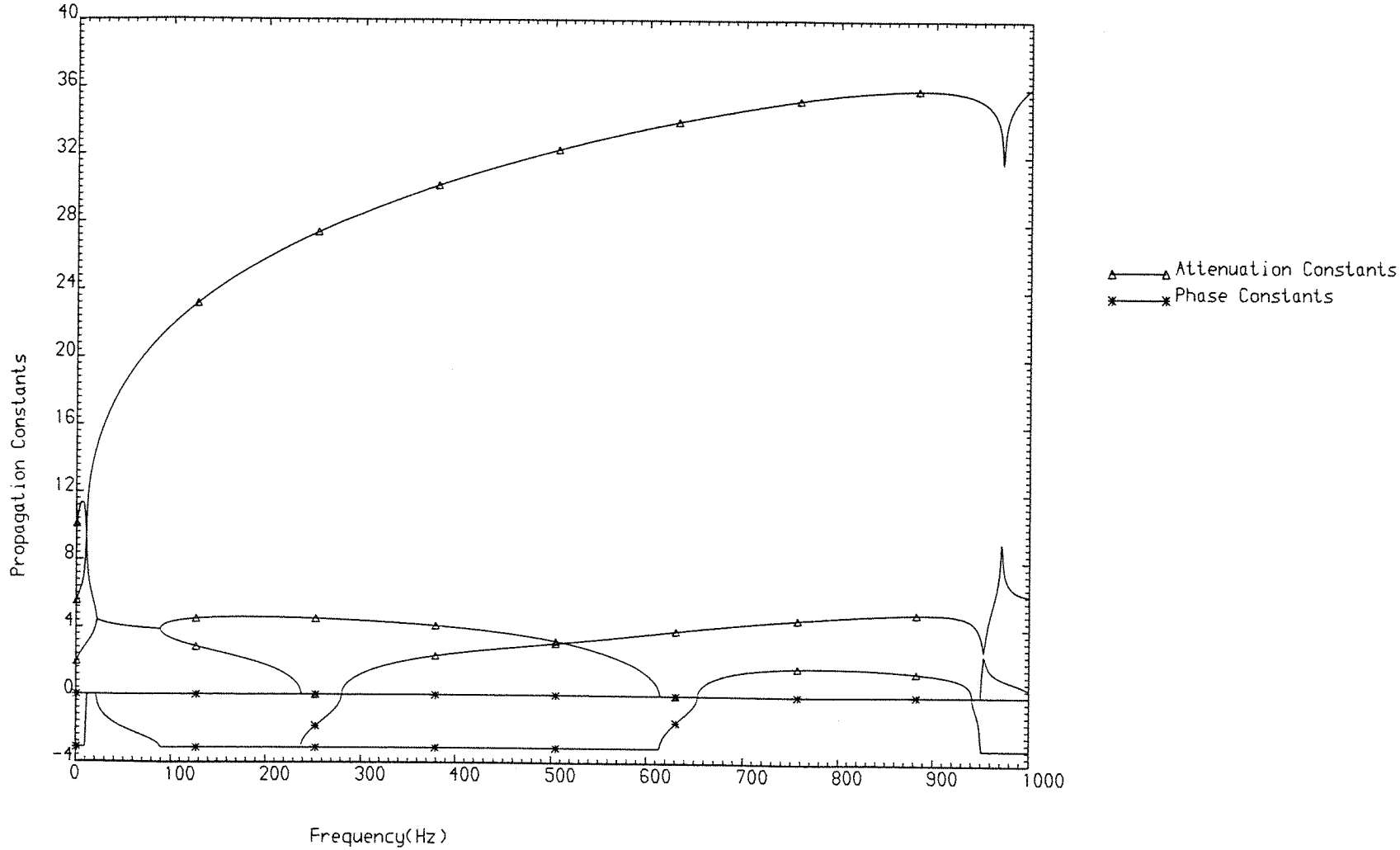

Fig. 77 Propagation Constants of Infinite, Periodic, Three-Layered Sandwich Plate (β = 0, Stiffeners without coupling and distortion)

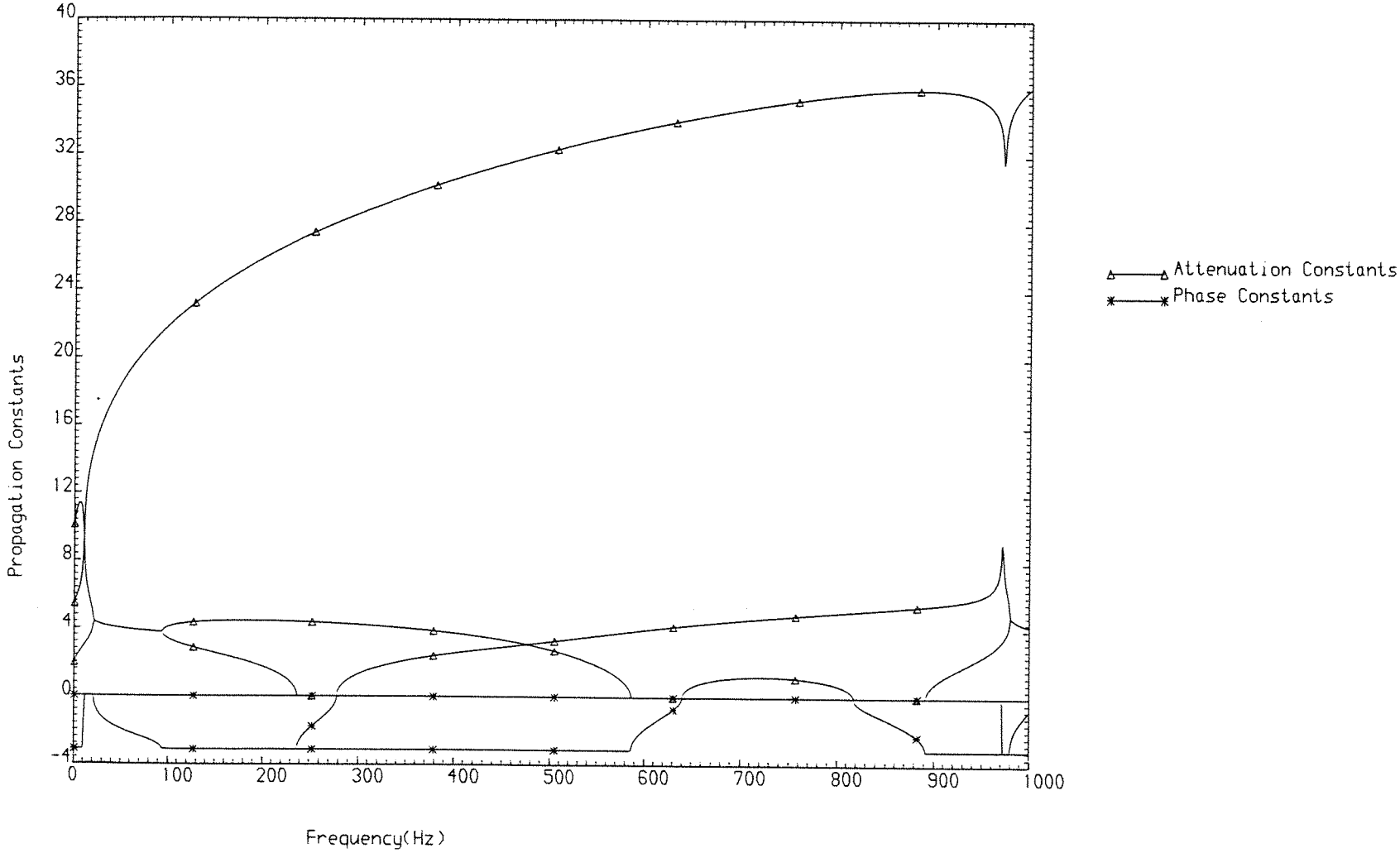

Fig. 78 Propagation Constants of Infinite, Periodic, Three-Layered Sandwich Plate (β = 0, Stiffeners without distortion)

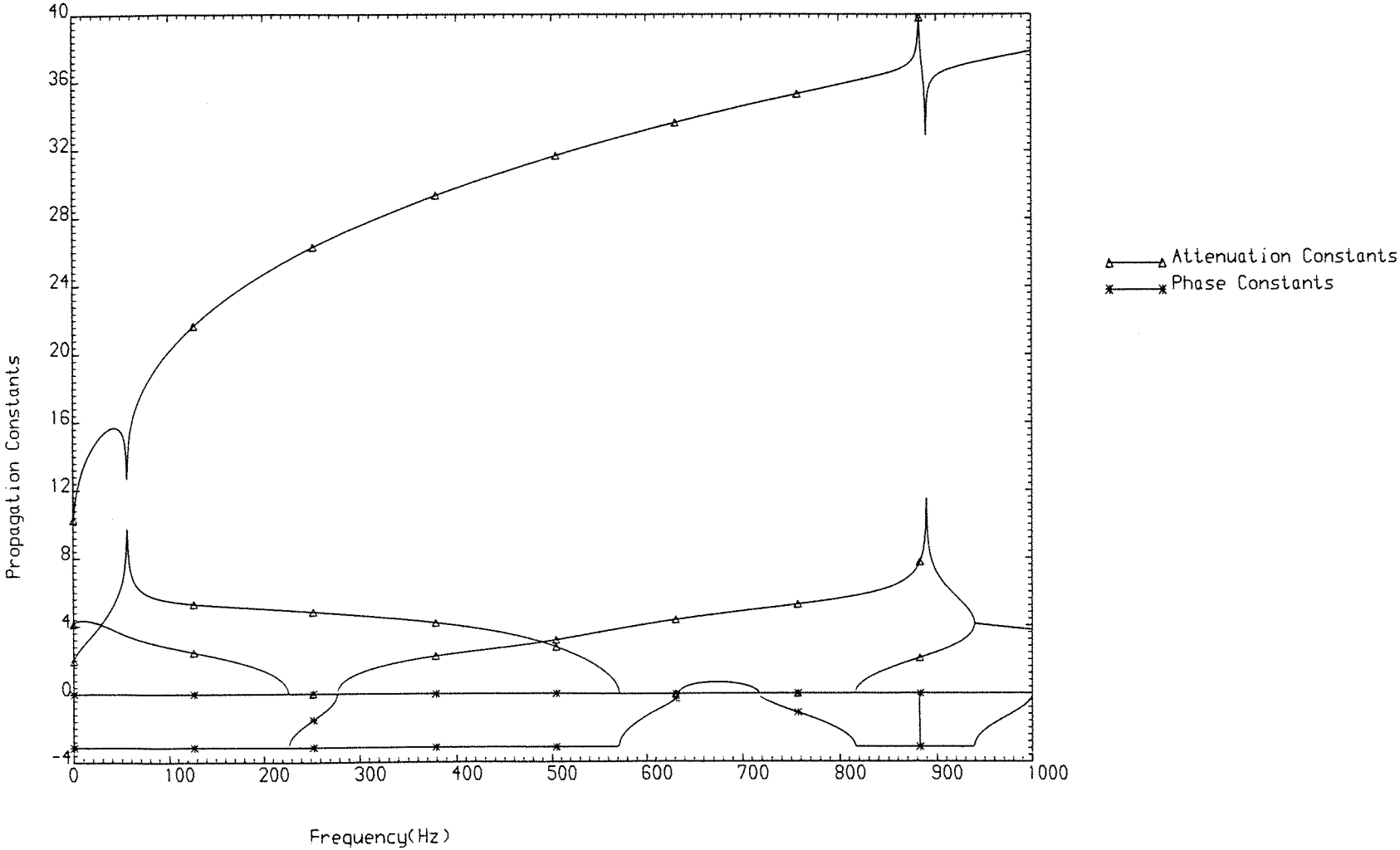

Fig. 79 **Propagation Constants of Infinite, Periodic, Three-Layered Sandwich Plate (β = 0, General Supports)**

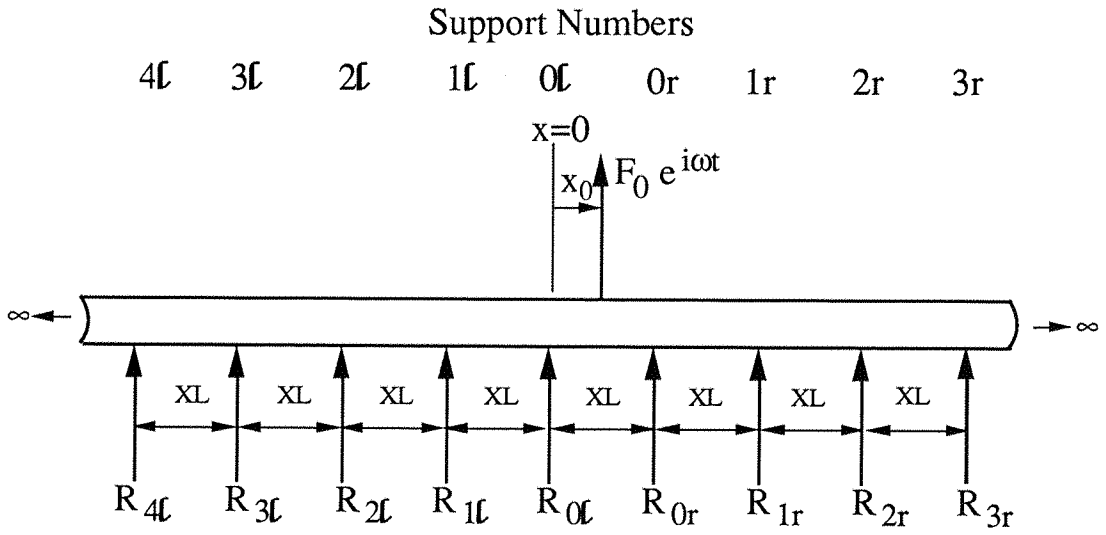

Figure 80: Reaction Forces on a Harmonically Forced and Periodically Supported Beam.

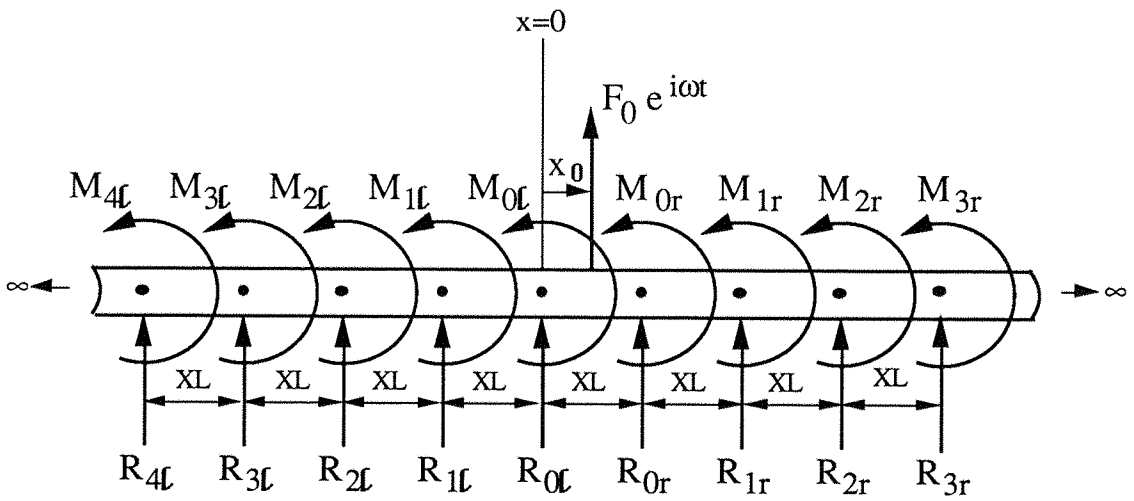

Figure 81: Reaction Forces and Moments on a Harmonically Forced and Periodically Supported Beam.

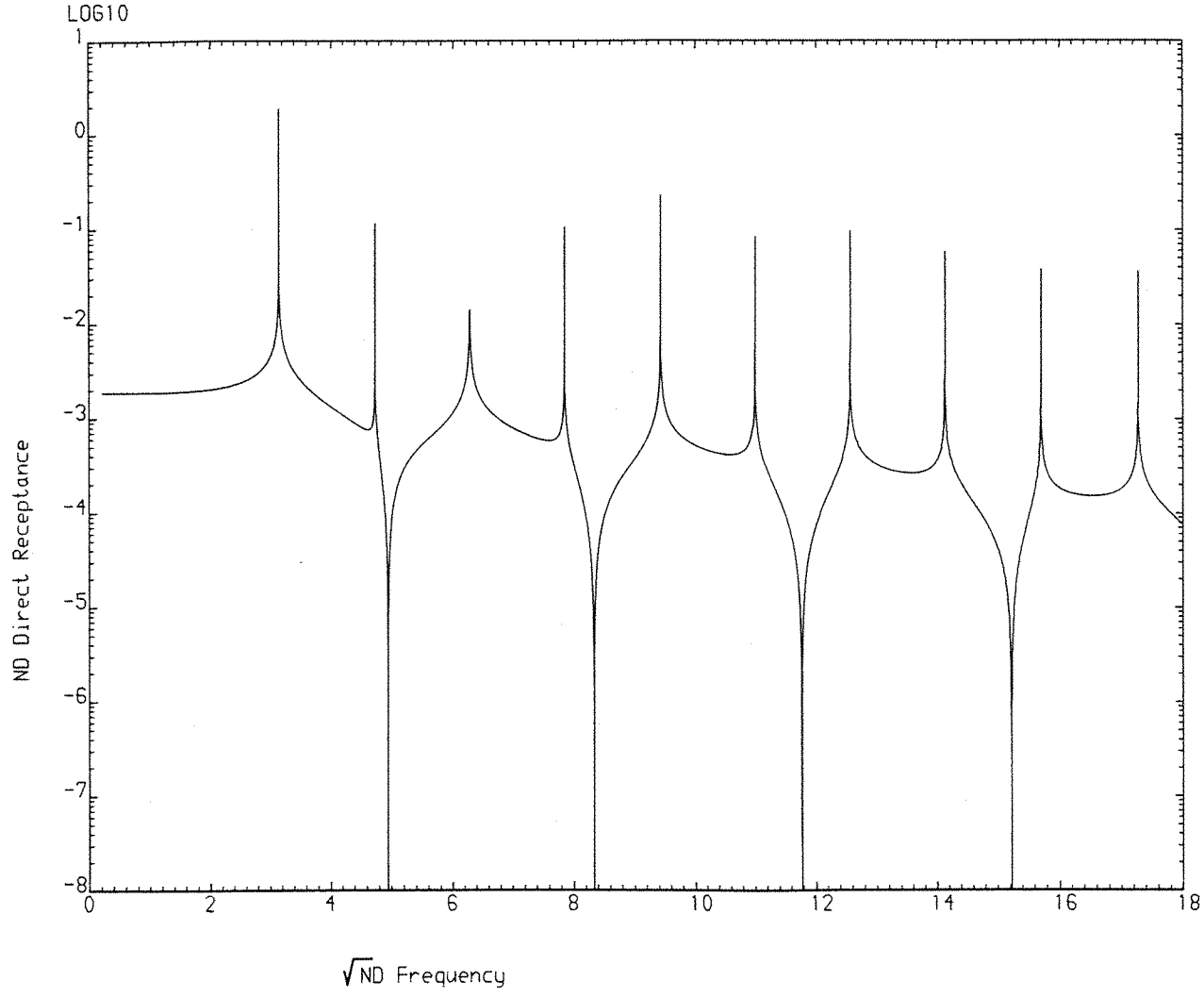

Fig. 82 Non-Dimensional Direct Transverse Receptance of Forced, Infinite, Periodic Simply-Supported Euler-Bernoulli Beam($\eta=10^{-6}$, $x_o=XL/8$)

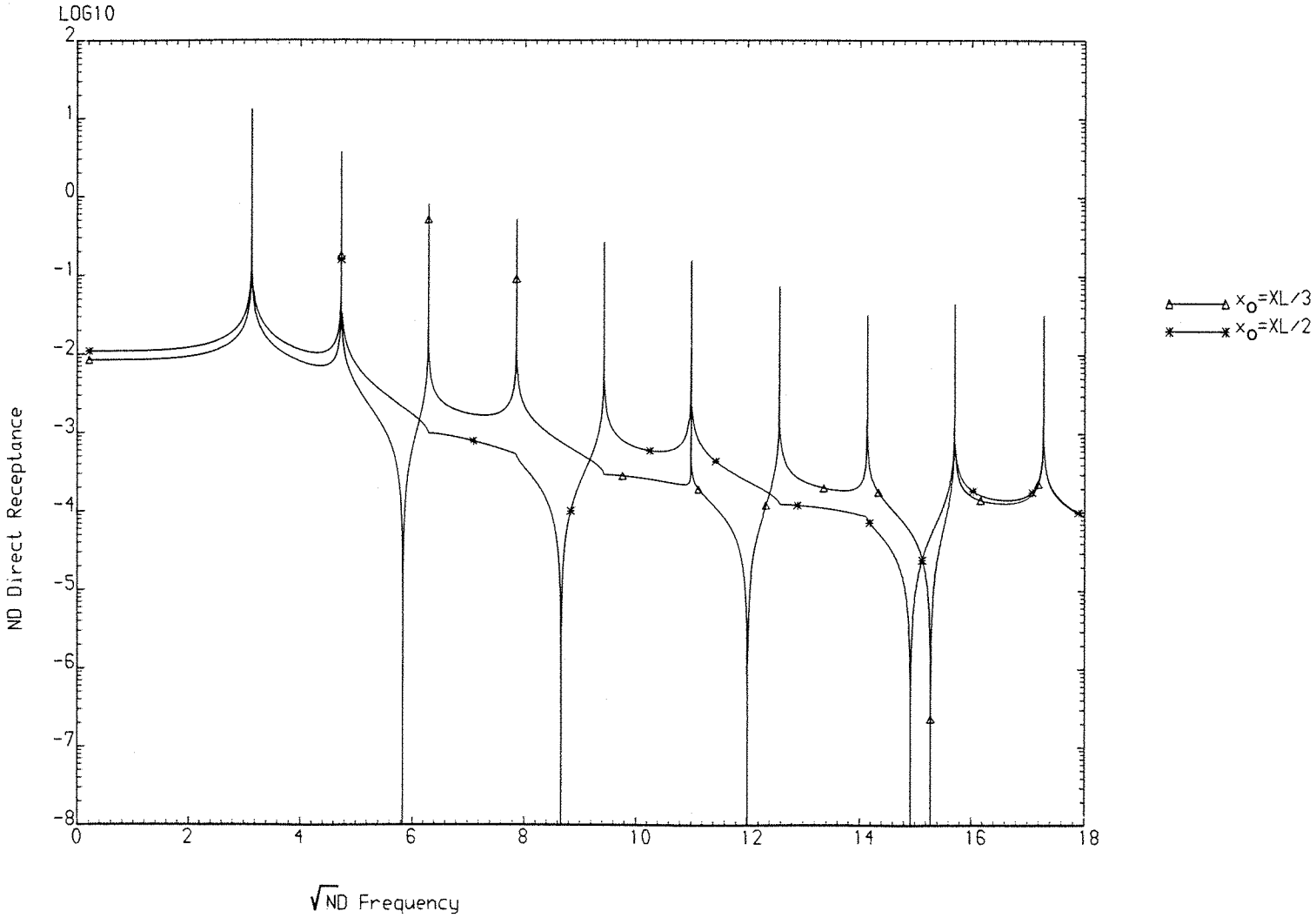

Fig. 83 Non-Dimensional Direct Transverse Receptance of Forced, Infinite Periodic Simply-Supported Euler-Bernoulli Beam ($\eta = 10^{-6}$)

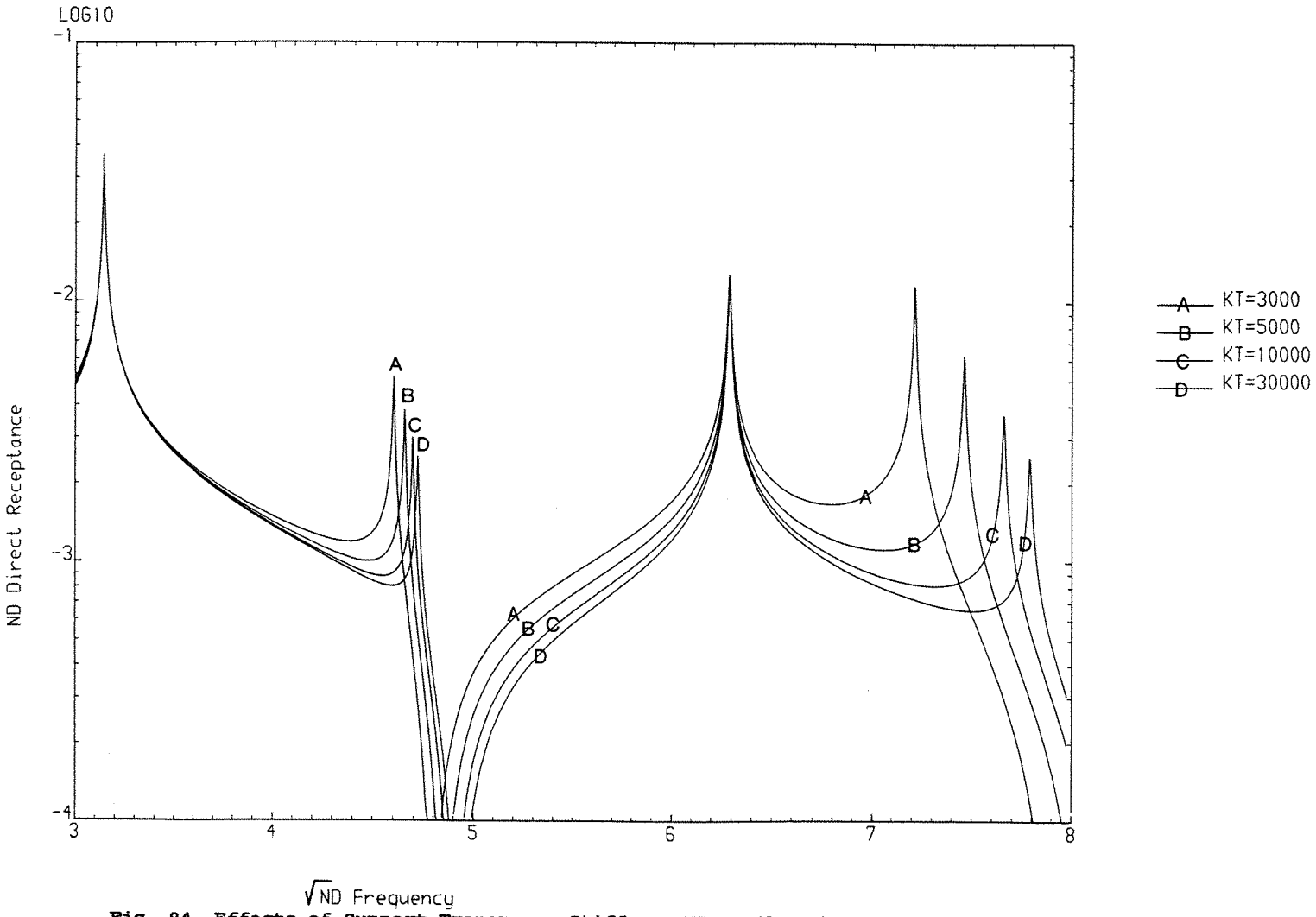

Fig. 84 Effects of Support Transverse Stiffness KT on the Direct Response of Forced, Infinite, Periodic Euler-Bernoulli Beam(η = 0.003, x_o = XL/8, KR = 0)

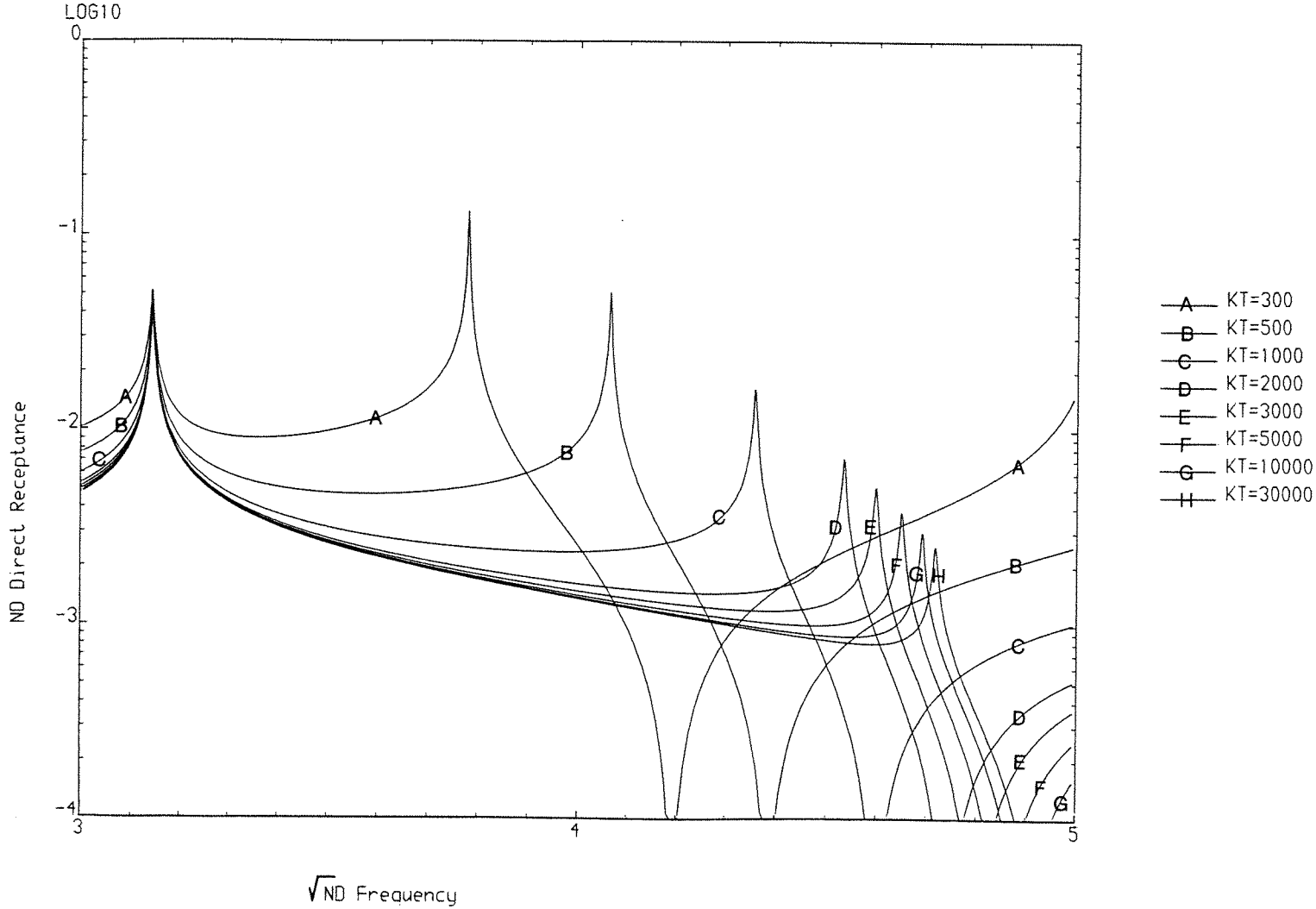

Fig. 85 Effects of Support Transverse Stiffness KT on the Direct Response of Forced, Infinite, Periodic Euler-Bernoulli Beam (η = 0.003, x_o = XL/8, KR = 0)

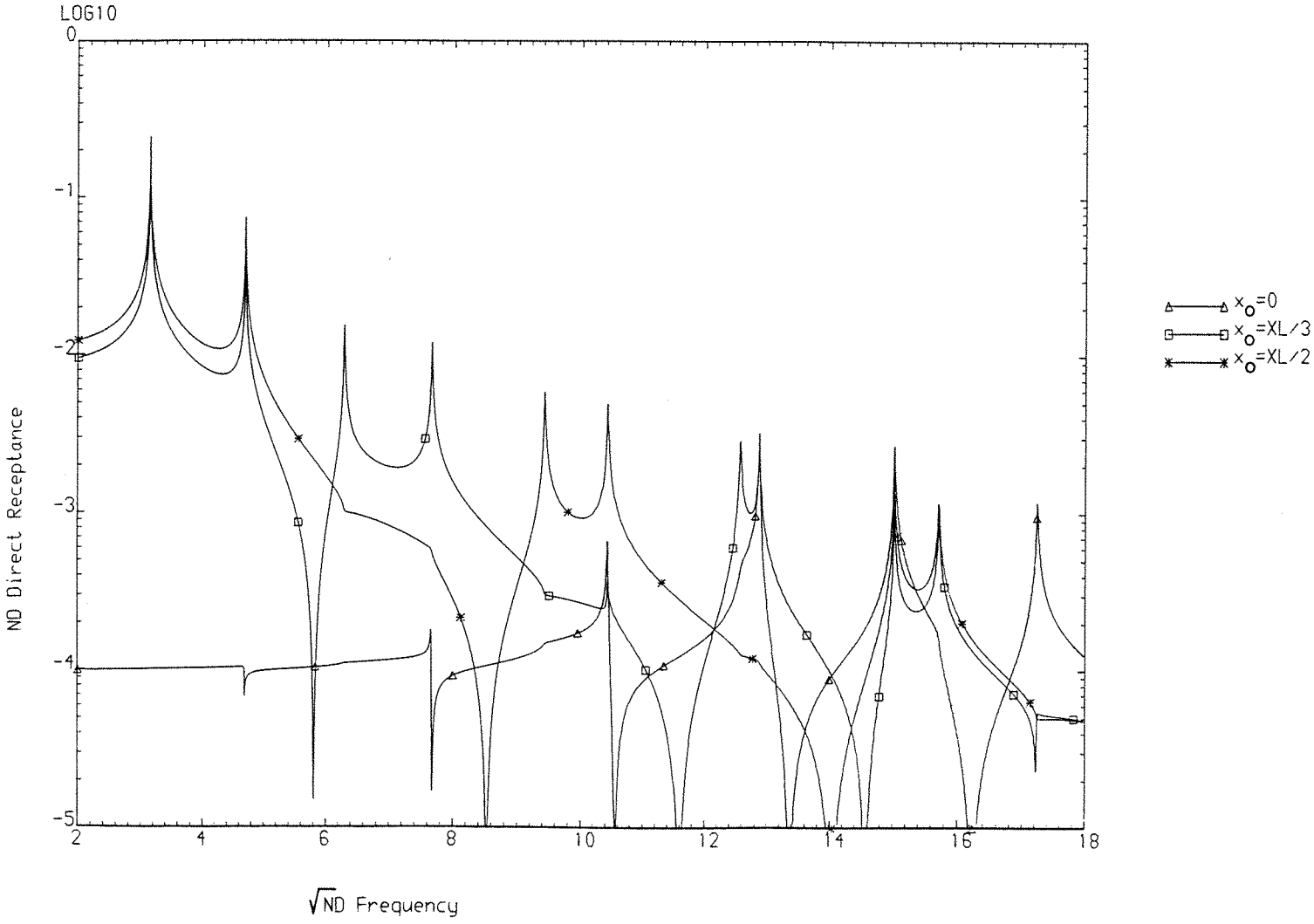

Fig. 86 Effects of Loading Position on the Direct Response of Forced, Infinite, Periodic Euler-Bernoulli Beam (η = 0.003, KT = 10000, KR = 0)

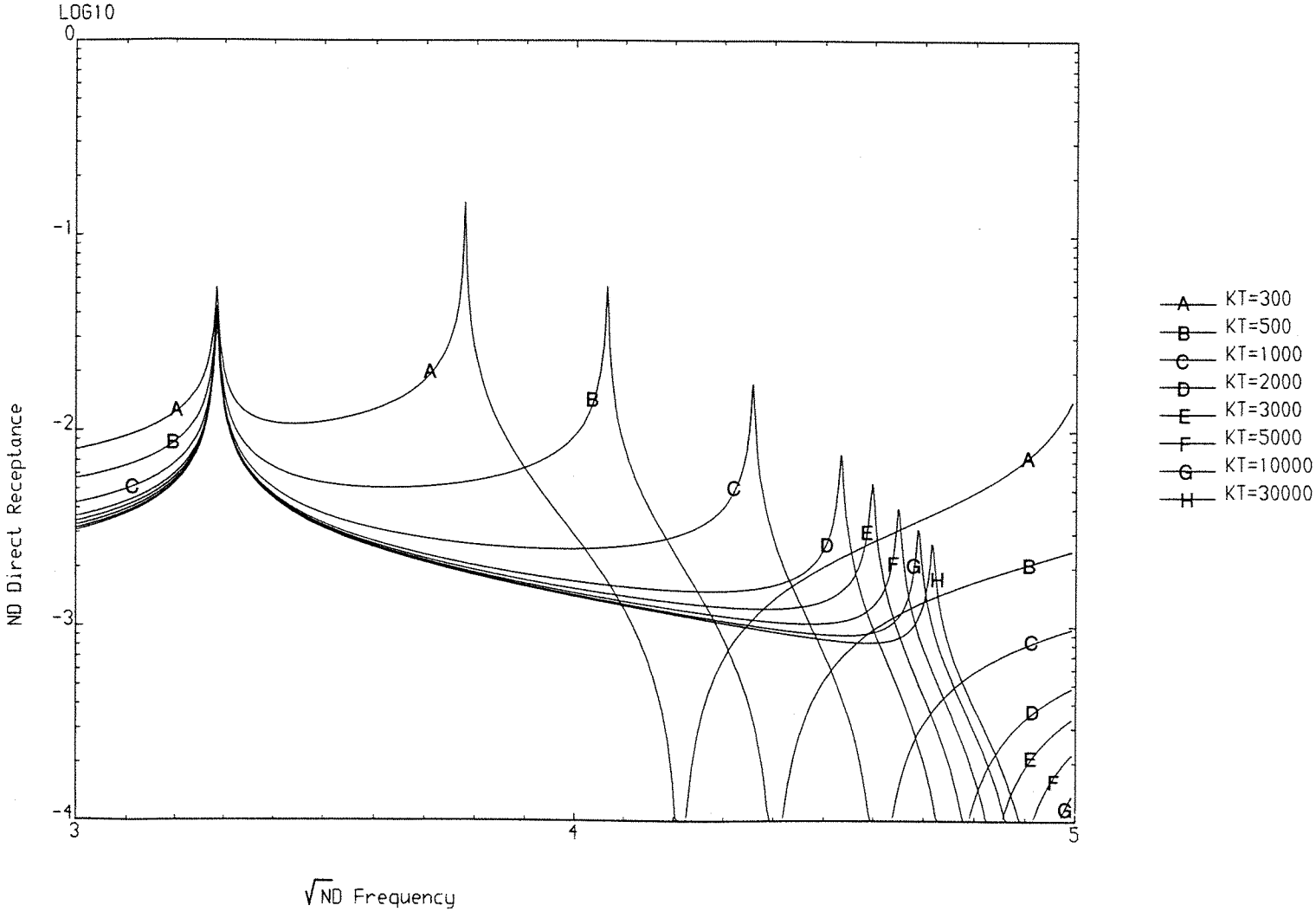

Fig. 87 Effects of Support Transverse Stiffness KT on the Direct Response of Forced, Infinite, Periodic Euler-Bernoulli Beam (η = 0.003, x_o = XL/8, KR = 1)

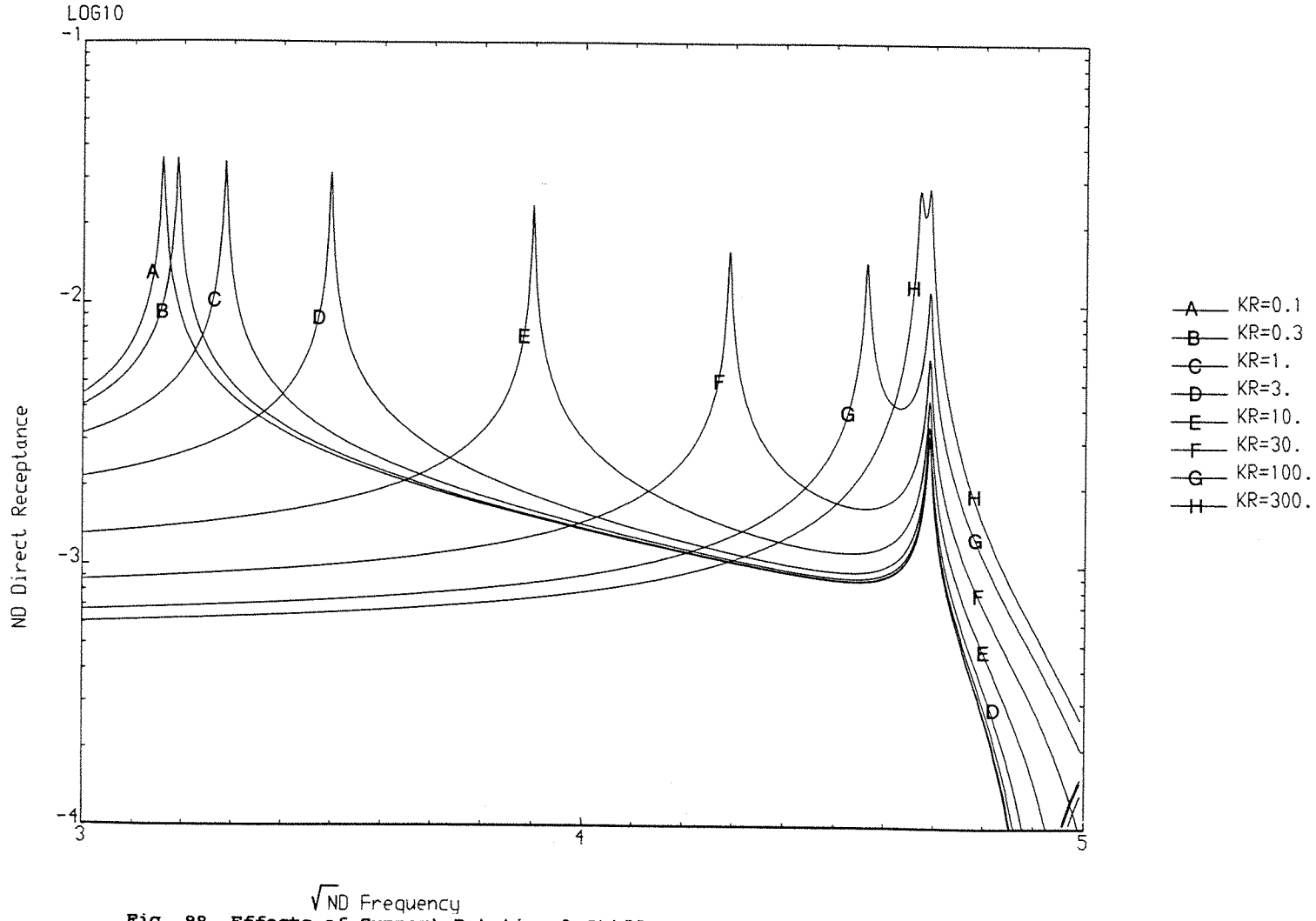

Fig. 88 Effects of Support Rotational Stiffness KR on the Direct Response of Forced, Infinite, Periodic Euler-Bernoulli Beam (η = 0.003, x_o = XL/8, KT = 10000)

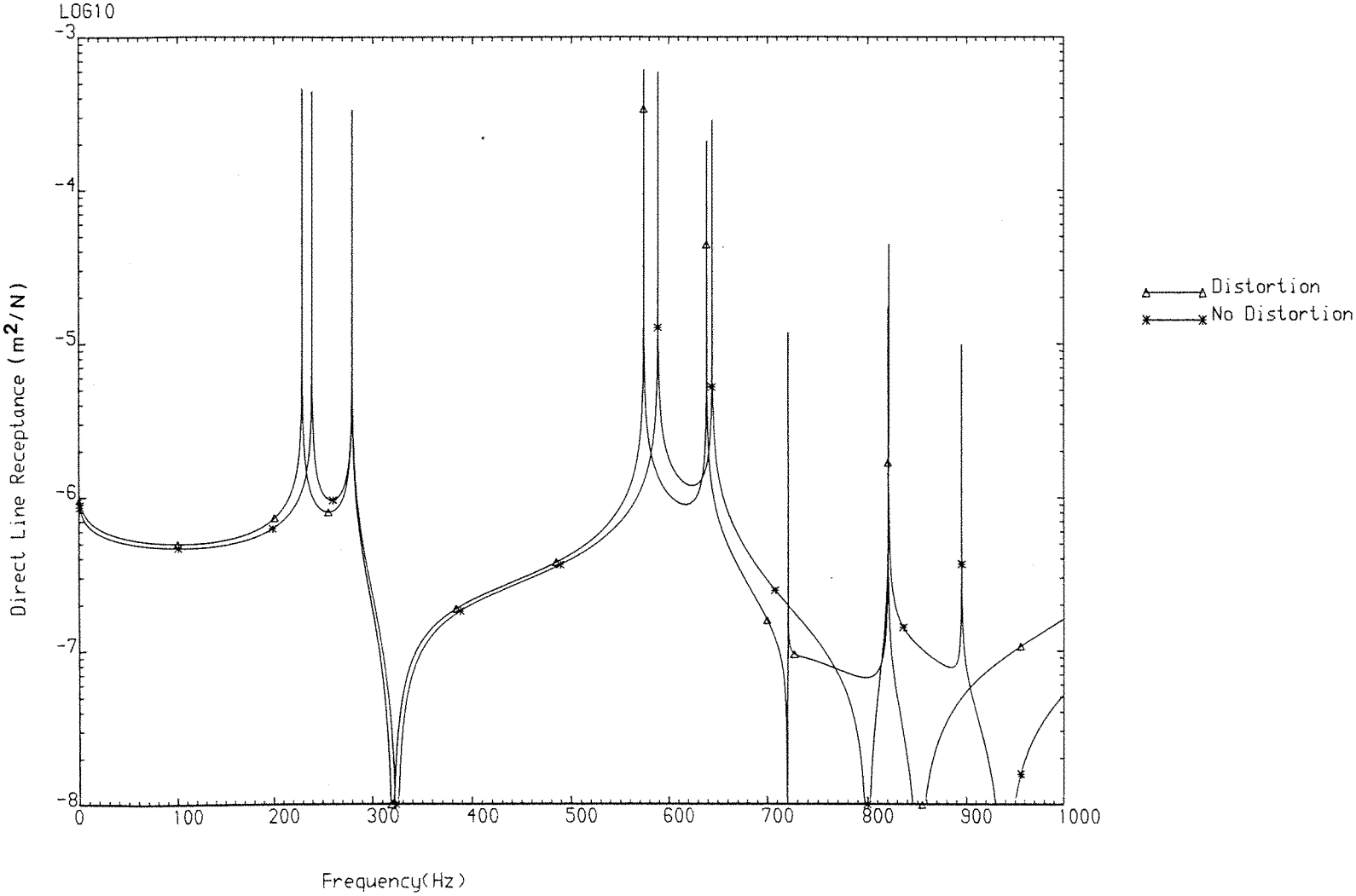

Fig. 89 **Direct Transverse Receptance of Forced, Infinite Periodic Three-Layered Sandwich Plate ($\beta = 10^{-6}$, General Supports, x_o=XL/8)**

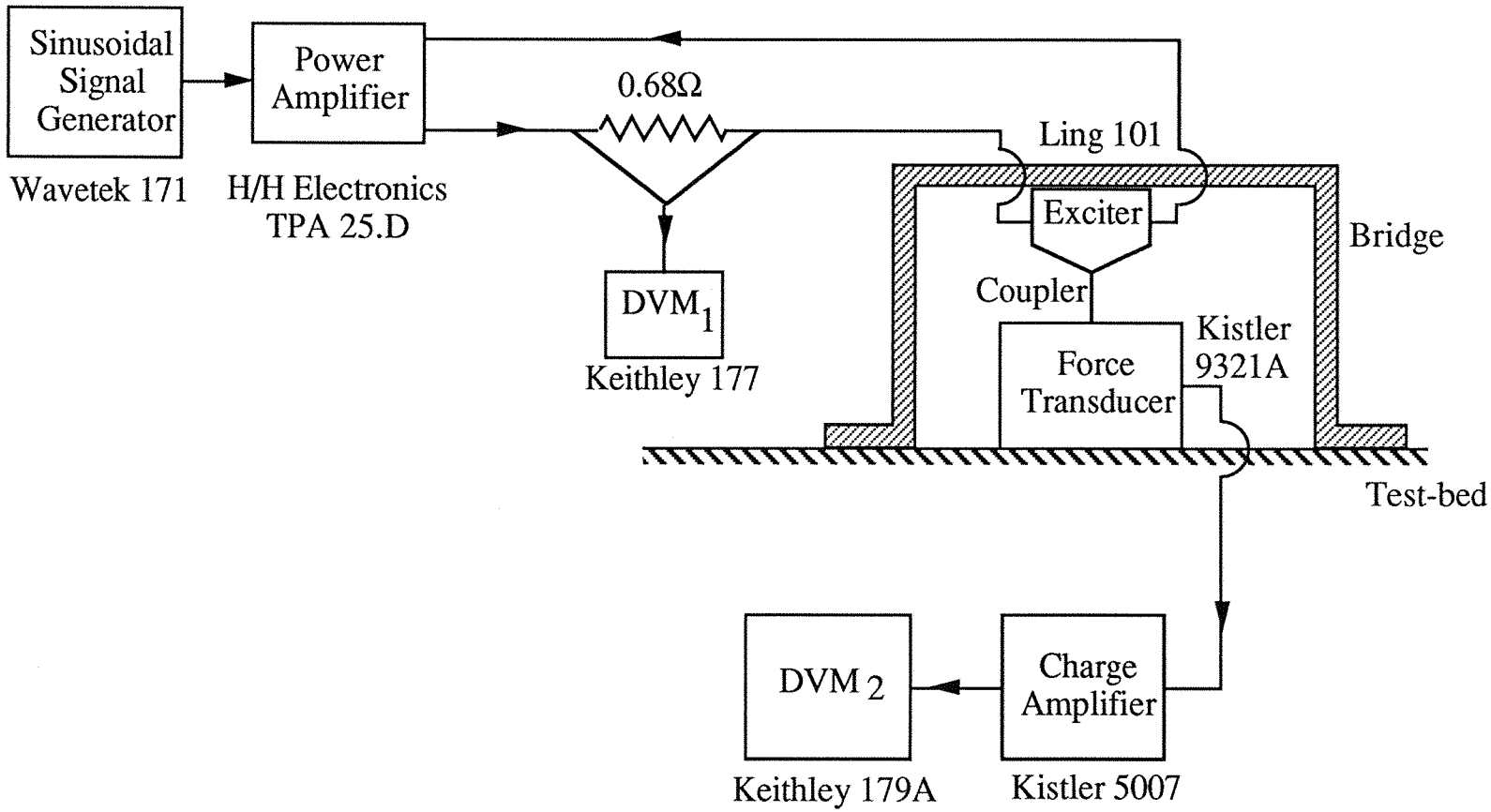

Figure 90 Block-Diagram of the Experimental Set-up and the Equipment Used for the Determination of Exciter Head Constants

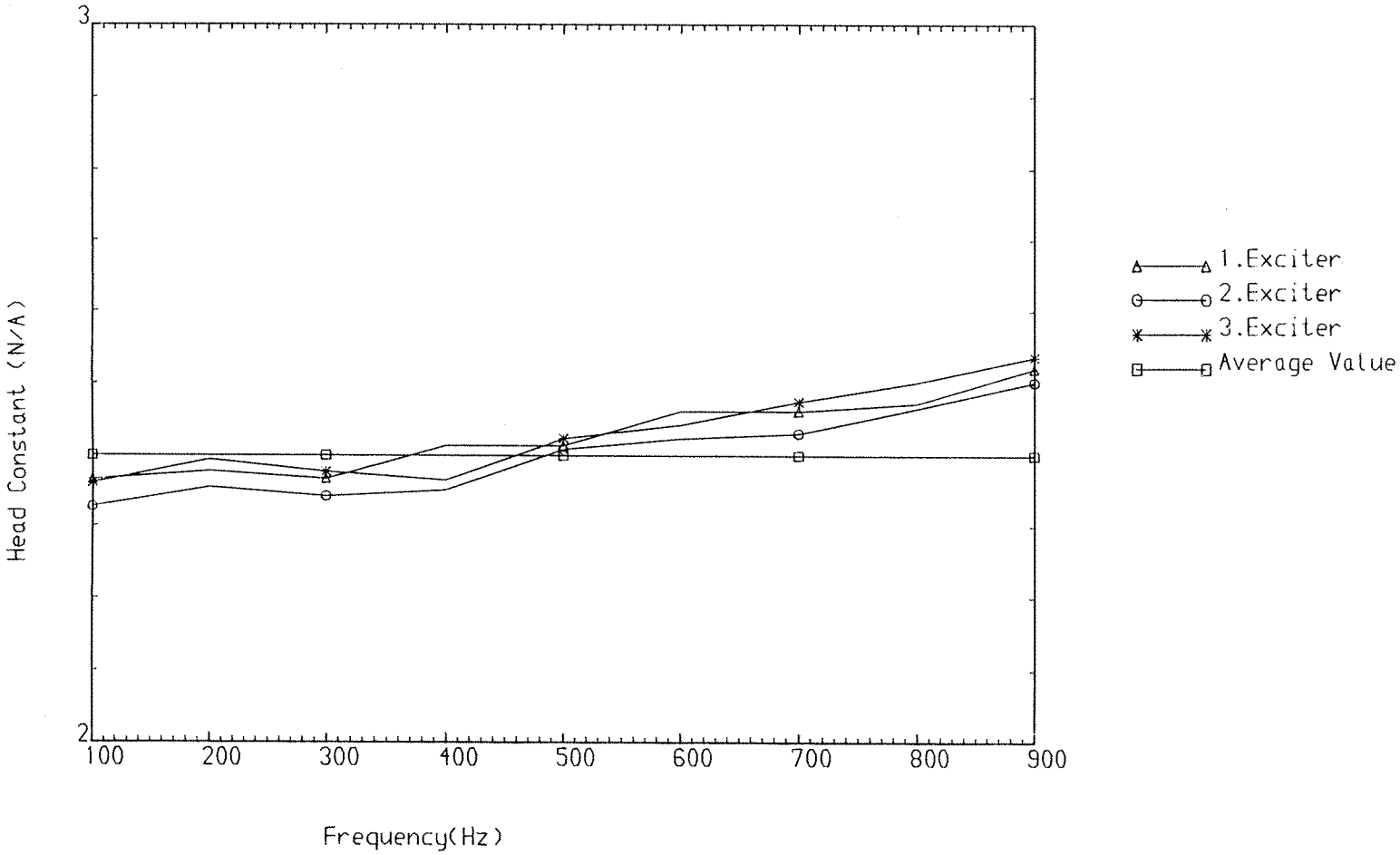

Fig. 91 Experimentally Determined Exciter Head Constants

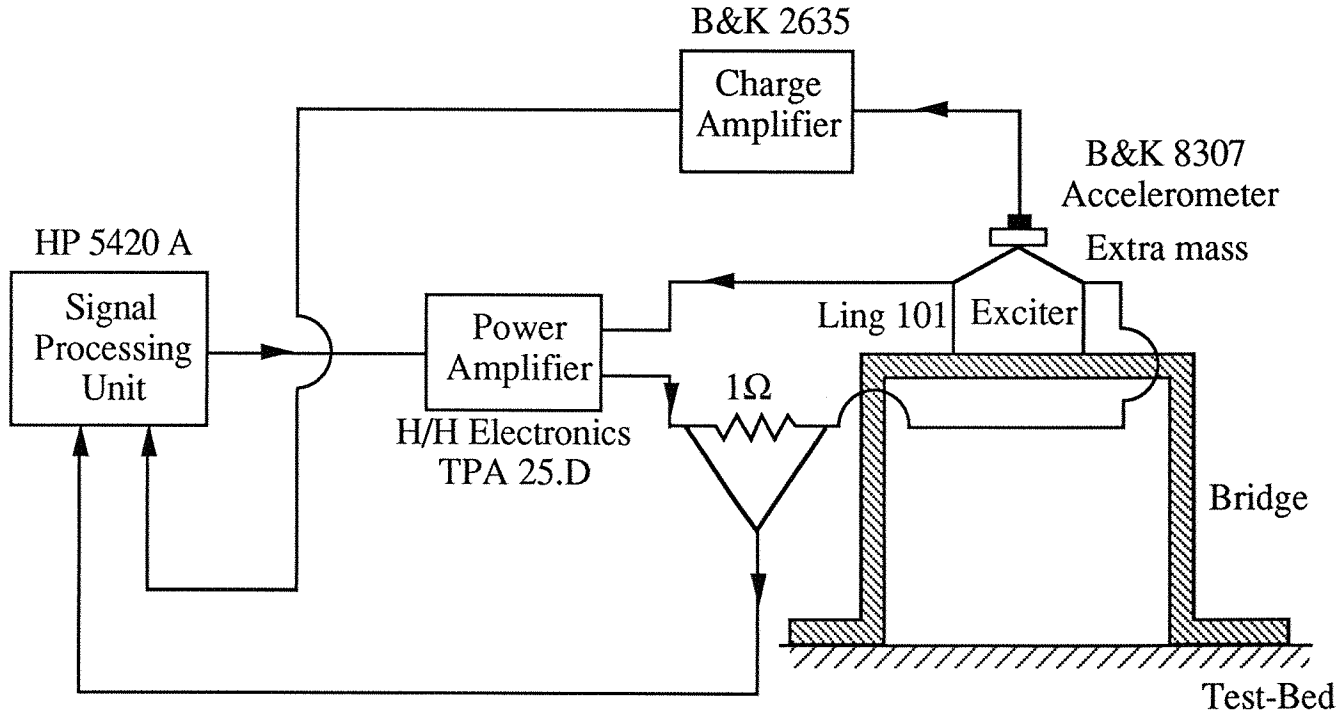

Figure 92: Block-diagram of the Experimental Set-up and the Equipment Used for the Calibration of the Exciter Moving Mass.

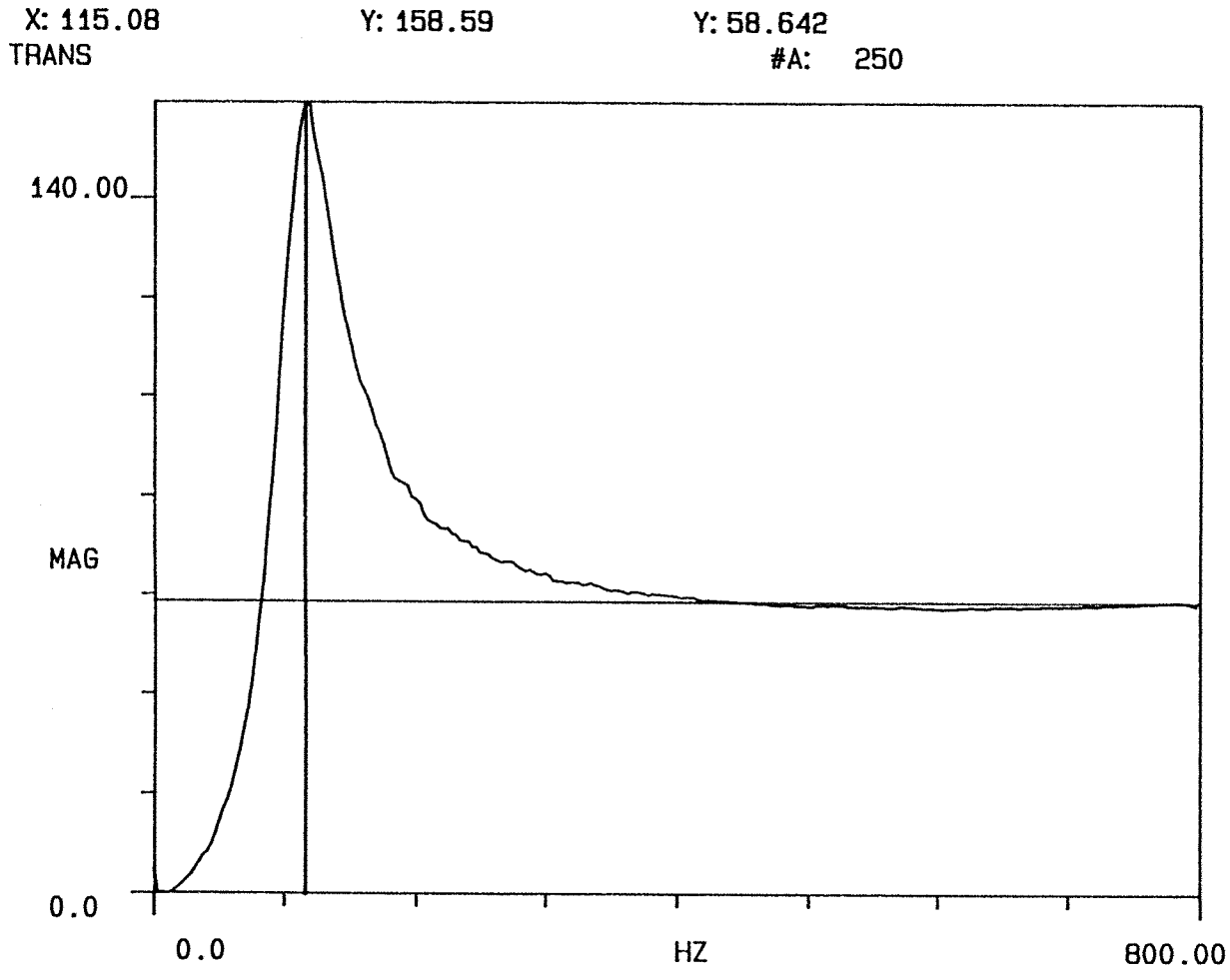

Fig. 93 Experimentally Obtained Random Transfer Function (Inertance) of the Exciter ($m_{extra} \cong 8.9$ [g])

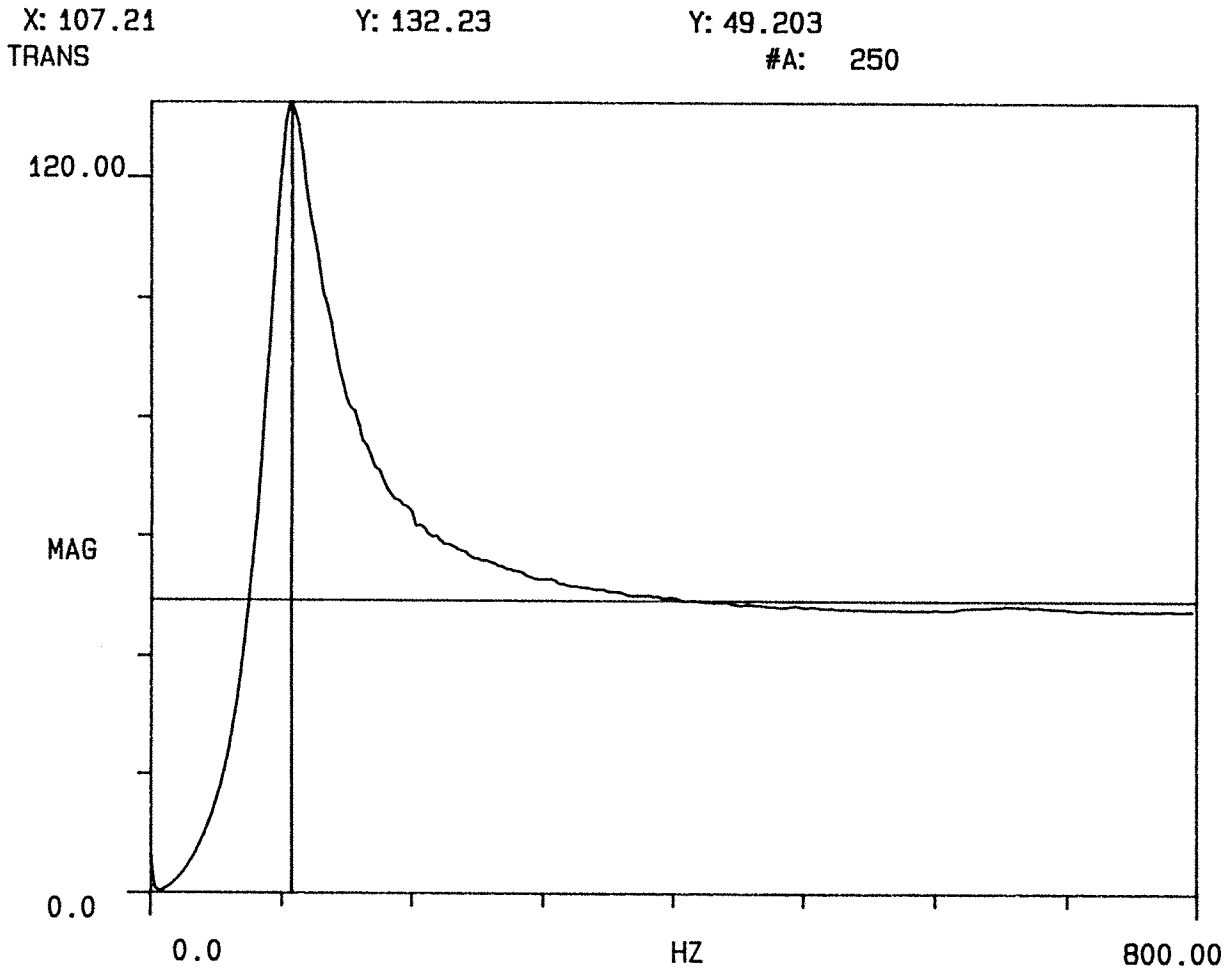

Fig. 94 Experimentally Obtained Random Transfer Function (Inertance) of the Exciter ($m_{extra} \cong 12.3$ [g])

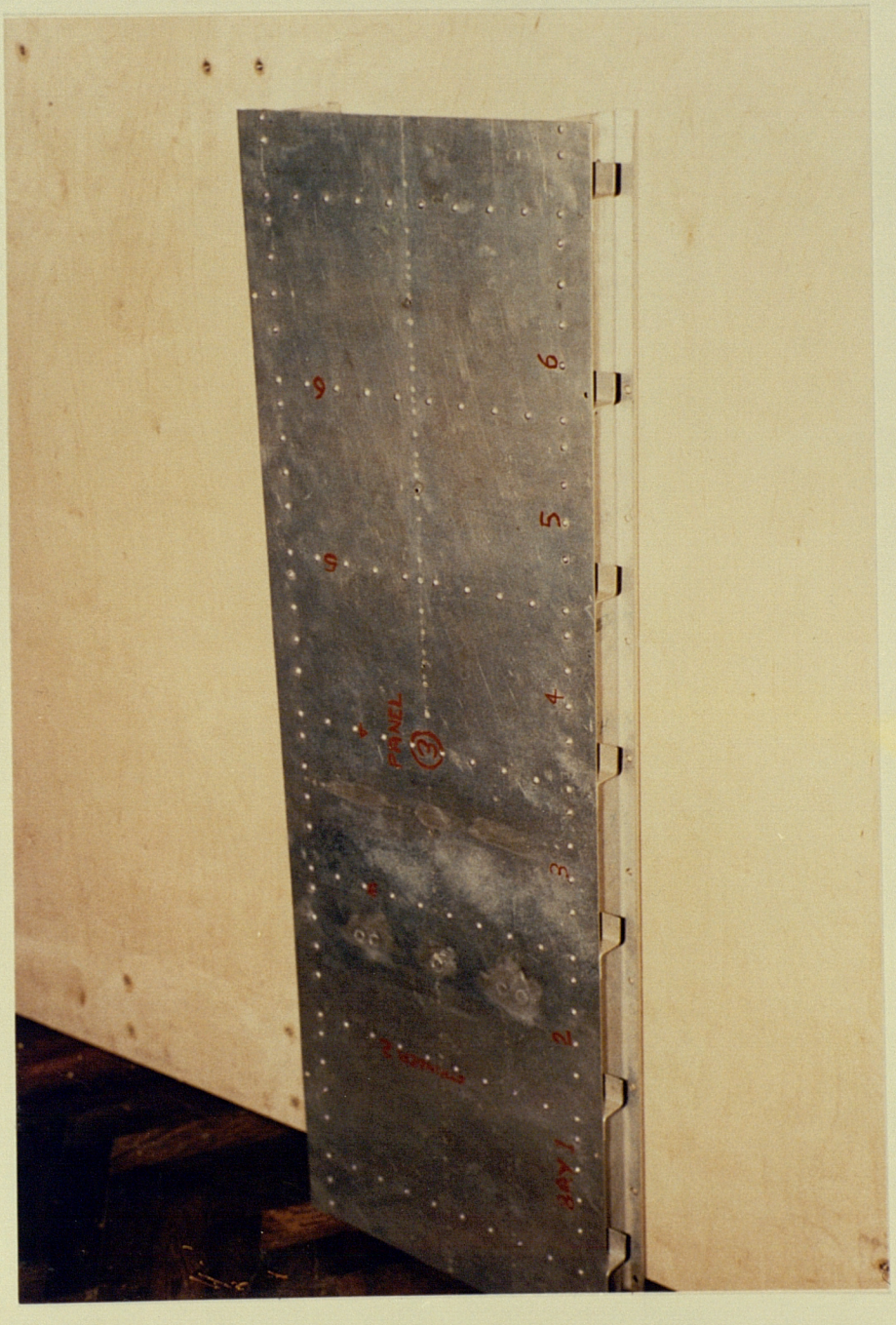

Fig. 95 Top View of the Eight-Bay, Stiffened Uniform Plate

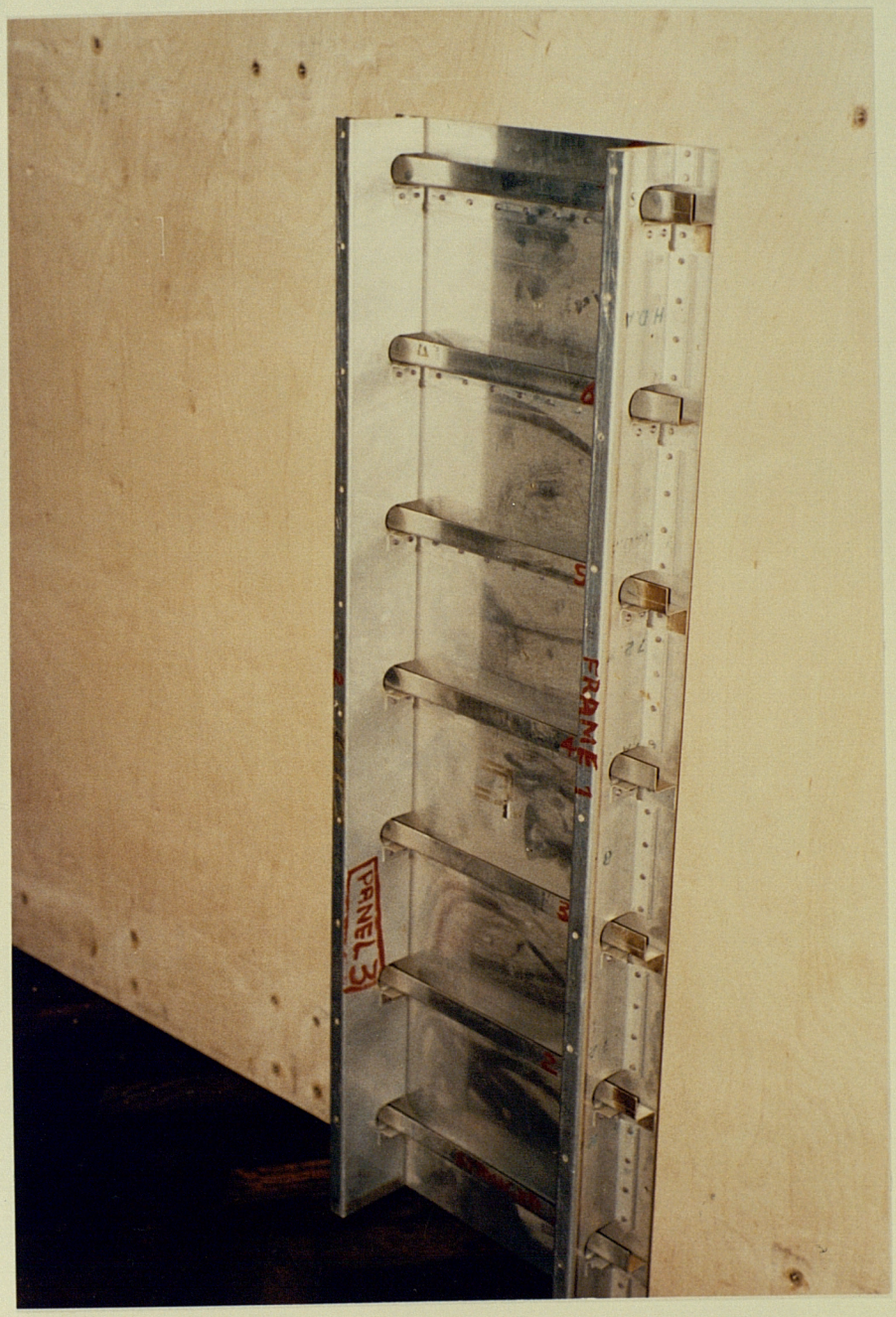

Fig. 96 Bottom View of the Eight-Bay, Stiffened Uniform Plate

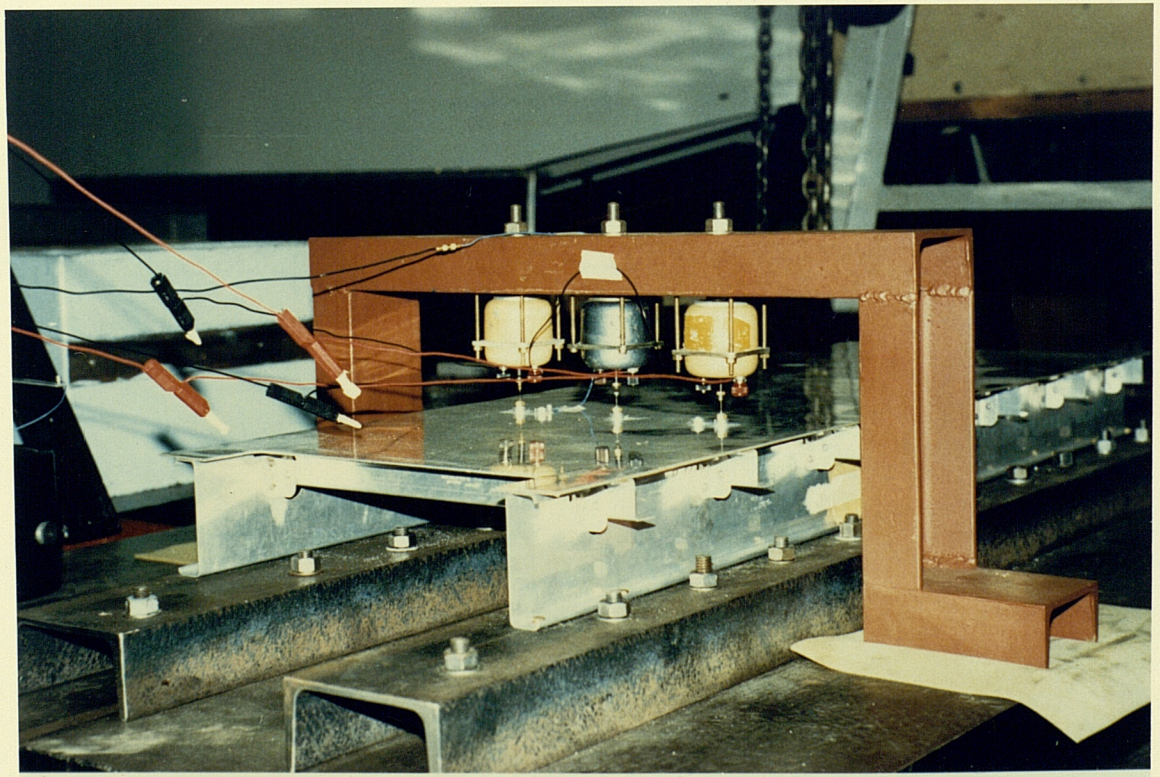

Fig. 97 Mounting of the Exciters and the Plate

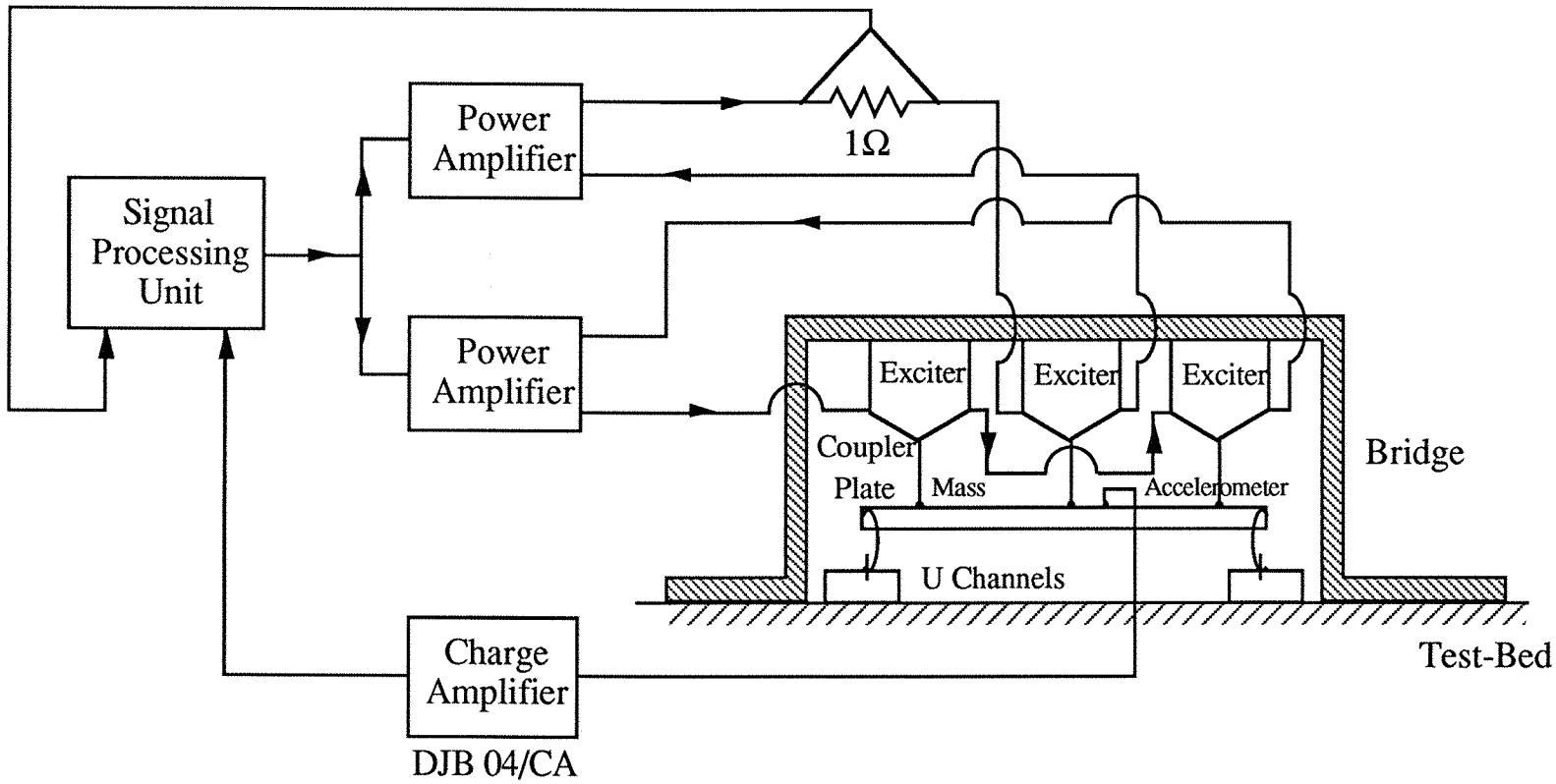

Exciters: Ling 101
Power Amplifiers: H/H Electronics TPA25.D
Accelerometer: B&K 8307

Figure 98: Block-diagram of the Experimental Set-up and the Equipment Used for the Frequency Response Measurements of the Eight-Bay, Stiffened Uniform Plate.

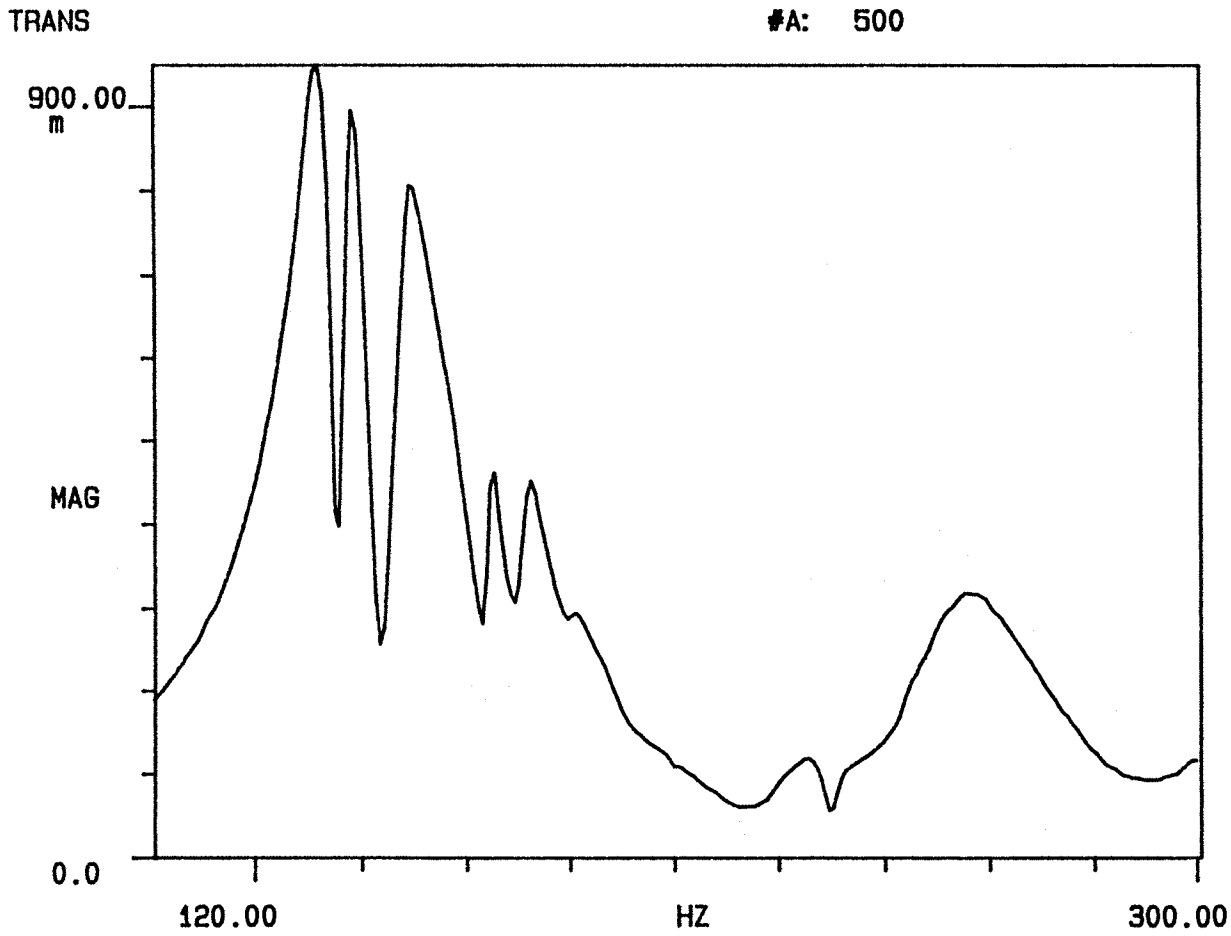

Fig. 99 Experimentally Obtained Frequency Response of the Eight-Bay, Stiffened Uniform Plate (m = 1)

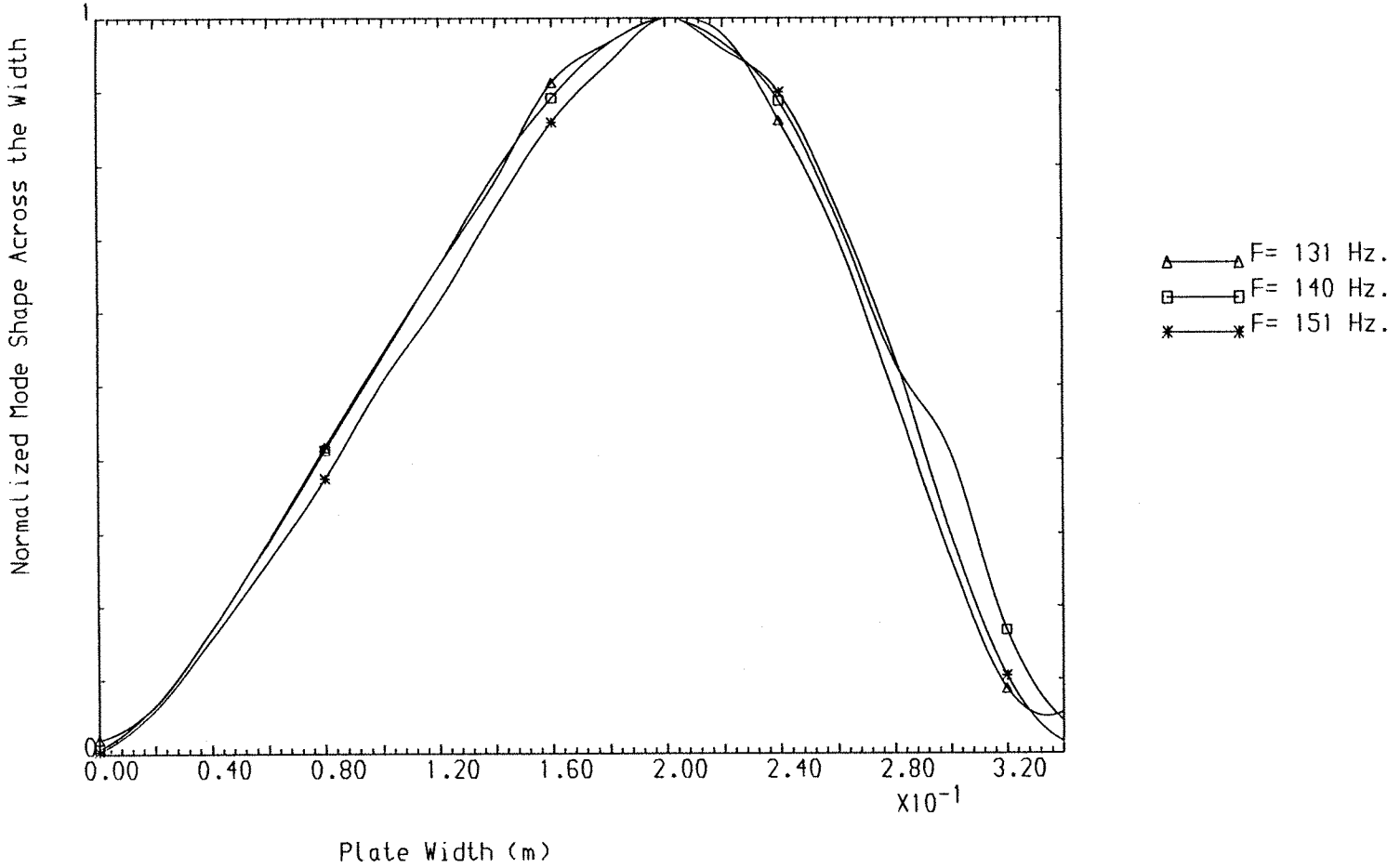

Fig. 100 Normalized Magnitudes of Experimentally Obtained Mode Shapes Across the Width of the Eight-Bay, Stiffened Uniform Plate (m = 1)

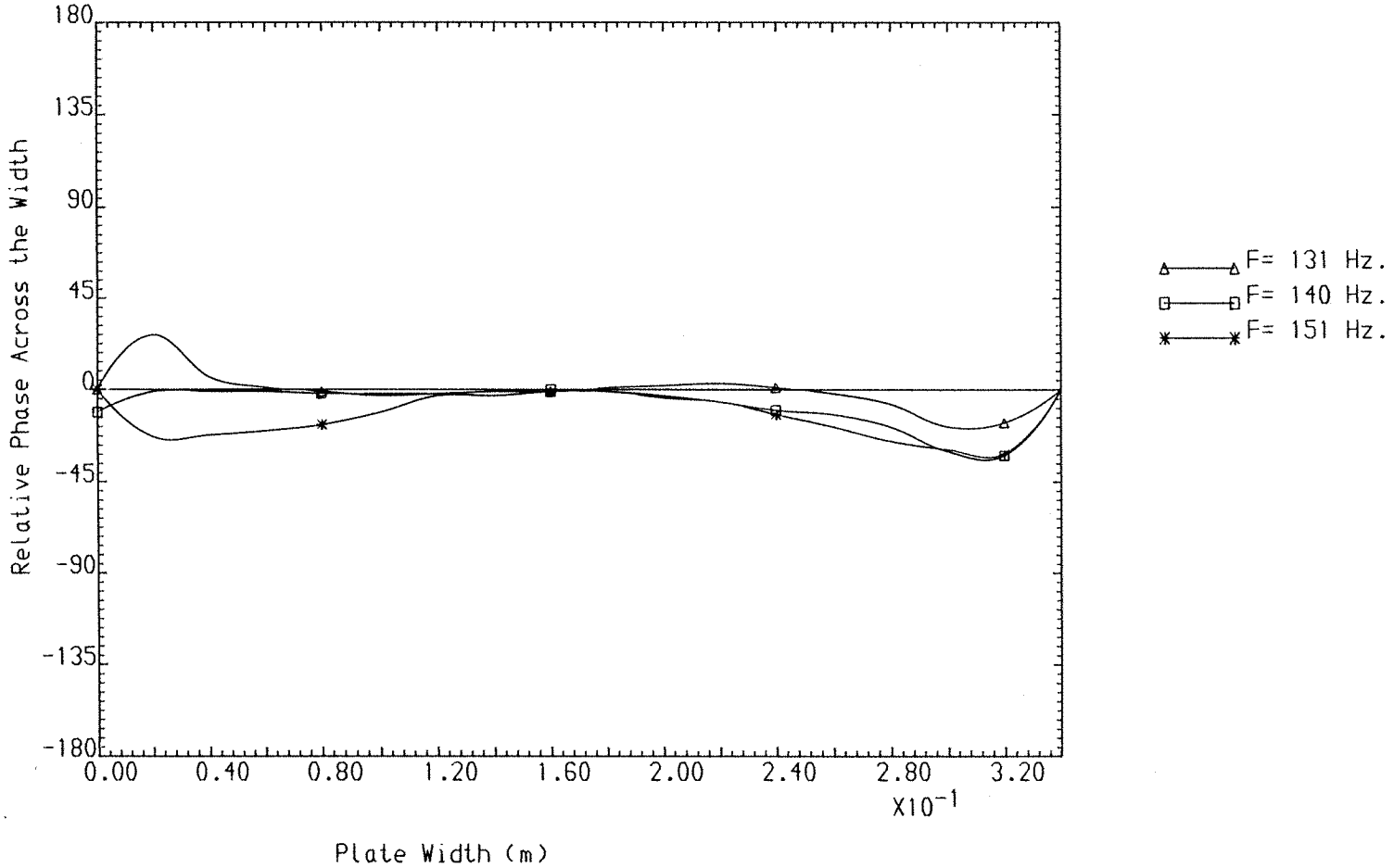

Fig. 101 Relative Phases of Experimentally Obtained Mode Shapes Across the Width of the Eight-Bay, Stiffened Uniform Plate (m = 1)

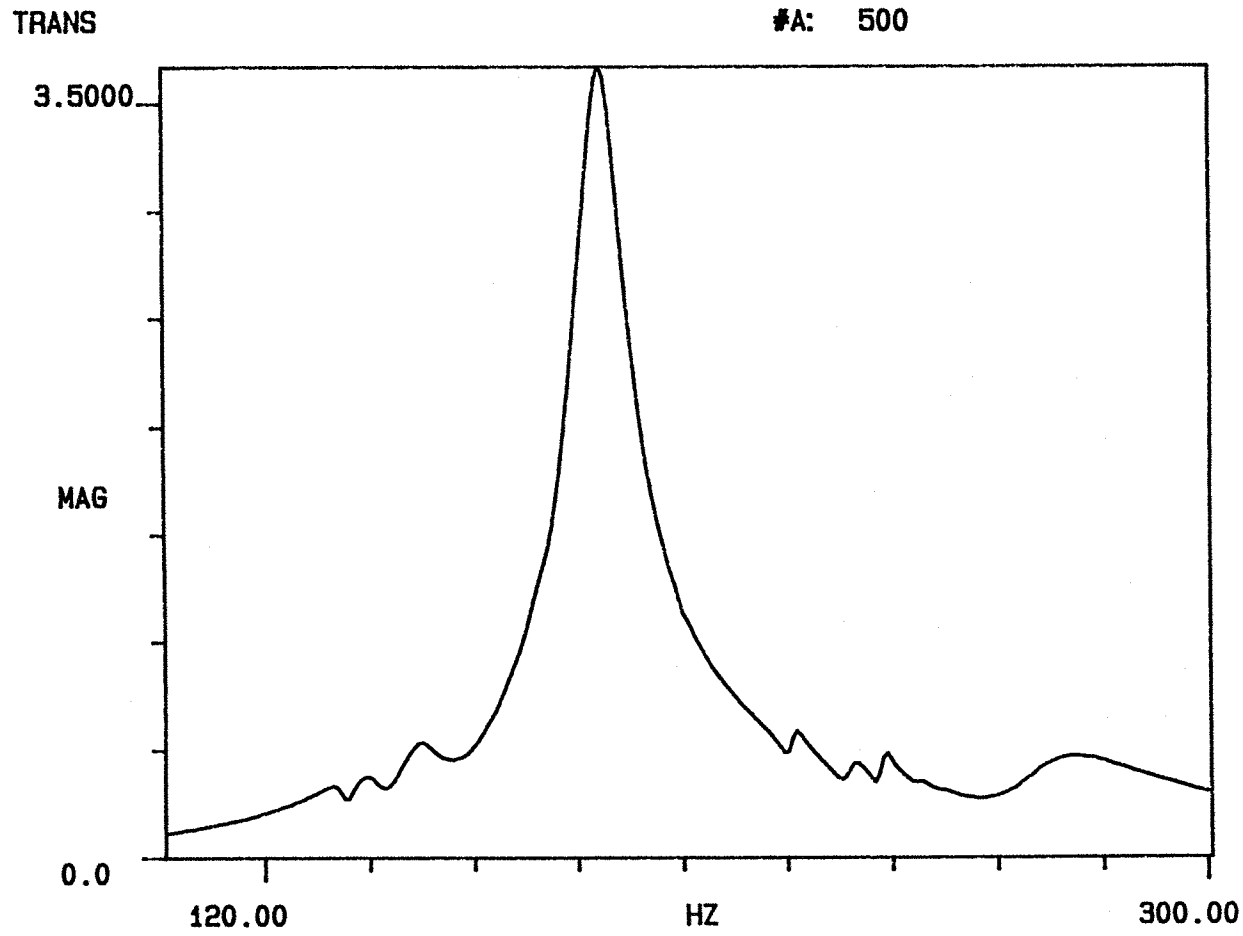

Fig. 102 Experimentally Obtained Frequency Response of the Eight-Bay, Stiffened Uniform Plate (m = 2)

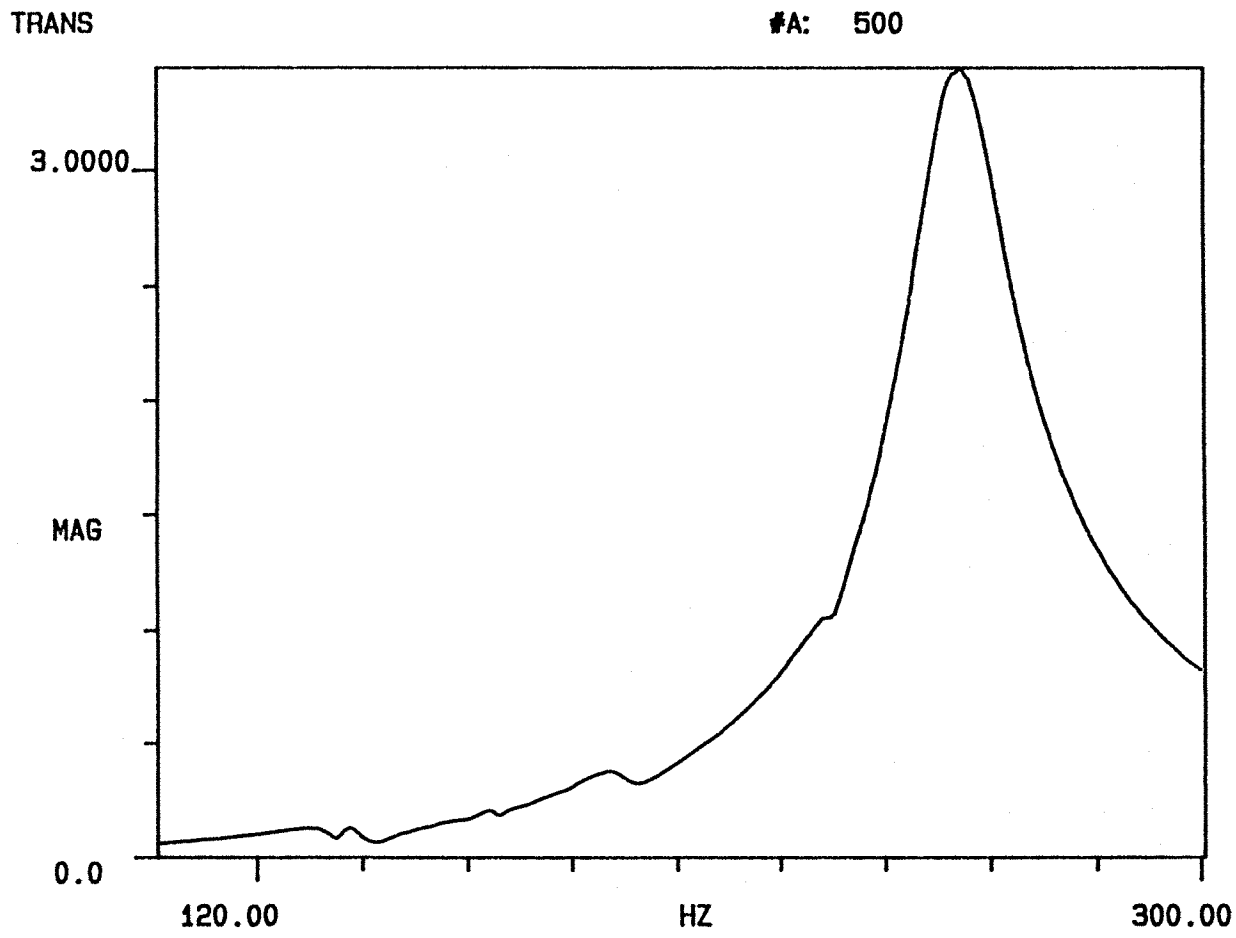

Fig. 103 Experimentally Obtained Frequency Response of the Eight-Bay, Stiffened Uniform Plate (m = 3)

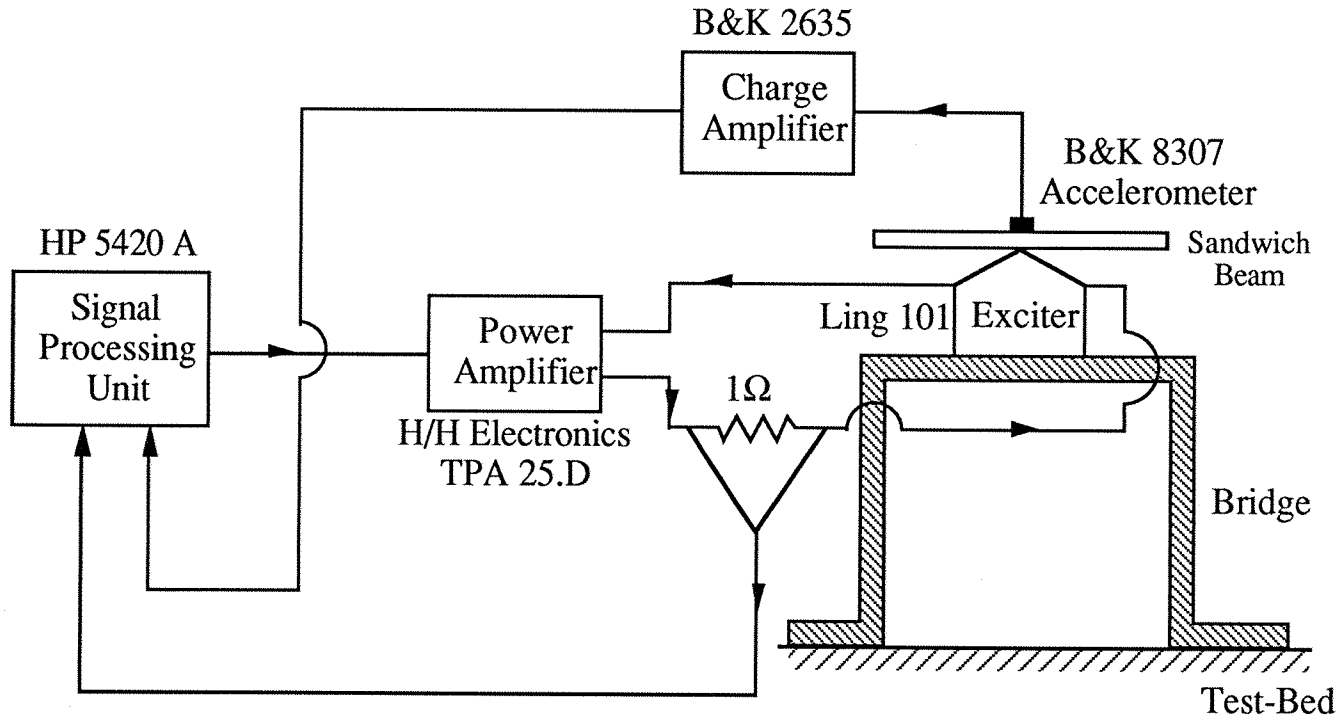

Figure 104: Block-diagram of the Experimental Set-up and the Equipment Used for the Frequency Response Measurements of the Free-Free Three-Layered Sandwich Beam by Using the Accelerometer

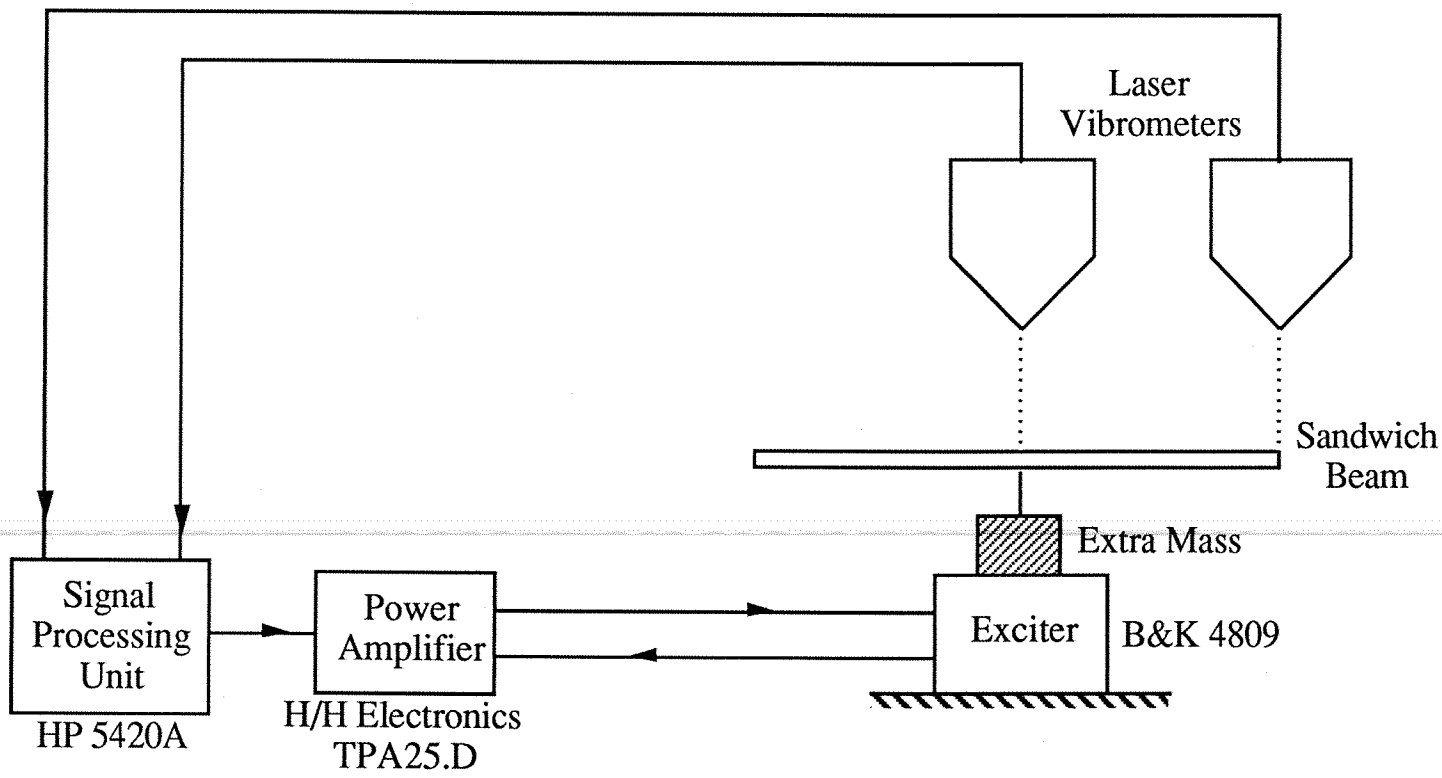

Figure 105: Block-diagram of the Experimental Set-up and the Equipment Used for the Frequency Response Measurements of the Free-Free Three-Layered Sandwich Beam by Using Laser Vibrometers.

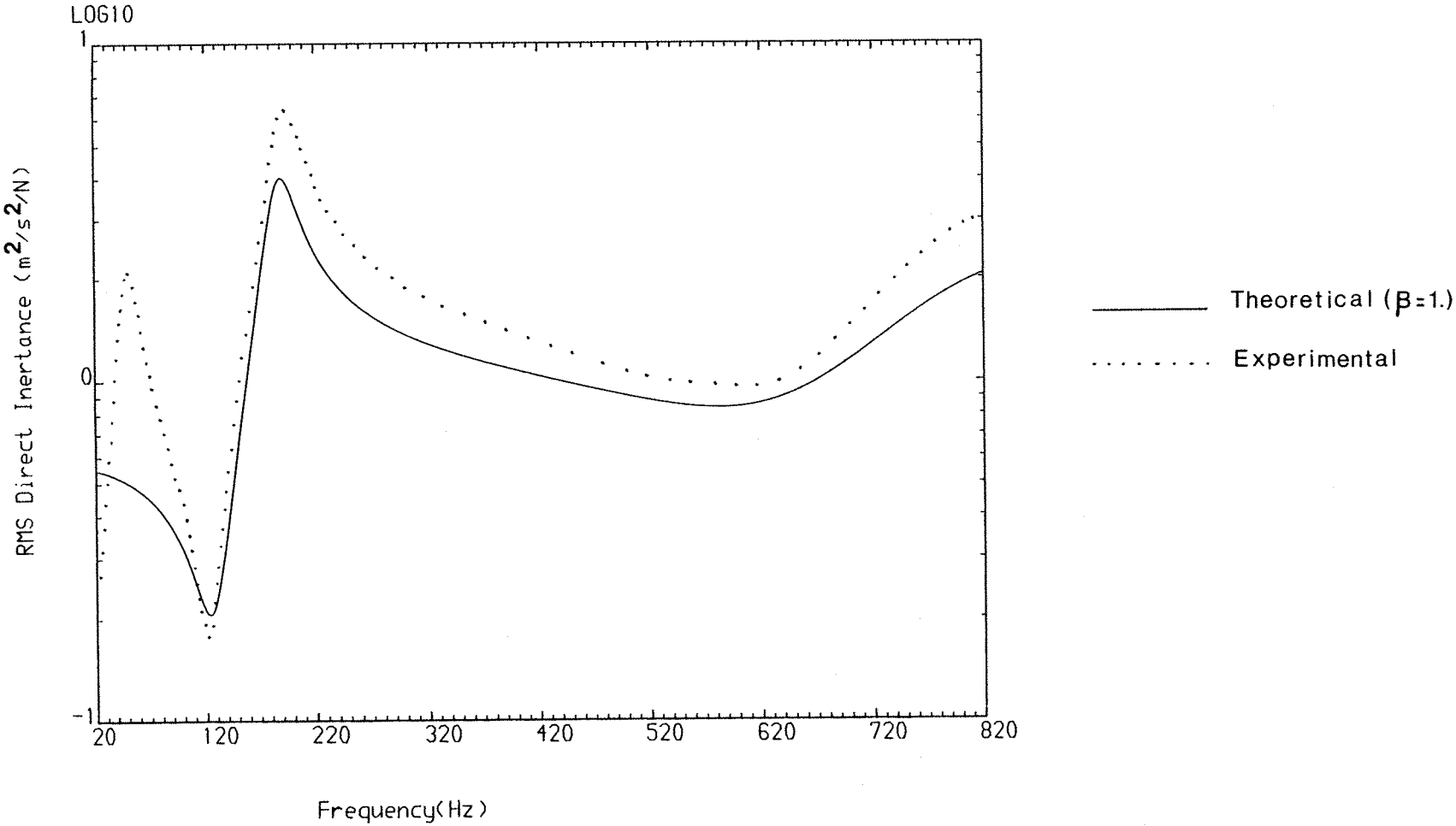

Fig. 106 Comparison of Theoretical and Experimental Transverse Direct Inertances of the Free-Free, Three-Layered Sandwich Beam (x = L/2)

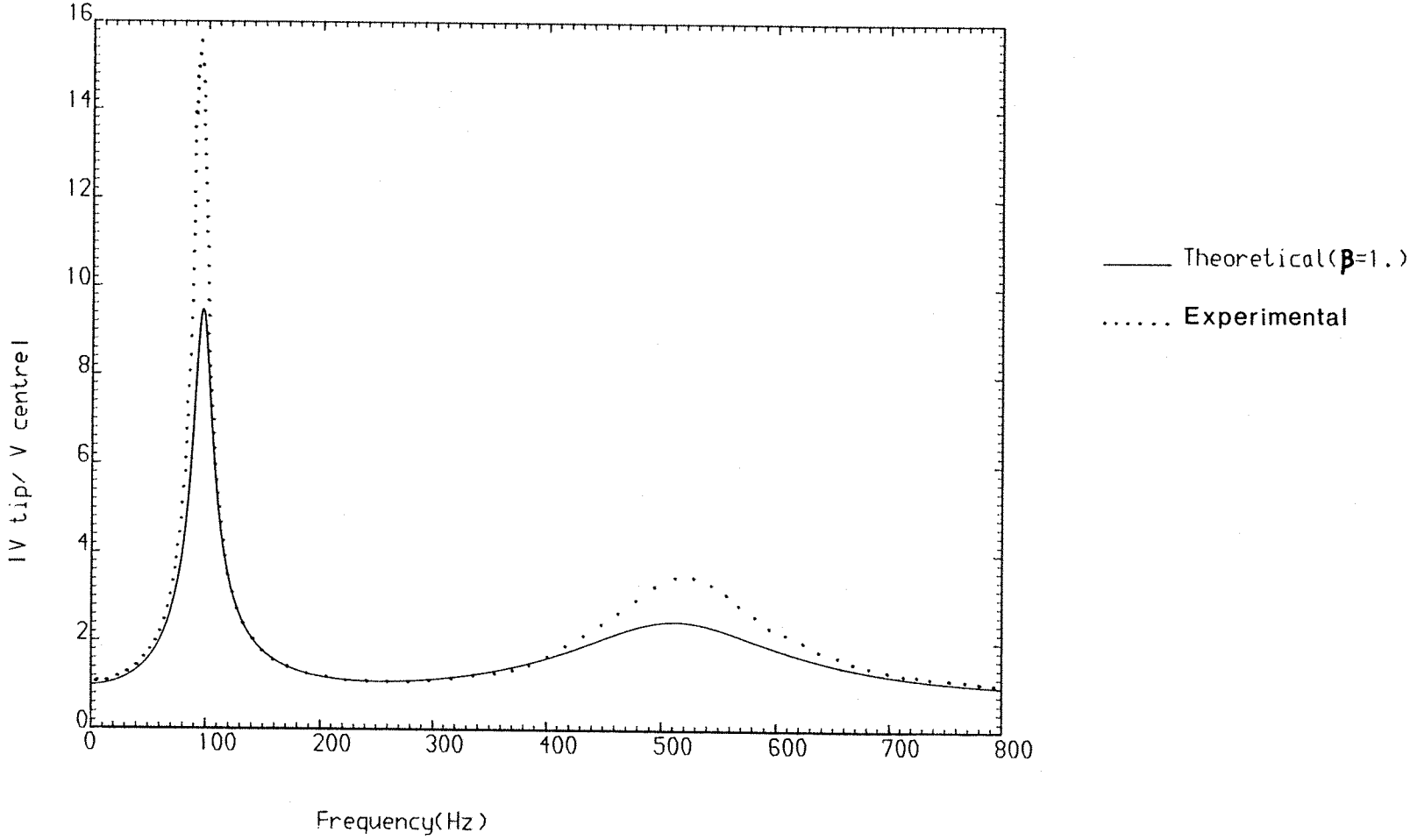

Fig. 107 Comparison of Theoretical and Experimental Ratios of Tip Transverse Response to Centre Transverse Response of the Free-Free, Three-Layered Sandwich Beam

Fig. 108 Top View of the Eight-Bay, Stiffened Three-Layered Sandwich Plate

Fig. 109 Bottom View of the Eight-Bay, Stiffened Three-Layered Sandwich Plate

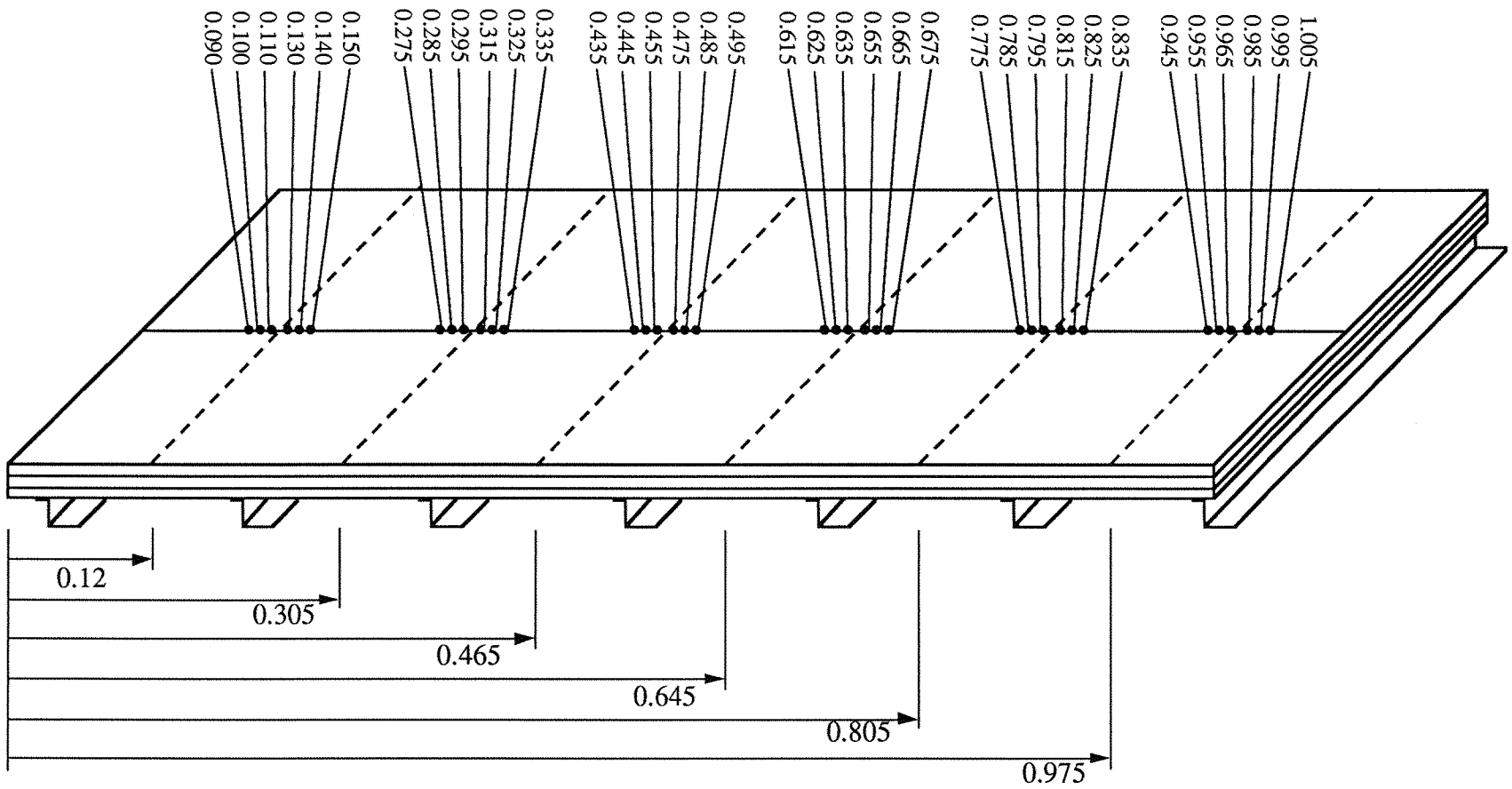

Figure: 110 Line of Excitations and Measurement Points [m] for the Frequency Response Measurements of the Eight-Bay, Stiffened Three-Layered Sandwich Plate . (--- Line of Excitations, • Measurement Points)

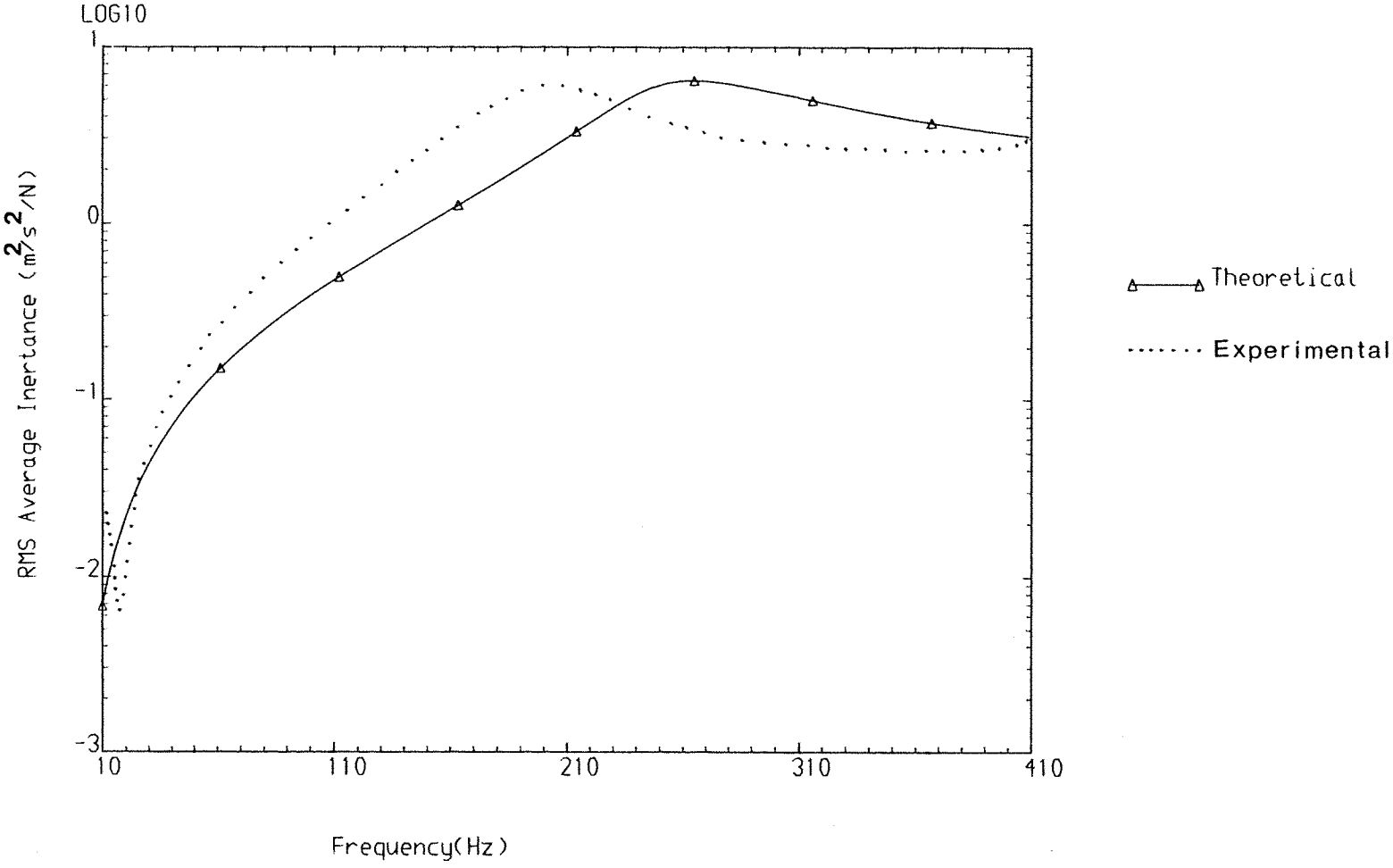

Fig. 111 Comparison of Theoretical and Experimental Transverse Line Inertances of the Eight-Bay, Stiffened, Three-LayeredSandwich Plate (x_o = 0.12 [m])

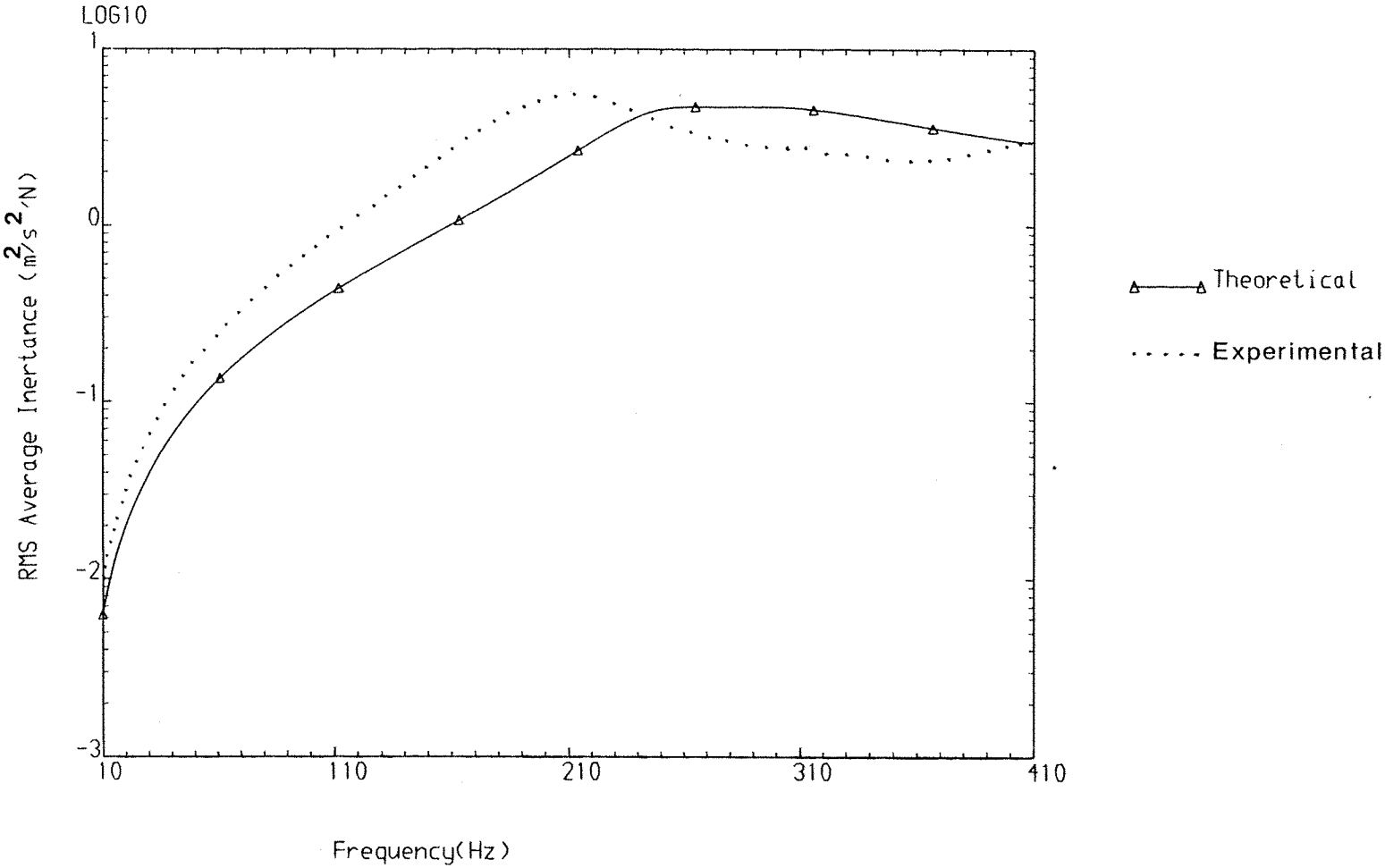

Fig. 112 Comparison of Theoretical and Experimental Transverse Line Inertances of the Eight-Bay, Stiffened, Three-Layered Sandwich Plate (x_o = 0.305 [m])

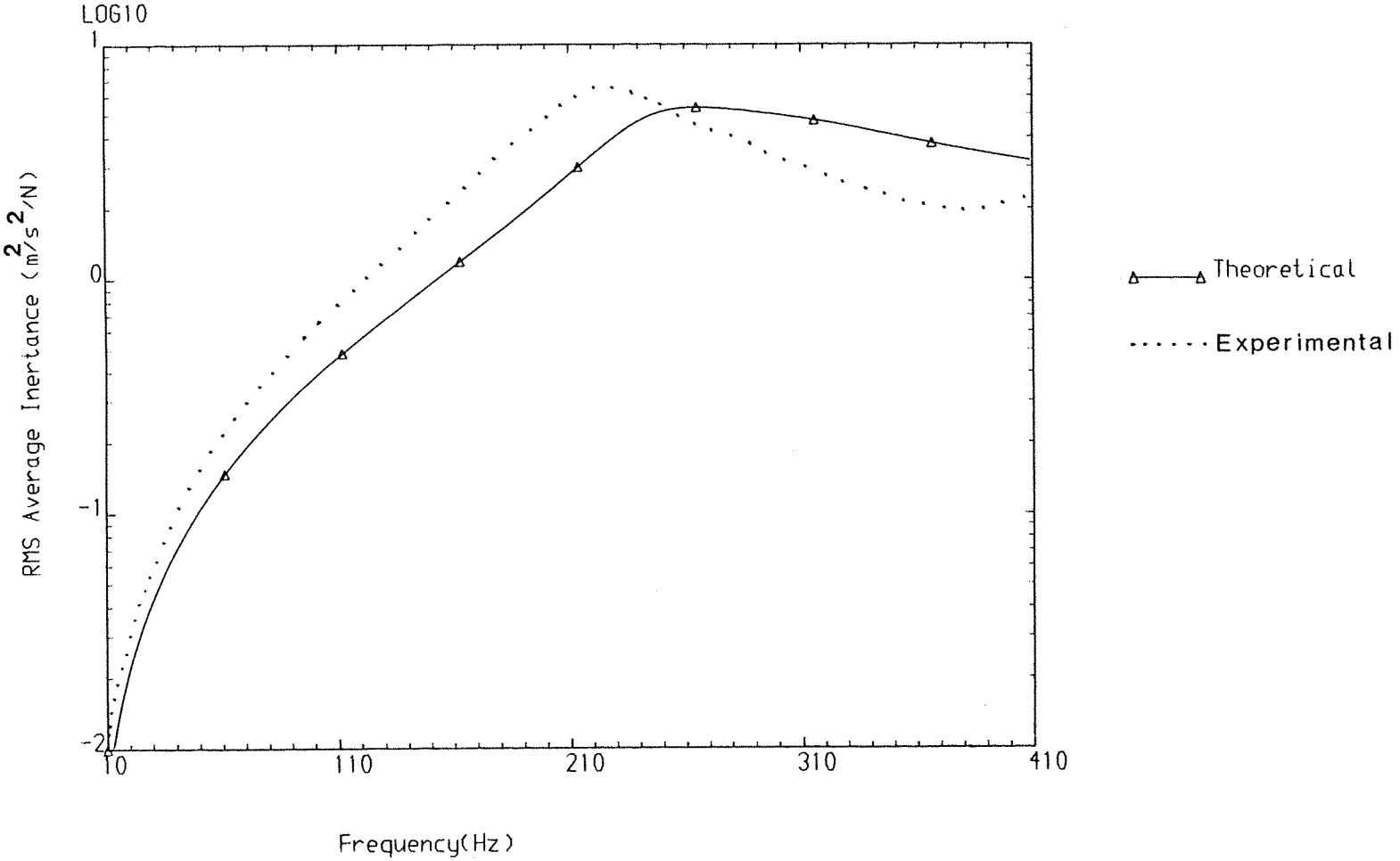

Fig. 113 Comparison of Theoretical and Experimental Transverse Line Inertances of the Eight-Bay, Stiffened, Three-Layered Sandwich Plate (x_o = 0.465 [m])

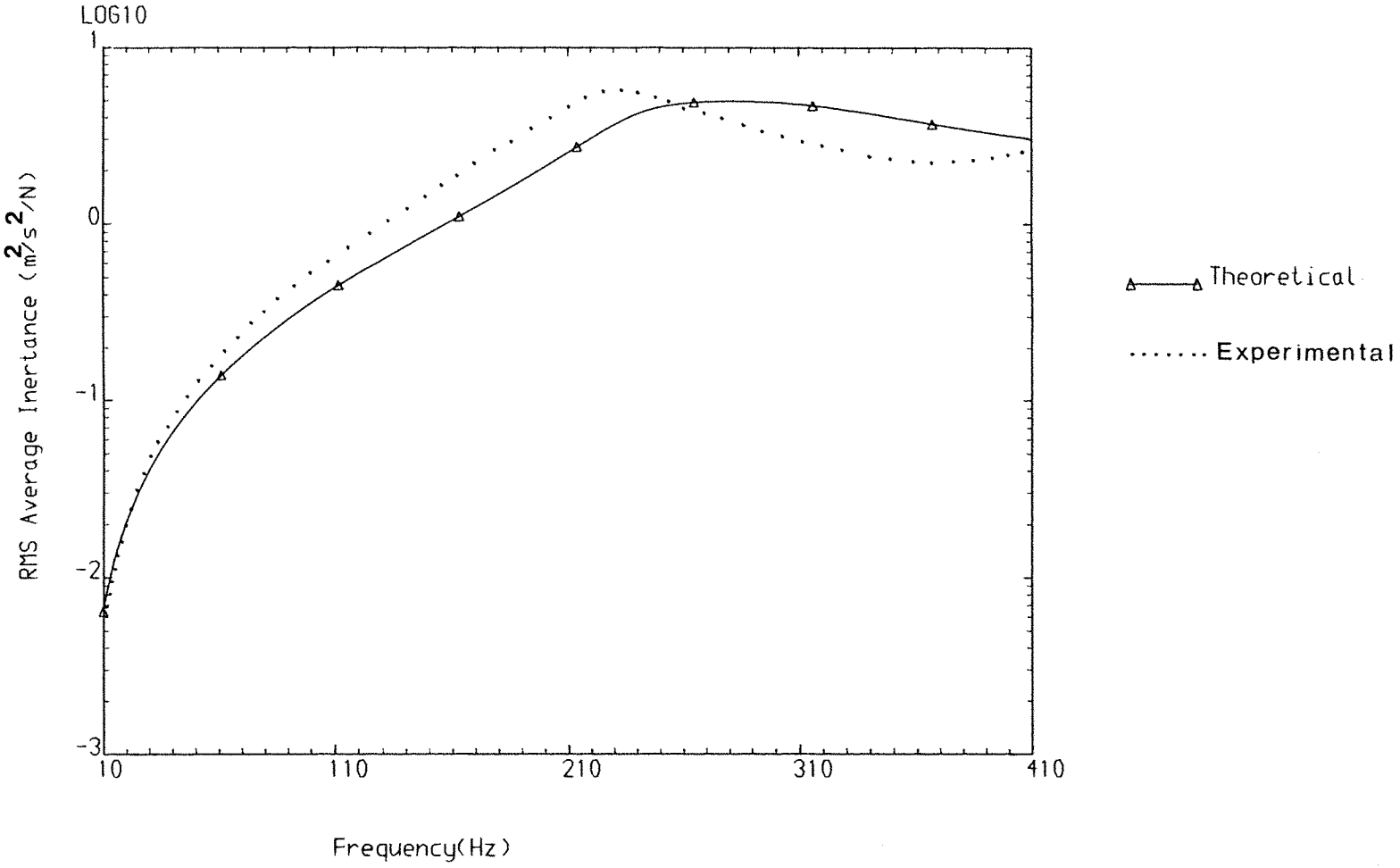

Fig. 114 Comparison of Theoretical and Experimental Transverse Line Inertances of the Eight-Bay, Stiffened, Three-Layered Sandwich Plate (x_o = 0.645 [m])

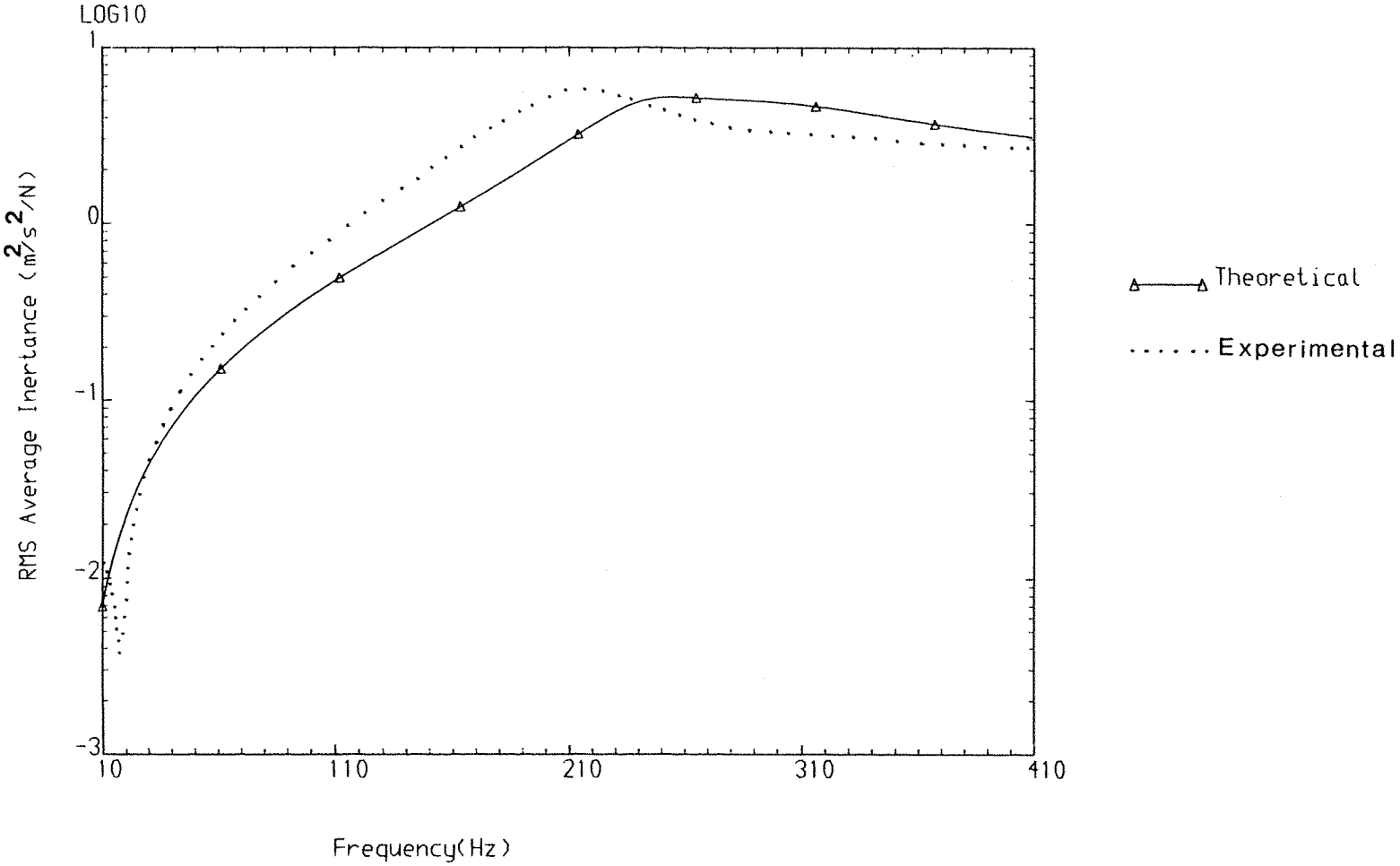

Fig. 115 Comparison of Theoretical and Experimental Transverse Line Inertances of the Eight-Bay, Stiffened, Three-Layered Sandwich Plate (x_o = 0.805 [m])

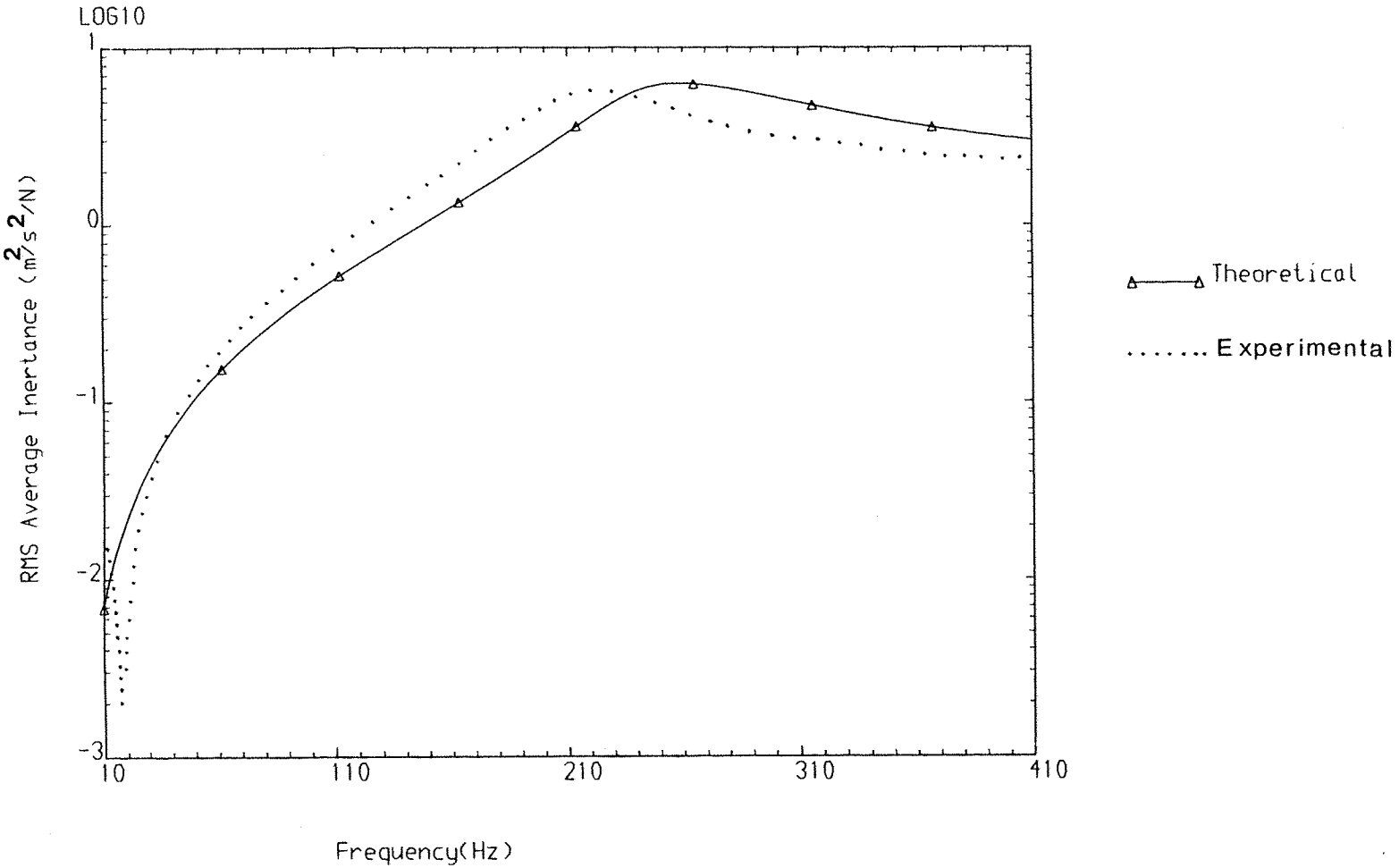

Fig. 116 Comparison of Theoretical and Experimental Transverse Line Inertances of the Eight-Bay, Stiffened, Three-Layered Sandwich Plate (x_o = 0.975[m])

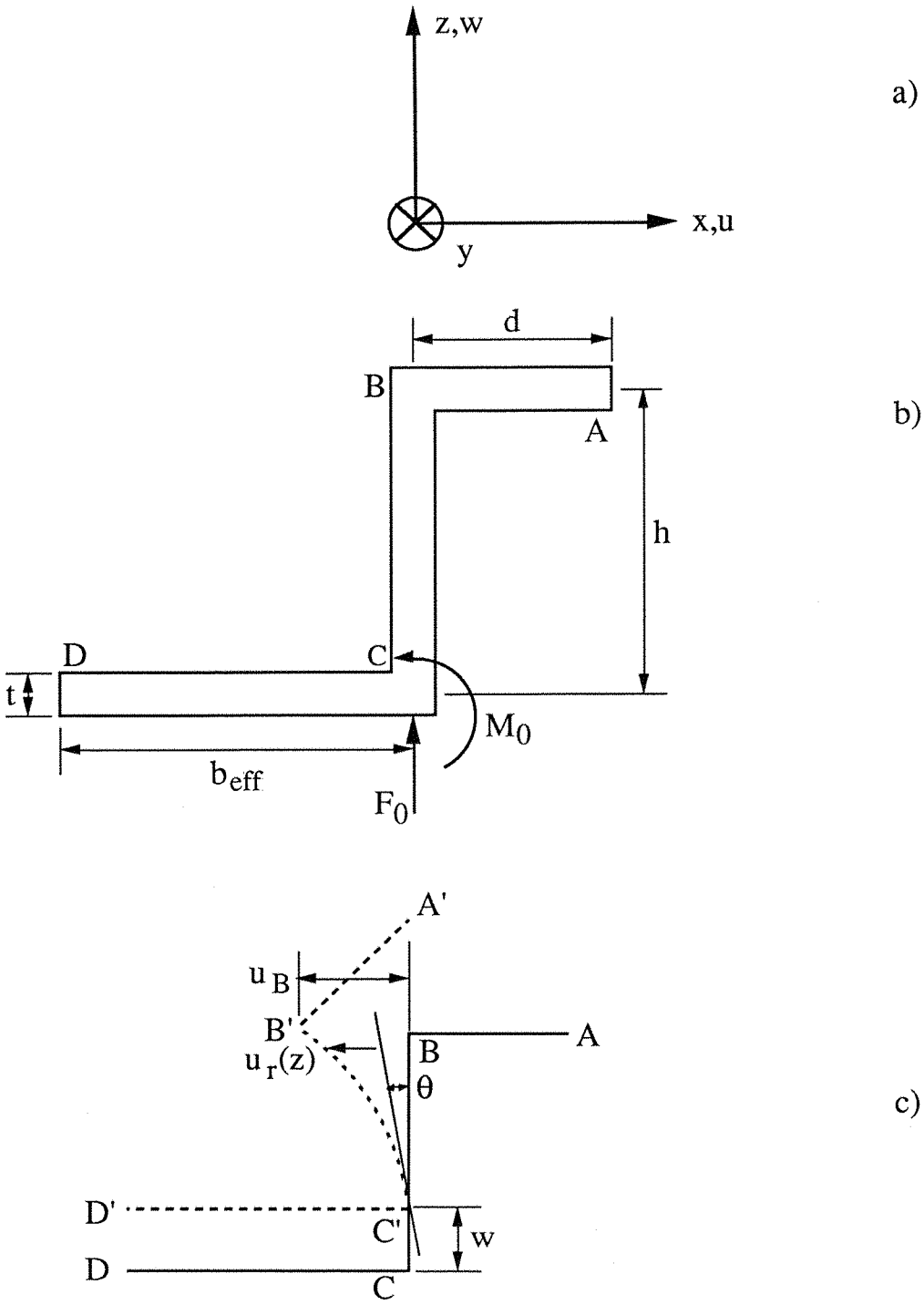

Figure C1: Coordinate, Displacement and Forcing Systems, Dimensions and the Total Deflection of a Z-Section Stiffener.

a) Coordinate and Displacement System
b) Dimensions and Forcing
c) ___ Static position, - - - Deflected Position

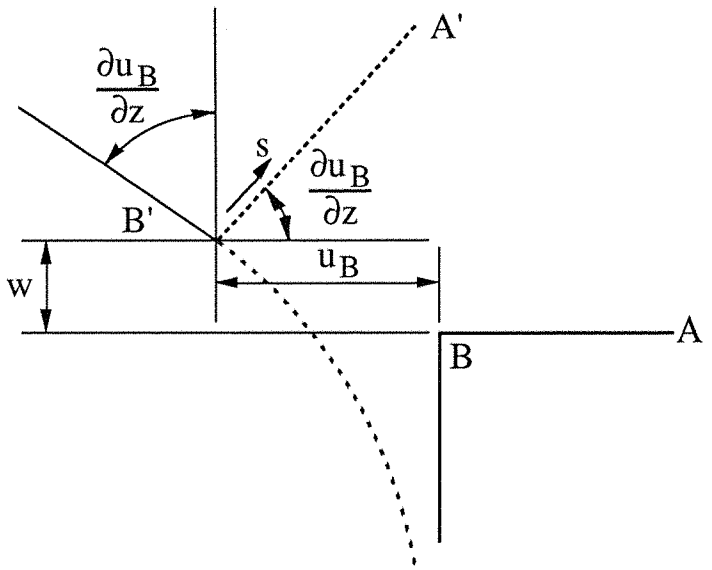

Figure C2: Total Deflection of Flange AB of the Stiffener.

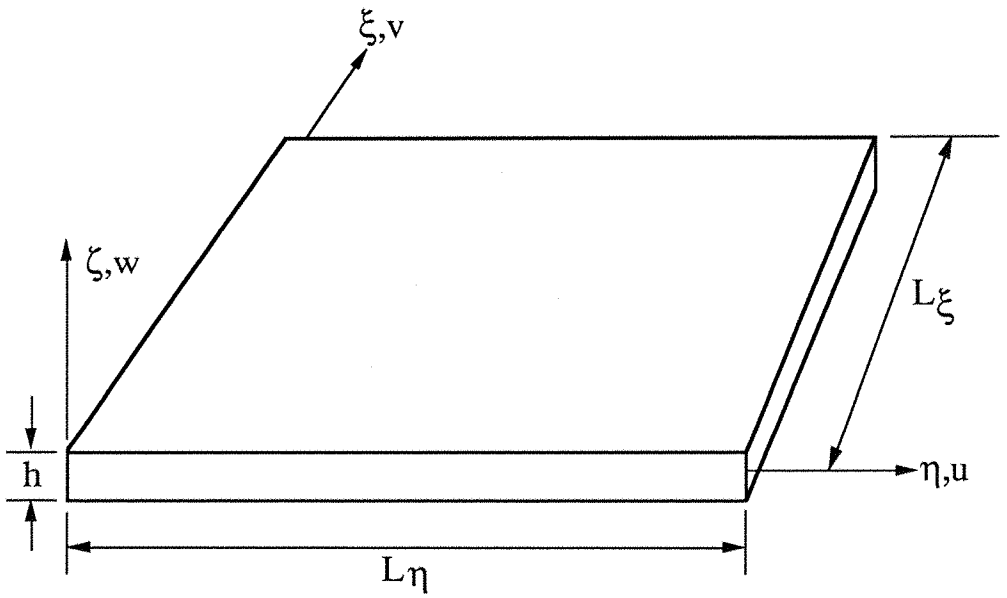

Figure C3: Coordinate, Displacement Systems and Dimensions of an Euler-Bernoulli Plate.

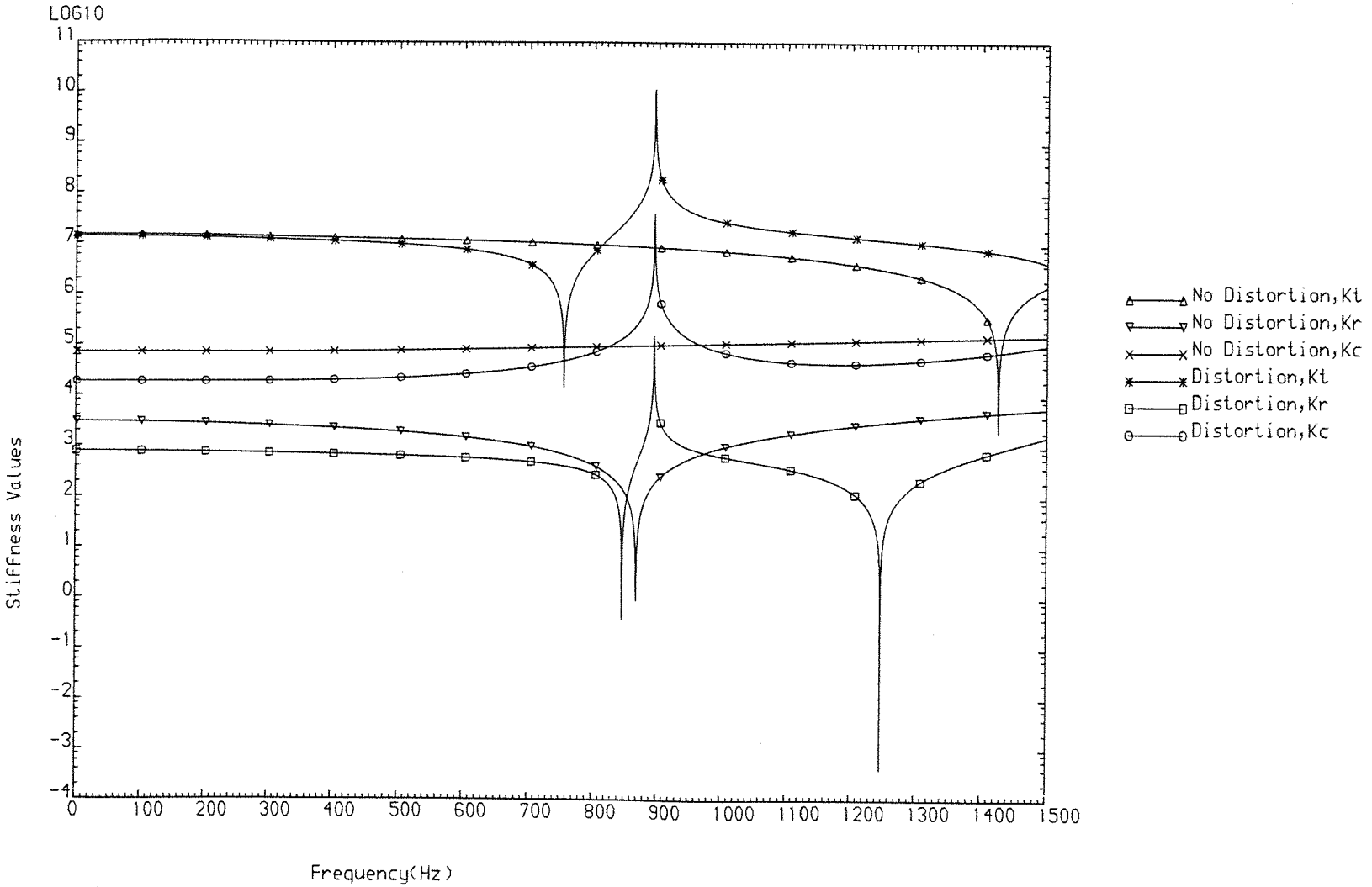

Fig. C.4 Effects of Cross-Sectional Distortion on the Dynamic Stiffnesses of the Stiffener

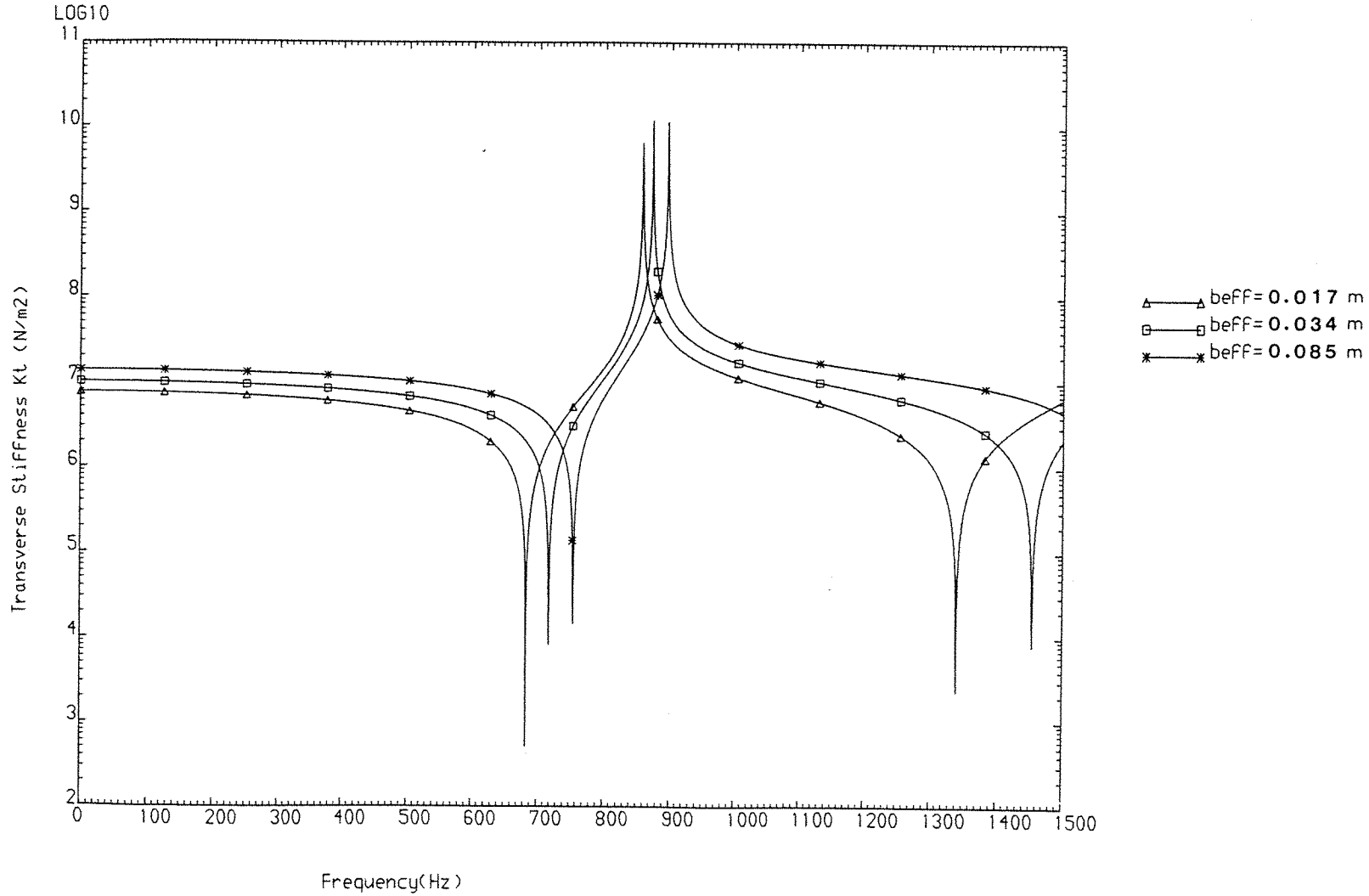

Fig. C.5 **Influence of Effective Width on the Dynamic Transverse Stiffness of the Stiffener**

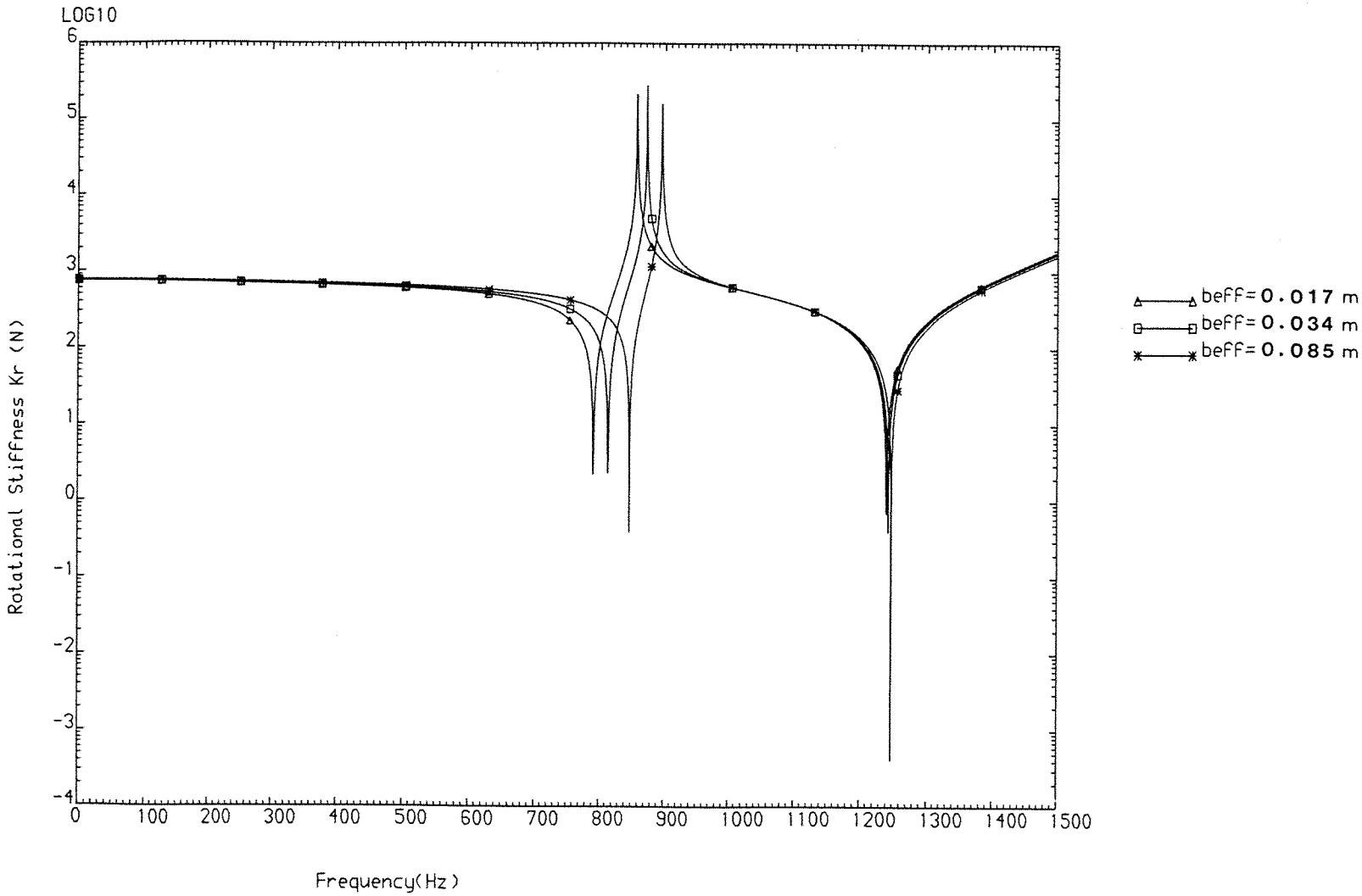

Fig. C.6 Influence of Effective Width on the Dynamic Rotational Stiffness of the Stiffener

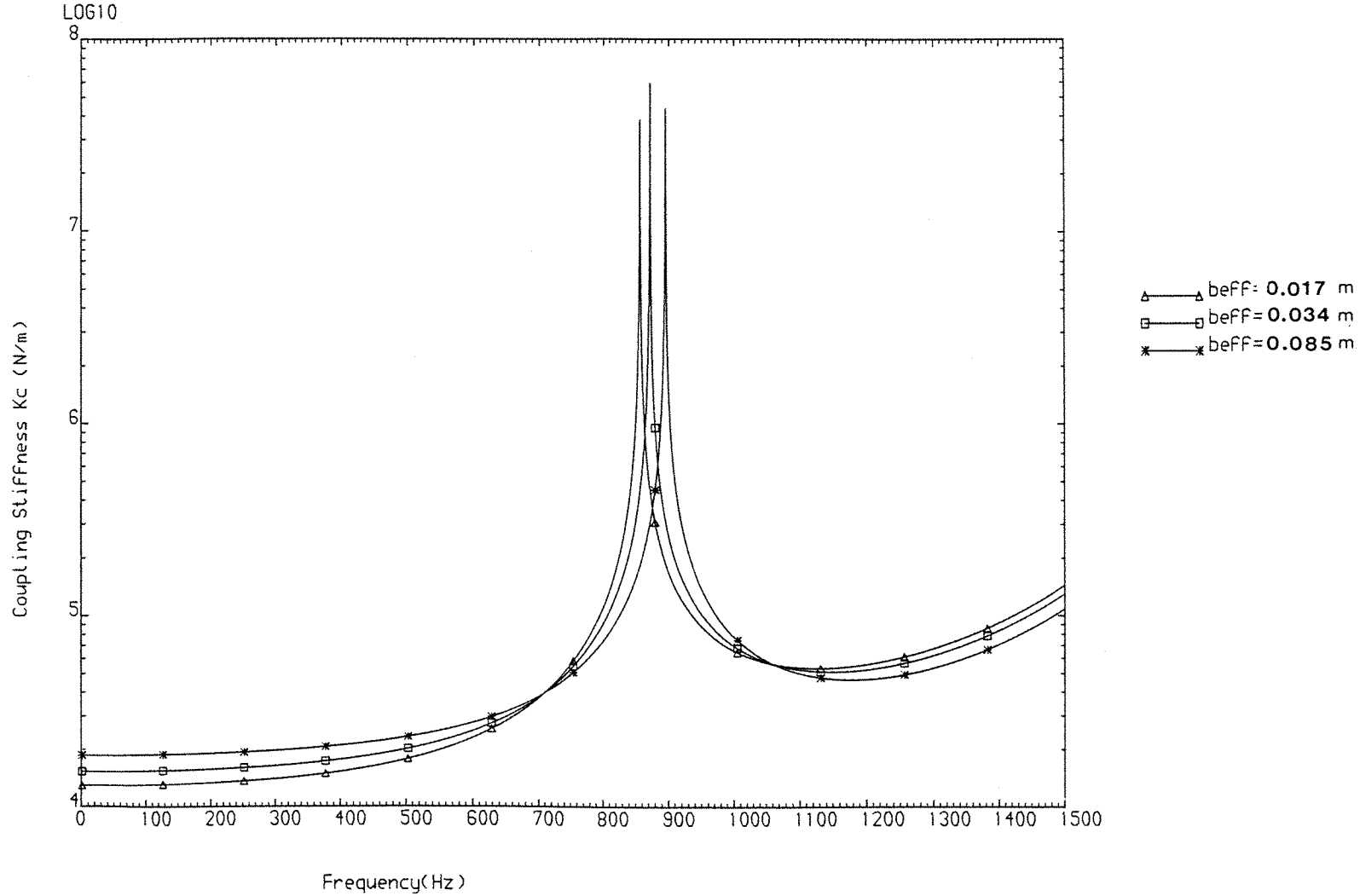

Fig. C.7 Influence of Effective Width on the Dynamic Stiffness Coupling of the Stiffener